

UC Santa Barbara

UC Santa Barbara Electronic Theses and Dissertations

Title

Interplay of molecular structure and photon response in select alternative nucleobases and pigments

Permalink

<https://escholarship.org/uc/item/4m87r45x>

Author

Gate, Gregory

Publication Date

2020

Peer reviewed|Thesis/dissertation

UNIVERSITY OF CALIFORNIA

Santa Barbara

Interplay of molecular structure and photon response in select alternative nucleobases and
pigments

A dissertation submitted in partial satisfaction of the
requirements for the degree Doctor of Philosophy
in Chemistry

by

Gregory Michael Gate

Committee in charge:

Professor Mattanjah de Vries, Chair

Professor Steven Buratto

Professor Martin Moskovits

Professor Joan-Emma Shea

December 2020

The dissertation of Gregory Michael Gate is approved.

Steven Buratto

Martin Moskovits

Joan-Emma Shea

Mattanjah de Vries, Committee Chair

December 2020

Interplay of molecular structure and photon response in select alternative nucleobases and
pigments

Copyright © 2020

by

Gregory Michael Gate

ACKNOWLEDGEMENTS

To my family, who have supported me throughout this entire process. They have patiently tolerated my frantic stress and grumpiness induced by grad school and the Army Reserves. To my friends who did their best to stay in touch thank you for always encouraging me and picking me when I was down. To the United States Army, for making me a better and stronger person, and continually taking me out of my academic bubble. To Mattanjah, for developing me into a scientist, and listening to my crazy ideas. To Michael, for encouraging my crazy ideas putting up with me for the past 5 years. And to all my intramural teams, to include Bucky Ballers I – XV, Bucky Ballers, and '96 Bullets thank you for keeping me sane and giving me something to look forward to throughout the week. We will forever be chasing those shirts.

VITA OF GREGORY MICHAEL GATE
December 2020

EDUCATION

Doctor of Philosophy in Chemistry, University of California, Santa Barbara, December 2020
Advisor: Prof. Mattanjah S. de Vries

Bachelor of Science in Biochemistry, Santa Clara University, June 2014 (cum laude)
Advisor: Prof. Steven W. Suljak

RESEARCH EXPERIENCE

Ph.D. Candidate, Physical Chemistry *December 2015 – December 2020*
de Vries Lab, Department of Chemistry and Biochemistry, UCSB

- Focus on *photodynamics* of canonical and non-canonical nucleobases
- Do *cold, gas-phase spectroscopy in high vacuum* to study photodynamics of isolated organic molecule free from thermal and solvent effects
- Employ *laser desorption jet-cooled mass spectrometry* to get large organic molecule in the gas phase and do action spectroscopy
- Utilize *resonance enhanced multiphoton ionization* for high resolution spectroscopy in the ultraviolet, visible, and infrared regions
- Utilize digital delay generator, digital oscilloscopes, and photodiode arrays to achieve time control *resolution down to single nanoseconds*
- Use *Python, Mathematica, and Labview* to run experiments and do data analysis

Research Assistant, Organic Synthesis *Fall 2014, Spring 2015*
Fuller Lab, Chemistry and Biochemistry Department, SCU

- Used solid-phase synthesis technique to synthesize peptoids with heterocycle backbone to mimic peptides with biological activity
- Used high pressure liquid chromatography and liquid chromatography-tandem mass spectrometry to purify and analyze peptoids
- Tested peptoids for biological activity

Research Assistant, Peptide Analysis and Aptamer Selection *Fall 2011 – June 2014*
Suljak Lab, Chemistry and Biochemistry Department, SCU

- Used manual and automated solid-phase peptide synthesis techniques to synthesize various peptides up to 26 amino acids long
- Used high pressure liquid chromatography and liquid chromatography-tandem mass spectrometry to purify and analyze peptides for use in biological assays
- Monitored fluorescently-tagged aptamer binding to protein using capillary electrophoresis

MILITARY EXPERIENCE

Observer, Coach, Trainer (OCT) team leader *November 2017 – Present*

- Lead about 10 soldiers
- Senior OCT, responsible for developing and executing OCT training and certifying soldiers
- Observe and evaluate other units' training, ensuring they are trained to standard and mission ready
- Ensure all soldiers on team are qualified OCTs to include identifying doctrinal tasks, public speaking, facilitating discussion, setting up a training lane
- Attended First Army Academy, learned how to setup training lanes, identify pertinent doctrine, OCT basics
- Combat Lifesaver Certified, having knowledge in tourniquet application, sucking chest wound, collapsed lung, Tactical Casualty Care

Combat engineer platoon leader

June 2014 – November 2017

- Led over 25 enlisted combat engineers
- Helped develop weekend-long training events for up to 90 soldiers, and ensured all necessary equipment and supplies were allocated and accounted for
- Ensured all soldiers were proficient in their combat engineer duties including infantry tactics, engineer recon, obstacle breaching, and urban breaching
- Assisted soldiers in their personal and civilian lives including receiving military benefits, job searching, school enrollment
- Led soldiers through extended combat exercises

ACADEMIC AWARDS

- Awarded Graduate Research Mentorship Program Fellowship 2019
- Awarded Outstanding Service to the Department Award 2018 and 2019
- Qualified for the semifinals of UCSB's Grad Slam 2018

PRESENTATIONS

- Photon Science Seminar talk on "Excited State Dynamics of Nucleobase Analogues Near Excitation Threshold" at SLAC 2020
- Presented poster on "Mixing Up the R-Groups on the Purines to Unravel the Photostability Mystery" at Pacific Conference for Spectroscopy and Dynamics 2020
- Gave talk on "Using Photostability to Help Select Life" at Chemical Student Speaker Seminars 2019
- Presented poster on "Looking at the isomeric side of life with isoguanine" at ACS Western Regional Meeting 2018
- Gave talk on "Excited state dynamics of a pair of alternative DNA bases" at Pacific Conference for Spectroscopy and Dynamics 2018
- Presented poster on "Probing Intrinsic Photodeactivation Pathways of Nucleobases and Dyes in a Molecular Beam" at Faraday Discussion 2019

PUBLICATIONS

- **G. Gate**, A. Williams, S. Boldissar, R. Szabla, M.S. de Vries, *Evidence for a barrier and intersystem crossing in two tautomers of 2,6-diaminopurine*, *In Preparation*
- **G. Gate**, A. Williams, R. Szabla, M.S. de Vries, *Experimental and theoretical photodynamics of xanthine and 9-methylxanthine in the gas phase*, *In Preparation*
- **G. Gate**, A. Fuller, G. Hill, M.S. de Vries, *Probing the solvent-free excimer dynamics of DNA using the DNA analogue, PNA*, *In Preparation*
- **G. Gate**, A. Williams, M.R. Haggmark, N. Svadlenak, M.S. de Vries, *Nucleobases as molecular fossils of prebiotic chemistry: Excited state dynamics of C2 and C6 substituted purines*, Royal Society of Chemistry, Book Title: *Prebiotic Chemistry*. Editors: Franz Saija and Giuseppe Cassone (In Press 2020)
- **G. Gate**, R. Szabla, M. Haggmark, R. Sobolewski, M.S. de Vries, *Photodynamics of alternative DNA base isoguanine*, *Phys. Chem. Chem. Phys.*, 2019, 21, 13474
2019 PCCP HOT Article
- J. Berenbeim, M. Haggmark, **G. Gate**, C. Patterson, M. Rode, M.S. de Vries, *Excited state intramolecular proton transfer in hydroxyanthraquinones: Toward predicting fading of organic red colorants in art*, *Science Advances*, 2019, 5(9), eaaw5227
- M.R. Haggmark, **G. Gate**, S. Boldissar, J. Berenbeim, A.L Sobolewski, M.S. de Vries, *Evidence for competing proton-transfer and hydrogen-transfer reactions in the S1 state of indigo*, *Chem. Phys.*, 2018, 515, 535-542
- J.A. Berenbeim, S. Boldissar, F.M. Siouri, **G. Gate**, M.R. Haggmark, B. Abalouche, T. Cohen, M.S. de Vries, *Excited-State Dynamics of Isocytosine: A Hybrid Case of Canonical Nucleobase Photodynamics*, *J. Phys. Chem. Lett.*, 2017, 8(20), 5184-5189
- A. Mohan, A.H.M. Koh, **G. Gate**, A.L. Alkins, K.N. McCormas, A.A. Fuller, *Solid-Phase Synthesis of Azole-Compromising Peptidomimetics and Coordination of a Designed Analog to Zn²⁺*, *Molecules*, 2018, 23(5), 1035

ABSTRACT

Interplay of molecular structure and photon response in select alternative nucleobases and pigments

by

Gregory Michael Gate

The spectroscopic analyses of organic molecules relevant to genetic material and the origin of life, as well as various culturally important pigments and dyes are reported. This analysis was conducted in the cold, gas phase using resonance enhanced multiphoton ionization (REMPI). REMPI allows for structural characterization and a temporal description of the excited state dynamics. This experimental technique, when combined with state-of-the-art theoretical calculations, creates a much clearer picture of what is occurring on the molecular and electronic levels. These studies are focused on the excited state dynamics of these systems – how do they react and get rid of their electronic energy after absorption of a photon. A photon is merely a packet of energy, which a molecule then converts to electronic energy upon resonant photon absorption. How these systems react to this added energy is a function of their electronic structure, which is ultimately dependent on their molecular structure. Slight changes in the molecular structure alter the excited state dynamics. It is our goal to develop a model to connect molecular structure to photostability.

Several nucleobase analogues have been studied to determine their photostability. These studies were conducted to help understand the role light hardness played in the evolution of

life's genetic material, long before the creation of the ozone layer. Photostability is determined by a system's excited state lifetime and the presence of any barriers along the pertinent relaxation pathways on the potential energy surfaces. Coupled with results from theoretical calculations, assignments for the relative photostabilities can be deduced. The results from these nucleobase analogues are then compared to the canonical nucleobases: adenine, cytosine, guanine, thymine, and uracil. First, the pyrimidine isocytosine was studied. Isocytosine has the same ligand substructure as guanine, helping to explain the ultrafast lifetimes of biological, keto guanine. A review of the spectroscopy of the C2 and C6 substituted purines follows. Finally, the dynamics of the purines isoguanine, 2,6-diaminopurine, xanthine, and their various tautomers are then explored. The canonical nucleobases are much more photostable than their analogues, supporting the theory that genetic material was selected, at least partially, for its enhanced photostability properties. Excited state dynamics and photostability are very subtle functions of molecular structure, but with no clear mechanism apparent.

Culturally relevant pigments and dyes were also studied spectroscopically. These molecules of interest were studied for their expansive use since antiquity in works of art, due to their visible colorant properties. A study of indigo revealed competing proton transfer and hydrogen transfer relaxation mechanisms, with the mechanism dependent on the exact vibronic mode excited. With enough excess energy, the more photostable proton transfer dynamics becomes the dominant pathway. Separately, the excited state dynamics of the red dye pigments alizarin and purpurin, along with several other hydroxyanthraquinones, were studied. This study was motivated by the apparent fading of some of these compounds in bulk (*e.g.* paint in a work of art). A mechanism heavily dependent on their -OH substitution was resolved to help explain their resistance to fading.

All the systems studied herein are noted for having undergone some form of selection process. For the nucleobases, that involved surviving the ultraviolet bombardment on an early Earth. For DNA, that meant meeting the necessary requirements for the genetic material of life. And for pigments and dyes, that required having the proper steady-state absorption properties for the artist's purposes. Ultimately, the response to these selection pressures were determined by these compounds' molecular structure. This work increases the understanding between molecular structure and excited state dynamics.

TABLE OF CONTENTS

I. Introduction	13
II. Excited state dynamics of alternative pyrimidine isocytosine.....	16
<i>I.</i> Excited state dynamics of isocytosine; a hybrid case of canonical nucleobase photodynamics	17
III. Excited state dynamics of the purines	34
<i>I.</i> Nucleobases as molecular fossils of prebiotic photochemistry: Excited state dynamics of C2 and C6 substituted purines.....	35
1. Introduction.....	35
2. Techniques	42
3. Excited state dynamics.....	45
4. The role of C2 and C6 substitutions	69
5. Outlook	73
<i>II.</i> Photodynamics of alternative DNA base isoguanine	84
1. Introduction.....	85
2. Methods	89
3. Results and discussion	94
<i>III.</i> The tautomer-specific excited-state dynamics of 2,6-diaminopurine using REMPI and quantum calculations.....	113
1. Introduction.....	113
2. Experimental.....	116
3. Results and discussion	118

IV. Experimental and theoretical photodynamics of xanthine and 9-methylxanthine in the gas phase	137
1. Introduction.....	137
2. Methods	141
3. Results and discussion	142
IV. Excited state dynamics of DNA base-stacking free from solvent	156
I. Probing the DNA stacking free from solvent using peptide nucleic acids	158
V. Photostability of organic pigments and dyes	176
I. Evidence for competing proton-transfer and hydrogen-transfer reactions in the S ₁ state of indigo	176
1. Introduction.....	177
2. Methods	180
3. Results.....	183
4. Discussion.....	193
II. Excited State Intramolecular Proton Transfer in Hydroxyanthraquinones: Towards Predicting Fading of Organic Red Colorants in Art	211
1. Introduction.....	212
2. Results.....	215
3. Discussion.....	226
4. Materials and Methods	231

I. Introduction

Life evolves from life. But there must have been a beginning. On an early Earth, life likely arose from inanimate matter. Four billion years ago, life was just beginning to take shape. During this time, our sun was emitting much more ultraviolet (UV) radiation. And the early Earth did not have an ozone layer to attenuate this enhanced UV bombardment. Meanwhile, the early Earth had a “primordial soup” of organic compounds that could be used for the genetic material of life. The diversity of organic compounds discovered on meteorites is evidence for this soup, as meteorite were the feedstock for Earth. Work done by others on the synthesis of nucleobases using prebiotic chemistry also support this diversity. From this wide selection, life selected five nucleobases, the canonical nucleobases, to use as its genetic material.

With the great diversity of life, many exceptions exist. But one aspect that has held constant for all life on Earth, is that they all use the same five canonical nucleobases: adenine, cytosine, guanine, thymine, and uracil. With many possible nucleobases to utilize, and plenty of time for deviations, life still only used the canonical nucleobases. Strong selection pressures must have guided this selection. Inherently, this would have been a chemical selection, as opposed to biological selection, as life had not yet formed. One possible selection was the need for photostability. With the ultraviolet bombardment occurring, life needed its genetic material to have light hardiness and remain chemically inert. If all the non-photostable nucleobases photodegraded upon UV exposure, only the photostable ones would remain. Thus, life would be forced to select the light-fast molecules, because all the other options faded away.

Indeed, the canonical nucleobases have all been found to be extremely resistant to light degradation. And a growing body of evidence shows that most of the non-canonical nucleobases are not photostable. This has helped spark the growing research in how light and matter interact.

Interest in the spectroscopy of the canonical nucleobases began over half a century ago. Then with the accessibility of lasers and the development of ultrafast probing techniques, research focused in on the study of the excited state dynamics of the canonical nucleobases at the beginning of the 21st century. This was coupled with the steady improvements of theoretical calculations with greater computing power allowing for higher demanding calculations. Much of this work went on for about the first decade of the century. This work was motivated by the photostability of the nucleobases, nucleosides, and nucleotides and how that property affected the origins of life and skin damage today. Unfortunately, creating a cohesive picture of the dynamics of life's genetic material proved difficult because there were only five data points available to develop a trend.

Thus, within the past decade, interest has switched to looking at the many variations of the canonical nucleobases. These variations include different tautomers, analogues, and derivatives of the nucleobases. Understanding the excited state dynamics of similar systems would provide more data points and hopefully a more cohesive picture.

Can knowledge of the molecular structure predict the photostability of a system? Photostability is mediated by the excited state dynamics. Excited state dynamics are influenced by electronic and nuclear structure. Here I will discuss my work on the excited state dynamics of various non-canonical nucleobases to help elucidate the answer to this problem. With these additional data points, can a mechanistic solution to the interplay between photostability and molecular structure be derived? I mainly focus on the various

permutations of purine with amino or oxo moieties substituted at the C2 and C6 positions. Preliminary work on the excited state dynamics induced by base stacking of single-stranded DNA using peptide nucleic acids (PNA) as a substitute are also presented. Though relatively small structural modifications, these substitutions can have disproportionate impact on the excited state dynamics, and hence photostability, of these systems.

In a similar manner, the electronic structure of pigments and dyes determine their absorption and scattering properties, hence mediating their color and appearance. Their visible appearance can help artists decide whether or not to use them. Just as life's genetic material underwent a chemical selection based on its electronic properties, so do dyes and paints undergo biological (artistic) selection. Certain pigments and dyes, now just referred to as pigments, were selected for their preferential electronic properties. The artist was unaware of these pigments' excited state properties though. If they were, the artist would have found a rich assortment of excited state dynamics depending on the exact molecular structure they chose.

The blue pigment indigo has been used as a colorant for millenia, with artifacts thousands of years old still retaining their blue hue. Today, indigo is one of the most widely produced pigments as it is the main chromophore in denim jeans. Indigo's ability to not fade over these long periods of time point to its photostability. Indeed, we have found its light-fastness derives from its ability to do both proton and hydrogen atom transfer with stable proton transfer preferred at higher excitation energies.

Organic red-hued pigments from the hydroxyanthraquinone family have been used as paint colorants in cultural works of art for centuries. It has been noted that some of these red hues fade and lose their distinct color faster than others. Since antiquity, alizarin and purpurin have been chosen as red colorants. Unbeknownst to the artist, some pigments were

more photostable than others, allowing their colors to last longer. I studied the effects of -OH substitution for a series of hydroxyanthraquinones on their respective photostability and excited state dynamics. The single -OH substitution motif at the 1 position had significantly higher photostability due to radiationless ultrafast relaxation via proton transfer while the 1,4 doubly-substituted motif had much longer lifetimes and lower photostability. This lower photostability for the 1,4 motif would lead to faster photodegradation of the pigment over time.

Just like the nucleobases, photostability is sensitive to molecular structure. This is because molecular structure determines the excited state dynamics, which ultimately regulates photostability. We have studied the hydroxyanthraquinone pigments and indigo free from thermal and solvent effects and found their photostability to be structure dependent. Selected for their visible appearance, little thought was given to the enduring capabilities of these pigments. This thesis looks at what happens to various nucleobases and pigments after photon absorption, and the implications for these actions.

II. Excited state dynamics of alternative pyrimidine isocytosine

The canonical nucleobases have been found to all be very photostable, having the ability to convert electronic energy to heat before any damaging chemical reactions can take place. With light-fastness as a possible chemical selection pressure, other nucleobase analogues likely do not share this trait, otherwise they would have been selected. And a growing body of evidence supports this. But certainly photostability was only *one* pressure, with other selection characteristics also driving this evolution.

Isocytosine has been studied for how it reacts to light. As the pyrimidine version of guanine, it shares surprisingly similar excited state dynamics, for both tautomers observed. Thus, its Watson Crick (WC) tautomer is very photostable. Meanwhile, enol cytosine was

also observed in the gas phase for the first time, and found to have a faster decay than its corresponding WC keto tautomer. The differences in dynamics between the various tautomers highlights how important molecular structure is in mediating reaction to light.

I. Excited state dynamics of isocytosine; a hybrid case of canonical nucleobase photodynamics

Jacob A. Berenbeim, Samuel Boldissar, Faady M. Siouri, Gregory Gate, Michael R. Haggmark, Briana Aboulache, Trevor Cohen, and Mattanjah S. de Vries

Department of Chemistry and Biochemistry, University of California Santa Barbara, CA 93106-9510

Abstract

We present resonant two-photon ionization (R2PI) spectra of isocytosine (isoC) and pump–probe results on two of its tautomers. IsoC is one of a handful of alternative bases that have been proposed in scenarios of prebiotic chemistry. It is structurally similar to both cytosine (C) and guanine (G). We compare the excited-state dynamics with the Watson–Crick (WC) C and G tautomeric forms. These results suggest that the excited-state dynamics of WC form of G may primarily depend on the heterocyclic substructure of the pyrimidine moiety, which is chemically identical to isoC. For WC isoC we find a single excited-state decay with a rate of $\sim 10^{10} \text{ s}^{-1}$, while the enol form has multiple decay rates, the fastest of which is 7 times slower than for WC isoC. The excited-state dynamics of isoC exhibits striking similarities with that of G, more so than with the photodynamics of C.

Without a fossil record of the prebiotic chemical world we are left to conjecture to understand the roadmap that led to RNA and DNA. One of the factors that may have played a role in the prebiotic chemistry on an early earth is the photochemistry that could have been important before modern enzymatic repair and before the formation of the ozone layer.¹⁻⁶ Nucleobases, when absorbing ultraviolet (UV) radiation, tend to eliminate the resulting

electronic excitation by internal conversion (IC) in picoseconds (ps) or less.^{4, 7-9} The availability of this rapid “safe” de-excitation pathway turns out to depend exquisitely on molecular structure. DNA and RNA bases are generally short lived in the excited state, and thus UV protected, while many closely related compounds are long lived and thus more prone to UV damage. This structure dependence suggests a mechanism for the chemical selection of the building blocks of life, implying that photochemical properties may be molecular fossils of the earliest stages of prebiotic chemistry.

It is therefore of great interest to study the photochemical properties of possible alternative bases in comparison to the canonical bases. Especially intriguing are structures that can form alternate base pairs with the same Watson–Crick (WC) motif as the canonical ones, such as the triple hydrogen bonded guanine/cytosine (G/C) pair.¹⁰⁻¹³ The alternative bases isocytosine (isoC) and isoguanine (isoG) were predicted in 1962 as a plausible third WC base pair.¹⁴ As pointed out by Saladino et al., isoC can form WC base pairs with cytosine (C) and isoguanine or a reversed WC base pair with guanine.¹⁵ Here we focus on isoC, which is not only an isomer of C but also an analogue of guanine (G), see Figure 1. Theoretical and experimental study has established the thermodynamic stability of the isoC/isoG base pair which nominally has greater free energy than G/C as well as of other possible base pair combinations with isoC.¹⁶⁻¹⁷ This has piqued interest in the prebiotic prevalence of these unnatural pairs in addition to their role in synthetic research and medical applications.¹⁸⁻¹⁹ Here we aim to understand the photostability of isoC.

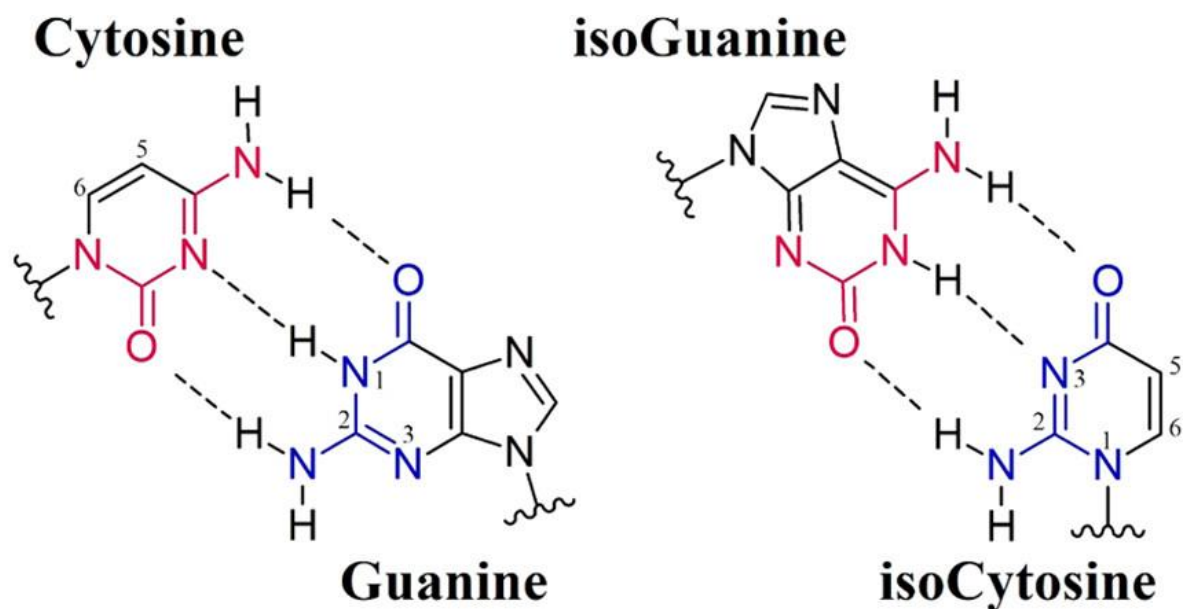


Figure 1. Structures of G/C and isoG/isoC arranged to emphasize heterocyclic substructure similarities, emphasized in red and blue.

We have arranged the bases within Figure 1 to emphasize the functional rearrangement from the standard base to its iso- analog about the pyrimidine heterocyclic centers. Doing so likens isoC to the core moiety of G. The difference between G and isoC is the five-membered ring in G (not present in isoC) which would have consequences for formation of a macromolecular structure. In this work, we find that the excited-state dynamics of isoC exhibits striking similarities with that of G and more so than with the photodynamics of C.

IsoC has previously been identified in the gas phase,²⁰ and its photo dynamics have been studied theoretically²¹⁻²² and in the condensed phase.²³⁻²⁵ However, no excited-state lifetime has been experimentally determined of isolated isoC in individual tautomeric forms. The two lowest-energy forms are enol and keto which can isomerize via an excited-state intramolecular proton transfer. This isomerization after UV excitation has been observed in solution²³ by time-dependent absorption spectroscopy and in a rare gas matrix by changes in the IR absorption.²⁴⁻²⁵ Chart 1 outlines the lowest energy tautomers in the gas phase. KA2

corresponds to the WC structure in the pairing with isoG in Figure 1. KA1 can also form similar triple hydrogen bonded structures with other tautomeric forms of G, such as the enol form.

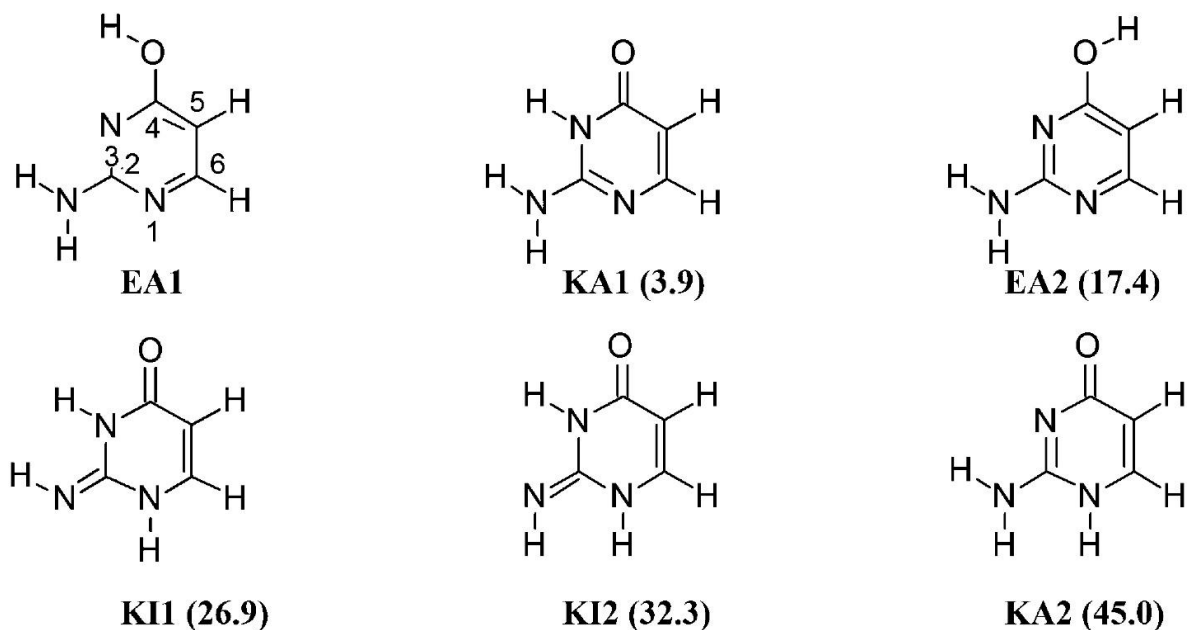


Chart 1: Lowest ground state energy structures ($\Delta E < 50$ kJ/mol). Heterocyclic atoms are numbered for EA1 but the convention is the same for all others. Arranged in order of relative energy given in parenthesis (kJ/mol). Zero point corrected energies were calculated by DFT analysis with the B3LYP hybrid functional and with a cc-pVTZ basis set.

Recent work by Szabla et. al used state-of-the-art surface-hopping adiabatic molecular dynamic simulations to predict the excited-state lifetime of isoC to be the following:

$\tau_{EA1}=533$ fs and $\tau_{KA1}=182$ fs.²¹ These lifetimes are from populating a continuum of mixed character electronic states S1–S6 at the 5.5 ± 0.2 eV spectral domain which proceed to relax through S1 IC. Three dominant conical intersection (CI) geometries are established in their work for the modeled EA1 and KA1 starting structures, whereby pyramidalization of the planar Franck–Condon (FC), i.e. excitation geometry, structure at the C2 position accounts for $\Phi_{EA1} = 0.60$ and $\Phi_{KA1} = 0.93$ nonradiative relaxation yields, while deformation about the C5=C6 bond accounts for a CI of negligible yield. Hu et al. also studied the KA1 form

computationally, comparing different levels of theory. They assumed excitation at energies closer to the vibrationless level and identified three CIs, all leading to IC to the ground state, one involving the C=O stretching vibration and two involving out-of-plane structures of the NH₂ group. They found the preferred pathway to depend on the computational method, as did the IC rate, leading to excited-state lifetimes ranging from 100 fs to 1 ps.²⁶ Surprisingly, both computational studies are contrary to the bulk of theoretical work done on pyrimidine relaxation dynamics, where the C1C5=C6 is understood to be a major pathway toward nonradiative deactivation by twisting of the H-C5=C6-H torsional angle to near ethylene geometry.²⁷⁻²⁹ Trachsel et al. most recently showed the importance of this particular bond deformation when they measured excited-state lifetimes of 5,6-trimethylenecytosine, a sterically constrained C analogue, in the gas phase.³⁰ This modified version yielded lifetimes attributed to IC six times greater than that of C, likely due to the absence of a CI_{C5=C6}.

Figure 2 two-color (2C) resonant two-photon ionization (R2PI) spectra of isocytosine with nanosecond (ns) and ps pulse sources. The ns spectrum (Figure 2a) has a well-defined origin transition at 35 292 cm⁻¹ (starred *) followed by a series of discrete peaks atop an elevated baseline over a range of 500 cm⁻¹. This elevated baseline extends to the red but is relatively low in intensity and devoid of features. The ps trace (Figure 2b) exhibits the same defined vibronic transitions seen in the ns spectrum but presents another unique feature at 33 266 cm⁻¹. Here, the elevated baseline features to the red of the starred origin are by contrast to the ns spectrum more intense. While this signal could result from other tautomers, we suspect that this feature is due to hot bands from the low-frequency breathing vibrational modes which are more efficiently excited with the 6 cm⁻¹ spectral line width of ps laser and artificially intensified by elevated laser power in that region. The sharp feature

at $35\,000\text{ cm}^{-1}$ is a laser power artifact and highlights the nonresonant nature of the absorption in this range. Furthermore, we could not obtain an IR–UV double-resonant signal from this part of the spectrum, which is also consistent with hot bands. We simultaneously recorded wavelength and mass spectra, shown as a two-dimensional plot in the Supporting Information (Figure S.1) to verify that there is no contribution to the isoC mass channel from potential higher-order clusters, including checking the M+1 mass channel.

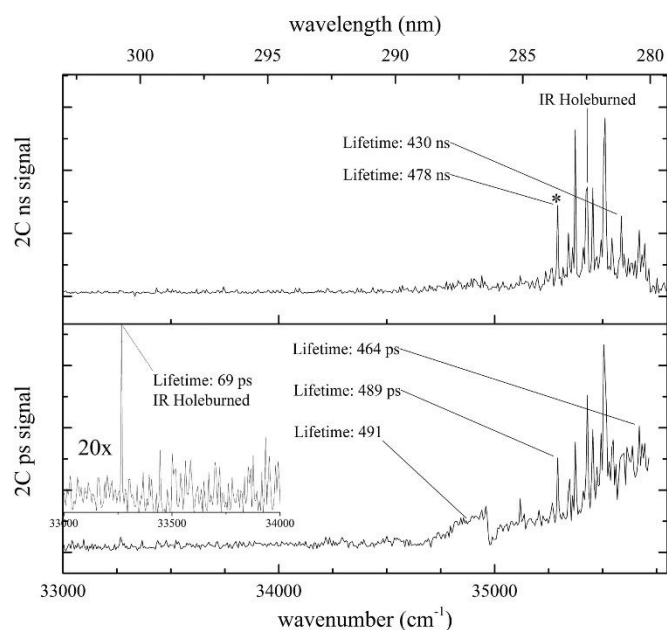


Figure 2. 2C R2PI spectra for isocytosine (a) ns excitation with 193 nm ionization and (b) ps excitation with 213 nm ionization (5th Nd:YAG harmonic). Lifetimes are pump–probe data. See text for details.

IR–UV double-resonance spectroscopy reveals the presence of the EA1 tautomer, with the origin at $35\,292\text{ cm}^{-1}$ and the KA2 tautomer, with the feature at $33\,266\text{ cm}^{-1}$, shown by Figure 3a. We matched IR–UV hole burning spectra (probed as annotated in Figure 3a) with anharmonic computations. The peaks observed in the ns 2C R2PI scan are all correlated with the EA1 tautomer by IR–UV double-resonance spectroscopy in which the IR resonance at $3\,470\text{ cm}^{-1}$ was held constant 200 ns prior to scanning the UV source (Figure 3b). We have

attached UV–UV hole burning results at 35 428 cm^{-1} as Figure S.2 which further confirms that all the peaks shown in the ns spectrum belong to a single tautomer which we identify as EA1. After characterization, the KA2 and EA1 electronic origin transition energies correlated to within 10% of those predicted for KA1 and EA1 by Szabla et al. and KA1 by Hu et al.^{21, 26}

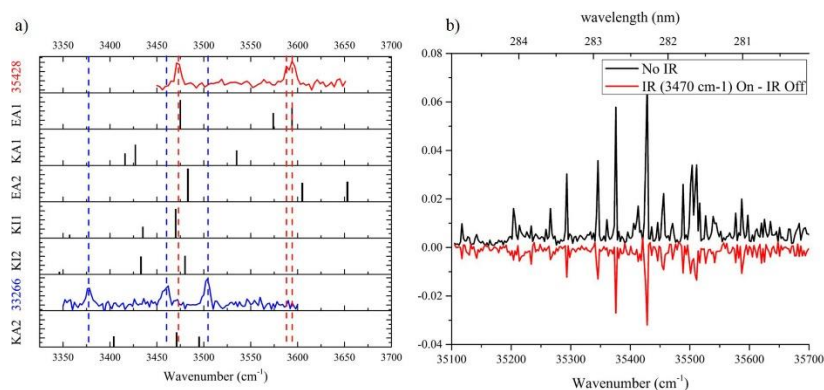


Figure 3. (a) IR UV hole burning results compared to anharmonic simulations for the six low-energy structures. Experimental spectra are from UV ns probe 35 428 (red) and ps probe 33 266 (blue) cm^{-1} , respectively. (b) Nanosecond 2C R2PI spectrum (black) and the difference trace below (red) when burning at the EA1 experimental wavelength of 3 470 cm^{-1} . Anharmonic DFT analysis calculated with the B3LYP hybrid functional and the cc-pVTZ basis set.

Referring to Chart 1, KA2 is predicted to be the highest-energy structure indicating that if this tautomer is present all other forms may be present in our beam as well. Jet-cooling is not an equilibrium process; therefore, we cannot predict the tautomer distribution, but in our experience in our setup usually the lowest-energy tautomers up to typically about 50 kJ/mol are present. Furthermore, the KA1 tautomer was observed in matrix isolation experiments.²⁴⁻
²⁵ Three possible reasons certain tautomers are not observed in our experiment are the following. (1) There can be tautomers that absorb in different ranges of the UV spectrum, which we have not covered. (2) Our experiment measures action spectroscopy rather than direct absorption. It is possible that a molecule is excited by the first photon but not ionized by the second. One way this situation can occur is when the excited-state lifetime is

significantly shorter than the ionizing laser pulse. A very similar situation exists for guanine: the lowest-energy keto tautomers, equivalent to KA1 in isoC, have not been observed so far by R2PI, although from direct absorption in microwave experiments and in He droplets they are known to exist.³¹⁻³² (3) A molecule may undergo fragmentation after excitation or ionization adding complexity to the action spectrum as we typically monitor only the parent ion mass. We did not observe any obvious nonstatistical fragmentation.

Figure 4 shows a selection of the pump-probe results from the origin transitions of EA1 and KA2; additional pump-probe fits are found in Figure S.3. The derived lifetimes are shown within Figure 2a,b. The 463–491 ps lifetime of the EA1 tautomer represents the decay rate of the excited state. All pump-probe curves were fit to a monoexponential decay.

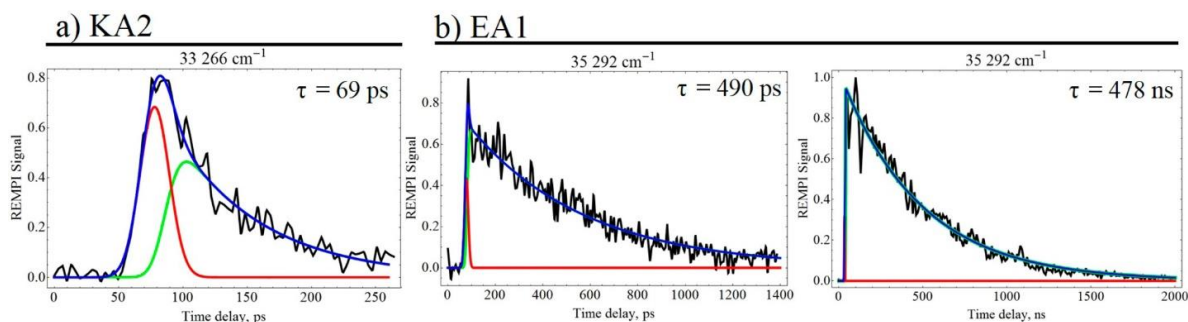


Figure 4. Pump-probe results from the origin bands of (a) the KA2 and (b) the EA1 tautomer in the ps and ns regimes. The data in panels a and b are fit to a curve (blue) which is the sum of a single exponential decay convolved with a Gaussian component (green) representative of our instrument response function (IRF) and the IRF itself (red).

We probed the broad elevated baseline signal present to the red of the EA1 origin in Figure 2a in hopes of attributing it to a specific species from Chart 1. The lifetime of 491 ps agrees with the ps component measured for EA1. We were unable to support this pump-probe correlation to EA1 with conclusive IR-UV hole burning results, like those from Figure 3a. The inability to obtain a clear IR-UV spectrum would be consistent with hot bands.

	keto KA1	keto KA2	enol
Isocytosine	N/O	69 ps	489 ps / 478 ns
Cytosine	N/O	730 ps ³³ / 290 ns ³⁴	*56 ps / *30.5 ns
Guanine	N/O	N/O	13 ns ³⁵ / 40 ns ³⁵

Table 1. Vibrationless excited state lifetimes. N/O = not observed. *These reported pump-probe results for enol-C were not obtained at the 0-0 transition but rather on the rising edge of its broad initial absorption region.

Table 1 lists vibrationless excited-state lifetimes, following 0–0 excitation unless otherwise noted, which we found here for isoC and compares those with the equivalent lifetimes for C and G. In terms of its photodynamics, isoC has elements of both G and C. The six-membered ring in G is an amino-pyrimidione, identical to isoC with a five-membered ring that immobilizes the C5=C6 bond that is free in isoC. Szabla et al. identified major conical intersections involving ring puckering, C=O stretching, NH₂ out-of-plane bending, and C=C rotation.²¹ The former three are similar to the CIs that dominate G dynamics,³⁶ while the latter cannot occur in G but is characteristic for pyrimidines, including cytosine.³⁷ We first compare isoC with G. Neither the 1H-9h-keto-amino (KA1 equiv) nor the 3H-keto-amino (KA2 equiv) have been identified yet by ps or ns R2PI. So in both isoC and G we do not observe the KA1 form (because of the difference in numbering between pyrimidines and purines, this is N3H for isoC and N1H for G, see Figure 1). For G this is the WC form and is slightly less in energy than the imino forms, which are observed.^{36, 38} As noted before, one likely reason for not observing a species with R2PI is an excited-state lifetime significantly shorter than the laser pulse length. In the G experiments pulse widths were of the order of 5 ns, and in the current isoC experiments they are lower limited at 30 ps. Excited states with lifetimes of the order of a few hundred femtoseconds could thus defy detection by R2PI in these experiments. Notably, the conical intersection that is most responsible for the ultrafast IC in the G keto case involves pyramidalization at the C2

position and does not involve the 5-membered ring.^{29, 36, 39-40} Therefore, it is possible for the isoC KA1 form to undergo very similar ultrafast IC. For the KA2 form of isoC we find a lifetime of 69 ps, while the equivalent form for G was not observed with R2PI although it is lower in energy than the imino forms that are observed with R2PI.^{31-32, 41} For both compounds the enol form is significantly longer-lived, with two independent decay channels of almost 0.5 ns and 0.5 μ s for isoC and 13 and 40 ns for G.³⁵ In both cases we consider that the long-lived dark state could be a triplet state and for G the 13 ns decay can be attributed to fluorescence.⁴² In the case of enol isoC the observation of two decays with a 3 orders of magnitude difference implies that those two channels do not decay from the same excited state. If they did, the higher rate process would have 3 orders of magnitude larger quantum yield and dwarf the signal from the lower rate process. Instead we assume an ultrafast population of a doorway state, possibly a triplet, which in turn decays at the slow rate.

In comparing isoC and C, we notice larger differences in excited-state dynamics. Again we do not see the KA1 equivalent form for C, which is about 30 kJ/mol higher in energy than the WC KA2 equivalent and enol forms. The KA2 form, which is the lowest-energy keto form for C, behaves very different from isoC. Leutwyler and co-workers have reported this case in great detail, finding a vibrationless decay time of 730 ps.^{33, 43-45} Nir et al. reported on a long-lived state, presumably a triplet, with a 290 ns lifetime.^{34, 46} These observations suggest different dynamics than for isoC where we found a single 69 ps decay. For the enol form of C we find a 56 ps short component which populates a longer-lived state with a 30.5 ns lifetime (shown in Figure S.4). Because the ns R2PI spectra of enol C, also reported by Nir et al., is broad and without a clear 0–0 transition,⁴⁶ we performed these pump–probe measurements on the rising edge of the broad signal which appears along with the ps 2C R2PI in Figure S.4. So for C the vibrationless excited state for the enol form is

shorter lived than for the keto form, contrary to the situation for both G and isoC. Szabla et al. find a CI for the isoC enol that involves the C5=C6 twist, which also plays a role in C; however, according to their calculations, only 14% of the trajectories follow this path in isoC.²¹ It should be noted that their trajectories start at 5.5 ± 0.2 eV, which is a full electronvolt more excited-state energy than what we impart in our experiments. This may suggest that the C5=C6 CI for EA1 has an energy barrier of up to 1 eV.

The conclusion that isoC resembles G in its photochemistry is just one of the considerations in evaluating its potential role in prebiotic scenarios. For example, we are currently investigating the photostability of isoguanine as one of its possible alternative base pair partners. Furthermore, the response to radiation is wavelength-dependent, and its consideration should not be limited to a single wavelength or small parts of the spectrum. The study of the dynamics near the threshold for absorption provides opportunities to probe the potential energy landscape close to the most relevant CIs and barriers. It is hoped that these data will serve as support for further detailed theoretical treatments.

Experimental Section

Here we report results which identify the EA1 and KA2 tautomers of cold isocytosine prepared in a molecular beam. We have investigated the absorption spectrum with 2C R2PI, identified the tautomers with IR–UV hole burning, and performed pump–probe experiments to probe excited-state relaxation dynamics in the ns and ps time regimes. The instrument and explanation of these specific techniques are detailed elsewhere and very briefly outlined here.^{35, 47} IsoC standard (Sigma, $\geq 99\%$) is entrained into a pulsed molecular beam by laser desorption and ionized by tunable 2C R2PI. The ps spectroscopic and pump–probe delay measurements are performed with a Nd:YAG driven optical parametric oscillator (OPG) laser system which produces ~ 30 ps laser pulses. The molecule is excited by the tunable

light from the OPG and ionized by 213 nm, which is mechanically delayed up to 1.5 ns before colineation with the OPG beam. A variable electronic delay between the OPG UV laser and an excimer laser (193 nm, 6 ns pulse width) is used for spectroscopic and pump–probe measurements in the ns time delay range.

For IR–UV double-resonant spectroscopy, an optical parametric oscillator/amplifier (OPO/OPA) precedes the 2C R2PI by 200 ns. IR resonant frequencies are compared to anharmonic DFT analysis calculated with the B3LYP hybrid functional with the cc-pVTZ basis set.

Supplemental Information

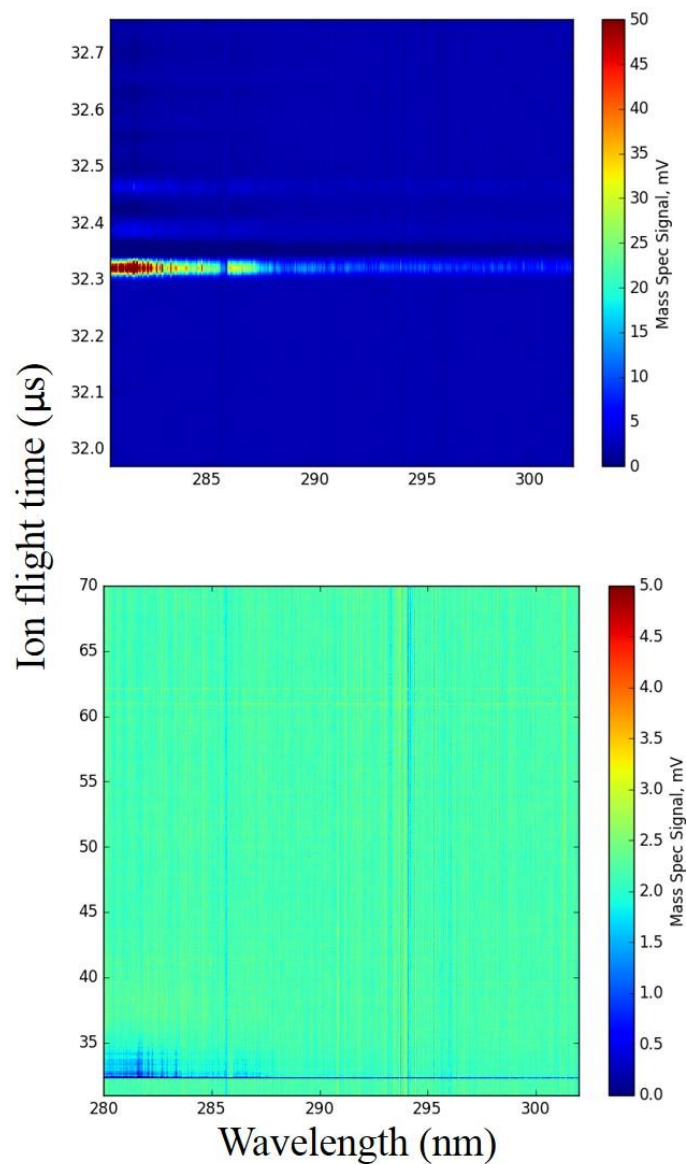


Figure S.1 The two-dimensional time-of-flight data showing ion signal intensity (z axis 0-50 mv top, 0-5 mv bottom) with respect to flight time (y axis) and excitation wavelength (x axis). The only signal is the parent mass of isoC at 32.3 us across all wavelengths. Therefore, no signal is due to the fragmentation of higher order mass ions.

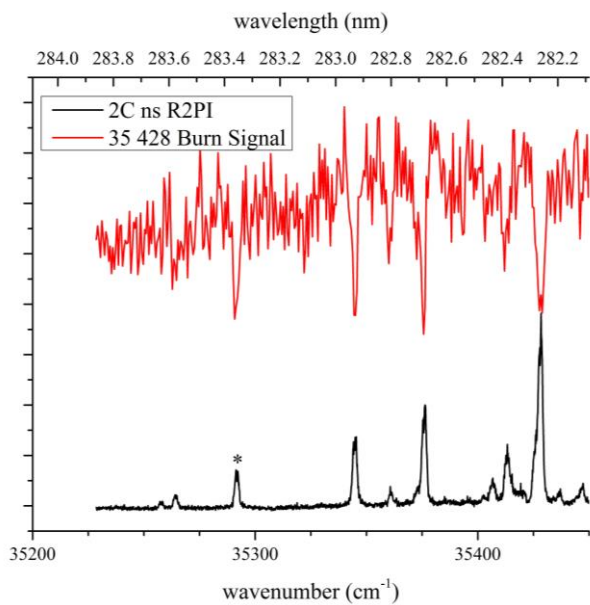


Figure S.2 The UV-UV of the EA1 region ($35,428\text{ cm}^{-1}$ probe) supporting the IR-UV in Figure 3b that all signal in the ns scan within the shown range is from the EA1 tautomer only. The EA1 origin of $35,292\text{ cm}^{-1}$ is starred (*).

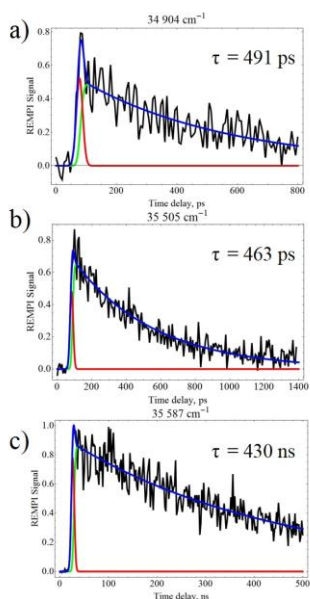


Figure S.3 The pump-probe results (a) through (c) at excitations other than the 0-0 transition wavelengths. The data in (a-c) is fit to a curve (blue) which is the sum of a single exponential decay convolved with a Gaussian component (green) representative of our instrument response function (IRF) and the IRF itself (red).

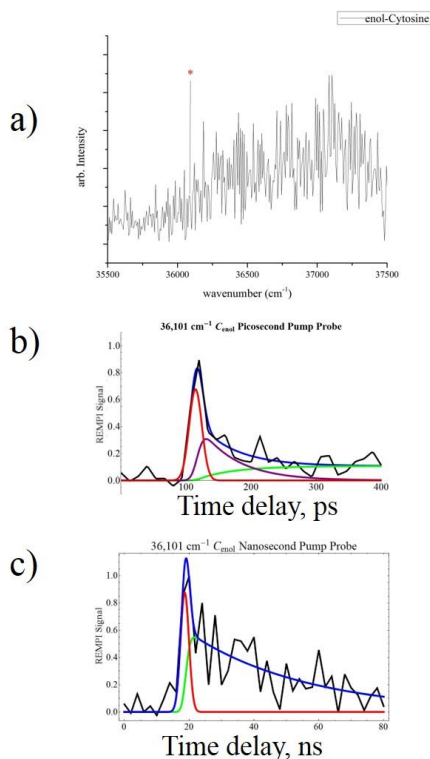


Figure S.4 The (a) ps 2C R2PI and (b) ps pump-probe results of enol C. 213 nm was the second color for both, and (c) ns pump-probe results of enol C with 193 nm as a second color. In the ps pump-probe two lifetimes were fit for, a short lifetime (purple) of 56 ps which populates a >5 ns secondary lifetime (green). The ns pump-probe fit to a single decay of 30.5 ns (green) In both the IRF is plotted in red. Our previous work on 6-TG showed the upper fitting limit of our ps setup to be ~5 ns, longer lifetimes need additional fitting in the ns regime.

References

1. Beckstead, A. A.; Zhang, Y. Y.; de Vries, M. S.; Kohler, B., Life in the light: nucleic acid photoproperties as a legacy of chemical evolution. *PCCP* **2016**, *18* (35), 24228-24238.
2. Nir, E.; Kleinermanns, K.; Grace, L.; de Vries, M. S., On the photochemistry of purine nucleobases. *Journal of Physical Chemistry A* **2001**, *105* (21), 5106-5110.
3. Rios, A. C.; Tor, Y., On the Origin of the Canonical Nucleobases: An Assessment of Selection Pressures across Chemical and Early Biological Evolution. *Isr J Chem* **2013**, *53* (6-7), 469-483.
4. Middleton, C. T.; de La Harpe, K.; Su, C.; Law, Y. K.; Crespo-Hernandez, C. E.; Kohler, B., DNA excited-state dynamics: from single bases to the double helix. *Annu Rev Phys Chem* **2009**, *60*, 217-39.
5. Miller, S. L.; Orgel, L. E., *The Origins of Life On the Earth*. Prentice-Hall: Englewood Cliffs, NJ, 1974.
6. Gustavsson, T.; Improta, R.; Markovitsi, D., DNA/RNA: Building Blocks of Life Under UV Irradiation. *J. Phys. Chem. Lett.* **2010**, *1* (13), 2025-2030.

7. Kohler, B., Nonradiative Decay Mechanisms in DNA Model Systems. *J. Phys. Chem. Lett.* **2010**, *1* (13), 2047-2053.
8. Kleineremanns, K.; Nachtigallová, D.; de Vries, M. S., Excited state dynamics of DNA bases. *International Reviews in Physical Chemistry* **2013**, *32* (2), 308-342.
9. Crespo-Hernandez, C. E.; Martinez-Fernandez, L.; Rauer, C.; Reichardt, C.; Mai, S.; Pollum, M.; Marquetand, P.; Gonzalez, L.; Corral, I., Electronic and Structural Elements That Regulate the Excited-State Dynamics in Purine Nucleobase Derivatives. *J. Am. Chem. Soc.* **2015**, *137* (13), 4368-4381.
10. Yang, Z. Y.; Hutter, D.; Sheng, P. P.; Sismour, A. M.; Benner, S. A., Artificially expanded genetic information system: a new base pair with an alternative hydrogen bonding pattern. *Nucleic Acids Res.* **2006**, *34* (21), 6095-6101.
11. Leontis, N. B.; Stombaugh, J.; Westhof, E., The non-Watson-Crick base pairs and their associated isostericity matrices. *Nucleic Acids Res.* **2002**, *30* (16), 3497-3531.
12. Wojciechowski, F.; Leumann, C. J., Alternative DNA base-pairs: from efforts to expand the genetic code to potential material applications. *Chem. Soc. Rev.* **2011**, *40* (12), 5669-79.
13. Cafferty, B. J.; Hud, N. V., Was a Pyrimidine-Pyrimidine Base Pair the Ancestor of Watson-Crick Base Pairs? Insights from a Systematic Approach to the Origin of RNA. *Isr. J. Chem.* **2015**, *55* (8), 891-905.
14. Rich, A., On the Problems of Evolution and Biochemical Information Transfer. In *Horizons in Biochemistry*, Michael Kasha, B. P., Ed. Academic Press: New York, 1962; pp 103-126.
15. Saladino, R.; Crestini, C.; Cossetti, C.; Di Mauro, E.; Deamer, D., Catalytic effects of Murchison Material: Prebiotic Synthesis and Degradation of RNA Precursors. *Origins Life Evol B* **2011**, *41* (5), 437-451.
16. Roberts, C.; Bandaru, R.; Switzer, C., Theoretical and experimental study of isoguanine and isocytosine: Base pairing in an expanded genetic system. *J. Am. Chem. Soc.* **1997**, *119* (20), 4640-4649.
17. Yang, X. L.; Sugiyama, H.; Ikeda, S.; Saito, I.; Wang, A. H., Structural studies of a stable parallel-stranded DNA duplex incorporating isoguanine:cytosine and isocytosine:guanine basepairs by nuclear magnetic resonance spectroscopy. *Biophys. J.* **1998**, *75* (3), 1163-71.
18. Sismour, A. M.; Benner, S. A., The use of thymidine analogs to improve the replication of an extra DNA base pair: a synthetic biological system. *Nucleic Acids Res.* **2005**, *33* (17), 5640-5646.
19. Hirao, I., Unnatural base pair systems for DNA/RNA-based biotechnology. *Curr. Opin. Chem. Biol.* **2006**, *10* (6), 622-627.
20. Lee, S. J.; Min, A.; Ahn, A.; Moon, C. J.; Choi, M. Y.; Ishiuchi, S.-I.; Miyazaki, M.; Fujii, M. In *Resonance Enhanced Multi-Photon Ionization (REMPI) and Double Resonance (UV-UV AND IR-UV) Spectroscopic Investigation Isocytosine*, OSU International Symposium on Molecular Spectroscopy, Ohio State University: 2013.
21. Szabla, R.; Gora, R. W.; Sponer, J., Ultrafast excited-state dynamics of isocytosine. *Phys Chem Chem Phys* **2016**, *18* (30), 20208-18.
22. Shukla, M. K.; Leszczynski, J., Investigations of the excited-state properties of isocytosine: An ab initio approach. *Int. J. Quantum Chem* **2000**, *77* (1), 240-254.
23. Bakalska, R. I.; Delchev, V. B., Comparative study of the relaxation mechanisms of the excited states of cytosine and isocytosine. *J. Mol. Model.* **2012**, *18* (12), 5133-5146.

24. Ivanov, A. Y.; Stepanian, S. G.; Adamowicz, L., Tautomeric transitions of isocytosine isolated in argon and neon matrices induced by UV irradiation. *J. Mol. Struct.* **2012**, *1025*, 92-104.
25. Vranken, H.; Smets, J.; Maes, G.; Lapinski, L.; Nowak, M. J.; Adamowicz, L., Infrared spectra and tautomerism of isocytosine; an ab initio and matrix isolation study. *Spectrochimica Acta Part A: Molecular Spectroscopy* **1994**, *50* (5), 875-889.
26. Hu, D.; Liu, Y. F.; Sobolewski, A. L.; Lan, Z., Nonadiabatic dynamics simulation of keto isocytosine: a comparison of dynamical performance of different electronic-structure methods. *Phys Chem Chem Phys* **2017**, *19* (29), 19168-19177.
27. Merchan, M.; Gonzalez-Luque, R.; Climent, T.; Serrano-Andres, L.; Rodriguez, E.; Reguero, M.; Pelaez, D., Unified model for the ultrafast decay of pyrimidine nucleobases. *J. Phys. Chem. B* **2006**, *110* (51), 26471-6.
28. Pepino, A. J.; Segarra-Marti, J.; Nenov, A.; Improta, R.; Garavelli, M., Resolving Ultrafast Photoinduced Deactivations in Water-Solvated Pyrimidine Nucleosides. *J. Phys. Chem. Lett.* **2017**, *8* (8), 1777-1783.
29. Improta, R.; Santoro, F.; Blancafort, L., Quantum Mechanical Studies on the Photophysics and the Photochemistry of Nucleic Acids and Nucleobases. *Chem. Rev.* **2016**, *116* (6), 3540-93.
30. Trachsel, M. A.; Lobsiger, S.; Schär, T.; Blancafort, L.; Leutwyler, S., Planarizing cytosine: The S1 state structure, vibrations, and nonradiative dynamics of jet-cooled 5,6-trimethylenecytosine. *The Journal of Chemical Physics* **2017**, *146* (24), 244308.
31. Choi, M. Y.; Miller, R. E., Four tautomers of isolated guanine from infrared laser spectroscopy in helium nanodroplets. *J Am Chem Soc* **2006**, *128* (22), 7320-8.
32. Mons, M.; Piuze, F.; Dimicoli, I.; Gorb, L.; Leszczynski, J., Near-UV resonant two-photon ionization spectroscopy of gas phase guanine: evidence for the observation of three rare tautomers. *J Phys Chem A* **2006**, *110* (38), 10921-4.
33. Blaser, S.; Trachsel, M. A.; Lobsiger, S.; Wiedmer, T.; Frey, H. M.; Leutwyler, S., Gas-Phase Cytosine and Cytosine-N1-Derivatives Have 0.1-1 ns Lifetimes Near the S1 State Minimum. *J Phys Chem Lett* **2016**, *7* (5), 752-7.
34. Nir, E.; Muller, M.; Grace, L. I.; de Vries, M. S., REMPI spectroscopy of cytosine. *Chem. Phys. Lett.* **2002**, *355* (1-2), 59-64.
35. Siouri, F. M.; Boldissar, S.; Berenbeim, J. A.; de Vries, M. S., Excited State Dynamics of 6-Thioguanine. *J Phys Chem A* **2017**, *121* (28), 5257-5266.
36. Marian, C. M., The guanine tautomer puzzle: quantum chemical investigation of ground and excited states. *J Phys Chem A* **2007**, *111* (8), 1545-53.
37. Kistler, K. A.; Matsika, S., Radiationless decay mechanism of cytosine: an ab initio study with comparisons to the fluorescent analogue 5-methyl-2-pyrimidinone. *J Phys Chem A* **2007**, *111* (14), 2650-61.
38. Mons, M.; Dimicoli, I.; Piuze, F., Isolated Guanine: Tautomerism, Spectroscopy And Excited State Dynamics. In *Radiation Induced Molecular Phenomena in Nucleic Acids: A Comprehensive Theoretical and Experimental Analysis*, Shukla, M. K.; Leszczynski, J., Eds. Springer Netherlands: Dordrecht, 2008; pp 343-367.
39. Chen, H.; Li, S., Ab initio study on deactivation pathways of excited 9H-guanine. *J Chem Phys* **2006**, *124* (15), 154315.
40. Yamazaki, S.; Domcke, W.; Sobolewski, A. L., Nonradiative decay mechanisms of the biologically relevant tautomer of guanine. *J Phys Chem A* **2008**, *112* (47), 11965-8.

41. Alonso, J. L.; Pena, I.; Lopez, J. C.; Vaquero, V., Rotational spectral signatures of four tautomers of guanine. *Angew Chem Int Ed Engl* **2009**, *48* (33), 6141-3.
42. Chin, W.; Mons, M.; Dimicoli, I.; Piuze, F.; Tardivel, B.; Elhanine, M., Tautomer contributions to the near UV spectrum of guanine: towards a refined picture for the spectroscopy of purine molecules. *The European Physical Journal D* **2002**, *20* (3), 347-355.
43. Lobsiger, S.; Etinski, M.; Blaser, S.; Frey, H. M.; Marian, C.; Leutwyler, S., Intersystem crossing rates of S1 state keto-amino cytosine at low excess energy. *J Chem Phys* **2015**, *143* (23), 234301.
44. Lobsiger, S.; Trachsel, M. A.; Frey, H. M.; Leutwyler, S., Excited-state structure and dynamics of keto-amino cytosine: the 1 $\pi\pi^*$ state is nonplanar and its radiationless decay is not ultrafast. **2013**, *117* (20), 6106-15.
45. Lobsiger, S.; Leutwyler, S., The Adiabatic Ionization Energy and Triplet T-1 Energy of Jet-Cooled Keto-Amino Cytosine. *J. Phys. Chem. Lett.* **2012**, *3* (23), 3576-3580.
46. Nir, E.; Hunig, I.; Kleinermanns, K.; de Vries, M. S., The nucleobase cytosine and the cytosine dimer investigated by double resonance laser spectroscopy and ab initio calculations. *Phys. Chem. Chem. Phys.* **2003**, *5* (21), 4780-4785.
47. Meijer, G.; Devries, M. S.; Hunziker, H. E.; Wendt, H. R., Laser Desorption Jet-Cooling of Organic-Molecules - Cooling Characteristics and Detection Sensitivity. *Appl Phys B-Photo* **1990**, *51* (6), 395-403.

III. Excited state dynamics of the purines

Alongside the noncanonical pyrimidine, isocytosine, various noncanonical purine systems have also been studied. First, a review of the excited state dynamics of the purines substituted with carbonyl and amino ligands at the C2 and C6 positions, including the canonical guanine and adenine, is presented. Then individual works on isoguanine, 2,6-diaminopurine, and xanthine follow. With the exception of enol isoguanine, all the other forms of these purines were found to have barriers to relaxation, leading to their decreased photostability. These data points further support the theory of photostability as a selection pressure and that even minor structural modifications can have disproportionate effects to the photodynamics.

A couple of notes about the works presented below. The purine review differs from the accepted manuscript. Due to a word and figure limit, the accepted manuscript is significantly shorter. The version presented below is much more thorough with more information. The articles on 2,6-diaminopurine and xanthine are not complete. All the experimental work is

done. Theoretical calculations to explain the experimental results are currently being completed by Prof. Rafal Szabla. I have included my results, results analysis, and a possible excited state dynamics explanation for the observed results. Rafal will certainly have more to say on the subject and will alter the manuscript accordingly.

I. Nucleobases as molecular fossils of prebiotic photochemistry: Excited state dynamics of C2 and C6 substituted purines

G. Gate^a, A. Williams^a, M.R. Haggmark^a, N.D. Svadlenak^a, G. Hill^b, M.S. de Vries^a

^aDepartment of Chemistry and Biochemistry, University of California Santa Barbara, CA 93106

^bInterdisciplinary Nanotoxicity Center, Department of Chemistry, Jackson State University, Jackson, MS 39217

Abstract

Many variations of the canonical nucleobases, such as different derivatives and analogues, would likely have been present in a primordial soup. Alternative combinations of molecular building blocks would conceivably have been possible to form self-replicating RNA like structures. The nucleobases that are involved in replication selectively exhibit short excited state lifetimes which provide high intrinsic stability against otherwise harmful UV photo-damage. The stark difference in response to UV irradiation between these structures and many of the alternative bases suggests the possibility of a photochemical selection of the molecular building blocks of life long before the advent of biological selection. It is thus conceivable that the molecular photo-properties of nucleobases are molecular fossils of the prebiotic chemistry that occurred 4 billion years ago. This chapter considers the excited state dynamics of the purine bases by comparing a full set of canonical and alternative nucleobases formed by oxo- and amino- substitutions of purine.

1. Introduction

The key components of the reproductive machinery are unlikely to have been selected by a biological evolution that requires that very machinery to begin with. Instead it is conceivable that choosing the molecular building blocks of life was mediated by a chemical selection that preceded biology. This hypothesis also implies that molecular properties of nucleobases, preserved unchanged from prebiotic times, can possibly serve as molecular fossils of that prebiotic chemistry.

The nucleobases that are involved in replication exhibit short excited state lifetimes which provide high intrinsic stability against otherwise harmful UV photo-damage.¹⁻³ UV protection comes about when electronic excitation is converted to heat by internal conversion at rates too fast for other more harmful reactive pathways to occur while subsequently safely dissipating the energy to the environment. The canonical nucleobases generally decay in less than 1 ps, orders of magnitude faster than in most other heterocyclic compounds. This property would have been highly advantageous for the first self-replicating molecules in prebiotic times before modern enzymatic repair or the formation of the ozone layer that would later attenuate the high levels of UV radiation penetrating the early atmosphere. The safe elimination of excess electronic energy in the canonical bases is exquisitely sensitive to molecular structure and much slower relaxation is observed in many closely related structures.

These many variations of the canonical nucleobases, such as different derivatives and analogues, would likely have been present in a primordial soup. Alternative combinations of molecular building blocks would conceivably have been possible to form self-replicating RNA like structures. However, while the structural differences appear relatively small, many of the alternative nucleobases have much longer excited state lifetimes, sometimes by orders of magnitude, which would allow a variety of possibly harmful photochemical processes and

thus render them much less photostable. The stark difference in response to UV irradiation between these structures suggests the possibility of a photochemical selection of the molecular building blocks of life long before the advent of biological selection. It is thus conceivable that the molecular photo-properties of nucleobases, which we study now, are relics from part of the prebiotic chemistry that occurred 4 billion years ago.

The rapid decay mechanism that provides photostability has primarily been studied for the canonical bases themselves, providing five data points, and in the case of the purine bases, just two. Purine itself has a long-lived excited state and the substitutions in C₂ and C₆, to form guanine and adenine, dramatically shorten the excited state lifetime. Other variations in those substitutions, however, lead to vastly different excited state dynamics. Therefore, to further understand these processes and the role of the C₂ and C₆ substitutions, we here examine a larger set of nine structures, formed by all combinations of oxo- and amino-derivatives in the C₂ and C₆ position (see Figure 1).

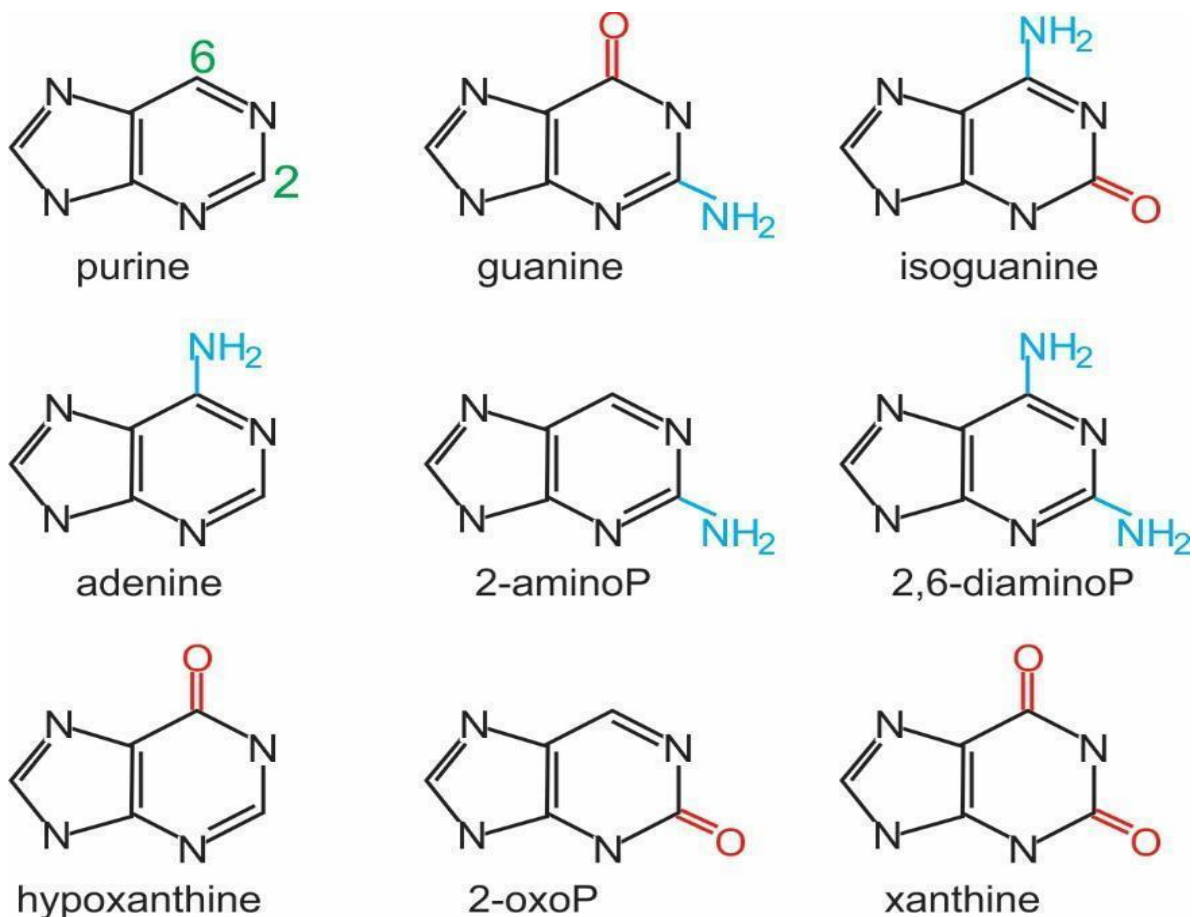


Figure 1: The 9 purine structures formed by all combinations of oxo- and amino-substitutions in the C₂ and C₆ positions. Only one tautomer is shown for each structure.

Each of these purine derivatives could conceivably form alternative base pairs with suitable complementary nucleobases, such as isoguanine with isocytosine, xanthine with 2,4-diaminopyrimidine, or 2,6-diaminopurine with uracil, as shown in Figure 2. Such alternative base pairs have been proposed as part of an alternative genetic lexicon and in various prebiotic scenarios.⁴⁻⁷ Therefore, the fundamental photochemistry needs to be understood both for the canonical bases that make up life as we know it today and for possible alternative bases that could have competed under plausible prebiotic conditions. UV sunlight is an attractive energy source for creating the organic molecules needed to start life on the early earth and not all competing processes are harmful, particularly when they trigger reactivity for synthetic steps.⁸ Generally, the molecular architecture for replication seems to

require rigid structures, which tend to be aromatic and therefore inevitably prone to UV absorption. Since UV excitation is unavoidable for such compounds, it is crucial to understand the possible competing pathways available to process the electronic excitation. At this point, the relaxation dynamics of the canonical nucleobases are well studied and focus has shifted to their derivatives and analogues. The goal is to determine if there is a mechanistic reason for the unique photostability of the canonical bases.

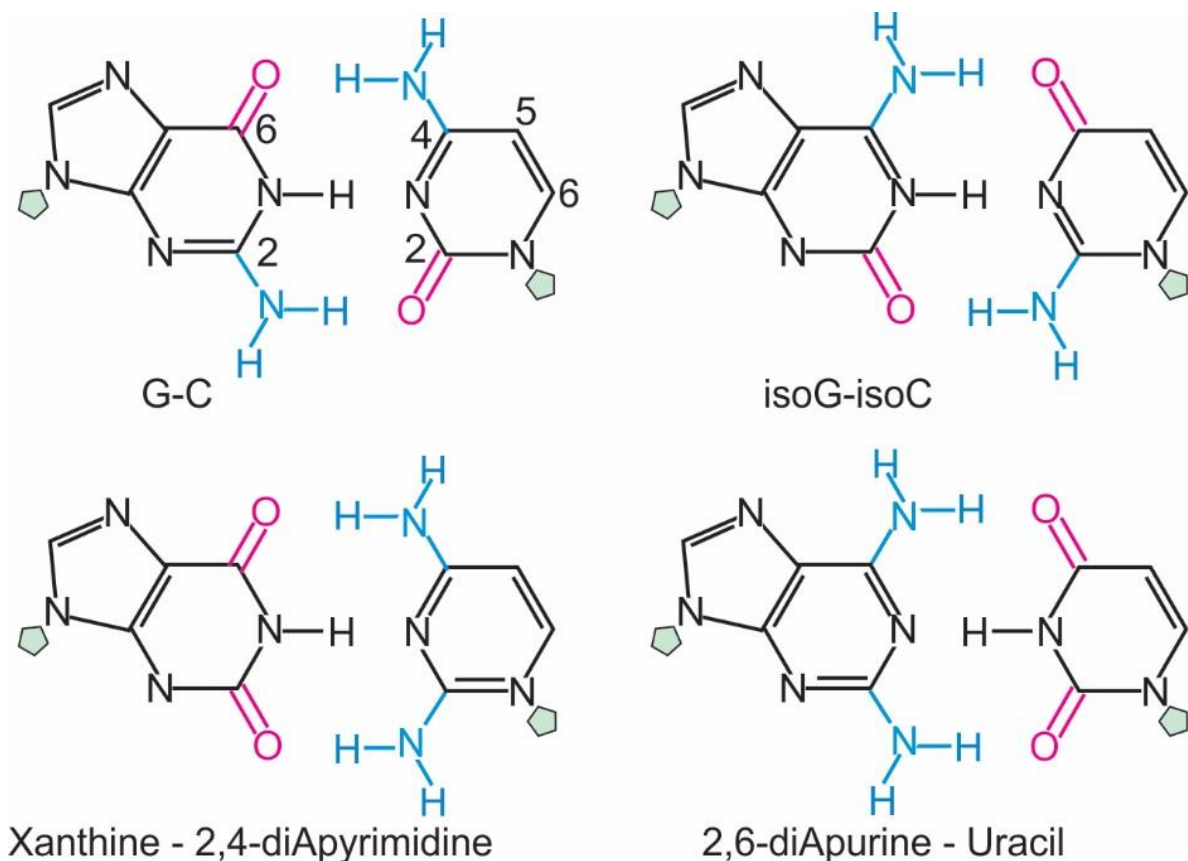


Figure 2: Examples of alternative base pairs formed with purine derivatives, compared with the canonical G–C pair. G=guanine, C=cytosine. Green pentagons indicate the position of the sugar moiety in corresponding nucleosides. The different numbering for purines and pyrimidines is shown in the G–C pair.

Figure 3 shows a schematic Jablonski diagram to illustrate some major competing excited state decay processes following UV absorption (purple). The only radiative process shown here is fluorescence (blue), which typically involves a timescale of nanoseconds. All

the other processes shown are non-radiative. Internal conversion processes (green) can be fast, on the order of ps or less, if trajectories are available to conical intersections (CIs). Lifetimes can become significantly longer if the system is trapped in a minimum below a barrier in the potential energy surface (barriers are schematically indicated in brown). For example, trapping in a bright $^1\pi\pi^*$ minimum may result in fluorescence. Intersystem crossing (red) can be fast, on the order of ps, when El Sayed allowed (I), or very slow, on the order of ns to μ s, when not el-Sayed allowed (II). Dashed grey arrows indicate intramolecular vibrational redistribution (IVR). If the $n\pi^*$ state is higher in energy than the $\pi\pi^*$ state, the only available pathways would be process i and fluorescence and to some extent ISC to the $^3\pi\pi^*$ state, which would be very slow. For the molecule to be most photostable, it is advantageous for the pathways that return it to the ground state to have the highest rates, competing favourably with processes that lead to ISC or to long times in the excited state.

Such a Jablonsky diagram is an oversimplification since potentials are a function of all internuclear coordinates and multiple trajectories are possible over complex multidimensional potential energy surfaces (PESs). Not only are the relative energies of S_1 , S_2 , T_1 , and T_2 important, but also the detailed shapes of the corresponding PESs, including location of minima, barriers, and conical intersections and seams. Especially the coordinates around C_2 and C_6 may affect the role of substituents in those positions. Conical intersections, required for fast internal conversion, involve distortions of the molecular frame relative to equilibrium structures. Several motifs have been discussed in the literature for the structure of CIs in purines, especially out of plane distortion at C_2 and sometimes C_6 .⁹⁻¹¹ Alternatively, substitution at C_6 has also been discussed as possibly affecting barriers on trajectories toward CIs.¹²⁻¹³ In the case of pyrimidines, distortion of the C_5 - C_6 bond often leads to a CI but for purines the additional 5 membered ring “flattens” the structure so this motif does not

play a role. Furthermore, the potential energy landscape is also affected by tautomeric form¹⁴⁻¹⁵ and solvent environment, further complicating relaxation pathways and photostability.¹⁶⁻¹⁷

In the following, we will assess the role of the oxo- and amino- groups at C₂ and C₆ by systematically examining all 9 derivative structures. To elucidate the intrinsic photochemical properties, we focus on gas phase data, obtained by us and others, and their comparison with high level computational theory. Gas phase data don't describe the entire dynamics because the solvent also plays a role, but they provide insight in the most fundamental intrinsic properties of the chromophore, provide the best comparison to the highest level computations, and allow for tautomer selection. In some cases, we will refer to solution data to discuss the additional role of the solvent or when gas phase data are scarce. As some of these systems have multiple tautomers present, both in solution and in the gas phase, we will primarily focus on the biologically relevant tautomer and briefly discuss other tautomers where the data are available, to highlight how tautomerization can affect the excited state dynamics.

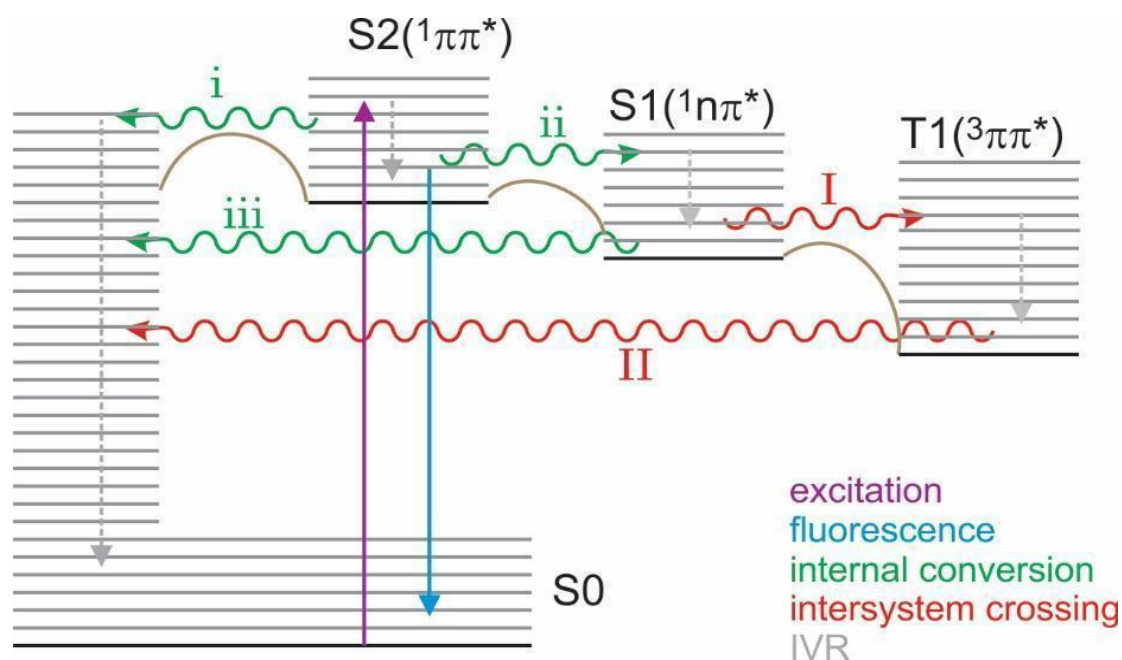


Figure 3: Schematic Jablonski diagram, indicating major competing excited state decay processes. All internal conversion processes (green) can be fast if trajectories are available to conical intersections. Lifetimes can become significantly longer if the system is trapped in a minimum below a potential barrier (barriers are indicated in brown). Intersystem crossing (red) can be fast when El Sayed allowed (I) or very slow when not El-Sayed allowed (II). If the $n\pi^*$ is higher in energy than the $\pi\pi^*$ state, only process i and fluorescence are possible while ISC to the $^3\pi\pi^*$ state would very slow.

2. Techniques

The photodynamics of nucleobases is typically studied either in the gas phase or in solution. Although the role of the solvent is important, there are four reasons why gas phase studies are useful. (i) The absence of intermolecular interactions reveals intrinsic properties of the chromophore, (ii) comparison with high level computations is facilitated, (iii) isomer selective spectroscopy is possible, and (iv) in combination with jet-cooling high resolution can be obtained. A major gas phase spectroscopy technique is resonance enhanced multiphoton ionization (REMPI), while photoelectron spectroscopy,¹⁸⁻²⁰ IR,²¹⁻²² and microwave absorption²³⁻²⁶ have also been employed.

In REMPI, commonly combined with laser desorption and jet-cooling, a first photon excites the molecule resonantly to an excited state and a second photon ionizes the excited molecule. The ions are detected in a mass spectrometer. Varying the time between the two photons – the pump and the probe pulse - allows the measurement of excited state lifetimes. Various double resonant techniques, such as IR-UV hole burning, allow identification and selection of individual isomers. This makes it possible to obtain excited state lifetimes of selected tautomers, cluster structures, or conformers.^{3, 27-29} We note that REMPI is a form of action spectroscopy in which the excited state population is observed through its photoionization. Therefore, small ionization efficiency leads to small or absent signal. This is especially important if the excited state lifetime is significantly shorter than the laser pulse width, preventing ionization. As a result, some states may only be observed with short laser pulses and the technique can be blind to very short-lived excited states.

Two major techniques in solution are excited state absorption, both steady state and transient, and fluorescence upconversion. Both techniques employ a pump pulse, usually from a fs laser, to excite the system, followed by monitoring the wavepacket evolution after absorption through the excited state. Fluorescence upconversion is mostly limited to monitoring the $^1\pi\pi^*$ states, as emission is predominately from these states. One benefit of solution is the, often employed, femtosecond resolution since narrow line width is not as important.

High-level theoretical calculations significantly aid in the analysis of these experimental results. There are a number of reviews and resources that present an in-depth review of theoretical background formulation and methods, specifically detailing strengths and weaknesses.³⁰⁻³⁴ The foundation of the ab initio theoretical approach is the solution to the time independent Schrodinger Equation as a complete description of the nuclei and the

electrons. Any practical solution requires approximations, especially to treat electron correlation and excited states.

Full Configuration Interaction (CI) best describes electron correlation because of its expansive description of multiple permutations of the electrons within virtual orbitals. This method can accurately describe the electron correlation, however, it is prohibitively expensive for systems of any significant size. Attempts to extend the application to reasonable systems include truncating the determinants by limiting the electrons to valence electrons and only including certain transitions, many body perturbation theory (MPn methods),³⁵ and using a cluster operator (Couple Cluster (CC) methods).³⁶ Density Functional Theory (DFT)³⁷⁻⁴⁰ attempts to determine the electron correlation, not by adding more excited state determinants, but by using the density of the electrons to enhance the wavefunction. This method is then corrected with coefficients parameterized with experimental values to produce hybrid functionals, which can give relatively good descriptions inexpensively.

However, these methods are challenged in describing molecules within the excited state. CIS (Configuration Interaction with single excitation) gives a basic description approximating the excitation via a singly excited determinant without including the ground state determinant.⁴¹ But, in the excited state, it does not include electron correlation and is often not accurate. To correct this, other methods solve the time-dependent Schrodinger equation instead of the time-independent Schrodinger equation. This produces TD-DFT approaches, which gives a reasonable approximation of excited state phenomena.⁴²⁻⁴³ However, TDDFT does not properly describe reactions within the excited state potential energy surface of a molecule.⁴⁴⁻⁴⁵ For these circumstances, Complete Active Space SCF (CASSCF) becomes a more appropriate choice. CASSCF, uses the SCF determinants for the

core electrons, but uses the most accurate Full CI for small groups of specific electrons.⁴⁶ The more electrons and orbitals are included, however, the more expensive the calculations. Therefore, great care must be taken to determine which electrons and which orbitals are included. The benefit of CASSCF is that the method better describes the potential energy surface of the molecule and is better equipped to study conical intersections and other calculations that require following PES reaction pathways in the excited state. most widely used and simplest way to study excited states.

Often, configuration interaction techniques are used for single point calculations at important geometries (Frank-Condon, minima, CIs). Then, complete active space (CAS) is used to calculate electronic energies and pathways between these points to determine relaxation pathways.

A note about fitting decay traces: Lifetimes can only be fit for dynamics that are about half the cross-correlation of the pulse widths of the pump/probe lasers or longer. The experiment is essentially blind to faster dynamics because they occur on a time resolution faster than the pulse width of the measurement. Furthermore, derived lifetimes can vary between studies, even when for the same system with the same technique. These differences can be due to many factors, from sample preparation to the fitting algorithm used. A single trace can sometimes be fit with different lifetimes and different numbers of exponentials depending on the pre-exponential factors.⁴⁷ Thus, lifetimes need to be interpreted with some caution to simply get a sense of the overall orders of magnitude and photostability of the system.

3. Excited state dynamics

Here we briefly summarize what is known about the excited state dynamics for each of the nine compounds. Of the set of compounds, we have studied guanine, adenine,

isoguanine, xanthine, and 2,6-diaminopurine. Together with data from many other groups, a fairly extensive picture emerges. Table 1 lists the excited state lifetimes as measured at the origin of the lowest $^1\pi\pi^*$ transition.

compound	R2	R6	tautomer	lifetime (ps)	S1	references
purine	H	H		long	$n\pi^*$	48
guanine	NH ₂	O	N1 keto	<1	$\pi\pi^*$	49-50
			enol	13,000/40,000	$\pi\pi^*$	51
isoguanine	O	NH ₂	N3,7 keto	>900	$n\pi^*$	52
			enol	<30	$n\pi^*$	
adenine	H	NH ₂		9	$n\pi^*$	53
2-AP	NH ₂	H		156	$n\pi^*$	16
2,6-dAP	NH ₂	NH ₂		655/6,300	$n\pi^*$	this work
hypoX	H	O		<1	$\pi\pi^*$	54
2-oxoP	O	H			$\pi\pi^*$	13
xanthine	O	O		30 ps/2 μ s	$n\pi^*$	this work

Table 1: Excited state lifetimes as measured at the origin of lowest $\pi\pi^*$ transition.

Purine

Purine is the base structure for all these systems. It is the chromophore and main contributor to the overall absorption spectrum for all these systems. In spite of that, it has its own unique excited state dynamics, different from the rest of the molecules of interest, i.e. the purine base structure is not responsible for the ultrafast relaxation dynamics of the canonical purines. Being the simplest case, we will consider purine's excited state dynamics first.

Purine is found exclusively in the 9H tautomer in the gas phase.⁵⁵ Only Schneider et al. have successfully studied the dynamics of purine experimentally in the gas phase.⁴⁸ They collected an R2PI spectrum and determined the lowest electronic state to be of $^1n\pi^*$ character, shown in Figure 4. Individual bands in the the spectrum could be observed up to +4000 cm^{-1} , though it starts to become diffuse after +2000 cm^{-1} , relative to the $^1n\pi^*$ origin. From the similarities in the spectra of purine to deuterated purine, they attributed the low vibronic transitions to skeletal motions, as opposed to hydrogen atom vibrations. The decay

of low energy transitions must not be ultrafast, owing to the sharpness of the R2PI spectrum for so many wavenumbers.

Due to copyright limits, this figure cannot be replicated. Please refer to figure 1 from reference 48

Figure 4. (a) R2PI spectrum of purine, with the $^1n\pi^*$ origin at 31309 cm^{-1} . Most peaks $+900\text{ cm}^{-1}$ can be assigned to the combination bands with two dominant modes, a^1 and b^1 . (b) R2PI spectrum of purine-d1, two isotopomers present. (c) H-atom action spectrum. From reference 48.

Mburu and Matsika investigated the substituent effects on the excited states of purine derivatives.⁵⁶ They found purine to be one of the few molecules to have the lowest electronic state to be $^1n\pi^*$. They claim this allows for quenching of fluorescent decay via nonadiabatic dynamics (electronic state changes) to a dark state. Borin et al. came to a similar conclusion studying the excited states of 7H and 9H purine.⁵⁷

Crespo-Hernandez et al. conducted a thorough investigation of purine and 9-methylpurine transient absorption spectroscopy, coupled with quantum calculations.¹² First, they compared the dynamics to 9-methylpurine because the 7H and 9H tautomers of purine exist in amount equal amounts in aqueous solution.⁵⁸⁻⁵⁹ Their calculations assign the lowest electronic states to a dark $S_1(n\pi^*)$ and a bright $S_2(\pi\pi^*)$ for 9-methylpurine and the 7H and 9H tautomers of purine. Further, all three systems have similar dynamics. After UV absorption to $S_2(\pi\pi^*)$, they internally convert to $S_1(n\pi^*)$ in $\sim 100\text{ fs}$ (Fig. 5). Vibrational cooling then occurs from the unrelaxed $^1n\pi^*$ to the relaxed $^1n\pi^*$ (6-15 ps). Once in S_1 , the system bifurcates to S_1/S_0 internal conversion and $S_1(n\pi^*)/T_2(\pi\pi^*)$ intersystem crossing. The triplet yield is expected near unity. The authors argue that amino or oxo substitution at C_6 prevents $^1n\pi^*$ access, promoting $^1\pi\pi^*/S_0$ internal conversion via a C_2 distortion conical

intersection instead.¹² This predominance of the triplet state is supported by other solution phase experiments.⁶⁰

Due to copyright limits, this figure cannot be replicated. Please refer to figure 9 from reference 12

Figure 5. General relaxation scheme for 9-methylpurine and purine after UV excitation to $S_2(\pi\pi^*)$. From reference 12.

Biologically relevant 9H purine is seen exclusively in the gas phase. The R2PI spectrum of the lowest energy electronic state, $^1n\pi^*$, is observed and extends for $\sim 4000\text{ cm}^{-1}$. The excited state lifetime of purine has not been measured in the gas phase, but was found to be 360 ps and 645 ps in acetonitrile and aqueous solution, respectively. Solution phase experiments are complicated by the near equal populations of the 7H and 9H tautomers. Theoretical calculations agree with solution phase experiments that after excitation to $S_2(\pi\pi^*)$, purine quickly internally converts to $S_1(\pi\pi^*)$. Once there, purine will undergo intersystem crossing to a triplet state with near unity quantum yield. Evidence supports the 7H tautomer having very similar dynamics to the 9H.

2-oxopurine

2-oxopurine is purine with an oxo group at the C_2 position. It was first observed in solution in 1954 with a spectrum characterized by two transitions at 321 nm and 239 nm (Fig. 6).⁶¹ Later in 2008, a study by Mburu and Matsika explained that both of these transitions are of $^1\pi\pi^*$ character.⁵⁶ Two dark $^1n\pi^*$ states lie in between. This study was the first theoretical study of 2-oxopurine as part of a larger comparison of substituted purines at the MRMP2 level of theory. Martinez-Fernandez and co-workers built off these findings to characterize the PES and expected photodynamics of 2-oxopurine in a 2019 theoretical

study.⁶² They confirmed that the excitation would most likely be into the $S_1(\pi\pi^*)$ state, as this is the brightest state, whose minimum lies 3.4 eV above the ground state minimum. To reach the conical intersection between the $S_1(\pi\pi^*)/S_0$ is a 0.6 eV barrier from the S_1 minimum. This conical intersection is characterized by further stretching of the C_2-O and N_3-C_4 bonds, puckering of the C_6 atom, and tilting of the H atom at C_6 . Calculations of spin orbit coupling show that the S_1 minimum also intersects with two triplets states of $^1\pi\pi^*$ character. Spin orbit coupling is high enough for relaxation to prefer intersystem crossing to a triplet state over internal conversion to the ground state. The relaxation scheme is shown in figure 7!

Due to copyright limits, this figure cannot be replicated. Please refer to figure 4 from reference 61

Figure 6. Absorption spectra of 2-oxopurine with A, the neutral molecule; B, anion; and C, cation. From reference 61.

Due to copyright limits, this figure cannot be replicated. Please refer to figure 2 from reference 62

Figure 7. Potential energy diagram of 2-oxopurine with energies in eV, relative to the ground, calculated at the MS-CASPT2 (a), ADC(2) (b), and M062X/PCM-M062X (c) levels of theory. From reference 62.

Later, theoretical calculations done by Guo and co-workers support the lifetime assignment of ~200 fs by elucidating the decay mechanisms responsible for the ultrafast dynamics.⁶⁶ They found each tautomer had two different conical intersections due to out-of-plane distortions of the C_2 atom. Both conical intersection reported were lower in energy than the Frank-Condon region with no barriers in between. Hypoxanthine decays directly

from its bright $S_1(\pi\pi^*)$ to the ground state. In another study, they found solvation slightly affects the dynamics of the two tautomers.⁶⁷ Solvation is expected to slightly decrease the lifetime of 7H and slightly increase the lifetime of 9H, though their decays are still predicted to be < 1 ps. This is shown in figure 9. They also confirmed the ultrafast dynamics observed experimentally in solution for inosine by modeling the dynamics of 9-methylhypoxanthine in solution.⁶⁸

Due to copyright limits, this figure cannot be replicated. Please refer to figure 3 from reference 67

Figure 9. Plot of the average amount of time 7H and 9H spend in the S_1 state, modeled in aqueous solution. From reference 67.

Overall, hypoxanthine is noted for having the fastest excited state lifetime and incredibly photostability. Hypoxanthine undergoes absorption into the bright $S_1(\pi\pi^*)$ which then quickly passes through an ultrafast barrierless S_1/S_0 conical intersection. Experimental results show both the 7H and 9H tautomers present in solution have almost identical dynamics. These experimental results are corroborated by theoretical calculations that show ultrafast internal conversion via out-of-plane deformation at C_2 .

Xanthine (2,6-dioxopurine) and 9-methylxanthine

Xanthine is a purine derivative with oxo moieties on both C_2 and C_6 , and thus can also be called 2,6-dioxopurine. It is the combination of 2-oxopurine and hypoxanthine. Xanthine is found in the human body, as the degradation product of the canonical purines, adenine and guanine. There is strong evidence that xanthine existed on an early Earth, as it was found on meteorites⁶⁹ and synthesized using prebiotic chemistry.⁷⁰⁻⁷¹

Xanthine was first studied spectroscopically in the gas phase in 2007 by Callahan et al.⁷² They collected an R2PI spectrum and determined that only the 7H tautomer, the lowest energy tautomer, was present. A combined theoretical and experimental study by Gate et al. further studied the photodynamics of 7H and 9-methylxanthine in the gas phase. This work is not yet complete. I am waiting on theoretical results and input from Rafal. 9-methylxanthine was used as a substitute for the 9H tautomer. 7H and 9-methylxanthine had similar dynamics with a < 30 ps and ultraslow decay components observed at all vibronic transitions (Fig. 10). These relaxation mechanisms were attributed to prompt internal conversion from the bright $^1\pi\pi^*$ to $^1n\pi^*$. From there, a slight barrier causes the < 30 ps lifetime to reach the ground state while also allowing significant long-lived triplet yield, explaining the ultraslow decay.

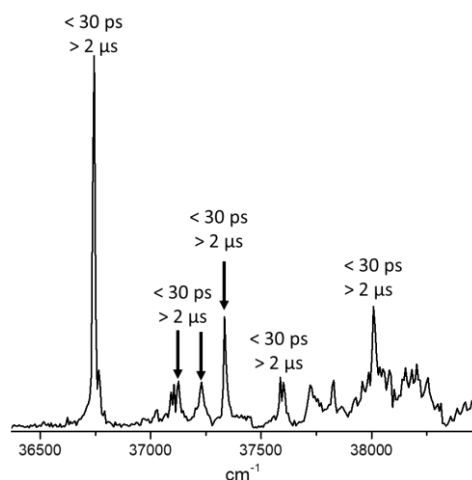


Figure 10. R2PI spectrum of 7H xanthine. Lifetimes for each peak are displayed above the respective peak. Similar decays were found for 9-methylxanthine.

Yamazaki et al. explain the lack of 9H tautomer in the gas phase is due to its poor Frank-Condon factors and its worse stability relative to 7H.⁷³ They found a near barrierless path from the Frank-Condon region of the bright $^1\pi\pi^*$ to the conical intersection defined by deformation of the 5-membered ring for 7H. The 9H had a much larger barrier to reach the

conical intersection. These potential energy surfaces are shown in Figure 11. This deformation of the 5-membered ring to reach the conical intersection stands in contrast to all other purine relaxation mechanisms that require deformation of the 6-membered ring. The authors attribute this to the single double bond across C₄C₅ in the 6-membered ring. They did not study conical intersections from the ¹nπ* because the conical intersection was significantly higher in energy than the ¹nπ* minimum. But the ¹nπ* was close in energy to the ¹ππ*, possibly allowing for significant vibronic coupling into the ¹nπ*. These results, calculated in the gas phase, disagree with experimental gas phase results.

Due to copyright limits, this figure cannot be replicated. Please refer to figure 5 from reference 73

Figure 11. Potential energy functions along the out-of-plane deformation coordinate ϕ of 7H xanthine (a) and 9H xanthine (b). Full lines with open squares (filled circles) indicate ¹ππ* energies at the CC2-optimized (CASSCF-optimized) geometries. Dashed lines with open circles show how the S₀ energies at the ¹ππ*-optimized geometries. From reference 73.

Xanthine does not dissolve in solution, so solution phase studies have used various forms of xanthosines and methylated xanthines. In 2012, Chen and Kohler studied the ultrafast nonradiative decay of hypoxanthine and several methylxanthines using fluorescence up-conversion.⁶⁴ They found all molecules have monoexponential decays with lifetimes < 600 fs. Using fluorescence up-conversion, Gustavsson and co-workers found the lifetimes of various methylated xanthines to all be ~1 ps in both H₂O and methanol (Fig. 12).⁷⁴ A combined fluorescence upconversion and transient absorption study on XMP and XMP⁻ also reveal < 1 ps lifetimes.⁷⁵ The ultrafast nonradiative decays of these various xanthines have been attributed to bright ¹ππ* relaxing directly to the ground state, in line with theoretical calculations.^{64, 74-75}

2-aminopurine

2-aminopurine is the isomer of adenine with the amino group moved to the C₂ position. It has been used for decades as an analogue of adenine in DNA. It can base pair with thymine. It is also highly fluorescent in solution, with diminished yields in the DNA helix. Thus, it has extensively been used as an environmental probe.

2AP was first observed in the gas phase in 2001.⁷⁶ In the gas phase, 2AP is mainly in the lowest energy and biologically relevant 9H tautomer.⁷⁷ The most significant contributions to the excited state dynamics of 2AP were done by Leutwyler et al. in an exciting series of articles. Using REMPI coupled with calculations, they observed two isomers of 9H-2AP·H₂O, differing only by their hydrogen bonding network (Fig. 13).⁷⁸ Vibronic analyses showed the cluster with H₂O hydrogen-bonded to the amino group (Fig. 13b) has more intense in-plane vibrational modes and less intense out-of-plane modes compared to the cluster without the amino group being hydrogen-bound (Fig. 13a). This study implied the cluster without the amino hydrogen-bonding had greater $^1L_a(\pi\pi^*)/{}^1n\pi^*$ vibronic coupling than the former. They were then able to observe 7H-2AP in the molecular beam, $\sim 1600\text{ cm}^{-1}$ to the red and 1000x weaker than 9H-2AP.⁷⁹ A vibronic analysis revealed mainly in-plane modes for 7H, predicting little vibronic coupling and a long lifetime. They also observed an ultraslow decay ($< 5\ \mu\text{s}$) for 9H, attributed to $S_1(n\pi^*)/T_1(\pi\pi^*)$ intersystem crossing. Most importantly, they measured a lifetime of 156 ps at the origin of isolated 2AP.⁸⁰⁻⁸¹ Single hydration increased the lifetime 4-100 fold, up to 14.5 ns, depending on the site of hydration. They correlated this lifetime increase with a greater ${}^1n\pi^* - {}^1\pi\pi^*$ energy gap which led to less vibronic coupling from Lim's proximity model (Figure 14). Hydration of the amino moiety

destabilized the $n\pi^*$, reducing the vibronic coupling and increasing the fluorescence and lifetime. This phenomenological approach would corroborate other mechanistic studies.

Due to copyright limits, this figure cannot be replicated. Please refer to figure 4 from reference 78

Figure 13. R2PI spectra of 9H-2AP·H₂O (a, b) and 9H-2AP (c). The spectrum in (a) is the cluster without the hydrogen bound amino group. The spectrum in (b) is the cluster with the hydrogen bound amino group. From reference 78.

Due to copyright limits, this figure cannot be replicated. Please refer to figure 3 from reference 81

Figure 14. Excited state lifetime of various 9H-2AP·(H₂O)_n clusters relative to their calculated ${}^1n\pi^*$ - ${}^1\pi\pi^*$ energy difference. 9H is isolated 9H-2AP. Note the near linearity of the lifetime with the calculated adiabatic energy gap, $E_{\text{calc}}({}^1n\pi^*) - E_{\text{calc}}({}^1\pi\pi^*)$. From reference 81.

Two competing relaxation pathways have been proposed by theoretical calculations for 9H-2AP. One put forth, first by Broo in 1998, is after initial excitation into the ${}^1L_a(\pi\pi^*)$, the system gets trapped in the ${}^1\pi\pi^*$ minimum, which explains 2AP's enhanced fluorescence over adenine.⁸²⁻⁸⁴ The ${}^1n\pi^*$ is too high in energy to affect the relaxation. This pathway assumes fluorescence and a long-lived state in both the gas phase and aqueous solution. The other proposes a slight barrier from the bright ${}^1L_a(\pi\pi^*)$ to the ${}^1n\pi^*$ allows for significant vibronic coupling and then decay to the ground state through the accessible ${}^1n\pi^*$.^{77, 84-85} This pathway would quench fluorescence in the gas-phase and in non-polar solvents. In aqueous solution, the ${}^1n\pi^*$ would destabilize to the point where it is no longer accessible and the excited system gets trapped in the ${}^1\pi\pi^*$ until it fluoresces back to S₀. Barbatti and Lischka confirmed

the latter pathway in a theoretical study that introduced individual H₂O molecules around 2AP.⁸⁶ They found in bare 2AP strong coupling between ¹ππ* and ¹nπ* and a small barrier to the ¹nπ*/S₀ conical intersection characterized by puckering at C₆ (Fig. 15). There is also a small S₁ – T₂ energy gap, such that staying in S₁ can induce intersystem crossing. Single hydration at the amino group destabilizes the ¹nπ*, trapping the system in the ¹ππ* and favoring fluorescence. This model explains the experimental work done by Leutwyler et al. using ππ* - nπ* energy differences as opposed to vibronic coupling.

Due to copyright limits, this figure cannot be replicated. Please refer to figure 5 from reference 86

Figure 15. Potential energy curves of 2AP (top) and 2AP with one H₂O hydrogen bonded to the amino group (bottom). Solid lines indicate diabatic connections of the excited states at the S₀ minimum. Dotted lines indicate adiabatic connections through the S₁ transition state. From reference 86.

Santhosh and Mishra did an extensive study comparing the absorption and excited state dynamics of 2AP and 2,6-dAP using absorption, fluorescence and emission spectroscopy coupled with calculations in 1991.⁸⁷ They found 2AP to have a 2.1 ns and 24.6 ns in aqueous solution, attributed to emission from the 9H and 7H tautomers. Later studies cast doubt on these numbers, finding 11.0 ns and 13.5 ns for the 9H and 7H tautomers.⁸⁸ This study also found though 9H-2AP is most stable, 40% is in the 7H form, due its increased dipole moment. Using several spectroscopic techniques, it was determined the lowest electronic state is of ¹ππ* character and the second lowest of ¹nπ* character.⁸⁹ Further, it was measured to have a 11.8 ns decay, which is consistent if fitting with a monoexponential. Two < 1 ps decay components were observed using fs-fluorescence upconversion, attributed to

solvation.⁹⁰ An ultralong process was also observed. Using 2APdr to exclude the 7H tautomer, Crespo-Hernandez et al. observed increasing triplet yield of 10 – 40% with decreased solvent polarity.⁹¹ Further, fluorescence decreased with decreasing solvent polarity. This triplet state exists for hundreds of ns, and is most likely populated via $^1\pi\pi^* \rightarrow ^1n\pi^* \rightarrow ^3\pi\pi^*$, confirming the work by Leutwyler and co-workers. They also observed a constant yield of 30% nonradiative decay, independent of solvent, therefore likely decay from $^1\pi\pi^*$. This overall solvent dependence is due to the stabilization (destabilization) of the $^1\pi\pi^*$ ($^1n\pi^*$) in polar solvent, reducing vibronic coupling between the two states. This is shown schematically in figure 16.

Due to copyright limits, this figure cannot be replicated. Please refer to scheme 1 from reference 91

Figure 16. Proposed kinetic mechanism for 2APdr in various solvents. ~30% of the excited population decays to the ground state nonradiatively. From reference 91.

In summary, 2AP is known for its fluorescent properties in H₂O and thus used in DNA as an adenine analogue and environmental probe. Its fluorescence decreases in less polar solvent, having a weak fluorescent signal in the gas phase. 9H-2AP is seen in the gas phase and has both an excited state lifetime that is relatively short (~100 ps) and ultralong (< 5 μ s). Fast internal conversion from the bright $^1\pi\pi^*$ leads to the $^1n\pi^*$. From there, the system will remain for ~100 ps before internally converting to the ground state or undergoing intersystem crossing to an ultralong triplet state. These dynamics are highly dependent on the hydrogen bonding environment though, with a single hydrogen bond at the amino moiety able increase the lifetime to aqueous solution decays. This is due to the extremely sensitive

interplay between the ${}^1\pi\pi^*$ - ${}^1n\pi^*$ states. Aqueous solvation stabilizes the lowest ${}^1L_a(\pi\pi^*)$ while destabilizing the ${}^1n\pi^*$, increasing the energy gap between the two states. This gap increase leads to reduced vibronic coupling and trapping of the excited system in the ${}^1\pi\pi^*$ leading to increased fluorescence and lifetime.

Adenine (6-aminopurine)

One of the two canonical purine nucleobases, adenine is also known as 6-aminopurine. It is found almost exclusively in the biologically relevant 9H tautomer in the gas phase^{53, 92} with a single, weaker peak identified belonging to the 7H tautomer by Plutzer and Kleinermanns.⁹³ In solution, about 80% is in the 9H configuration and the rest in 7H.⁹⁴⁻⁹⁵

The lowest electronic states are ${}^1n\pi^*$, ${}^1L_b(\pi\pi^*)$, ${}^1L_a(\pi\pi^*)$, and ${}^1\pi\sigma^*$. Kim et al. first observed adenine, including the dark ${}^1n\pi^*$ in 2000 using REMPI and LIF at 35503 cm^{-1} and the higher ${}^1L_b(\pi\pi^*)$ at 36105 cm^{-1} .⁹⁶ These assignments were later confirmed using helium nanodroplets absorption spectroscopy⁹⁷ and REMPI⁹³. This helium nanodroplet experiment and Kim used the decrease in lifetime coupled with theory to assign the broad spectrum above $\sim 36800 \text{ cm}^{-1}$ to the ${}^1L_a(\pi\pi^*)$ state.⁹⁷⁻⁹⁸ The gas phase spectrum is dominated by the ${}^1L_b(\pi\pi^*)$ origin transition (peak D in Fig. 17). A few weaker peaks are observed to the red of this origin, assigned to the ${}^1n\pi^*$ state (peak A) and 7H tautomer (peaks B). Well-resolved peaks from the ${}^1L_b(\pi\pi^*)$ are observed to the blue of the origin for $\sim 500 \text{ cm}^{-1}$ before the spectrum broadens and contributions are then mainly from the ${}^1L_a(\pi\pi^*)$.

Due to copyright limits, this figure cannot be replicated. Please refer to figure 1 from reference 96

Fig. 17. R2PI spectrum of adenine. Peak A is the origin band of the ${}^1n\pi^*$. D is the origin band of the ${}^1L_b(\pi\pi^*)$. The peaks assigned to B are due to the 7H tautomer. The wave number

scale on the top is relative to the origin band of the $^1n\pi^*$ state. The inset shows the spectrum over a much broader range. The broadening of the spectrum starting at $\sim 36800\text{ cm}^{-1}$ and above is caused by mainly the absorption of the $^1L_a(\pi\pi^*)$. From reference 96.

Adenine is noted for having an ultrafast decay in the gas phase. Fischer and co-workers conducted the first time-resolved study on adenine in the gas phase in 2001 using REMPI, extracting a lifetime of 9 ps at the $^1L_b(\pi\pi^*)$ origin. Various fs pump-probe transient spectroscopy and photoelectron spectroscopy studies have concluded that the initially bright states (1L_b and 1L_a) decay to the dark $^1n\pi^* < 100$ fs, and this state decays to the ground state < 1 ps.⁹⁸⁻¹⁰⁶ Thus the transients are fitted using biexponentials. Direct $^1\pi\pi^*/S_0$ internal conversion may also contribute to this < 100 fs component. The $^1n\pi^*/S_0$ decay lifetime decreases with excess excitation energy due to a small energy barrier in the $^1n\pi^*$ to the conical intersection. Smith et al. were able to observe adenine, adenine dimer, and adenine – H₂O clusters in the gas phase using photoelectron spectroscopy.¹⁰⁶ They observed the < 100 fs and 1 ps decay of adenine monomer in the gas phase due to the $^1\pi\pi^*$ and $^1n\pi^*$, respectively. But the addition of three H₂O molecules completely removed the 1 ps component. This supports the conclusion that the $^1n\pi^*$ state is not active in decay dynamics of hydrated adenine. Their data, which includes a typical transient spectrum from fs pump probe spectroscopy for adenine is displayed in Figure 18. There is also experimental evidence for a long-lived small triplet state component.⁹⁹⁻¹⁰¹

Due to copyright limits, this figure cannot be replicated. Please refer to figure 3 from reference 106

Figure 18. Time-resolved ion signals from photoelectron spectroscopy for adenine, adenine dimer, and water clusters. A typical transient ion signal of adenine is shown in the top left. From reference 106.

The experimental evidence for the activity of the $^1\pi\sigma^*$ is difficult to detect due to its dark nature and expected ultrafast dynamics to its repulsive nature. Repulsion of the N₉-H bond in the excited state is stabilized by its bond lengthening, leading to possible H atom ejection at N₉. This state is estimated only to be viable with an excitation 0.5 – 1.0 eV above the vertical excitation of the $^1L_b(\pi\pi^*)$.^{102, 107-109} Using deuterated and methylated adenine derivatives in combination with fs pump-probe spectroscopy and photoelectron spectroscopy no evidence for the $^1\pi\sigma^*$ decay route was observed.^{104-105, 110-111} Other studies using photoelectron spectroscopy and theory show possible evidence to $\pi\sigma^*$.^{100-102, 107-110, 112-113}

The photophysics and photochemistry of adenine has also attracted much theoretical effort. Different studies will differ on things such as the contribution of the $^1\pi\sigma^*$ to nonradiative decay and exact state ordering. But the general consensus for the majority of excited state decay is that the low-energy vibronic transitions excite the $^1L_b(\pi\pi^*)$ state, and vibronic coupling and a barrierless path fill a nearly degenerate $^1n\pi^*$ state.^{82, 107-110, 114-116} This accounts for the < 100 fs decay observed experimentally. Direct $^1\pi\pi/S_0$ relaxation is thought to contribute to this as well. Once in the $^1n\pi^*$, adenine undergoes significant ring puckering and out-of-plane deformation at the C2N3 and C6 to reach a conical intersection and relax back to the ground state.^{82, 107-109, 116-117} This $^1n\pi^*/S_0$ internal conversion accounts for the ~ 1 ps decay observed experimentally. Figure 19 displays this general relaxation scheme graphically. Higher energy excitations to $^1L_a(\pi\pi^*)$ lead to branching of $^1L_a(\pi\pi^*)$ to $^1n\pi^*$ and $^1\pi\sigma^*$. Serrano-Andres et al. and Corral and co-workers proposed an alternative model.^{12, 83} In this model, adenine relaxes via similar structural deformations to reach $^1\pi\pi^*/S_0$ conical intersections. This picture completely excludes the $^1n\pi^*$.

The 7H tautomer of adenine has been noted for a barrier to access the $n\pi^*$ conical intersection, which explains its experimentally observed longer lifetime and increase fluorescence.⁸²⁻⁸³ This is another example of the subtle function of molecular structure and excited state dynamics.

Due to copyright limits, this figure cannot be replicated. Please refer to figure 3 from reference 108

Figure 19. Potential energy diagram of adenine calculated with CASPT2. This shows the decay path calculated from the local minimum (LM) geometry of adenine at the $^1n\pi^*$ to the saddle point (SP) to the out-of-plane conical intersection (CI_{32}). From reference 108.

In aqueous solution using fs transient absorption and fluorescence upconversion, adenine is noted for a biexponential decay with lifetimes of ~ 0.2 and 8 ps.^{94-95, 112, 118} This longer lifetime was shown to be due to the significantly more fluorescent 7H tautomer using dAMP, and methylated adenines.^{94, 112, 118} Figure 20 shows the typical decay observed for adenine, adenosine, and dAMP in aqueous solution using fluorescence upconversion. Adenosine was found to have a similarly fast lifetime of 0.3 fs.^{112, 118-120} Note, some studies find biexponential decays for adenosine, but these lifetimes are still consistently < 0.5 ps. Because adenosine does not have a 7H tautomer, and therefore no long 8 ps decay, adenosine was also used to study the dynamics of intermolecular vibrational cooling in the ground state.¹¹⁹⁻¹²¹ Others have studied the dynamics of adenosine in the context of making comparisons to adenine homo-oligonucleotides.^{111, 121-123} They too have found similar lifetimes for adenosine. Mechanistically, it is unclear whether in solution adenine decays using the $^1n\pi^*$ state. Some studies point to its contribution,^{94, 118} while others do not.^{106, 111}

Due to copyright limits, this figure cannot be replicated. Please refer to figure 3 from reference 118

Figure 20. Fluorescence upconversion decay curves for adenine, adenosine, and dAMP in aqueous solution. These curves are similar to fluorescence upconversion and transient absorption curves from other studies. From reference 118.

Overall, 9H-adenine has slightly different excited state dynamics in gas phase and aqueous solution. In the gas phase, adenine has two decay components. One is a < 100 fs component due to the decay of the initially bright state, either $^1L_b(\pi\pi^*)$ or $^1L_a(\pi\pi^*)$, to the $^1n\pi^*$ or S_0 . The longer component is on the order of 1 ps, due to the decay of the $^1n\pi^*$ through a conical intersection by out-of-plane deformations along the 6-membered ring. In aqueous solution, study of the dynamics also involved studying adenosine, dAMP, and methylated derivatives due to presence of the 7H tautomer and vibrational cooling with the solvent. Nonradiative decay in solution occurs on the < 1 ps timescale due to low-lying conical intersections. It is inconclusive so far if the $^1n\pi^*$ contributes to this decay in solution.

2,6-diaminopurine

2,6-diaminopurine (2,6-dAP) is the combination of 2AP and 6AP, with amino moieties at both C_2 and C_6 . 2,6-dAP likely existed on an early Earth, as it was found in meteorite samples⁶⁹ and could be synthesized under the same conditions with the same starting materials as the canonical nucleobases.¹²⁴

2,6-dAP was first observed in the gas phase in 2001.⁷⁶ Gengeliczki et al. then determined the presence of both the 7H and 9H diamino tautomers in the molecular beam with the 7H origin red-shifted ~ 2600 cm^{-1} relative to the 9H origin.¹²⁵ Using ns pump probe, they also measured excited state lifetimes of 8.7 ns and 6.3 ns for the 7H and 9H tautomers,

respectively. Recently, Gate and co-workers did an extensive gas-phase excited state dynamics study using both REMPI and quantum calculations. This work is also not complete. I am waiting for theoretical calculations and input from Rafal for 2,6-dAP as well. For the 7H tautomer, they observed a sizable barrier to internal conversion from the bright $S_1(\pi\pi^*)$ leading to a ~ 25 ns lifetime and significant triplet yield with a > 2 μ s lifetime (Fig. 21). On the other hand, the 9H tautomer has a small barrier to the $S_1(\pi\pi^*)/S_0$, yielding a small fluorescent quantum yield for the first few vibronic transitions before disappearing. Further, a 600 ps decay was also observed for the first few vibronic bands that reduces to 9 ps at $+800$ cm^{-1}

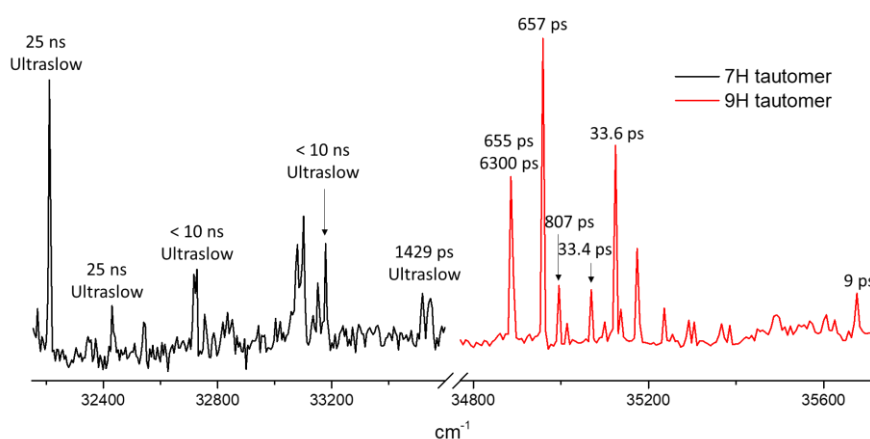


Figure 21. R2PI spectra of the 7H (black) and 9H (red) tautomers of 2,6-dAP. The origins are at 32216 cm^{-1} and 34885 cm^{-1} for the 7H and 9H, respectively. The lifetimes derived for each peak are listed above the peaks. Ultraslow has a decay of $> 2\mu$ s.

These experimental results are supported by theoretical calculations. The 7H has a barrier from its Frank-Condon excitation to S_0 conical intersection, requiring significant nuclear motion, explaining the 25 ns decay. The intersystem crossing geometry is very similar to the Frank-Condon geometry. This similar geometry, coupled with the amount of time 7H stays in the $S_1(\pi\pi^*)$, allows for significant triplet yield and competitive intersystem crossing. The intersystem crossing is competitive at all probed wavelengths. The 9H has a

small barrier between the Frank-Condon excitation and the ground state. This small barrier allows for a small fluorescent yield, explaining the 6.3 ns decay. The rest of the wavepacket decays nonradiatively, attributed to the ps decay. With only a small amount of energy, the barrier is quickly overcome and the fluorescent yield disappears, outcompeted by the much more efficient nonradiative decay. The significant drop in lifetime of the ps decay and broadening of the R2PI spectrum are evidence to this.

Santhosh and Mishra also studied 2,6-dAP in aqueous solution using absorption, fluorescence and excitation spectroscopies.⁸⁷ They also conducted ns pump probe, and observed a 4.0 ns fluorescent decay. Virta et al. characterized 2,6-dAP using fluorescent spectroscopy.¹²⁶ They found a 1.7 ns fluorescent lifetime with a fluorescence quantum yield of 0.02. As far as we can tell, no one has determined the tautomer distribution of 2,6-dAP in aqueous solution. But we assume both tautomers and contribute to the fluorescence signal. The 9H tautomer is slightly more stable than the 7H tautomer in the gas phase, similar to 2AP and 6AP. And the 7H tautomers make up 40% and 20% of the aqueous population for 2AP⁸⁸ and 6AP,⁹⁴⁻⁹⁵ respectively. It is therefore likely that both the 7H and 9H tautomers of 2,6-dAP are present in sizable amount in solution.

The biologically relevant 9H tautomer of 2,6-dAP has a small fluorescent component at low excitation energies. It also has a fast nonradiative decay that becomes more efficient and competitive with small increases in excess energy, on the order of $\sim 500 \text{ cm}^{-1}$. This is due to a small barrier from the bright $S_1(\pi\pi^*)$ to the ${}^1\pi\pi^*/S_0$ conical intersection. In solution, 2,6-dAP has small fluorescent yield with a lifetime of ~ 2 ns. These results stand in contrast to the 7H tautomer, which has significantly different excited state dynamics.

Isoguanine

Isoguanine is the isomer of guanine with the oxo and amino moieties switched. Interest in isoguanine grew after Rich in 1962 suggested isoguanine and isocytosine could form a highly stable Watson-Crick base pair that could biologically be incorporated into DNA.¹²⁷ Scientists now believe that the canonical nucleobases were selected partially because of their pairing fidelity and tautomeric stability. Later studies showed that isoguanine defies both of those standards. Studies have shown that isoguanine exists in multiple different tautomeric forms in DNA¹²⁸⁻¹²⁹ and can base pair with guanine,¹³⁰ cytosine,^{128, 131-132} thymine,¹²⁸ and isocytosine.¹²⁷ Isoguanine can also form parallel strand helices¹³¹ and tetraplexes¹³² with cytosine. Because of the many important tautomers of isoguanine, two of the more influential studies by Sepiol et al.¹³³ and Seela et al.¹³⁴ focused on assigning the predominant tautomeric forms. Sepiol et al. used spectrophotometric titration on isoguanosine and other isoguanine analogues and concluded both keto-amino and enol-amino were present depending on the solvent polarity.¹³³ Seela et al. fixed the tautomerization using alkylation and confirmed that the keto-amino 1H tautomer of isoguanosine was present in aqueous solution.¹³⁴ Other studies have found evidence for other tautomers, showing that the tautomerization of isoguanine is a complex situation.^{128, 130}

The latest study of isoguanine by Gate et al. in 2019 also appears to be the first to assign gas phase tautomers and study the relaxation dynamics.¹³⁵ They observed the keto-3,7H and enol-7H in the gas phase (Fig. 22). The keto form was found to have a lifetime around 950 ps at all transitions. The enol form could not be measured and was proposed due to an ultrafast lifetime. Quantum calculations were carried out on the two tautomers above as well as the lowest energy and biologically relevant tautomers, enol-N9 and keto-N1,9 (Fig. 23). The keto-3,7H $S_1(n\pi^*)$ minimum is 0.98 eV below the ground state conical intersection. This barrier explains the 950 ps lifetime observed. Two conical intersections with smaller

barriers were observed for the enol-7H tautomer. Consequently, the enol form is expected to have a fast excited state lifetime which explains the small amount of signal and unsuccessful pump probe experiments. Calculations were also done on the unobserved enol-9H, the lowest energy tautomer. They showed no barrier to the ground state conical intersection leading to an ultrafast decay, and possibly explaining the lack of signal from enol-9H.

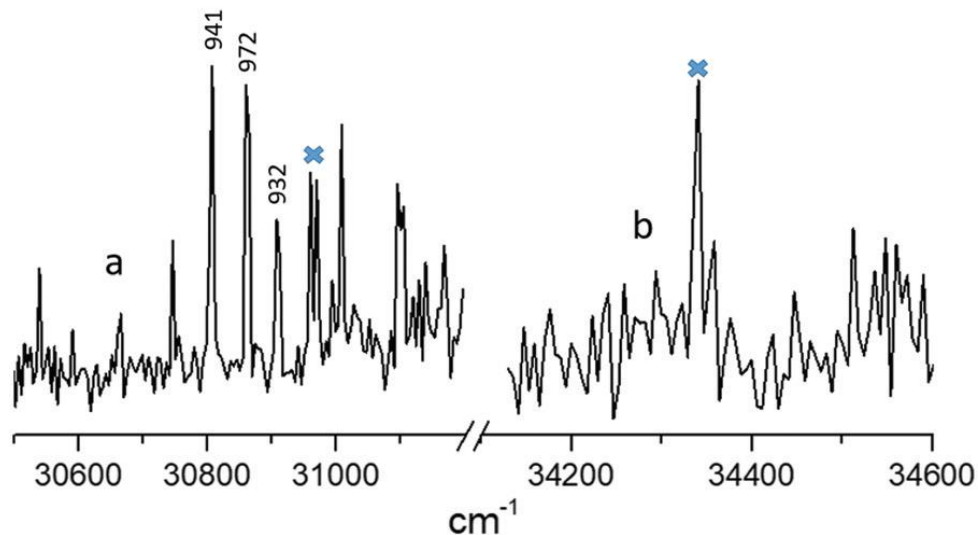


Figure 22. R2PI spectra of keto-3.7H (a) and enol-7H (b). Lifetimes, in ps, are displayed above each peak. Peaks where pump probe was unsuccessfully attempted are marked with crosses. Reproduced without permission.¹³⁵

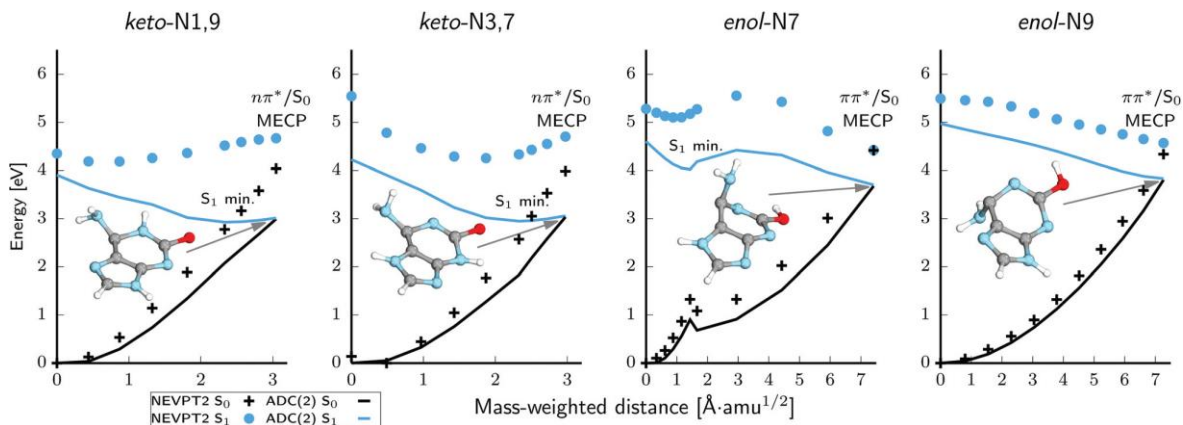


Figure 23. Potential energy profiles for the predicted dominant photodeactivation pathways of keto and enol isoguanine. The inserted structure corresponds to the S_1/S_0 minimum-energy crossing point (MECP) geometry (conical intersection). For a description of the

applicability of NEVPT2 and ADC(2), refer to the reference. Reproduced without permission.¹³⁵

Isoguanine has several tautomeric forms present, apparently in both solution and gas phase. This is similar to the situation with guanine. The experimentally observed keto-3,7H had a lifetime of 950 ps at all peaks, explained theoretically by a large barrier to internal conversion. The unobserved keto-1,9H was predicted to have similar dynamics. Enol-7H, the other experimentally observed tautomer had only small amount of signal, attributed to a smaller barrier and faster internal conversion. Enol-9H was predicted to have ultrafast dynamics.

Guanine

Guanine is a canonical nucleobase with a purine structure and an amino group at the C₂ and an oxo group at the C₆. In this way, it is a combination of hypoxanthine and 2AP. A high resolution gas phase spectrum of guanine was first taken by Nir et al. in 1999.¹³⁶ This was followed shortly after by the vibronic spectrum of guanosine.¹³⁷ IR-UV double resonance experiments, coupled with calculated structure stabilities were used to assign tautomers in the gas phase. Four tautomers are seen in the gas phase (Fig. 24). At first, they were assigned to the lowest energy tautomers: keto 9H, keto 7H, enol 9H, and enol 7H.¹³⁸⁻¹⁴⁰ The keto 9H, keto 7H, enol 9H(trans), and enol 9H(cis) were then definitely seen by Choi and Miller in helium nanodroplets and IR laser spectroscopy in 2006.¹⁴¹ The IR spectra acquired in this study did not match previous studies on the tautomers of guanine. It was later confirmed that enol 9H, enol 7H, and two imino-keto 7H, are observed in the gas phase using a molecular beam.¹⁴²⁻¹⁴⁴ These tautomers are 3-7 kcal/mol higher in energy than the lowest energy keto 9H. This caused a reassignment of the tautomers observed in previous studies using

molecular beams. Though the biologically relevant guanine tautomer has been observed in the gas phase,^{141, 145} it has not been done with a technique that can probe its excited state dynamics with tautomer-specificity. A couple of early attempts to probe the dynamics of guanine found < 1 ps lifetimes, but this was without tautomer resolution. The ultrafast relaxations support that these authors were probing biological guanine.^{99, 105} Other tautomers have lifetimes on the order of tens of nanoseconds, though these were found using techniques that could only observe nanosecond decays.^{51, 140} Note that analyses done before the tautomer reassignment in 2006/2007 may have been assuming the wrong tautomers. These also highlight how small structural rearrangements as tautomerization also significantly impact excited state dynamics.

Due to copyright limits, this figure cannot be replicated. Please refer to figure 1 from reference 142

Figure 24. R2PI spectrum of guanine. The origins of the four different tautomers are marked with arrows. From reference 142.

Theoretical calculations have explained why biological guanine is not observed in molecular beam experiments. It has poor Frank-Condon factors¹⁴⁴. Further it is predicted to have ultrafast decay due to a barrierless conical intersection directly from the bright $^1\pi\pi^*$ to S_0 from puckering at C_2 .^{144, 146-148} Figure 25 shows a general scheme for this decay model. Another barrierless conical intersection opens up via hydrogen-abstraction from a $^1\pi\sigma^*$ state due to stabilization of guanine's large static dipole moment.^{144, 146-147} Unlike 9H-adenine, the $^1n\pi^*$ is negligibly involved in the excited state dynamics due to its prohibitively high energy. Thiel and co-workers conducted a nonadiabatic dynamics study in simulated aqueous solution and found these dynamics to be faster than *in vacuo*.¹⁴⁹ This was due to a smaller

energy gap between ${}^1L_a(\pi\pi^*)$ and ${}^1L_b(\pi\pi^*)$ and a new conical intersection by out-of-plane motion of the carbonyl group.

Due to copyright limits, this figure cannot be replicated. Please refer to figure 3 from reference 146

Figure 25. General relaxation scheme for guanine going from a bright ${}^1\pi\pi^*$ down a barrierless path directly to a conical intersection with the ground state. From reference 146.

Guanine has been scantily studied in solution due to its poor solubility. Instead, solution phase studies have focused on guanosine and GMP and dGMP. The biologically relevant amino-keto tautomer is found in aqueous solution for guanosine and GMP.¹⁵⁰⁻¹⁵² Like adenine, these systems have been noted for two low-energy bright states, the ${}^1L_a(\pi\pi^*)$ and ${}^1L_b(\pi\pi^*)$. For guanine, the state ordering is reversed though, with ${}^1L_a(\pi\pi^*)$ lower in energy than ${}^1L_b(\pi\pi^*)$. The fluorescence spectrum of GMP is much broader and red-shifted relative to other nucleotides with a tail out to 700 nm.^{120, 151} This red tail is due to the relatively flat ${}^1L_a(\pi\pi^*)$ PES leading to the S_1/S_0 conical intersection. Excitation of the higher energy ${}^1L_b(\pi\pi^*)$ leads to < 100 fs internal conversion to ${}^1L_a(\pi\pi^*)$.^{119-120, 151-154} The ${}^1L_a(\pi\pi^*)$ then decays along a barrierless, though flat, PES to the S_1/S_0 conical intersection, leading to a < 1 ps lifetime (Figure 26).

Due to copyright limits, this figure cannot be replicated. Please refer to figure 2 from reference 119

Figure 26. Transient absorption spectra of guanosine in aqueous solution with pump at 263 nm and at the set probe wavelengths. The curves have been offset vertically for clarity. From reference 119.

Overall, the biologically relevant amio-keto 9H tautomer of guanine presumably decays on < 1 ps timescale in solution and gas phase. This lifetime assignment is complicated by the fact that guanine will not dissolve in aqueous solution and thus guanosine and GMP must be used instead. Further, biological guanine has not been definitively probed in gas phase due to its likely ultrafast decay, as explained by theory. Guanine has two bright states, an $^1L_a(\pi\pi^*)$ and a higher $^1L_b(\pi\pi^*)$. Guanine will decay from the $^1L_b(\pi\pi^*)$ to $^1L_a(\pi\pi^*)$ in under < 100 fs and then reach a $^1L_a(\pi\pi^*)/S_0$ conical intersection via mainly C_2 pyramidalization under < 1 ps. $^1\pi\sigma^*$ and $^1n\pi^*$ may be reached at higher excitation energies. Unlike adenine the $^1n\pi^*$ is not accessed in biological guanine due to its much higher energy. This destabilization may be due to the presence of the electron-donating oxo moiety. Though this cannot be the whole story, as the photostability is still tautomer dependent.

4. The role of C_2 and C_6 substitutions

Photostability follows from the ability to return to the electronic ground state at time scales short enough to outcompete all other possible processes. This scenario requires a potential energy landscape that allows barrierless trajectories to efficient conical intersections. The dependence on structure comes about because even minor changes in the PES can affect the positions and levels of minima, CIs, barriers, or ordering of states which can have large effects on the excited state dynamics. The structure dependence is subtle and even tautomers of the same compound can have excited state lifetimes that differ by orders of magnitude. As a result, it is hard to formulate general trends. A number of models have been proposed to generalize the structural effects and each of those describe important elements. However, the complete description still appears to require the inclusion of additional details.

While comparing the effects of different C₂ and C₆ substitutions, it should be noted that the excited state lifetimes are not a single number but are, rather, a function of absorption wavelength. The focus here is on absorption close to the origin, because the excited state dynamics at threshold energies are the most sensitive measure of the topography of the PE landscapes. Moreover, at high excitation energy, above all barriers, deactivation rates tend to increase and thus may not be an accurate reflection of photostability. For the molecule to rapidly and safely diffuse electronic excitation, no significant part of the spectrum should be trapped in the excited state, including the part absorbed near threshold. In some of the non-canonical bases, such as xanthine and 2AP, ultrafast dynamics occur, but at the same time ISC occurs as well with a significant quantum yield, thus threatening the long-term stability upon radiation. Furthermore, under prebiotic conditions, absorption further to the red in the spectrum may have implied more exposure to damaging radiation.

The base structure of these substitutions is purine. Purine itself is long-lived via the mechanism of a S₂(¹ππ^{*})/S₁(¹nπ^{*}) CI in 100 fs followed by a near 100% QY for ISC to a long-lived triplet state. So the chromophore by itself is not responsible for the photostability of the purine nucleobases. Substitutions of oxo- or amino- groups at the C₂ and C₆ position modify the dynamics to produce different outcomes for each of the other eight structures, including producing photostability for selected ones. This is not unique to the purine nucleobases as Arpa et al. have pointed out that “The pyrimidine chromophore is not responsible for the photostability of the nucleobases”.¹⁵⁵ In this case C₂ and C₄ functionalization with amino- and/or oxo- substituents modifies the PES landscape, creating ultrafast pathways through CIs to the ground state. For purine based structures, four major motifs have emerged in describing how the excited state dynamics is affected by the potential energy landscapes of purine and its oxo- and amino- derivatives.

(i) The first motif is the order of $\pi\pi^*$ and $n\pi^*$ states which the substituents modify through stabilization/destabilization effects of the added groups.⁹ Generally, the $\pi\pi^*$ state is the bright state. If the $n\pi^*$ is lower in energy in the FC region or its minimum is below that of the $\pi\pi^*$ state, then there may be conical intersections between the two that allow the $n\pi^*$ to be populated and to serve as a doorway state or a dark state.¹⁵⁶⁻¹⁵⁷ This is the reported arrangement in all cases, except guanine, hypoxanthine, 2-oxopurine and enol isoguanine. However, while an accessible $n\pi^*$ state creates a more complex PE landscape, it does not suffice to characterize excited state dynamics. Even when the $n\pi^*$ state is not accessible, there may or may not be a barrierless path to the ground state, as in keto vs. enol guanine. Conversely, when the $^1n\pi^*$ state can be reached, it may subsequently lead to the ground state, as in adenine, or lead to for example intersystem crossing to a $^3\pi\pi^*$ state as in purine and 2-oxopurine, and possibly xanthine, 2,6-diaminopurine, and 2-aminopurine.

(ii) A major motif, in many cases, is C_2 puckering in the CI geometry.^{13, 158} It has been argued that this geometry is responsible for the short lifetime of two structures without a C_2 substituent, adenine and hypoxanthine. The most often cited example is the lifetime difference between adenine and 2-aminopurine. For 2-aminopurine, it has been argued that the out of-plane rotation of the C_2 -amino group takes longer than the C_2 -H bond rotation in adenine, resulting in the longer observed lifetime. However, this trend does not hold for purine which has no C_2 substituent but still has a long lifetime. It is also contradicted by the fact that ketoG and enol isoG with an amino- and oxo- substituent in C_2 , respectively, have fast excited state lifetimes.

(iii) Puckering at C_6 can also define conical intersection geometries to a lesser extent.¹⁵⁹ For example, it provides an additional deactivation channel in adenine, which becomes significant only at higher excitation energies.¹⁶⁰ C_6 substitution has also been proposed to

play a role in reducing the barrier in the $\pi\pi^*$ state. The effect is illustrated with the observation that adenine and hypoxanthine decay fast relative to purine. However, the observations that 2,6-dAP is slower than 2AP and that enol-G and keto-isoG are slow complicate this explanation.

(iv) When considering the fate of photoexcited nucleobases, the possibility of intersystem crossing is of particular concern. Only rapid return to the ground state, either directly or through a doorway state, effectively transforms electronic excitation to heat but some nonradiative transitions lead to a longer-lived dark state. Purine, 2,6-dAP, and xanthine all have significant ISC with the major pathway involving a $^1n\pi^*/^3\pi\pi^*$ CI, which is El-Sayed allowed. Large spin-orbit coupling, as in the case of 2-oxopurine and 2-aminopurine can also contribute to this strength of this ISC pathway.

While this review is based on insights from gas phase data, other aspects, such as the solvent, of course play a role. A prime example is 2AP, which is known for its long excited state lifetime in solution, but in the gas phase has a 156 ps lifetime at the origin. Lobsiger et al. have shown that it takes only three water molecules for that lifetime to lengthen to 14.5 ns. Computations predict a reduction in the barrier for tautomerisation upon solvation for all canonical nucleobases. For example, a reduction from 190 to 112 kJ/mol and from 230 to 126 kJ/mol was predicted for thymine and cytosine respectively by Valadbeigi et al.¹⁶¹ Although the barriers are not easy to compute and their values strongly depend on the computation level, all the computational works report that solvation by water reduces the barriers by about ~ 120 kJ/mol.¹⁶² Intrastrand hydrogen bonding can also affect the excited state dynamics. For example, Zeleny et al. found computationally that in the GC base pair the out of plane motions of the guanine NH_2 are restricted, affecting the associated CI.¹⁶³ On

the other hand, the base pair forms a charge transfer state along the N₁-H coordinate, which provides another fast decay trajectory.^{28, 164}

It should also be noted that a longer stay in an excited state may not always need to lead to photochemical damage. An example is the formation of excitons in stacked bases, which return to the ground state by charge recombination at a time scale of 100 ps.¹⁶⁵

One might speculate that the oxo- and amino- substitutions did not only provide the purine and pyrimidine skeletons with the necessary hydrogen bonding structures – for which many combinations were possible – but at the same time also with UV hardness – for which only a subset was preferred. To understand which structures could provide the fastest deactivation dynamics back to the ground state requires careful computations to map out all potential energy surfaces in comparison with detailed experimental data. In putting these observations and trends together, we observe that the dynamics is governed by distortions of the 6 ring and the resulting potentials do depend on the structure around the ring. But structural trends combine in very nuanced ways; the effects of individual substitutions don't simply add up and the end result cannot be intuitively predicted.

5. Outlook

While from all the data, described here, an extensive picture emerges of the entire landscape of 2,6 oxo-/amino- substituted purines, a few pieces of the puzzle are still missing. Notably, no gas phase data are yet available for 2-oxopurine, hypoxanthine, and keto guanine. For the latter two, presumably the sub-picosecond excited state lifetime is too short for REMPI detection. Alternative approaches, such as population of the hot ground state following internal conversion may provide additional data.

Possible next steps may include the following considerations. (i) When considering prebiotic scenarios, one may consider recent proposals that the difficulty of plausible glycosylation pathways for the nucleobases suggest the possibility that nucleosides were synthesized directly to form the first building blocks.¹⁶⁶ Following this work on nucleobases, it will therefore be important to study the nucleoside photochemistry, some of which has already been reported for the canonical nucleosides.¹⁶⁷⁻¹⁶⁸ (ii) Some of the effects of hydrogen-bonding in base pairs and in water have been mentioned above, but much more work is called for, especially on clusters with water. (iii) Another possible structural motif that leads to intermolecular interactions is pi-stacking. Upon excitation, stacking can lead to exciplexes, which provides additional photochemical pathways. Some of those dynamics has been studied in solution¹⁶⁹⁻¹⁷⁰ but not in the gas phase because nucleobases tend only to form hydrogen bonded structures in the gas phase.^{121, 171-174} (iv) In addition to substitutions, it will be of interest to the prebiotic community to consider the photostability of analogues, such as triazines.⁷

This field has been progressing, and continues to do so, thanks to parallel developments in experiments and in theory, allowing the study of molecules of increasing size in the gas phase and with ever higher levels of computational theory. Finally, in addition to the prebiotic importance of photostability of the molecular building blocks of life, complete understanding of the structure dependence of photostability might one day help in the design of compounds with desired photochemical properties.

References

1. Abo-Riziq, A.; Grace, L.; Nir, E.; Kabelac, M.; Hobza, P.; de Vries, M. S., Photochemical selectivity in guanine-cytosine base-pair structures. *Proc. Natl. Acad. Sci. U.S.A.* **2005**, *102* (1), 20-23.

2. Weinkauff, R.; Schermann, J. P.; de Vries, M. S.; Kleinermanns, K., Molecular physics of building blocks of life under isolated or defined conditions. *European Physical Journal D* **2002**, *20* (3), 309-316.
3. Nir, E.; Kleinermanns, K.; de Vries, M. S., Pairing of isolated nucleic-acid bases in the absence of the DNA backbone. *Nature* **2000**, *408* (6815), 949-951.
4. Boldissar, S.; de Vries, M. S., How nature covers its bases. *Phys Chem Chem Phys* **2018**, *20*, 9701-9716.
5. Hutter, D.; Benner, S. A., Expanding the genetic alphabet: Non-epimerizing nucleoside with the pyDDA hydrogen-bonding pattern. *J. Org. Chem.* **2003**, *68* (25), 9839-9842.
6. Hoshika, S.; Leal, N. A.; Kim, M. J.; Kim, M. S.; Karalkar, N. B.; Kim, H. J.; Bates, A. M.; Watkins, N. E.; SantaLucia, H. A.; Meyer, A. J.; DasGupta, S.; Piccirilli, J. A.; Ellington, A. D.; SantaLucia, J.; Georgiadis, M. M.; Benner, S. A., Hachimoji DNA and RNA: A genetic system with eight building blocks. *Science* **2019**, *363* (6429), 884-+.
7. Hud, N. V.; Cafferty, B. J.; Krishnamurthy, R.; Williams, L. D., The Origin of RNA and "My Grandfather's Axe". *Chem Biol* **2013**, *20* (4), 466-474.
8. Powner, M. W.; Gerland, B.; Sutherland, J. D., Synthesis of activated pyrimidine ribonucleotides in prebiotically plausible conditions. *Nature* **2009**, *459* (7244), 239-242.
9. Mburu, E.; Matsika, S., An Ab Initio Study of Substituent Effects on the Excited States of Purine Derivatives. *J. Phys. Chem. A* **2008**, *112* (48), 12485-12491.
10. Gengeliczki, Z.; Callahan, M. P.; Svadlenak, N.; Pongor, C. I.; Sztaray, B.; Meerts, L.; Nachtigallova, D.; Hobza, P.; Barbatti, M.; Lischka, H.; de Vries, M. S., Effect of substituents on the excited-state dynamics of the modified DNA bases 2,4-diaminopyrimidine and 2,6-diaminopurine. *Phys. Chem. Chem. Phys.* **2010**, *12* (20), 5375-5388.
11. Nachtigallova, D.; Barbatti, M.; Szymczak, J. J.; Hobza, P.; Lischka, H., The photodynamics of 2,4-diaminopyrimidine in comparison with 4-aminopyrimidine: The effect of amino-substitution. *Chem. Phys. Lett.* **2010**, *497* (1-3), 129-134.
12. Crespo-Hernandez, C. E.; Martinez-Fernandez, L.; Rauer, C.; Reichardt, C.; Mai, S.; Pollum, M.; Marquetand, P.; Gonzalez, L.; Corral, I., Electronic and structural elements that regulate the excited-state dynamics in purine nucleobase derivatives. *J Am Chem Soc* **2015**, *137* (13), 4368-81.
13. Martinez-Fernandez, L.; Arslanacan, S.; Ivashchenko, D.; Crespo-Hernandez, C. E.; Corral, I., Tracking the origin of photostability in purine nucleobases: the photophysics of 2-oxopurine. *Phys Chem Chem Phys* **2019**, *21*, 13467-13473.
14. Lobsiger, S.; Sinha, R. K.; Trachsel, M.; Leutwyler, S., Low-lying excited states and nonradiative processes of the adenine analogues 7H-and 9H-2-aminopurine. *J. Chem. Phys.* **2011**, *134* (11).
15. Cohen, B.; Hare, P. M.; Kohler, B., Ultrafast excited-state dynamics of adenine and monomethylated adenines in solution: Implications for the nonradiative decay mechanism. *J. Am. Chem. Soc.* **2003**, *125* (44), 13594-13601.
16. Lobsiger, S.; Blaser, S.; Sinha, R. K.; Frey, H. M.; Leutwyler, S., Switching on the fluorescence of 2-aminopurine by site-selective microhydration. *Nat Chem* **2014**, *6* (11), 989-993.
17. Reichardt, C.; Wen, C. W.; Vogt, R. A.; Crespo-Hernandez, C. E., Role of intersystem crossing in the fluorescence quenching of 2-aminopurine 2'-deoxyriboside in solution (vol 12, pg 1341, 2013). *Photoch. Photobio. Sci.* **2013**, *12* (12), 2203-2203.

18. Ullrich, S.; Schultz, T.; Zgierski, M. Z.; Stolow, A., Electronic relaxation dynamics in DNA and RNA bases studied by time-resolved photoelectron spectroscopy. *Phys. Chem. Chem. Phys.* **2004**, *6* (10), 2796-2801.
19. Mohamadzade, A.; Bai, S.; Barbatti, M.; Ullrich, S., Intersystem crossing dynamics in singly substituted thiouracil studied by time-resolved photoelectron spectroscopy: Micro-environmental effects due to sulfur position. *Chem. Phys.* **2018**.
20. Smith, V. R.; Samoylova, E.; Ritze, H. H.; Radloff, W.; Schultz, T., Excimer states in microhydrated adenine clusters. *Phys. Chem. Chem. Phys.* **2010**, *12* (33), 9632-9636.
21. Casaes, R.; Provencal, R.; Paul, J.; Saykally, R. J., High resolution pulsed infrared cavity ringdown spectroscopy: Application to laser ablated carbon clusters. *J. Chem. Phys.* **2002**, *116* (15), 6640-6647.
22. Viant, M. R.; Fellers, R. S.; McLaughlin, R. P.; Saykally, R. J., Infrared-Laser Spectroscopy of Uracil in a Pulsed Slit Jet. *J. Chem. Phys.* **1995**, *103* (21), 9502-9505.
23. Alonso, J. L.; Pena, I.; Lopez, J. C.; Vaquero, V., Rotational Spectral Signatures of Four Tautomers of Guanine. *Angew Chem Int Edit* **2009**, *48* (33), 6141-6143.
24. Sanz, M. E.; Blanco, S.; Lopez, J. C.; Alonso, J. L., Rotational probes of six conformers of neutral cysteine. *Angew Chem Int Edit* **2008**, *47* (33), 6216-6220.
25. Vaquero, V.; Sanz, M. E.; Lopez, J. C.; Alonso, J. L., The structure of uracil: A laser ablation rotational study. *J. Phys. Chem. A* **2007**, *111* (18), 3443-3445.
26. Lopez, J. C.; Pena, M. I.; Sanz, M. E.; Alonso, J. L., Probing thymine with laser ablation molecular beam Fourier transform microwave spectroscopy. *J. Chem. Phys.* **2007**, *126* (19).
27. Nir, E.; Janzen, C.; Imhof, P.; Kleinermanns, K.; de Vries, M. S., Guanine tautomerism revealed by UV-UV and IR-UV hole burning spectroscopy. *J. Chem. Phys.* **2001**, *115*, 4604-4611.
28. Nir, E.; Janzen, C.; Imhof, P.; Kleinermanns, K.; de Vries, M. S., Pairing of the nucleobases guanine and cytosine in the gas phase studied by IR-UV double-resonance spectroscopy and ab initio calculations. *Phys. Chem. Chem. Phys.* **2002**, *4* (5), 732-739.
29. Nir, E.; Hünig, I.; Kleinermanns, K.; de Vries, M. S., Conformers of guanosines and their vibrations in the electronic ground and excited states, as revealed by double-resonance spectroscopy and ab initio calculations. *ChemPhysChem* **2004**, *5* (1), 131-137.
30. Cramer, C. J., *Essentials of Computational Chemistry: Theories and Models* 2nd Edition ed.; Wiley.
31. Jensen, F., *Introduction to Computational Chemistry* 3rd Edition ed.; Wiley.
32. Foresman, J. B.; Frisch, A., *Exploring Chemistry with Electronic Structure Methods*. 3rd edition ed.; (Gaussian, Inc.: , Wallingford, CT, 2015.
33. Adamo, C.; Jacquemin, D., The calculations of excited-state properties with Time-Dependent Density Functional Theory. *Chem. Soc. Rev.* **2013**, *42* (3), 845-856.
34. Schlegel, H. B.; McDouall, J. J., In *Computational Advances in Organic Chemistry*, Ögretir, C.; Csizmadia, I. G., Eds. Kluwer Academic: the Netherlands, 1991; pp 137-185.
35. Moller, C.; Plesset, M. S., Note on an Approximation Treatment for Many-Electron Systems. *Phys Rev* **1934**, *46*, 618-622.
36. Bartlett, R. J.; Purvis, G. D., Many-Body Perturbation-Theory, Coupled-Pair Many-Electron Theory, and Importance of Quadruple Excitations for Correlation Problem. *Int. J. Quantum Chem.* **1978**, *14* (5), 561-581.
37. Kohn, W.; Becke, A. D.; Parr, R. G., Density functional theory of electronic structure. *J. Phys. Chem.* **1996**, *100* (31), 12974-12980.

38. Ziegler, T., Approximate Density Functional Theory as a Practical Tool in Molecular Energetics and Dynamics. *Chem. Rev.* **1991**, *91* (5), 651-667.
39. Hohenberg, P.; Kohn, W., Inhomogeneous Electron Gas. *Phys Rev B* **1964**, *136* (3b), B864-+.
40. Kohn, W.; Sham, L. J., Self-Consistent Equations Including Exchange and Correlation Effects. *Phys Rev* **1965**, *140* (4a), 1133-&.
41. Headgordon, M.; Rico, R. J.; Oumi, M.; Lee, T. J., A Doubles Correction to Electronic Excited-States from Configuration-Interaction in the Space of Single Substitutions. *Chem. Phys. Lett.* **1994**, *219* (1-2), 21-29.
42. Bauernschmitt, R.; Ahlrichs, R., Treatment of electronic excitations within the adiabatic approximation of time dependent density functional theory. *Chem. Phys. Lett.* **1996**, *256* (4-5), 454-464.
43. Dreuw, A.; Head-Gordon, M., Single-reference ab initio methods for the calculation of excited states of large molecules. *Chem. Rev.* **2005**, *105* (11), 4009-4037.
44. Tozer, D. J.; Handy, N. C., Improving virtual Kohn-Sham orbitals and eigenvalues: Application to excitation energies and static polarizabilities. *J. Chem. Phys.* **1998**, *109* (23), 10180-10189.
45. Shao, Y. H.; Head-Gordon, M.; Krylov, A. I., The spin-flip approach within time-dependent density functional theory: Theory and applications to diradicals. *J. Chem. Phys.* **2003**, *118* (11), 4807-4818.
46. Bernardi, F.; Bottoni, A.; Mcdouall, J. J. W.; Robb, M. A.; Schlegel, H. B., Mcscf Gradient Calculation of Transition Structures in Organic-Reactions. *Faraday Symp Chem S* **1984**, (19), 137-147.
47. Haggmark, M. R.; Gate, G.; Boldissar, S.; Berenbeim, J.; Sobolewski, A. L.; de Vries, M. S., Evidence for competing proton-transfer and hydrogen-transfer reactions in the S1 state of indigo. *Chemical Physics* **2018**, *515*, 535-542.
48. Schneider, M.; Hain, T.; Fischer, I., Resonance-enhanced multiphoton ionisation of purine. *Chemphyschem* **2009**, *10* (4), 634-6.
49. Barbatti, M.; Szymczak, J. J.; Aquino, A. J. A.; Nachtigallova, D.; Lischka, H., The decay mechanism of photoexcited guanine – A nonadiabatic dynamics study. *J. Chem. Phys.* **2011**, *134*, 014304.
50. Yamazaki, S.; Domcke, W.; Sobolewski, A. L., Nonradiative Decay Mechanisms of the Biologically Relevant Tautomer of Guanine. *J. Phys. Chem. A* **2008**, *112* (47), 11965-11968.
51. Siouri, F. M.; Boldissar, S.; Berenbeim, J. A.; de Vries, M. S., Excited State Dynamics of 6-Thioguanine. *J Phys Chem A* **2017**, *121* (28), 5257-5266.
52. Gate, G.; Szabla, R.; Haggmark, M. R.; Sponer, J.; Sobolewski, A. L.; de Vries, M. S., Photodynamics of alternative DNA base isoguanine. *Phys. Chem. Chem. Phys.* **2019**, *21* (25), 13474-13485.
53. Lührs, D. C.; Viallon, J.; Fischer, I., Excited state spectroscopy and dynamics of isolated adenine and 9-methyladenine. *Physical Chemistry Chemical Physics* **2001**, *3* (10), 1827-1831.
54. Chen, J. Q.; Kohler, B., Ultrafast nonradiative decay by hypoxanthine and several methylxanthines in aqueous and acetonitrile solution. *Phys. Chem. Chem. Phys.* **2012**, *14* (30), 10677-10682.
55. Caminati, W.; Maccaferri, G.; Favero, P. G.; Favero, L. B., Free jet absorption millimeter wave spectrum of purine. *Chemical Physics Letters* **1996**, *251* (3-4), 189-192.

56. Mburu, E.; Matsika, S., An ab initio study of substituent effects on the excited states of purine derivatives. *J Phys Chem A* **2008**, *112* (48), 12485-91.
57. Borin, A. C.; Serrano-Andrés, L.; Fülischer, M. P.; Roos, B. O., A Theoretical Study of the Electronic Spectra of N9 and N7 Purine Tautomers. *The Journal of Physical Chemistry A* **1999**, *103* (12), 1838-1845.
58. Gonnella, N. C.; Roberts, J. D., Studies of the tautomerism of purine and the protonation of purine, and its 7- and 9-methyl derivatives, by nitrogen-15 nuclear magnetic resonance spectroscopy. *Journal of the American Chemical Society* **1982**, *104* (11), 3162-3164.
59. Majoube, M.; Millié, P.; Chinsky, L.; Turpin, P. Y.; Vergoten, G., Resonance Raman spectra for purine. *Journal of Molecular Structure* **1995**, *355* (2), 147-158.
60. Quinones, E.; Arce, R., Photochemistry and photophysics of purine free base and 6-methylpurine. *Journal of the American Chemical Society* **1989**, *111* (21), 8218-8223.
61. Mason, S. F., Purine studies. Part II. The ultra-violet absorption spectra of some mono- and poly-substituted purines. *Journal of the Chemical Society (Resumed)* **1954**.
62. Martinez-Fernandez, L.; Arslançan, S.; Ivashchenko, D.; Crespo-Hernandez, C. E.; Corral, I., Tracking the origin of photostability in purine nucleobases: the photophysics of 2-oxopurine. *Phys Chem Chem Phys* **2019**, *21* (25), 13467-13473.
63. Röttger, K.; Siewertsen, R.; Temps, F., Ultrafast electronic deactivation dynamics of the rare natural nucleobase hypoxanthine. *Chemical Physics Letters* **2012**, *536*, 140-146.
64. Chen, J.; Kohler, B., Ultrafast nonradiative decay by hypoxanthine and several methylxanthines in aqueous and acetonitrile solution. *Phys Chem Chem Phys* **2012**, *14* (30), 10677-82.
65. Villabona-Monsalve, J. P.; Noria, R.; Matsika, S.; Peon, J., On the accessibility to conical intersections in purines: hypoxanthine and its singly protonated and deprotonated forms. *J Am Chem Soc* **2012**, *134* (18), 7820-9.
66. Guo, X.; Lan, Z.; Cao, Z., Ab initio insight into ultrafast nonadiabatic decay of hypoxanthine: keto-N7H and keto-N9H tautomers. *Phys Chem Chem Phys* **2013**, *15* (26), 10777-82.
67. Guo, X.; Zhao, Y.; Cao, Z., A QM/MM MD insight into photodynamics of hypoxanthine: distinct nonadiabatic decay behaviors between keto-N7H and keto-N9H tautomers in aqueous solution. *Phys Chem Chem Phys* **2014**, *16* (29), 15381-8.
68. Guo, X.; Yuan, H.; An, B.; Zhu, Q.; Zhang, J., Ultrafast excited-state deactivation of 9-methylhypoxanthine in aqueous solution: A QM/MM MD study. *J Chem Phys* **2016**, *144* (15), 154306.
69. Callahan, M. P.; Smith, K. E.; Cleaves, H. J., 2nd; Ruzicka, J.; Stern, J. C.; Glavin, D. P.; House, C. H.; Dworkin, J. P., Carbonaceous meteorites contain a wide range of extraterrestrial nucleobases. *Proc Natl Acad Sci U S A* **2011**, *108* (34), 13995-8.
70. Piccirilli, J. A.; Krauch, T.; Moroney, S. E.; Benner, S. A., Enzymatic incorporation of a new base pair into DNA and RNA extends the genetic alphabet. *Nature* **1990**, *343* (6253), 33-7.
71. Saladino, R.; Crestini, C.; Neri, V.; Brucato, J. R.; Colangeli, L.; Ciciriello, F.; Di Mauro, E.; Costanzo, G., Synthesis and degradation of nucleic Acid components by formamide and cosmic dust analogues. *ChemBiochem* **2005**, *6* (8), 1368-74.
72. Callahan, M. P.; Crews, B.; Abo-Riziq, A.; Grace, L.; de Vries, M. S.; Gengeliczki, Z.; Holmes, T. M.; Hill, G. A., IR-UV double resonance spectroscopy of xanthine. *Phys Chem Chem Phys* **2007**, *9* (32), 4587-91.

73. Yamazaki, S.; Sobolewski, A. L.; Domcke, W., Photophysics of xanthine: computational study of the radiationless decay mechanisms. *Phys Chem Chem Phys* **2009**, *11* (43), 10165-74.
74. Changenet-Barret, P.; Kovacs, L.; Markovitsi, D.; Gustavsson, T., Xanthenes Studied via Femtosecond Fluorescence Spectroscopy. *Molecules* **2016**, *21* (12).
75. Rottger, K.; Stellmacher, R.; Stuhldreier, M. C.; Temps, F., Ultrafast Electronic Deactivation Dynamics of Xanthosine Monophosphate. *Molecules* **2017**, *22* (1).
76. Nir, E.; Kleinermands, K.; Grace, L.; de Vries, M. S., On the photochemistry of purine nucleobases. *Journal of Physical Chemistry A* **2001**, *105* (21), 5106-5110.
77. Seefeld, K. A.; Plutzer, C.; Lowenich, D.; Haber, T.; Linder, R.; Kleinermands, K.; Tatchen, J.; Marian, C. M., Tautomers and electronic states of jet-cooled 2-aminopurine investigated by double resonance spectroscopy and theory. *Phys Chem Chem Phys* **2005**, *7* (16), 3021-6.
78. Sinha, R. K.; Lobsiger, S.; Trachsel, M.; Leutwyler, S., Vibronic spectra of jet-cooled 2-aminopurine.H₂O clusters studied by UV resonant two-photon ionization spectroscopy and quantum chemical calculations. *J Phys Chem A* **2011**, *115* (23), 6208-17.
79. Lobsiger, S.; Sinha, R. K.; Trachsel, M.; Leutwyler, S., Low-lying excited states and nonradiative processes of the adenine analogues 7H- and 9H-2-aminopurine. *J Chem Phys* **2011**, *134* (11), 114307.
80. Blaser, S.; Frey, H. M.; Heid, C. G.; Leutwyler, S., Gas-phase lifetimes of nucleobase analogues by picosecond pump-ionization and streak techniques. *Chimia (Aarau)* **2014**, *68* (4), 260-3.
81. Lobsiger, S.; Blaser, S.; Sinha, R. K.; Frey, H. M.; Leutwyler, S., Switching on the fluorescence of 2-aminopurine by site-selective microhydration. *Nat Chem* **2014**, *6* (11), 989-93.
82. Broo, A., A Theoretical Investigation of the Physical Reason for the Very Different Luminescence Properties of the Two Isomers Adenine and 2-Aminopurine. *The Journal of Physical Chemistry A* **1998**, *102* (3), 526-531.
83. Serrano-Andres, L.; Merchan, M.; Borin, A. C., Adenine and 2-aminopurine: paradigms of modern theoretical photochemistry. *Proc Natl Acad Sci U S A* **2006**, *103* (23), 8691-6.
84. Perun, S.; Sobolewski, A. L.; Domcke, W., Ab initio studies of the photophysics of 2-aminopurine. *Molecular Physics* **2006**, *104* (5-7), 1113-1121.
85. Rachofsky, E. L.; Ross, J. B. A.; Krauss, M.; Osman, R., CASSCF Investigation of Electronic Excited States of 2-Aminopurine. *The Journal of Physical Chemistry A* **2001**, *105* (1), 190-197.
86. Barbatti, M.; Lischka, H., Why water makes 2-aminopurine fluorescent? *Phys Chem Chem Phys* **2015**, *17* (23), 15452-9.
87. Santhosh, C.; Mishra, P. C., Electronic spectra of 2-aminopurine and 2,6-diaminopurine: phototautomerism and fluorescence reabsorption. *Spectrochimica Acta Part A: Molecular Spectroscopy* **1991**, *47* (12), 1685-1693.
88. Neely, R. K.; Magennis, S. W.; Dryden, D. T. F.; Jones, A. C., Evidence of Tautomerism in 2-Aminopurine from Fluorescence Lifetime Measurements. *The Journal of Physical Chemistry B* **2004**, *108* (45), 17606-17610.
89. Holmén, A.; Nordén, B.; Albinsson, B., Electronic Transition Moments of 2-Aminopurine. *Journal of the American Chemical Society* **1997**, *119* (13), 3114-3121.

90. Pal, S. K.; Peon, J.; Zewail, A. H., Ultrafast decay and hydration dynamics of DNA bases and mimics. *Chemical Physics Letters* **2002**, *363* (1-2), 57-63.
91. Reichardt, C.; Wen, C.; Vogt, R. A.; Crespo-Hernandez, C. E., Role of intersystem crossing in the fluorescence quenching of 2-aminopurine 2'-deoxyriboside in solution. *Photochem Photobiol Sci* **2013**, *12* (8), 1341-50.
92. Plützer, C.; Nir, E.; de Vries, M. S.; Kleinermanns, K., IR–UV double-resonance spectroscopy of the nucleobase adenine. *Physical Chemistry Chemical Physics* **2001**, *3* (24), 5466-5469.
93. Plützer, C.; Kleinermanns, K., Tautomers and electronic states of jet-cooled adenine investigated by double resonance spectroscopy. *Phys. Chem. Chem. Phys.* **2002**, *4* (20), 4877-4882.
94. Cohen, B.; Hare, P. M.; Kohler, B., Ultrafast excited-state dynamics of adenine and monomethylated adenines in solution: implications for the nonradiative decay mechanism. *J Am Chem Soc* **2003**, *125* (44), 13594-601.
95. Buchner, F.; Ritze, H. H.; Lahl, J.; Lubcke, A., Time-resolved photoelectron spectroscopy of adenine and adenosine in aqueous solution. *Phys Chem Chem Phys* **2013**, *15* (27), 11402-8.
96. Kim, N. J.; Jeong, G.; Kim, Y. S.; Sung, J.; Keun Kim, S.; Park, Y. D., Resonant two-photon ionization and laser induced fluorescence spectroscopy of jet-cooled adenine. *The Journal of Chemical Physics* **2000**, *113* (22), 10051-10055.
97. Smolarek, S.; Rijs, A. M.; Buma, W. J.; Drabbels, M., Absorption spectroscopy of adenine, 9-methyladenine, and 2-aminopurine in helium nanodroplets. *Phys Chem Chem Phys* **2010**, *12* (48), 15600-6.
98. Kang, H.; Chang, J.; Lee, S. H.; Ahn, T. K.; Kim, N. J.; Kim, S. K., Excited-state lifetime of adenine near the first electronic band origin. *J Chem Phys* **2010**, *133* (15), 154311.
99. Kang, H.; Lee, K. T.; Jung, B.; Ko, Y. J.; Kim, S. K., Intrinsic Lifetimes of the Excited State of DNA and RNA Bases. *J Am Chem Soc* **2002**, *124*, 12958 - 12959.
100. Ullrich, S.; Schultz, T.; Zgierski, M. Z.; Stolow, A., Direct Observation of Electronic Relaxation Dynamics in Adenine via Time-Resolved Photoelectron Spectroscopy. *J Am Chem Soc* **2004**, *126*, 2262 - 2263.
101. Ullrich, S.; Schultz, T.; Zgierski, M. Z.; Stolow, A., Electronic relaxation dynamics in DNA and RNA bases studied by time-resolved photoelectron spectroscopy. *Physical Chemistry Chemical Physics* **2004**, *6* (10).
102. Evans, N. L.; Ullrich, S., Wavelength dependence of electronic relaxation in isolated adenine using UV femtosecond time-resolved photoelectron spectroscopy. *J Phys Chem A* **2010**, *114* (42), 11225-30.
103. Samoylova, E.; Schultz, T.; Hertel, I. V.; Radloff, W., Analysis of ultrafast relaxation in photoexcited DNA base pairs of adenine and thymine. *Chemical Physics* **2008**, *347* (1-3), 376-382.
104. Kang, H.; Jung, B.; Kim, S. K., Mechanism for ultrafast internal conversion of adenine. *The Journal of Chemical Physics* **2003**, *118* (15), 6717-6719.
105. Canuel, C.; Mons, M.; Piuze, F.; Tardivel, B.; Dimicoli, I.; Elhanine, M., Excited states dynamics of DNA and RNA bases: characterization of a stepwise deactivation pathway in the gas phase. *J Chem Phys* **2005**, *122* (7), 074316.
106. Smith, V. R.; Samoylova, E.; Ritze, H. H.; Radloff, W.; Schultz, T., Excimer states in microhydrated adenine clusters. *Phys Chem Chem Phys* **2010**, *12* (33), 9632-6.

107. Marian, C. M., A new pathway for the rapid decay of electronically excited adenine. *J Chem Phys* **2005**, *122* (10), 104314.
108. Perun, S.; Sobolewski, A. L.; Domcke, W., Photostability of 9H-adenine: mechanisms of the radiationless deactivation of the lowest excited singlet states. *Chemical Physics* **2005**, *313* (1-3), 107-112.
109. Perun, S.; Sobolewski, A. L.; Domcke, W., Ab initio studies on the radiationless decay mechanisms of the lowest excited singlet states of 9H-adenine. *J Am Chem Soc* **2005**, *127* (17), 6257-65.
110. Barbatti, M.; Lischka, H., Nonadiabatic Deactivation of 9H-Adenine A Comprehensive Picture Based on Mixed Quantum-Classical Dynamics. *J Am Chem Soc* **2008**, *130*, 6831 - 6839.
111. Kwok, W. M.; Ma, C.; Phillips, D. L., Femtosecond time- and wavelength-resolved fluorescence and absorption spectroscopic study of the excited states of adenosine and an adenine oligomer. *J Am Chem Soc* **2006**, *128* (36), 11894-905.
112. Pancur, T.; Schwalb, N. K.; Renth, F.; Temps, F., Femtosecond fluorescence up-conversion spectroscopy of adenine and adenosine: experimental evidence for the $\pi\sigma^*$ state? *Chemical Physics* **2005**, *313* (1-3), 199-212.
113. Wells, K. L.; Roberts, G. M.; Stavros, V. G., Dynamics of H-loss in adenine via the $1\pi\sigma^*$ state using a combination of ns and fs laser spectroscopy. *Chemical Physics Letters* **2007**, *446* (1-3), 20-24.
114. Fabiano, E.; Thiel, W., Nonradiative deexcitation dynamics of 9H-adenine: an OM2 surface hopping study. *J Phys Chem A* **2008**, *112* (30), 6859-63.
115. Picconi, D.; Avila Ferrer, F. J.; Improta, R.; Lami, A.; Santoro, F., Quantum-classical effective-modes dynamics of the $\pi\pi^* \rightarrow n\pi^*$ decay in 9H-adenine. A quadratic vibronic coupling model. *Faraday Discussions* **2013**, *163*.
116. Chen, H.; Li, S., Theoretical study toward understanding ultrafast internal conversion of excited 9H-adenine. *J Phys Chem A* **2005**, *109* (38), 8443-6.
117. Plasser, F.; Crespo-Otero, R.; Pedersoli, M.; Pittner, J.; Lischka, H.; Barbatti, M., Surface Hopping Dynamics with Correlated Single-Reference Methods: 9H-Adenine as a Case Study. *J Chem Theory Comput* **2014**, *10* (4), 1395-405.
118. Gustavsson, T.; Sharonov, A.; Onidas, D.; Markovitsi, D., Adenine, deoxyadenosine and deoxyadenosine 5'-monophosphate studied by femtosecond fluorescence upconversion spectroscopy. *Chemical Physics Letters* **2002**, *356* (1-2), 49-54.
119. Pecourt, J.-M. L.; Peon, J.; Kohler, B., DNA Excited-State Dynamics: Ultrafast Internal Conversion and Vibrational Cooling in a Series of Nucleosides. *Journal of the American Chemical Society* **2001**, *123* (42), 10370-10378.
120. Onidas, D.; Markovitsi, D.; Marguet, S.; Sharonov, A.; Gustavsson, T., Fluorescence Properties of DNA Nucleosides and Nucleotides: A Refined Steady-State and Femtosecond Investigation. *The Journal of Physical Chemistry B* **2002**, *106* (43), 11367-11374.
121. Su, C.; Middleton, C. T.; Kohler, B., Base-stacking disorder and excited-state dynamics in single-stranded adenine homo-oligonucleotides. *J Phys Chem B* **2012**, *116* (34), 10266-74.
122. Chen, J.; Kohler, B., Base stacking in adenosine dimers revealed by femtosecond transient absorption spectroscopy. *J Am Chem Soc* **2014**, *136* (17), 6362-72.
123. Crespo-Hernández, C. E.; Kohler, B., Influence of Secondary Structure on Electronic Energy Relaxation in Adenine Homopolymers. *The Journal of Physical Chemistry B* **2004**, *108* (30), 11182-11188.

124. Miyakawa, S.; Cleaves, H. J.; Miller, S. L., The cold origin of life: B. Implications based on pyrimidines and purines produced from frozen ammonium cyanide solutions. *Orig Life Evol Biosph* **2002**, *32* (3), 209-18.
125. Gengeliczki, Z.; Callahan, M. P.; Svadlenak, N.; Pongor, C. I.; Sztaray, B.; Meerts, L.; Nachtigallova, D.; Hobza, P.; Barbatti, M.; Lischka, H.; de Vries, M. S., Effect of substituents on the excited-state dynamics of the modified DNA bases 2,4-diaminopyrimidine and 2,6-diaminopurine. *Phys Chem Chem Phys* **2010**, *12* (20), 5375-88.
126. Virta, P.; Koch, A.; Roslund, M. U.; Mattjus, P.; Kleinpeter, E.; Kronberg, L.; Sjöholm, R.; Klika, K. D., Synthesis, characterisation and theoretical calculations of 2,6-diaminopurine etheno derivatives. *Org Biomol Chem* **2005**, *3* (16), 2924-9.
127. Rich, A., On the Problems of Evolution and Biochemical Information Transfer. In *Horizons in Biochemistry*, Kasha, M.; Pullman, B., Eds. Academic Press: New York, 1962; pp 103-126.
128. Blas, J. R.; Luque, F. J.; Orozco, M., Unique Tautomeric Properties of Isoguanine. *J Am Chem Soc* **2003**, *126*, 154-164.
129. Robinson, H.; Gao, Y. G.; Bauer, C.; Roberts, C.; Switzer, C.; Wang, A. H., 2'-Deoxyisoguanosine adopts more than one tautomer to form base pairs with thymidine observed by high-resolution crystal structure analysis. *Biochemistry* **1998**, *37* (31), 10897-905.
130. Eschenmoser, A., Hexose nucleic acids. *Pure and Applied Chemistry* **1993**, *65* (6), 1179-1188.
131. Roberts, C.; Chaput, J. C.; Switzer, C., Beyond guanine quartets: cation-induced formation of homogenous and chimeric DNA tetraplexes incorporating iso-guanine and guanine. *Chemistry & Biology* **1997**, *4* (12), 899-908.
132. Sugiyama, H.; Ikeda, S.; Saito, I., Remarkably Stable Parallel-Stranded Oligonucleotides Containing 5-Methylisocytosine and Isoguanine. *Journal of the American Chemical Society* **1996**, *118* (41), 9994-9995.
133. Sepiol, J.; Kazimierczuk, Z.; Shugar, D., Tautomerism of isoguanosine and solvent-induced keto-enol equilibrium. *Z Naturforsch C* **1976**, *31* (7-8), 361-70.
134. Seela, F.; Wei, C.; Kazimierczuk, Z., Substituent Reactivity and Tautomerism of Isoguanosine and Related Nucleosides. *Helvetica Chimica Acta* **1995**, *78* (7), 1843-1854.
135. Gate, G.; Szabla, R.; Haggmark, M. R.; Sponer, J.; Sobolewski, A. L.; de Vries, M. S., Photodynamics of alternative DNA base isoguanine. *Phys Chem Chem Phys* **2019**, *21* (25), 13474-13485.
136. Nir, E.; Grace, L.; Brauer, B.; de Vries, M. S., REMPI Spectroscopy of Jet-Cooled Guanine. *Journal of the American Chemical Society* **1999**, *121* (20), 4896-4897.
137. Nir, E.; Imhof, P.; Kleinermanns, K.; de Vries, M. S., REMPI Spectroscopy of Laser Desorbed Guanosines. *J Am Chem Soc* **2000**, *122* (33), 8091-8092.
138. Nir, E.; Janzen, C.; Imhof, P.; Kleinermanns, K.; de Vries, M. S., Guanine tautomerism revealed by UV-UV and IR-UV hole burning spectroscopy. *The Journal of Chemical Physics* **2001**, *115* (10), 4604-4611.
139. Piuzzi, F.; Mons, M.; Dimicoli, I.; Tardivel, B.; Zhao, Q., Ultraviolet spectroscopy and tautomerism of the DNA base guanine and its hydrate formed in a supersonic jet. *Chemical Physics* **2001**, *270* (1), 205-214.
140. Chin, W.; Mons, M.; Dimicoli, I.; Piuzzi, F.; Tardivel, B.; Elhanine, M., Tautomer contributions to the near UV spectrum of guanine: towards a refined picture for the spectroscopy of purine molecules. *The European Physical Journal D* **2002**, *20* (3), 347-355.

141. Choi, M. Y.; Miller, R. E., Four tautomers of isolated guanine from infrared laser spectroscopy in helium nanodroplets. *J Am Chem Soc* **2006**, *128* (22), 7320-8.
142. Mons, M.; Piuze, F.; Dimicoli, I.; Gorb, L.; Leszczynski, J., Near-UV resonant two-photon ionization spectroscopy of gas phase guanine: evidence for the observation of three rare tautomers. *J Phys Chem A* **2006**, *110* (38), 10921-4.
143. Seefeld, K.; Brause, R.; Haber, T.; Kleinermanns, K., Imino tautomers of gas-phase guanine from mid-infrared laser spectroscopy. *J Phys Chem A* **2007**, *111* (28), 6217-21.
144. Marian, C. M., The guanine tautomer puzzle: quantum chemical investigation of ground and excited states. *J Phys Chem A* **2007**, *111* (8), 1545-53.
145. Alonso, J. L.; Pena, I.; Lopez, J. C.; Vaquero, V., Rotational spectral signatures of four tautomers of guanine. *Angew Chem Int Ed Engl* **2009**, *48* (33), 6141-3.
146. Yamazaki, S.; Domcke, W.; Sobolewski, A. L., Nonradiative decay mechanisms of the biologically relevant tautomer of guanine. *J Phys Chem A* **2008**, *112* (47), 11965-8.
147. Barbatti, M.; Szymczak, J. J.; Aquino, A. J.; Nachtigallova, D.; Lischka, H., The decay mechanism of photoexcited guanine - a nonadiabatic dynamics study. *J Chem Phys* **2011**, *134* (1), 014304.
148. Chen, H.; Li, S., Ab initio study on deactivation pathways of excited 9H-guanine. *J Chem Phys* **2006**, *124* (15), 154315.
149. Heggen, B.; Lan, Z.; Thiel, W., Nonadiabatic decay dynamics of 9H-guanine in aqueous solution. *Phys Chem Chem Phys* **2012**, *14* (22), 8137-46.
150. Ashwood, B.; Ortiz-Rodriguez, L. A.; Crespo-Hernandez, C. E., Excited-State Dynamics in O(6)-Methylguanosine: Impact of O(6)-Methylation on the Relaxation Mechanism of Guanine Monomers. *J Phys Chem Lett* **2017**, *8* (18), 4380-4385.
151. Miannay, F. A.; Gustavsson, T.; Banyasz, A.; Markovitsi, D., Excited-state dynamics of dGMP measured by steady-state and femtosecond fluorescence spectroscopy. *J Phys Chem A* **2010**, *114* (9), 3256-63.
152. Karunakaran, V.; Kleinermanns, K.; Improta, R.; Kovalenko, S. A., Photoinduced dynamics of guanosine monophosphate in water from broad-band transient absorption spectroscopy and quantum-chemical calculations. *J Am Chem Soc* **2009**, *131* (16), 5839-50.
153. Peon, J.; Zewail, A. H., DNA/RNA nucleotides and nucleosides: direct measurement of excited-state lifetimes by femtosecond fluorescence up-conversion. *Chemical Physics Letters* **2001**, *348* (3-4), 255-262.
154. Pecourt, J.-M. L.; Peon, J.; Kohler, B., Ultrafast Internal Conversion of Electronically Excited RNA and DNA Nucleosides in Water. *Journal of the American Chemical Society* **2000**, *122* (38), 9348-9349.
155. Arpa, E. M.; Brister, M. M.; Hoehn, S. J.; Crespo-Hernandez, C. E.; Corral, I., On the Origin of the Photostability of DNA and RNA Monomers: Excited State Relaxation Mechanism of the Pyrimidine Chromophore. *J Phys Chem Lett* **2020**, 5156-5161.
156. Perun, S.; Sobolewski, A. L.; Domcke, W., Ab initio studies on the radiationless decay mechanisms of the lowest excited singlet states of 9H-adenine. *J. Am. Chem. Soc.* **2005**, *127* (17), 6257-6265.
157. Picconi, D.; Ferrer, F. J. A.; Improta, R.; Lami, A.; Santoro, F., Quantum-classical effective-modes dynamics of the $\pi \pi^* \rightarrow n \pi^*$ decay in 9H-adenine. A quadratic vibronic coupling model. *Faraday Discuss.* **2013**, *163*, 223-242.
158. Broo, A., A theoretical investigation of the physical reason for the very different luminescence properties of the two isomers Adenine and 2-Aminopurine. *J.Phys. Chem.* **1998**, *A 102*, 526-531.

159. Serrano-Andres, L.; Merchan, M.; Borin, A. C., Adenine and 2-aminopurine: Paradigms of modern theoretical photochemistry. *Proc. Natl. Acad. Sci. U.S.A.* **2006**, *103* (23), 8691-8696.
160. Plasser, F.; Crespo-Otero, R.; Pederzoli, M.; Pittner, J.; Lischka, H.; Barbatti, M., Surface Hopping Dynamics with Correlated Single-Reference Methods: 9H-Adenine as a Case Study. *J Chem Theory Comput* **2014**, *10* (4), 1395-1405.
161. Valadbeigi, Y.; Soleiman-Beigi, M.; Sahraei, R., Catalysis effect of micro-hydration on the intramolecular proton transfer in cytosine. *Chem. Phys. Lett.* **2015**, *629*, 1-7.
162. Mejía-Mazariegos, L.; Hernández-Trujillo, J., Electron density analysis of tautomeric mechanisms of adenine, thymine and guanine and the pairs of thymine with adenine or guanine. *Chem. Phys. Lett.* **2009**, *482* (1-3), 24-29.
163. Zeleny, T.; Ruckebauer, M.; Aquino, A. J. A.; Muller, T.; Lankas, F.; Dršata, T.; Hase, W. L.; Nachtigallova, D.; Lischka, H., Strikingly Different Effects of Hydrogen Bonding on the Photodynamics of Individual Nucleobases in DNA: Comparison of Guanine and Cytosine. *J. Am. Chem. Soc.* **2012**, *134* (33), 13662-13669.
164. Sobolewski, A. L.; Domcke, W., Ab Initio studies on the photophysics of the guanine-cytosine base pair. *Phys. Chem. Chem. Phys.* **2004**, *6*, 2763-2771.
165. Chen, J. Q.; Zhang, Y. Y.; Kohler, B., Excited States in DNA Strands Investigated by Ultrafast Laser Spectroscopy. *Top Curr Chem* **2015**, *356*, 39-87.
166. Xu, J.; Chmela, V.; Green, N. J.; Russell, D. A.; Janicki, M. J.; Gora, R. W.; Szabla, R.; Bond, A. D.; Sutherland, J. D., Selective prebiotic formation of RNA pyrimidine and DNA purine nucleosides. *Nature* **2020**, *582* (7810), 60-66.
167. Nir, E.; Imhof, P.; Kleinermanns, K.; de Vries, M. S., REMPI spectroscopy of laser desorbed guanosines. *J. Am. Chem. Soc.* **2000**, *122* (33), 8091-8092.
168. Abo-Riziq, A.; Crews, B. O.; Compagnon, I.; Oomens, J.; Meijer, G.; Von Helden, G.; Kabelac, M.; Hobza, P.; de Vries, M. S., The Mid-IR spectra of 9-ethyl guanine, guanosine, and 2-Deoxyguanosine. *J. Phys. Chem. A* **2007**, *111* (31), 7529-7536.
169. Su, C.; Middleton, C. T.; Kohler, B., Base-Stacking Disorder and Excited-State Dynamics in Single-Stranded Adenine Homo-oligonucleotides. *J. Phys. Chem. B* **2012**, *116* (34), 10266-10274.
170. Chen, J. Q.; Kohler, B., Base Stacking in Adenosine Dimers Revealed by Femtosecond Transient Absorption Spectroscopy. *J. Am. Chem. Soc.* **2014**, *136* (17), 6362-6372.
171. Crespo-Hernandez, C. E.; Cohen, B.; Kohler, B., Base stacking controls excited-state dynamics in A.T DNA. *Nature* **2005**, *436* (7054), 1141-4.
172. Crespo-Hernandez, C. E.; de La Harpe, K.; Kohler, B., Ground-state recovery following UV excitation is much slower in G center dot C - DNA duplexes and hairpins than in mononucleotides. *J. Am. Chem. Soc.* **2008**, *130* (33), 10844-+.
173. Kwok, W. M.; Ma, C. S.; Phillips, D. L., Femtosecond time- and wavelength-resolved fluorescence and absorption spectroscopic study of the excited states of adenosine and an adenine oligomer. *J. Am. Chem. Soc.* **2006**, *128* (36), 11894-11905.
174. Buchvarov, I.; Wang, Q.; Raytchev, M.; Trifonov, A.; Fiebig, T., Electronic energy delocalization and dissipation in single- and double-stranded DNA. *Proc. Natl. Acad. Sci. U.S.A.* **2007**, *104* (12), 4794-4797.

II. Photodynamics of alternative DNA base isoguanine

Gregory Gate^a, Rafal Szabla^{bc}, Michael R. Haggmark^a, Jiří Šponer^c, Andrej L. Sobolewski^b, Mattanjah de Vries^a

^a Department of Chemistry and Biochemistry, University of California, Santa Barbara, California 93106-9510, USA.

^b Institute of Physics, Polish Academy of Sciences, Al. Lotników 32/46, 02-668 Warsaw, Poland

^c Institute of Biophysics of the Czech Academy of Sciences, Královopolská 135, 61265 Brno, Czech Republic.

Abstract

Isoguanine is an alternative nucleobase that has been proposed as a component of expanded genetic codes. It has also been considered as a molecule with potential relevance to primordial informational polymers. Here, we scrutinize the photodynamics of isoguanine, because photostability has been proposed as a critical criterion for the prebiotic selection of biomolecular building blocks on an early Earth. We discuss resonance-enhanced multiphoton ionization, IR-UV double resonance spectroscopy and pump–probe measurements performed for this molecule to track the excited-state behaviour of its different tautomeric forms in the gas phase. These experiments, when confronted with highly accurate quantum chemical calculations and nonadiabatic dynamics simulations provide a complete mechanistic picture of the tautomer-specific photodynamics of isoguanine. Our results indicate that UV-excited enol tautomers of isoguanine are relatively short lived and therefore photostable. In contrast, the biologically more relevant keto forms are trapped in dark $n\pi^*$ states which are sufficiently long lived to participate in destructive photochemistry. The resulting lower photostability compared to canonical nucleobases may have been one of the reasons why isoguanine was not incorporated into DNA and RNA.

1. Introduction

Alternative nucleobases have long been considered as potential components of primordial informational polymers. Studies of their possible role on the Archean Earth were largely inspired by substantial difficulties in designing a prebiotically plausible synthesis of a complete set of canonical RNA nucleosides.¹ This resulted in the consideration of nucleobase analogs which undergo efficient glycosidation, namely triaminopyrimidine and barbituric acid, as potential components of a hypothetical predecessor of RNA.^{2,3} Presence of extraterrestrial nucleobase analogs was also reported in carbon-rich meteorites including examples like 2,6-diaminopurine, 6,8-diaminopurine, hypoxanthine and xanthine.⁴ Other alternative nucleobases as 2-aminopurine and isocytosine (isoC) were found as the products of formamide condensation catalysed by meteoritic materials,⁵⁻⁷ which indicates that these compounds could have been delivered to the surface of our planet or otherwise formed locally from readily available prebiotic precursor molecules. The fact that biology has selected a very narrow alphabet of RNA and DNA building blocks raises the question why the remaining nucleobase analogs never constituted biologically relevant nucleosides and were eradicated during the course of abiogenesis.

Recent estimates of plausible solar input and absorption properties of the terrestrial atmosphere in the prebiotic era indicate that UV light could have been a major (if not dominant) source of energy for primordial prebiotic reactions.^{8,9} In point of fact, canonical DNA and RNA bases and nucleosides are characterized by remarkable photostability which signifies that their analogs might have been eliminated owing to lower resistance to damage from UV light.¹⁰⁻¹² In particular, photostability is manifested by ultrashort excited-state lifetimes and nearly barrierless photorelaxation pathways which have consistently been reported for all the crucial components of RNA and DNA.¹³⁻²⁰ Recent experimental work by Brister *et al.*,²¹ showed that two promising candidates for prebiotic ancestors of RNA bases,

i.e. 2,4,6-triaminopyrimidine and barbituric acid, exhibit sub-picosecond excited-state lifetimes which could protect their chemical integrity in UV-rich environments. In contrast, some alternative nucleobases like 2-aminopurine and 2,6-diaminopurine, exhibit longer excited-state lifetimes which could result in fluorescence and are often sufficient to trigger bimolecular destructive photochemical reactions leading to relatively quick depletion of the starting material.²²⁻²³ Nevertheless, the fates of electronically excited states in many non-biological nucleobases were not examined so far.

Experimental and theoretical efforts in understanding the photochemistry and photophysics of isocytosine (isoC) revealed the existence of relatively efficient radiationless deactivation mechanisms in the enol tautomer and a longer-lived $S_1(n\pi^*)$ state in the keto form.²⁴⁻²⁶ However, the photodynamics of its Watson–Crick (WC) partner isoguanine (isoG) has not been investigated yet. It is worth noting, that isoG, also denoted as 2-hydroxy-adenine can be occasionally present in biological DNA as the product of oxidative damage of adenine.²⁷ When incorporated into DNA, isoG could further pair with cytosine (C) in parallel strand orientation, form $d(T_4\text{-isoG}_4\text{-T}_4)$ tetraplexes, and form anti-parallel strands with isoC by WC base pairing.²⁸ Such WC isoG–isoC base pair was demonstrated to be thermodynamically as stable as the biological G–C WC pair,²⁹⁻³⁰ and was also used for expanding the genetic code and incorporating non-biological amino acid L-iodotyrosine into polypeptides by means of ribosome-based translation.³¹⁻³³ It is important to note that isoG exists in more than one stable tautomeric form, with evident preference for the enol form in apolar environments.³⁴⁻³⁶ This might result in infidelity and might have been one of the reasons why isoG was eventually not utilized by biology.³⁷

In this work, we focused on studying the excited-state dynamics of four different tautomers of isoG in the gas phase from experimental and theoretical perspectives (see Fig.

1). In particular, we investigated the excited-state dynamics of two jet-cooled tautomers of isoG, *i.e.* keto and enol forms. We identified the absorption spectrum with 2-color R2PI, analyzed these tautomers by means of IR-UV hole burning, and performed pump-probe spectroscopic experiments in the picosecond time regime. For the complete interpretation of the experimental results we further performed static explorations of excited-state (S_1) potential energy (PE) surfaces using the algebraic diagrammatic construction to the second order [ADC(2)].³⁸⁻⁴⁰ method and the more accurate n -electron valence state perturbation theory (NEVPT2) approach for these two tautomers.⁴¹⁻⁴³ In addition, we performed analogous electronic structure calculations for two keto and enol tautomers which we did not observe in our gas-phase experiments, but which are representative of isoG in nucleic acid polymers. We also performed surface-hopping nonadiabatic molecular dynamics simulations⁴⁴ for two of the enol tautomers of isoG using the ADC(2) method for electronic structure calculations. Our results indicate that keto tautomers of isoG exhibit excited state properties similar to the keto form of cytosine, which are determined by a long lived $n\pi^*$ excitation,⁴⁵⁻⁵⁰ while the enol tautomers are characterized by more efficient photorelaxation mechanisms dominated by the lowest-lying singlet $\pi\pi^*$ states.

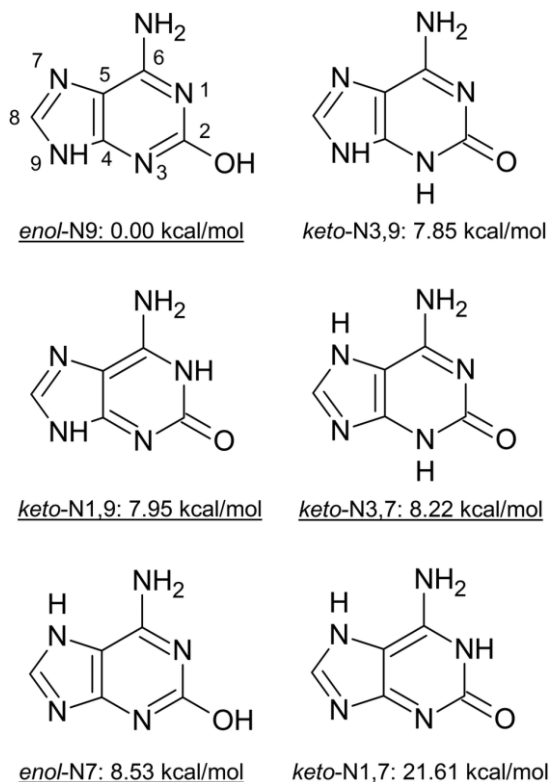


Figure 1. Different tautomeric forms of isoG considered for the initial determination of the experimentally studied tautomers. The relative energies were calculated at the CCSD(T)/def2-TZVPP level of theory. The photodynamics of the underlined tautomers was investigated in this work.

2. Methods

Experimental section

The experimental methods have been described extensively previously,⁵¹ and only a short description follows. In this study, we used laser desorption, jet-cooling coupled with resonance enhanced multi-photon ionization (REMPI). IsoG was placed on a translating graphite bar and desorbed with a focused Nd:YAG pulse (1064 nm, 1 mJ, 8 ns pulsewidth) from a Continuum Minilite II. The desorbed material was entrained in a supersonic jet expansion of argon gas (8 atm backing pressure, 30 μ s pulse width) to achieve jet cooling. The cold, gaseous molecules were resonantly ionized and detected in a reflectron time-of-flight mass spectrometer.

Two-color resonance two-photon ionization (2C-R2PI) is performed using an EKSPLA PL2251 Nd:YAG laser system producing 30 ps pulses. The 355 nm output pumps an optical parametric generator (OPG) (80–120 μJ per pulse) to produce tunable UV pulses, while the unused 1064 nm and 532 nm were combined to harmonically generate 213 nm light (0.3 mJ). The 213 nm pulses were used as the second color for ionization.

IR light was generated in a Laser Vision tunable optical parametric oscillator/optical parametric amplifier (OPO/OPA) (mid-IR output over the range 3200–3800 cm^{-1} of 1–2 mJ per pulse, 3 cm^{-1} spectral line width). For IR-UV double resonance spectroscopy, IR light preceded the ionization pulse by 200 ns. The IR laser was scanned across a target wavelength region, while the following ionization pulse was held at a constant R2PI transition for a given tautomer. Whenever the IR pulse excited a resonant vibrational transition, it burned out the cold ground state of the given tautomer, preventing the resonant transition needed for ionization. A resonant vibrational transition was thus detected as a loss in ion signal. All double resonance spectroscopic experiments were digitally chopped to compare the experimental (burn) signal to background (burn laser fired 800 ns after R2PI lasers) signal, with alternating shots collecting burn and background signal.

Pump–probe experiments were conducted by holding the pump pulse on a resonant R2PI transition. The probe (ionization) pulse, was then walked back in time relative to the pump pulse. In this way, a growing delay occurs between excitation and ionization. This delay allows the excited molecule to decay to different states, and will produce less signal as the delay grows. Pump–probe experiments were conducted in the picosecond (ps) and nanosecond (ns) regime. In the ps regime, the pump pulse was generated from the OPG and tuned to a resonant transition and the probe pulse was the harmonically generated 213 nm. The 213 nm pulse was mechanically delayed up to 1.8 ns. In the ns regime, the pump pulse

was again generated from the OPG, whereas the probe pulse was generated from a GAM excimer laser (193 nm, 1.5–2 mJ per pulse, 8 ns pulsewidth). Pump–probe experiments were conducted in two different time regimes to account for possible faster and slower processes. The method for deriving lifetimes was based on previous work, and described in detail there.⁵² Briefly, lifetimes were derived from the kinetic equations and solving the system of ordinary differential equations. This involved convolving the instrument response function (IRF) with a monoexponential decay function. The IRF was represented by a Gaussian function centered around t_0 .

Computational methods

The minimum-energy ground-state geometries of the enol-N7, enol-N9, keto-N1,9, keto-N3,7, keto-N3,9 and keto-N1,7 tautomers of isoG were optimized with the Kohn–Sham density functional theory (DFT). The two latter tautomers of isoG were not considered in the subsequent excited-state calculations. We applied the B3LYP hybrid functional and B2PLYP double hybrid functional⁵³ for these geometry optimizations. We also performed additional comparative optimizations of the ground-state geometries at the MP2/cc-pVTZ level, which is methodologically consistent with the method [ADC(2)] used for excited-state calculations. The MP2 optimizations yielded virtually identical structures as the two DFT functionals. The geometries obtained with both of the DFT methods were virtually identical and we further performed anharmonic frequency calculations^{54,55} using the B2PLYP functional which was suggested to provide highly accurate vibrational frequencies for small and medium sized organic molecules.⁵⁶ The anharmonic vibrational frequencies computed at the B2PLYP/def2-TZVP level were used for the assignment of the tautomers recorded in our experimental setup. While the harmonic vibrational frequencies calculated at the B2PLYP and B3LYP levels were nearly quantitatively consistent, we used the latter set of results for

the simulations of UV-vis absorption spectra with the ensemble method.⁵⁷ The relative ground-state energies of all the six tautomers were calculated at the CCSD(T)/def2-TZVPP level of theory. Vertical excitation energies, excited-state geometries, UV absorption spectra, energies and gradients in the surface-hopping nonadiabatic dynamics simulations were all computed employing the algebraic diagrammatic construction to the second order [ADC(2)]³⁸⁻⁴⁰ method and the aug-cc-pVDZ correlation consistent basis set. Vertical excitation energies computed with a larger aug-cc-pVTZ basis set can be found in the ESI, for comparison.

The minimum-energy crossing points were optimized using our in-house implementation of the protocol proposed by Levine and co-workers,⁵⁸ coupled with the ADC(2) and MP2 methods for energy and gradient calculations and the Broyden–Fletcher–Goldfarb–Shanno quasi-Newton geometry optimization scheme implemented in the Turbomole 7.2 package.^{59,60} This protocol was recently tested against multireference methods of quantum chemistry and protocols employing explicit calculation of nonadiabatic couplings, and was shown to provide very accurate geometries of $\pi\pi^*/S_0$ conical intersections.^{24,61} We additionally optimized the $n\pi^*/S_0$ conical intersections in the keto tautomers of isoG at the MRCIS(6,5)/cc-pVDZ level because of the highly multireference character of the ground-state electronic wave function at these state crossings, which was also reported previously for keto isoC.²⁴

The PE profiles were prepared by linear interpolation in internal coordinates between the crucial stationary points located for each tautomer, *i.e.* the ground-state geometry, S_1 minimum and the S_1/S_0 conical intersection. Energies of the ground and excited states necessary to construct the PE profiles were calculated at the MP2 and ADC(2) levels respectively. For these PE profiles, we additionally computed NEVPT2⁴¹⁻⁴³ energies on top

of the SA-2-CASSCF(10,9)/cc-pVTZ wave function, in order to test the accuracy of our ADC(2) calculations. The active space used in simulations of all the considered tautomers of isoG comprised of 10 electrons correlated in 9 molecular orbitals, which were selected based on the rules proposed by Veryazov, Malmqvist and Roos.⁶² More precisely, the complete active space (CAS) included orbitals with occupations ranging between 0.02 and 1.98.

We performed the surface-hopping nonadiabatic molecular dynamics simulations using the Tully fewest switches algorithm including the decoherence correction of Granucci and Persico (decoherence parameter was set to 0.1 Hartree). To select the initial conditions we first simulated UV absorption spectra using the nuclear ensemble method,⁵⁷ and generating 600 points for each tautomer based on the Wigner distribution for all vibrational normal modes of the ground-state minimum-energy structures. In the UV absorption spectra simulations we considered 8 lowest-lying excited singlet states, and 4 lowest-lying excited singlet states were considered in the subsequent nonadiabatic molecular dynamics simulations. We simulated 58, 64 and 53 trajectories for the enol-N7, enol-N9 and keto-N1,9 tautomers. These trajectories were initiated in the 4.26 ± 0.05 eV and 4.70 ± 0.05 eV spectral windows in the case of the enol-N7 and enol-N9. The trajectories simulated for the keto-N1,9 form were initiated in the 3.83 ± 0.05 eV spectral window and only the initial stage of the excited-state dynamics of this tautomer was analyzed owing to the incorrect description of the $n\pi^*/S_0$ crossing seam at the ADC(2)/MP2 level. In the case of the enol-N7 tautomer 45 and 13 trajectories were initiated in the S_1 and S_2 states, respectively. 55 and 9 trajectories for the enol-N9 tautomer were simulated from the S_1 and S_2 states, respectively. All of the trajectories simulated for the keto-N1,9 form were initiated in the S_1 state. All the trajectories were terminated when the energy gap between the S_1 and S_0 states dropped below 0.15 eV or otherwise propagated for the maximum time of 500 fs. Therefore,

nonadiabatic transitions were enabled only between electronically excited states. The classical equations for nuclear motion were propagated with the time step of 0.5 fs, while the semi-classical approximation with the time step of 0.025 fs was applied for the propagation of the electronic time-dependent Schrödinger equation. A similar computational protocol was previously applied for the simulations of the photodynamics of adenine and its reliability was confirmed against surface hopping nonadiabatic molecular dynamics simulations.⁶³

The B3LYP geometries and harmonic vibrational frequencies and all the ADC(2) and MP2 calculations were performed with the Turbomole 7.2 program.^{59,60} The B2PLYP geometries, energies and anharmonic vibrational frequencies were computed using the Gaussian09 package.⁶⁴ The NEVPT2 and CCSD(T) calculations were performed with the ORCA 4.0.1 program.⁶⁵ Optimizations of conical intersections at the MRCIS level were carried out using the Columbus 7.0 software.⁶⁶

3. Results and discussion

2C-R2PI spectra

Fig. 2 shows 2C-R2PI spectra (focused) of isoG. We assign the peaks at 30 807 and 34 340 cm^{-1} as the origin transitions of isoguanine amino-keto (a), and amino-enol (b), based on IR-UV burning as detailed below. The lifetimes of the probed peaks are displayed in ps. Crosses mark peaks for which pump–probe measurements were unsuccessful. The origin peaks are separated by approximately 3500 cm^{-1} (0.43 eV). Despite thorough searching to the red and blue, no other features were identified. The spectrum between the 30 800 and 34 300 cm^{-1} region consists of nonresonant signal and is devoid of any indicative features.

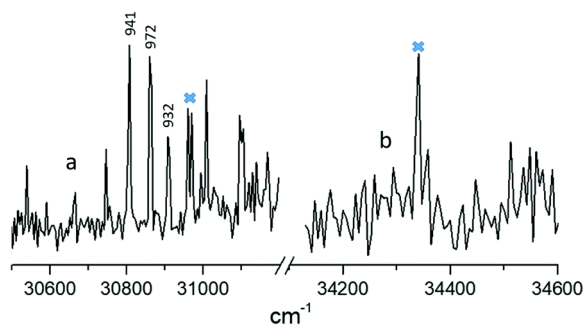


Figure 2. 2C-R2PI spectrum (focused) of isoguanine amino-keto (a), and amino-enol (b). Only one repeatable peak was found for the amino-enol tautomer. The lifetimes of the probed peaks are displayed in ps. Pump–probe was unsuccessfully attempted at peaks with crosses above them, owing to low signal-to-noise ratio.

Structural Determination

To determine the number and types of tautomers observed experimentally, we conducted IR-UV double resonance spectroscopy measurements (Fig. 3). The experimental data are displayed as the negative log of the raw data, probed at 30 807 cm^{-1} (red trace) and 34 340 cm^{-1} (blue trace). Spectra with probe wavelengths set to the other peaks within the 30 800 cm^{-1} region were practically identical and matched the red trace, confirming that all the peaks within this energy region corresponded to the same tautomer. Comparison of these spectra with the anharmonic vibrational frequencies simulated at the B2PLYP/def2-TZVP level, reveals that they could correspond to one of the keto tautomers with the best agreement for the keto-N3,7 tautomer (where the N3 and N7 heteroatoms of the purine ring are bonded to an H atom; see Fig. 1), with differences within 15–20 cm^{-1} . In contrast, differences between the experimental (red trace) and theoretical vibrational frequencies obtained for the remaining keto tautomers are generally larger and exceed 30 cm^{-1} in extreme cases.

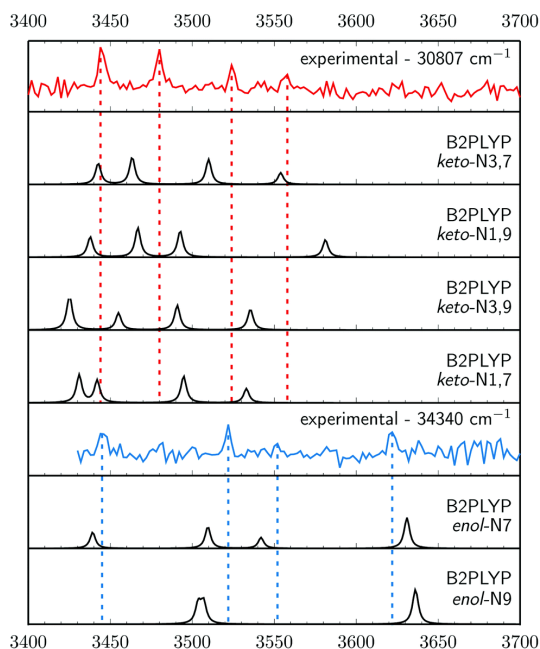


Figure 3. IR-UV hole burning results compared to anharmonic vibrational frequency simulations performed using the B2PLYP/def2-TZVP approach.

The double resonant spectrum recorded with the UV probe wavelength fixed at 34 340 cm⁻¹ (blue trace in Fig. 3) is in excellent agreement with the anharmonic vibrational frequencies simulated for the enol-N7 tautomer (having the N7 heteroatom bonded to a hydrogen atom). The anharmonic frequencies calculated for the enol-N9 tautomer contain two groups of nearly overlapping peaks (two peaks in each group) at ~3505 and ~3638 cm⁻¹ which is very different from the experimentally determined spectral structure of four well-separated peaks. The peak at 3552 cm⁻¹ of the blue trace is close to the S/N limit and we have carefully determined it to be real based on multiple IR scans and averaging of the results, as shown in Fig. S1 (ESI). It is also worth noting, that this assignment is further supported by almost identical vibrational frequencies of the NH stretching modes of the N7H and NH₂ groups in the keto-N3,7 and enol-N7 forms. These groups have very similar molecular environments in the assigned tautomers and such similarities in the IR spectra are thus expected.

According to the tautomer energies computed at the CCSD(T)/def2-TZVPP level of theory (Fig. 1) the assigned keto-N3,7 and enol-N7 structures are among the higher energy tautomeric forms of isoG and we were unable to detect the lower energy tautomers in our experiments, *i.e.* enol-N9, keto-N3,9 and keto-N1,9. However, having detected the higher energy tautomers, we expect that all the lower energy forms should be present in our beam as well. In fact, we cannot predict the plausible distribution of these tautomers, since jet-cooling is a nonequilibrium process. There may be several reasons why the lowest energy tautomers were not detected in our experiments. (1) Laser-desorbed isoG might have been trapped in local minima corresponding to higher energy tautomeric forms during the jet-cooling process, and some of the lower-energy tautomers might not be accessible within the timescales of our measurements. (2) It is likely that some of the tautomers excited with the first photon might not be ionized with the second, for instance when the excited-state lifetime is substantially shorter than the ionizing laser pulse. This behavior is typical for action spectroscopic measurements and was suggested as the reason why low-energy tautomers of guanine were not observed in analogous studies.^{25,67} (3) Some of these tautomers might undergo fragmentation upon photoexcitation which could increase the complexity of the action spectrum, particularly since we focused on monitoring the parent ion mass. However, we did not notice any apparent signs of nonstatistical fragmentation.

It is worth noting that the keto-N1,9 form was observed experimentally to exist in neutral aqueous solution, while the lowest energy enol-N9 tautomer is prevalent in apolar solvents.^{34, 35} In addition, these tautomers are expected as the dominant forms of isoG in a DNA strand,⁶⁸ allowing for wobble base pairing. Therefore, in the subsequent excited-state electronic structure calculations we considered the keto-N3,7 and enol-N7 tautomers

identified above, as well as the keto-N1,9 and enol-N9 tautomers more relevant for aqueous environments and modified DNA strands.

Pump-probe measurements

Fig. 4 shows the pump-probe measurements performed for the tautomers assigned above. The excited-state lifetimes are displayed above the probed peaks in Fig. 2. We were able to probe three peaks for the keto-N3,7 form shown in Fig. 2. Pump probe experiments on other peaks in the spectral region corresponding to this keto tautomer were unsuccessful owing to very low signal-to-noise ratio. Similarly none of the peaks of the enol-N7 tautomer could be probed owing to low signal and lack of two-color enhancement. In fact, low signal and the appearance of a single peak followed by spectral broadening indicates that the enol-N7 tautomer exhibits ultrafast excited state dynamics below the probe resolution of 30 ps. Given that R2PI is action spectroscopy, the molecule may not be ionized efficiently, if the probe pulse is significantly longer than the excited-state lifetime. In contrast, the peaks probed for the keto-N3,7 tautomer exhibited a lifetimes of 941, 972 and 932 ps. Our pump-probe measurements of the keto-N3,7 tautomer in the nanosecond regime yielded a trace that matched the instrument response function (IRF = ~ 8 ns). The IRF provides an upper limit for the lifetime of the probed transition and which signifies no long-lived state with any appreciable yield was populated in the keto-N3,7 form.

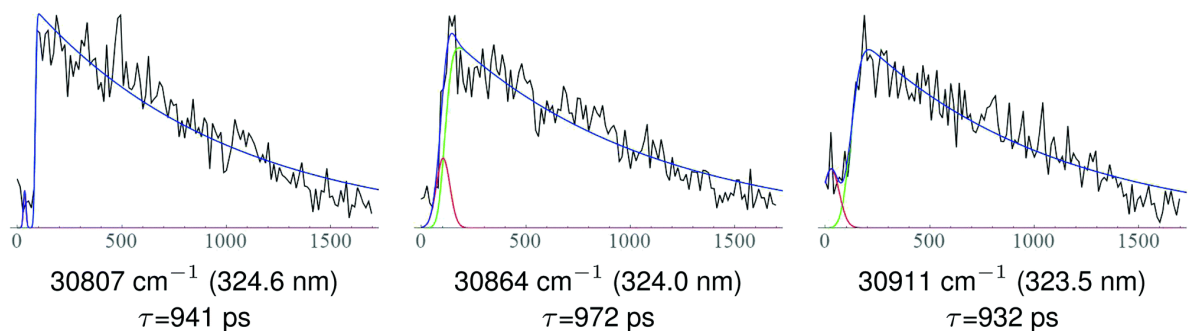


Figure 4. Pump–probe measurements performed on the three peaks assigned to the keto-N3,7 tautomer. The blue curve is a sum of a Gaussian and mono-exponential functions fitted to the data from the pump–probe measurements, where the Gaussian component represents the instrument response function.

Vertical excitation energies and UV-vis spectra

To characterize the photophysical and photochemical properties of isoG in different contexts we performed excited-state calculations for the biologically more relevant keto-N1,9 and enol-N9 tautomers in addition to the keto-N3,7 and enol-N7 tautomers identified in our IR-UV hole burning experiments. The vertical excitation energies of the six lowest excited singlet states calculated using the ADC(2) method on top of the optimized S_0 geometries are shown in Table 1. In the Franck–Condon regions of all the studied tautomers of isoG, the lowest-lying singlet states can be classified as optically bright $\pi\pi^*$ excitations. Similarly to cytosine and isocytosine, the keto-N1,9 and keto-N3,7 tautomers have rather low excitation energies for these $\pi\pi^*$ transitions (3.91 and 4.23 eV) which indicates that they could absorb much longer UV wavelengths than the enol-N7 and enol-N9 forms (4.59 and 4.97 eV). Each of these tautomers also displays higher-energy optically bright $\pi\pi^*$ excitations which could give rise to additional, higher-energy absorption maxima. Furthermore, both the keto tautomers have low-lying $n_O\pi^*$ states which were suggested as important contributors to the photochemistry of nucleobases containing carbonyl groups.^{45, 48, 69} This is particularly evident for the keto-N3,7 tautomer, for which the $n_O\pi^*$ is the S_2 state in the Franck–Condon region and this state might participate in the photorelaxation of this tautomeric form upon UV-excitation. While photorelaxation of enol tautomers of nucleobases is usually dominated by $\pi\pi^*$ states, both the enol-N7 and enol-N9 forms are also characterized by low-lying $n_N\pi^*$ states, which might become important at higher excitation energies.

State/transition		E_{exc} [eV]	f_{osc}	λ [nm]
Keto-N1,9				
S ₁	$\pi\pi^*$	3.91	0.141	317.1
S ₂	$\pi\sigma_{NH}^*$	4.49	2.40×10^{-3}	276.1
S ₃	$n_N\pi^*$	4.96	2.57×10^{-4}	250.0
S ₄	$\pi\sigma_{NH}^*$	4.98	1.78×10^{-4}	249.0
S ₅	$n_O\pi^*$	5.27	2.14×10^{-5}	235.3
S ₆	$\pi\pi^*$	5.36	0.171	231.3
Keto-N3,7				
S ₁	$\pi\pi^*$	4.23	0.162	293.8
S ₂	$\pi\sigma_{NH}^*$	4.62	1.28×10^{-3}	259.9
S ₃	$n_O\pi^*$	4.78	1.52×10^{-3}	256.2
S ₄	$n_N\pi^*$	5.15	2.80×10^{-3}	242.6
S ₅	$\pi\sigma_{NH}^*$	5.46	5.16×10^{-3}	219.1
S ₆	$\pi\pi^*$	5.52	0.100	225.0
Enol-N7				
S ₁	$\pi\pi^*$	4.59	0.141	293.1
S ₂	$\pi\sigma_{NH}^*$	4.75	9.18×10^{-3}	261.0
S ₃	$n_N\pi^*$	4.89	3.02×10^{-3}	253.5
S ₄	$\pi\sigma_{NH}^*$	5.52	1.11×10^{-2}	224.6
S ₅	$\pi\sigma_{NH}^*$	5.60	3.07×10^{-3}	221.4
S ₆	$\pi\pi^*$	5.66	6.46×10^{-2}	219.1
Enol-N9				
S ₁	$\pi\pi^*$	4.97	0.191	249.5
S ₂	$\pi\sigma_{NH}^*$	5.19	5.09×10^{-3}	238.9
S ₃	$n_N\pi^*$	5.40	1.39×10^{-3}	229.6
S ₄	$\pi\pi^*$	5.47	0.106	226.7
S ₅	$\pi\sigma_{NH}^*$	5.52	3.17×10^{-3}	224.6
S ₆	$n_N\pi^*$	5.88	7.09×10^{-3}	210.9

Table 1. Vertical excitation energies (in eV) of the four considered tautomers of isoG, computed using the ADC(2)/aug-cc-pVDZ method, assuming the ground-state minimum energy structures optimized at the B3LYP/def2-TZVPP level

The UV-absorption spectra simulated using the molecular ensemble method essentially reflect the implications inferred from the analyses of vertical excitations energies (see Fig. 5). Consequently, the onset of the absorption of the two keto tautomers can be observed at approximately 3.2 eV (387.4 nm), which is 0.7 eV lower than for the enol-N7 tautomer. This difference in absorption energies between the keto and enol-N7 is also consistent with the assigned origin transitions in the 2C-R2PI spectra. The enol-N9 tautomer, not observed in our beam absorbs at even higher UV energies, *i.e.* above 4.2 eV (295 nm). Therefore the keto tautomers of isoG absorb at much longer wavelengths than biologically relevant keto

guanine (G), within the UV-A range which is much less efficiently shielded by various atmospheric components and was most likely highly abundant on the Archean Earth. Consequently, if present on the early Earth's surface, isoG would be a better UV absorber than the canonical nucleobases and more prone to deleterious photochemistry in the absence of efficient photodeactivation pathways. As indicated by the shaded areas in Fig. 5, the pump pulses sampled the lower energy bands of the UV-absorption spectra of both keto-N3,7 and enol-N7 forms. Such low-energy excitation predominantly populates the lowest-lying singlet states in each of these tautomers (bright $\pi\pi^*$ states). Consequently, we anticipate that the excited-state dynamics of isoG within the experimental setup will be dominated by the S1 state with a very limited and temporary contribution from higher excitations.

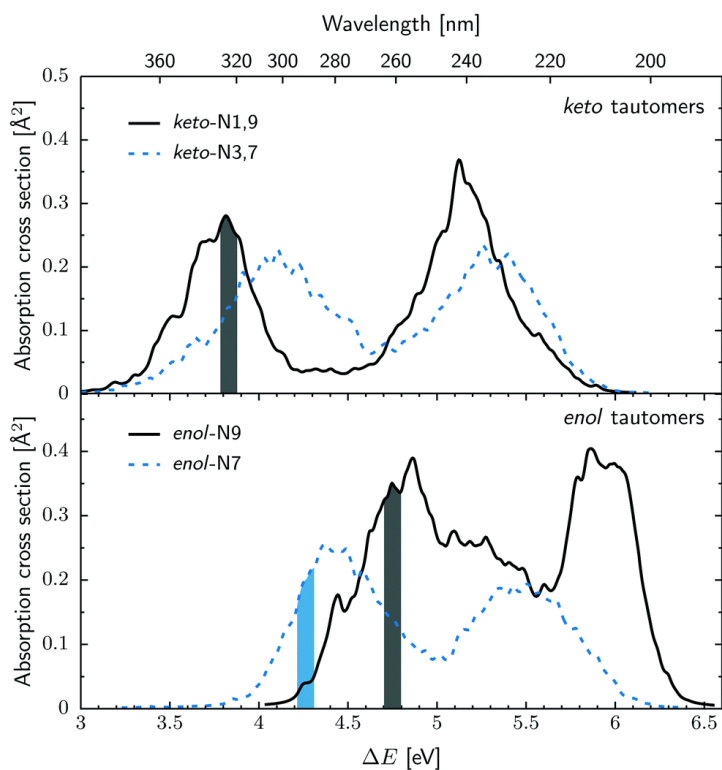


Figure 5. UV absorption spectra simulated at the ADC(2)/aug-cc-pVDZ method using the nuclear ensemble method.⁵⁷

Minimum energy geometries located in the S₁ state in each of the studied tautomers of isoG using the ADC(2)/aug-cc-pVDZ method

The ADC(2)-optimized minimum-energy geometries of the keto and enol tautomers in their lowest excited singlet states reveal further interesting details of their photochemistry (see Fig. 6). In particular, the S₁ minima of the keto-N1,9 and keto-N3,7 forms have both n_Oπ* character. Therefore, these geometries are characterized by slight pyramidalization of the C6 carbon atoms leading to an out-of-plane tilt of the amino groups and elongation of the C2=O bonds by ~0.18 Å when compared to the ground-state geometries, *i.e.* up to 1.39 and 1.40 Å for keto-N1,9 and keto-N3,7 respectively. Geometrically similar S₁(n_Oπ*) minima were also reported for the keto tautomers of C, G and isoC.^{24, 45-47, 50, 70} However, surface-hopping nonadiabatic molecular dynamics simulations executed for G showed that this local minimum is sampled by sparse trajectories and the prevalent photodeactivation channel drives keto-G towards the ππ*/S₀ conical intersection.⁷⁰ Our direct optimization of the S₁ minimum of keto-G initiated from the S₀ geometry also did not stabilize the n_Oπ* state, whereas the same optimization procedure returned the S₁(n_Oπ*) minima for both of the studied keto tautomers of isoG. This result indicates that the dark n_Oπ* states might have a much more significant contribution to the photorelaxation of the keto-N1,9 and keto-N3,7 tautomers of isoG as compared to canonical G.

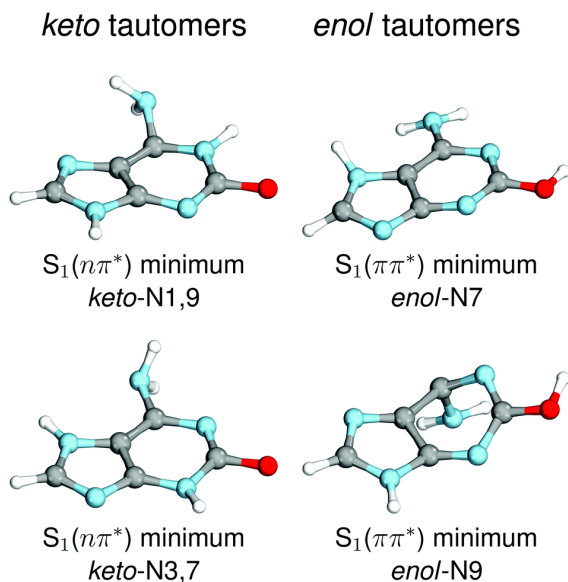


Figure 6. Minimum-energy geometries of the studied tautomers of isoG optimized at the ADC(2)/aug-cc-pVDZ level of theory.

Previous investigations of the photochemistry of keto isoC and thiocytosine revealed potential pitfalls of the ADC(2) approach in describing the low-lying $nO\pi^*$ state outside the Franck–Condon region.^{24, 71} In particular, ADC(2) incorrectly predicted the topography of the $nO\pi^*$ surface between S_1 and the corresponding conical intersection with the ground-state, owing to the multireference character of the electronic ground state for these geometries.²⁴ Therefore, we reoptimized the $S_1(nO\pi^*)$ minima of the keto-N1,9 and keto-N3,7 tautomers at the MRCIS(6,5) level and calculated NEVPT2/SA-CASSCF(10,9) energies to verify whether a similar behavior can be found in isoG. The MRCIS minimum energy geometries optimized for the $S_1(nO\pi^*)$ state were qualitatively consistent with the outcome of ADC(2) calculations (including the extent of ring-puckering and out-of-plane tilting visible in Fig. 6). Nevertheless, we observed an essential difference in the C2=O bond lengths, which were shorter by approximately 0.11 and 0.08 Å in the case of the S_1 optimized for the keto-N1,9 and keto-N3,7 tautomers at the MRCIS level. Furthermore, the S_1 – S_0 energy gap computed at the ADC(2) level for the respective $S_1(nO\pi^*)$ minima

amounts to 0.85 and 1.11 eV, whereas the same quantity calculated with NEVPT2 on top of MRCIS-optimized S_1 minima amounts to 2.92 and 2.68 eV for the keto-N1,9 and keto-N3,7 forms, respectively. These findings indicate that ADC(2) might be an inappropriate method for the description of $n\sigma\pi^*$ states of isoG already in the vicinity of the corresponding S_1 minima.

The excited-state geometry optimizations carried out for the enol-N7 and enol-N9 tautomers returned S_1 minima associated with the optically bright $\pi\pi^*$ states. In the case of the enol-N7 tautomer the associated virtual π^* molecular orbital has the highest contribution residing on the five-membered imidazole ring. This is reflected by the geometrical changes associated with N7–C8 bond elongation and out-of-plane tilting of the N7–H and C8–H bonds. The vertical S_1 – S_0 energy gap at this geometry amounts to 3.12 eV, which indicates that this S_1 minimum is separated from the nearby S_1/S_0 conical intersections by an energy barrier and the enol-N7 tautomer might not exhibit ultrafast excited-state photodeactivation.

In contrast, the geometry in the S_1 minimum of the enol-N9 tautomer is associated with substantial puckering of the pyrimidine ring, which originates from the associated virtual π^* molecular orbital located in this part of the molecule. Significant elongation of the C5–C6 bond from 1.41 to 1.51 Å demonstrates that this S_1 should be situated close to a typical ethylenic conical intersection also observed in C and isoC.^{24,45} However, unlike the analogous ring-puckered S_1 geometries reported for enol tautomers of C and isoC, the S_1 minimum of enol-N9 practically coincides with the $S_1(\pi\pi^*)/S_0$ conical intersection ($\Delta E_{S_1-S_0} = 0.03$ eV at the ADC(2) level of theory; consistent with NEVPT2 calculations). Good semi-quantitative agreement between the NEVPT2 and ADC(2) results indicate that the ADC(2)

method should provide a correct description of excited-state dynamics for the enol tautomers of isoG.

Supplemental Information

Vibration type	Theory (anharmonic) [cm ⁻¹]
<i>keto-N3,7</i>	
symmetric NH ₂ stretching (amino group)	3443
N3H stretching	3463
N7H stretching	3510
symmetric NH ₂ stretching (amino group)	3554
<i>keto-N1,9</i>	
symmetric NH ₂ stretching (amino group)	3438
N1H stretching	3467
N9H stretching	3493
asymmetric NH ₂ stretching (amino group)	3581
<i>keto-N3,9</i>	
symmetric NH ₂ stretching (amino group)	3425
N3H stretching	3455
N9H stretching	3491
asymmetric NH ₂ stretching (amino group)	3535
<i>keto-N1,7</i>	
symmetric NH ₂ stretching (amino group)	3431
N1H stretching	3442
N7H stretching	3495
asymmetric NH ₂ stretching (amino group)	3533
<i>enol-N7</i>	
symmetric NH ₂ stretching (amino group)	3439
N7H stretching	3510
asymmetric NH ₂ stretching (amino group)	3542
OH stretching	3631
<i>keto-N9</i>	
symmetric NH ₂ stretching (amino group)	3504
N9H stretching	3507
asymmetric NH ₂ stretching (amino group)	3636
OH stretching	3637

Table S1. The key (anharmonic) vibrational frequencies in the spectral region tracked in the IR-UV hole burning experiments obtained at the B2PLYP/def2-TZVP level.

State / Transition	$E_{\text{exc}}/[\text{eV}]$	f_{osc}	$\lambda/[\text{nm}]$	
<i>keto-N1,9</i>				
S ₁	$\pi\pi^*$	3.89	0.142	318.7
S ₂	$\pi\sigma_{NH}^*$	4.71	$2.23 \cdot 10^{-3}$	263.2
S ₃	$n_N\pi^*$	4.93	$2.27 \cdot 10^{-4}$	251.5
S ₄	$\pi\sigma_{NH}^*$	5.20	$1.78 \cdot 10^{-4}$	238.4
S ₅	$n_O\pi^*$	5.24	$3.94 \cdot 10^{-5}$	236.6
S ₆	$\pi\pi^*$	5.35	0.176	231.7
<i>keto-N3,7</i>				
S ₁	$\pi\pi^*$	4.22	0.162	293.8
S ₂	$n_O\pi^*$	4.77	$1.53 \cdot 10^{-3}$	259.9
S ₃	$\pi\sigma_{NH}^*$	4.84	$1.16 \cdot 10^{-3}$	256.2
S ₄	$n_N\pi^*$	5.11	$2.42 \cdot 10^{-3}$	242.6
S ₅	$\pi\pi^*$	5.51	0.145	225.0
S ₆	$\pi\sigma_{NH}^*$	5.66	$2.80 \cdot 10^{-3}$	219.1
<i>enol-N7</i>				
S ₁	$\pi\pi^*$	4.57	0.144	271.3
S ₂	$n_N\pi^*$	4.84	$2.94 \cdot 10^{-3}$	256.2
S ₃	$\pi\sigma_{NH}^*$	4.97	$5.46 \cdot 10^{-3}$	249.5
S ₄	$\pi\pi^*$	5.62	$6.21 \cdot 10^{-2}$	220.6
S ₅	$n\sigma_{NH}^*$	5.71	$1.52 \cdot 10^{-2}$	217.1
S ₆	$\pi\sigma_{OH}^*$	5.81	$1.22 \cdot 10^{-3}$	213.4
<i>enol-N9</i>				
S ₁	$\pi\pi^*$	4.94	0.188	251.0
S ₂	$n_N\pi^*$	5.35	$2.52 \cdot 10^{-3}$	231.7
S ₃	$\pi\sigma_{NH}^*$	5.39	$3.45 \cdot 10^{-3}$	230.0
S ₄	$\pi\pi^*$	5.45	0.113	227.5
S ₅	$\pi\sigma_{NH}^*$	5.73	$7.36 \cdot 10^{-4}$	216.4
S ₆	$n_N\pi^*$	6.07	$1.06 \cdot 10^{-3}$	204.3

Table S2 Vertical excitation energies (in eV) of the four considered tautomers of isoG, computed using the ADC(2)/aug-cc-pVTZ method, assuming the ground-state minimum energy structures optimized at the B3LYP/def2-TZVPP level.

State / Transition	$E_{exc}/[eV]$	f_{osc}	$\lambda/[nm]$	
<i>keto-N1,9</i>				
S ₁	$\pi\pi^*$	3.84	0.138	322.9
S ₂	$\pi\sigma_{NH}^*$	4.71	$2.15 \cdot 10^{-3}$	263.2
S ₃	$n_N\pi^*$	4.89	$3.26 \cdot 10^{-4}$	253.5
S ₄	$\pi\sigma_{NH}^*$	5.20	$2.65 \cdot 10^{-4}$	238.4
S ₅	$n_O\pi^*$	5.22	$6.39 \cdot 10^{-5}$	237.5
S ₆	$\pi\pi^*$	5.31	0.181	233.5
<i>keto-N3,7</i>				
S ₁	$\pi\pi^*$	4.22	0.169	293.8
S ₂	$n_O\pi^*$	4.74	$2.05 \cdot 10^{-3}$	261.6
S ₃	$\pi\sigma_{NH}^*$	4.88	$1.23 \cdot 10^{-3}$	254.1
S ₄	$n_N\pi^*$	5.11	$2.66 \cdot 10^{-3}$	242.6
S ₅	$\pi\pi^*$	5.55	0.104	223.4
S ₆	$\pi\sigma_{NH}^*$	5.66	$3.16 \cdot 10^{-3}$	219.1
<i>enol-N7</i>				
S ₁	$\pi\pi^*$	4.56	0.145	275.5
S ₂	$n_N\pi^*$	4.86	$2.83 \cdot 10^{-3}$	255.1
S ₃	$\pi\sigma_{NH}^*$	5.03	$4.98 \cdot 10^{-3}$	246.5
S ₄	$\pi\pi^*$	5.63	$6.38 \cdot 10^{-2}$	220.2
S ₅	$n\sigma_{NH}^*$	5.79	$1.15 \cdot 10^{-2}$	214.1
S ₆	$\pi\sigma_{OH}^*$	5.81	$5.04 \cdot 10^{-3}$	213.4
<i>enol-N9</i>				
S ₁	$\pi\pi^*$	4.90	0.188	253.0
S ₂	$n_N\pi^*$	5.36	$2.69 \cdot 10^{-3}$	231.3
S ₃	$\pi\sigma_{NH}^*$	5.41	$4.26 \cdot 10^{-3}$	229.2
S ₄	$\pi\pi^*$	5.45	0.110	227.5
S ₅	$\pi\sigma_{NH}^*$	5.76	$2.10 \cdot 10^{-3}$	215.3
S ₆	$\pi\sigma^*$	6.11	$1.36 \cdot 10^{-2}$	202.9
S ₇	$n_N\pi^*$	6.12	$7.79 \cdot 10^{-3}$	202.6

Table S3 Vertical excitation energies (in eV) of the four considered tautomers of isoG, computed using the ADC(2)/aug-cc-pVTZ method, assuming the ground-state minimum energy structures optimized at the MP2/cc-pVTZ level.

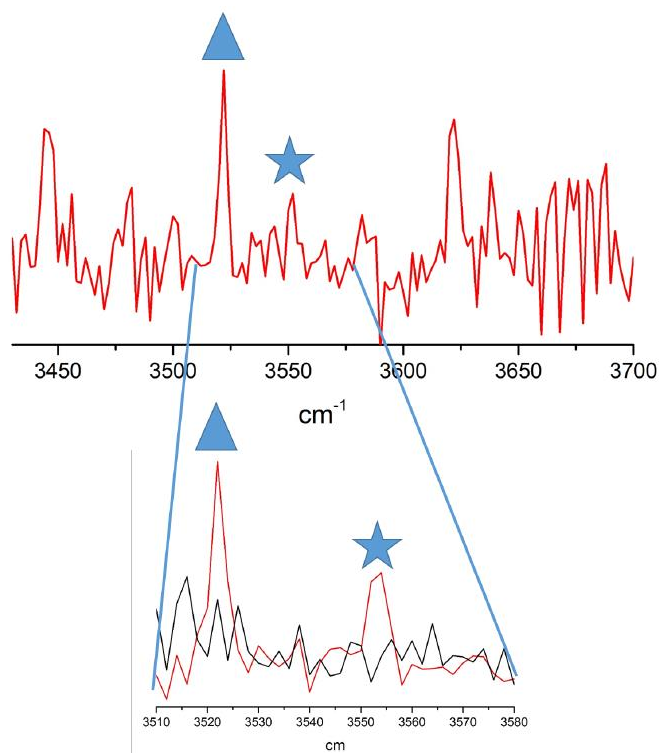


Figure S1. Rescaled experimental data of the right spectrum of figure 2 (IR-UV double resonance spectrum probing at $34\,340\text{ cm}^{-1}$). Red trace is burn signal and black is background signal. The peak marked by the triangle is at 3522 cm^{-1} and the peak marked by the star is at 3552 cm^{-1} . The inset displays the same experimental data, with the background signal displayed as well. This result demonstrates that the signal at 3552 cm^{-1} for the enol-N7 tautomer is a real peak.

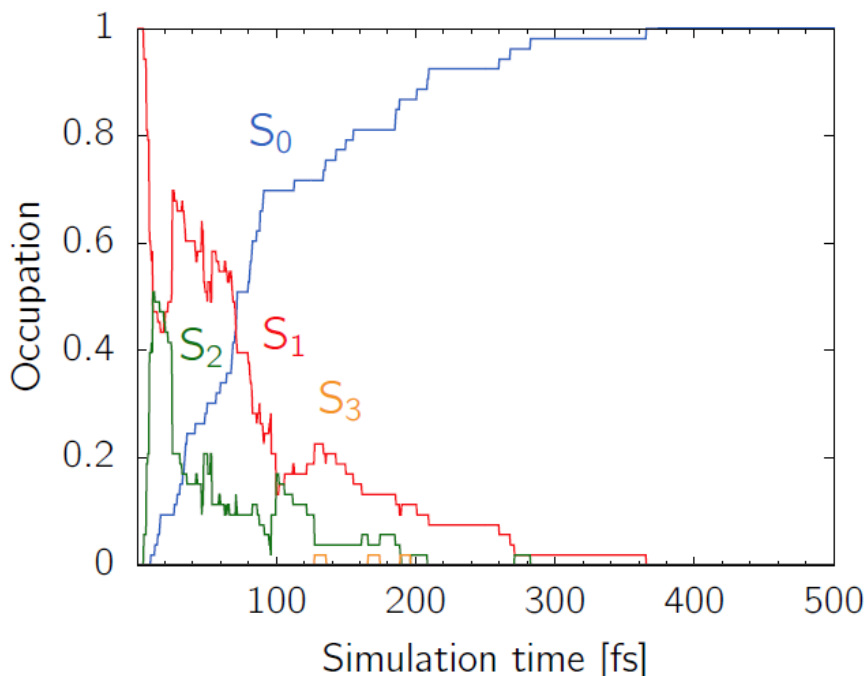


Figure S2. Adiabatic populations of electronic states extracted from nonadiabatic molecular dynamics simulations performed for the keto-N1,9 tautomer. Very fast recovery of the electronic ground state is assigned here to the incorrect description of the topography of the $S_1(n\pi^*)/S_0$ state crossing in this particular tautomer (see the main article for more information).

References

1. L. E. Orgel, *Crit. Rev. Biochem. Mol. Biol.*, 2004, **39**, 99–123
2. B. J. Cafferty, I. Gállego, M. C. Chen, K. I. Farley, R. Eritja and N. V. Hud, *J. Am. Chem. Soc.*, 2013, **135**, 2447–2450
3. B. J. Cafferty and N. V. Hud, *Isr. J. Chem.*, 2015, **55**, 891–905
4. M. P. Callahan, K. E. Smith, H. J. Cleaves, J. Ruzicka, J. C. Stern, D. P. Glavin, C. H. House and J. P. Dworkin, *Proc. Natl. Acad. Sci. U. S. A.*, 2011, **108**, 13995–13998
5. R. Saladino, V. Neri, C. Crestini, G. Costanzo, M. Graciotti and E. Di Mauro, *J. Am. Chem. Soc.*, 2008, **130**, 15512–15518
6. R. Saladino, C. Crestini, C. Cossetti, E. Di Mauro and D. Deamer, *Origins Life Evol. Biospheres*, 2011, **41**, 437–451
7. R. Saladino, G. Botta, M. Delfino and E. Di Mauro, *Chem. – Eur. J.*, 2013, **19**, 16916–16922
8. S. Ranjan and D. D. Sasselov, *Astrobiology*, 2016, **16**, 68–88
9. S. Ranjan and D. D. Sasselov, *Astrobiology*, 2017, **17**, 169–204
10. S. Boldissar and M. S. d. Vries, *Phys. Chem. Chem. Phys.*, 2018, **20**, 9701–9716
11. R. J. Rapf and V. Vaida, *Phys. Chem. Chem. Phys.*, 2016, **18**, 20067–20084

12. A. A. Beckstead, Y. Zhang, M. S. d. Vries and B. Kohler, *Phys. Chem. Chem. Phys.*, 2016, **18**, 24228–24238
13. D. Tuna, A. L. Sobolewski and W. Domcke, *J. Phys. Chem. A*, 2014, **118**, 122–127
14. D. Tuna, A. L. Sobolewski and W. Domcke, *J. Phys. Chem. B*, 2016, **120**, 10729–10735
15. A. L. Sobolewski and W. Domcke, *Europhys. News*, 2006, **37**, 20–23
16. C. T. Middleton, K. d. L. Harpe, C. Su, Y. K. Law, C. E. Crespo-Hernández and B. Kohler, *Annu. Rev. Phys. Chem.*, 2009, **60**, 217–239
17. S. D. Camillis, J. Miles, G. Alexander, O. Ghafur, I. D. Williams, D. Townsend and J. B. Greenwood, *Phys. Chem. Chem. Phys.*, 2015, **17**, 23643–23650
18. H. Satzger, D. Townsend, M. Z. Zgierski, S. Patchkovskii, S. Ullrich and A. Stolow, *PNAS*, 2006, **103**, 10196–10201
19. A. Abo-Riziq, L. Grace, E. Nir, M. Kabelac, P. Hobza and M. S. d. Vries, *PNAS*, 2005, **102**, 20–23
20. A. L. Sobolewski, W. Domcke and C. Hättig, *Proc. Natl. Acad. Sci. U. S. A.*, 2005, **102**, 17903–17906
21. M. M. Brister, M. Pollum and C. E. Crespo-Hernández, *Phys. Chem. Chem. Phys.*, 2016, **18**, 20097–20103
22. S. Lobsiger, S. Blaser, R. K. Sinha, H.-M. Frey and S. Leutwyler, *Nat. Chem.*, 2014, **6**, 989–993
23. Z. Gengeliczki, M. P. Callahan, N. Svadlenak, C. I. Pongor, B. Sztáray, L. Meerts, D. Nachtigallová, P. Hobza, M. Barbatti, H. Lischka and M. S. d. Vries, *Phys. Chem. Chem. Phys.*, 2010, **12**, 5375–5388
24. R. Szabla, R. W. Góra and J. Šponer, *Phys. Chem. Chem. Phys.*, 2016, **18**, 20208–20218
25. J. A. Berenbeim, S. Boldissar, F. M. Siouri, G. Gate, M. R. Haggmark, B. Aboulache, T. Cohen and M. S. de Vries, *J. Phys. Chem. Lett.*, 2017, **8**, 5184–5189
26. D. Hu, Y. F. Liu, A. L. Sobolewski and Z. Lan, *Phys. Chem. Chem. Phys.*, 2017, **19**, 19168–19177
27. H. Kamiya, *Nucleic Acids Res.*, 2003, **31**, 517–531
28. F. Seela and C. Wei, *Helv. Chim. Acta*, 1997, **80**, 73–85
29. C. Roberts, R. Bandaru and C. Switzer, *J. Am. Chem. Soc.*, 1997, **119**, 4640–4649
30. X. L. Yang, H. Sugiyama, S. Ikeda, I. Saito and A. H. Wang, *Biophys. J.*, 1998, **75**, 1163–1171
31. J. D. Bain, C. Switzer, R. Chamberlin and S. A. Benner, *Nature*, 1992, **356**, 537–539
32. S. Hoshika, N. A. Leal, M.-J. Kim, M.-S. Kim, N. B. Karalkar, H.-J. Kim, A. M. Bates, N. E. Watkins, H. A. SantaLucia, A. J. Meyer, S. DasGupta, J. A. Piccirilli, A. D. Ellington, J. SantaLucia, M. M. Georgiadis and S. A. Benner, *Science*, 2019, **363**, 884–887

33. O. Bande, R. Abu El Asrar, D. Braddick, S. Dumbre, V. Pezo, G. Schepers, V. B. Pinheiro, E. Lescrinier, P. Holliger, P. Marlière and P. Herdewijn, *Chem. – Eur. J.*, 2015, **21**, 5009–5022
34. F. Seela, C. Wei and Z. Kazimierczuk, *Helv. Chim. Acta*, 1995, **78**, 1843–1854
35. J. Sepioł, Z. Kazimierczuk and D. Shugar, *Z. Naturforsch. C*, 2014, **31**, 361–370
36. N. B. Karalkar, K. Khare, R. Molt and S. A. Benner, *Nucleosides, Nucleotides Nucleic Acids*, 2017, **36**, 256–274
37. A. Jaworski, J. S. Kwiatkowski and B. Lesyng, *Int. J. Quantum Chem.*, 1985, **28**, 209–216
38. A. B. Trofimov and J. Schirmer, *J. Phys. B: At., Mol. Opt. Phys.*, 1995, **28**, 2299
39. C. Hättig, *Advances in Quantum Chemistry*, Academic Press, 2005, vol. 50, pp. 37–60
40. A. Dreuw and M. Wormit, *Wiley Interdiscip. Rev.: Comput. Mol. Sci.*, 2015, **5**, 82–95
41. C. Angeli, R. Cimiraglia, S. Evangelisti, T. Leininger and J.-P. Malrieu, *J. Chem. Phys.*, 2001, **114**, 10252–10264
42. C. Angeli, R. Cimiraglia and J.-P. Malrieu, *J. Chem. Phys.*, 2002, **117**, 9138–9153
43. C. Angeli, R. Cimiraglia and J.-P. Malrieu, *Chem. Phys. Lett.*, 2001, **350**, 297–305
44. R. Crespo-Otero and M. Barbatti, *Chem. Rev.*, 2018, **118**, 7026–7068
45. M. Barbatti, A. J. A. Aquino, J. J. Szymczak, D. Nachtigallova and H. Lischka, *Phys. Chem. Chem. Phys.*, 2011, **13**, 6145–6155
46. M. Richter, P. Marquetand, J. González-Vázquez, I. Sola and L. González, *J. Phys. Chem. Lett.*, 2012, **3**, 3090–3095
47. S. Mai, P. Marquetand, M. Richter, J. González-Vázquez and L. González, *ChemPhysChem*, 2013, **14**, 2920–2931
48. P. M. Hare, C. E. Crespo-Hernández and B. Kohler, *Proc. Natl. Acad. Sci. U. S. A.*, 2007, **104**, 435–440
49. R. Szabla, H. Kruse, J. Šponer and R. W. Góra, *Phys. Chem. Chem. Phys.*, 2017, **19**, 17531–17537
50. A. J. Pepino, J. Segarra-Martí, A. Nenov, I. Rivalta, R. Improta and M. Garavelli, *Phys. Chem. Chem. Phys.*, 2018, **20**, 6877–6890
51. G. Meijer, M. S. de Vries, H. E. Hunziker and H. R. Wendt, *Appl. Phys. B*, 1990, **51**, 395–403
52. F. M. Siouri, S. Boldissar, J. A. Berenbeim and M. S. de Vries, *J. Phys. Chem. A*, 2017, **121**, 5257–5266
53. S. Grimme, *J. Chem. Phys.*, 2006, **124**, 034108
54. V. Barone, *J. Chem. Phys.*, 2004, **122**, 014108
55. J. Bloino, *J. Phys. Chem. A*, 2015, **119**, 5269–5287
56. M. Biczysko, P. Panek, G. Scalmani, J. Bloino and V. Barone, *J. Chem. Theory Comput.*, 2010, **6**, 2115–2125
57. R. Crespo-Otero and M. Barbatti, *Theor. Chem. Acc.*, 2012, **131**, 1–14
58. B. G. Levine, J. D. Coe and T. J. Martínez, *J. Phys. Chem. B*, 2008, **112**, 405–413

59. R. Ahlrichs, M. Bär, M. Häser, H. Horn and C. Kölmel, *Chem. Phys. Lett.*, 1989, **162**, 165–169
60. *TURBOMOLE V7.0 2015, a development of University of Karlsruhe and Forschungszentrum Karlsruhe GmbH, 1989–2007, TURBOMOLE GmbH, since 2007*, available from <http://www.turbomole.com>
61. D. Tuna, D. Lefrancois, Ł. Wolański, S. Gozem, I. Schapiro, T. Andruniów, A. Dreuw and M. Olivucci, *J. Chem. Theory Comput.*, 2015, **11**, 5758–5781
62. V. Veryazov, P. Å. Malmqvist and B. O. Roos, *Int. J. Quantum Chem.*, 2011, **111**, 3329–3338
63. F. Plasser, R. Crespo-Otero, M. Pederzoli, J. Pittner, H. Lischka and M. Barbatti, *J. Chem. Theory Comput.*, 2014, **10**, 1395–1405
64. M. J. Frisch, G. W. Trucks, H. B. Schlegel, G. E. Scuseria, M. A. Robb, J. R. Cheeseman, G. Scalmani, V. Barone, B. Mennucci, G. A. Petersson, H. Nakatsuji, M. Caricato, X. Li, H. P. Hratchian, A. F. Izmaylov, J. Bloino, G. Zheng, J. L. Sonnenberg, M. Hada, M. Ehara, K. Toyota, R. Fukuda, J. Hasegawa, M. Ishida, T. Nakajima, Y. Honda, O. Kitao, H. Nakai, T. Vreven, J. Montgomery, J. E. Peralta, F. Ogliaro, M. Bearpark, J. J. Heyd, E. Brothers, K. N. Kudin, V. N. Staroverov, R. Kobayashi, J. Normand, K. Raghavachari, A. Rendell, J. C. Burant, S. S. Iyengar, J. Tomasi, M. Cossi, N. Rega, J. M. Millam, M. Klene, J. E. Knox, J. B. Cross, V. Bakken, C. Adamo, J. Jaramillo, R. Gomperts, R. E. Stratmann, O. Yazyev, A. J. Austin, R. Cammi, C. Pomelli, J. W. Ochterski, R. L. Martin, K. Morokuma, V. G. Zakrzewski, G. A. Voth, P. Salvador, J. J. Dannenberg, S. Dapprich, A. D. Daniels, O. Farkas, J. B. Foresman, J. V. Ortiz, J. Cioslowski and D. J. Fox, *Gaussian 09, revision C.01*, Gaussian Inc., Wallingford CT, 2009
65. F. Neese, *Wiley Interdiscip. Rev.: Comput. Mol. Sci.*, 2012, **2**, 73–78
66. H. Lischka, R. Shepard, I. Shavitt, R. M. Pitzer, M. Dallos, T. Müller, P. G. Szalay, F. B. Brown, R. Ahlrichs, H. J. Böhm, A. Chang, D. C. Comeau, R. Gdanitz, H. Dachsel, C. Ehrhardt, M. Ernzerhof, P. Höchtl, S. Irle, G. Kedziora, T. Kovar, V. Parasuk, M. J. M. Pepper, P. Scharf, H. Schiffer, M. Schindler, M. Schüler, M. Seth, E. A. Stahlberg, J.-G. Zhao, S. Yabushita, Z. Zhang, M. Barbatti, S. Matsika, M. Schuurmann, D. R. Yarkony, S. R. Brozell, E. V. Beck, J.-P. Blaudeau, M. Ruckebauer, B. Sellner, F. Plasser and J. J. Szymczak, *Columbus, Release 7.0 2012, an Ab Initio Electronic Structure Program*, 2012
67. M. Y. Choi and R. E. Miller, *J. Am. Chem. Soc.*, 2006, **128**, 7320–7328
68. H. Robinson, Y.-G. Gao, C. Bauer, C. Roberts, C. Switzer and A. H.-J. Wang, *Biochemistry*, 1998, **37**, 10897–10905
69. R. Szabla, J. Campos, J. E. Šponer, J. Šponer, R. W. Góra and J. D. Sutherland, *Chem. Sci.*, 2015, **6**, 2035–2043
70. M. Barbatti, J. J. Szymczak, A. J. A. Aquino, D. Nachtigallová and H. Lischka, *J. Chem. Phys.*, 2011, **134**, 014304
71. M. J. Janicki, R. Szabla, J. Šponer and R. W. Góra, *Chem. Phys.*, 2018, **515**, 502–508

72. F. Plasser, S. Gómez, M. F. S. J. Menger, S. Mai and L. González, *Phys. Chem. Chem. Phys.*, 2019, **21**, 57–69
73. A. L. Sobolewski, W. Domcke, C. Dedonder-Lardeux and C. Jouvet, *Phys. Chem. Chem. Phys.*, 2002, **4**, 1093–1100
74. M. Z. Zgierski, T. Fujiwara, W. G. Kofron and E. C. Lim, *Phys. Chem. Chem. Phys.*, 2007, **9**, 3206–3209
75. M. A. Trachsel, S. Lobsiger, T. Schär, L. Blancafort and S. Leutwyler, *J. Chem. Phys.*, 2017, **146**, 244308

III. The tautomer-specific excited state dynamics of 2,6-diaminopurine using REMPI and quantum calculations

Gregory Gate^a, Ann Williams^a, Samuel Boldissar^a, Rafal Szabla^b, Mattanjah de Vries^a

^a Department of Chemistry and Biochemistry, University of California Santa Barbara, CA 93106

^b Department of Chemistry, University of Edinburgh

1. Introduction

The current understanding of the photochemistry of the canonical nucleobases is that they are very photostable thanks to rapid internal conversion to the ground state. This process efficiently converts electronic excitation to heat that can be safely dissipated.¹⁻⁸ Excited state lifetimes of the order of single picoseconds or less protect life's genetic code from possible photochemical damage. By contrast, many derivatives, isomers, and analogues of the canonical nucleobases have much longer excited state lifetimes, with competing and potentially hazardous photochemical pathways. These excited state dynamics are a subtle function of molecular structure.⁹ Generally, it appears that the heterosubstituted purines (guanine and isoguanine¹⁰) are more photostable than the homosubstituted purines (2,6-dAP and xanthine). Further, singly substituted purines (adenine, 2AP, 2-oxopurine, and hypoxanthine) are more photostable than doubly substituted purines, with the possible exception of guanine.

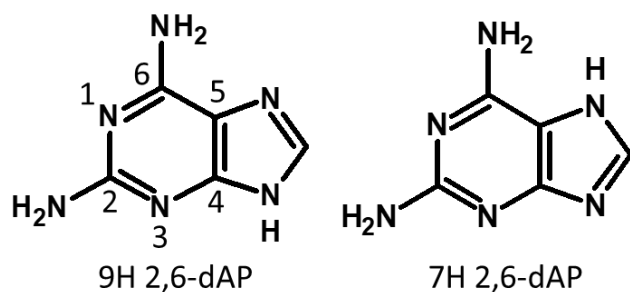
However, these general trends tend to oversimplify the structure dependence on photostability. First, one should consider the role of the solvent as the dynamics in solution and the gas may sometimes differ. A well-known example of this structure dependence is the difference between adenine, which is 6-aminopurine, and its isomer 2-aminopurine (2AP). 2AP has a strong fluorescence signature when in aqueous solution, while adenine does not. Adenine in the gas phase has a lifetime in the single picoseconds or less depending on the exact measurement technique, with similar lifetimes in solution.^{5, 11-14} In the gas phase, adenine exists almost exclusively as the lowest-energy 9H tautomer¹¹, while in solution about 80% is in the 9H form and the remaining 20% in the 7H form.¹⁵⁻¹⁶ Adenine has been described by several studies to have $n\pi^*$ characteristics for its lowest state and significant $^1n\pi^*/^1\pi\pi^*$ mixing after initial excitation, which causes its ~ 1 ps lifetime in the gas phase.^{4, 12, 15-18} Gustavsson et al. compared adenine to deoxyadenosine and deoxyadenosine 5'-monophosphate in solution using fluorescence upconversion and found the nucleosides to have similar, though slightly faster dynamics.¹⁹ Theoretically, the general consensus is that the low-energy vibronic transitions excite the $^1L_b(\pi\pi^*)$ state, and vibronic coupling and a barrierless path fill a nearly degenerate $n\pi^*$ state²⁰⁻²⁴. Adenine subsequently undergoes significant ring puckering and out-of-plane deformation at the C2N3 position to reach a conical intersection (CI) with some contribution from puckering at the C6, with a barrier of about 0.1 eV, to relax back to the ground state.^{13, 20-23, 25} Lobsiger et al. have found 2AP to have an excited state lifetime of 150 ps, significantly longer than adenine, at the origin in the gas-phase. Further, they observed another decay component with a lifetime of more than 2 μ s, attributed to ISC. The lifetime increases significantly upon microhydration, up to a hundredfold compared to the isolated gas-phase when selectively creating hydrogen bonds with the C2 amino group. This increase presumably corresponds to the fluorescence decay

noted for solvated 2AP. These experimental results are corroborated by theoretical calculations²⁶⁻²⁹.

Second, the excited state dynamics depends on the wavelength, especially near threshold where dynamics can slow and barriers to conical intersections can modify competing pathways. At higher electronic energies, adenine can also relax via hydrogen abstraction from a $^1\pi\sigma^*$ state.^{20-23, 30} While for 2AP, the lifetime of 150 ps decreases by about half after exciting with $\sim 1500\text{ cm}^{-1}$ excess energy, relative to the origin.³¹

Third, structural motifs do not always predict trends in potential energy surfaces and effects of substitutions do not necessarily add up. Excited state dynamics cannot *a priori* be predicted from 2AP and adenine for a purine with amino groups on both C2 and C6.

To highlight this and help shed more light on photodynamics of amino substituted purines we have 2,6-diaminopurine (2,6-dAP). 2,6-dAP is the hybrid of 2AP and adenine with amino groups on both the C2 and C6 positions. Most likely, 2,6-dAP existed on an early Earth with adenine and 2AP. 2,6-dAP was found in meteorite samples alongside other DNA analogues.³² Further, 2,6-dAP could be synthesized from the same starting materials and under the same conditions as the canonical nucleobases.³³ We have looked at both the biologically relevant 9H tautomer, and the 7H tautomer. In previous work³⁴ we found 6.3 and 8.7 ns lifetimes for the isolated 9H and 7H tautomers at their respective origins. These lifetimes stand out from those in both adenine and 2AP. To gain further insight, we investigated the dynamics of 2,6-dAP in the picosecond regime and found an additional fast decay pathway with barriers for each tautomer. We discuss the potential mechanisms that could explain observed lifetimes. By comparing with adenine, and 2AP, we attempt to reconcile the excited state dynamics with properties of the molecular structure.



Scheme 1. 9H (left) and 7H (right) tautomers of 2,6-diaminopurine

2. Experimental

The experimental setup has been described in detail elsewhere³⁵, and only a short description follows. 2,6-dAP (Aldrich, 98% purity) is placed on a translating graphite bar and desorbed via a focused Nd:YAG pulse (1064 nm, ~1 mJ/pulse at 10 Hz). A pulsed argon molecular beam (8 atm backing pressure, 30 μ s pulse width) entrains the gaseous molecules in a supersonic jet expansion, quickly cooling them. Downstream, resonance enhanced multiphoton ionization (REMPI) ionizes these cold, gaseous molecules and the ions enter into a reflectron time-of-flight mass spectrometer for detection.

We perform two-color resonant two-photon ionization (2C-R2PI) using an EKSPLA PL2251 Nd:YAG laser system producing ~30 ps pulses. The 355 nm output pumps the tunable optical parametric generator (OPG) (UV output of ~100 μ J). Leftover 1064 nm and 532 nm light from the pump are combined to generate the 5th harmonic at 213 nm (0.3 mJ), to be used as the ionization pulse. We also used the 193 nm output from a GAM excimer to ionize (2 mJ per pulse, 8 ns pulse width).

A Laser Vision tunable optical parametric oscillator/optical parametric amplifier (OPO/OPA) (mid-IR output over the range 3200-3800 cm^{-1} of ~2 mJ/pulse, 3 cm^{-1} spectral line width) generates IR light. IR light precedes the excitation/ionization pulses by ~200 ns. We use two variations of IR double resonant spectroscopy. In mode I, the IR laser scans

across IR wavelengths, while the ionization pulse is held constant at a resonant R2PI transition for a given tautomer. When the IR pulse is resonant with a vibrational mode, it modifies the ground state vibrational population, taking the excitation pulse out of resonance and causing a decrease in signal. This will produce the IR spectrum for the specific tautomer that is being ionized. In mode II, the IR pulse is held constant at a resonant vibrational transition, while the ionization pulse scans the R2PI spectrum. In this method, a tautomer is labeled by a vibrational stretch and signal decreases wherever the transition is shared. All double resonance spectroscopic experiments are digitally chopped to compare the alternating burn and control signals.

Pump-probe experiments were conducted to measure lifetimes. For this, the pump pulse from the OPG laser system, is tuned to a resonant transition, while the probe is the 5th harmonic (213 nm) from the pump laser for the OPG. The pulse of the 5th harmonic can be mechanically delayed up to 1.8 ns in time, relative to the OPG pulse. With ps pulse widths for both the pump and probe pulses, this allows probing of dynamics in the ps regime. Alternatively, we conducted pump probe using the OPG laser system for the pump and the excimer 193 nm to probe. The 193 nm pulse was delayed using electronic delay. Due to the 8 ns pulse width of the 193 nm, it is blind to < 1 ns dynamics. Therefore, probing with 213 or 193 nm are complementary techniques allowing us to observe both fast and slow dynamics.

The method for deriving lifetimes is based on previous work, and explained in more detail there.³⁶ Briefly, lifetimes are derived from the kinetic equations and solving the system of ordinary differential equations. This involves convolving the instrument response function (IRF) with exponential decay functions. The IRF is represented by a Gaussian function centered around t_0 , corresponding to the pump and probe pulses overlapping in time.

3. Results and discussion

Distinguishing the 7H and 9H tautomers of 2,6-dAP

First, an initial R2PI scan was taken of 2,6-dAP to find resonant electronic transitions. Two distinct regions of the spectrum provided signal, offset by $\sim 2500\text{ cm}^{-1}$ (see below). With known electronic resonances, we set about determining which tautomers of 2,6-dAP were in the beam. Using mode I and mode II (see supplemental) we confirmed the presence of both the 7H and 9H tautomers, in accordance with earlier work done by Gengeliczki.³⁴

2,6-dAP (7H) dynamics

The 2C-R2PI spectrum of 2,6-dAP (7H) is presented in Fig. 1. The origin is at 32216 cm^{-1} , which matches well with the origin found by Gengeliczki et al.³⁴ The R2PI displayed was taken using the ns 193 nm as the second color. The R2PI was also taken using ps 213 nm as the second color and had similar features, but at worse signal to noise (Fig. S1). The spectrum becomes diffuse and matches noise beyond 33600 cm^{-1} .

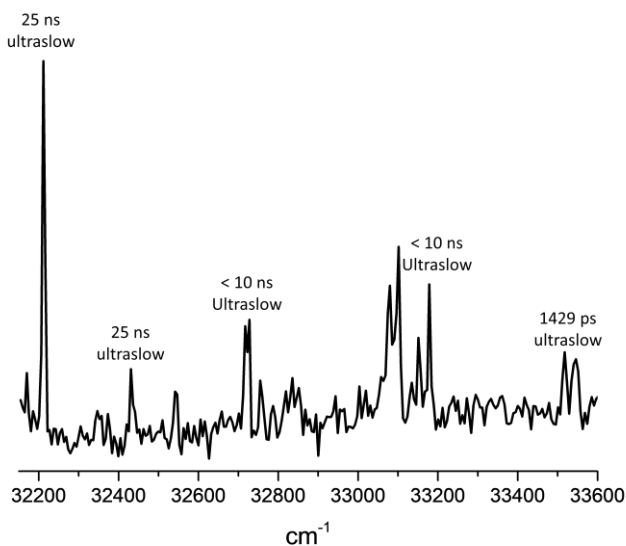


Figure 1. 2C-R2PI spectrum using the ns 193 nm as probe. Lifetimes are displayed above each peak. All lifetimes were taken from pump probes using the ns 193 nm probe. The only exception is the 1429 ps lifetime, which used the ps 213 nm probe. Lifetimes were measured at the origin, 32216 cm^{-1} , and then $+214$, $+511$, $+984$, and $+1307\text{ cm}^{-1}$, relative to the origin.

The lifetimes were derived from the pump probes, and are displayed in Figs. S4 – S6. A sample of the traces are shown in figure 1. The ns decay traces for the origin and +214 cm^{-1} peaks were similar and fit using biexponentials (Fig. 2a). We could fit the first two peaks using a 25 ns and 15000 ns lifetimes. These are best fits; they are not unique and indicate a range of times that could fit. As shown previously, biexponential decays can be fit with a range of times depending on the relative amplitudes of the two exponentials.³⁷ Qualitatively, the 25 ns fits well the shorter decay and the 15000 ns represents a very long-lived component. The ps pump probe traces just showed long-lived states at these first two peaks. Note, the origin decay we measured differs from the one measured by Gengeliczki et al.³⁴, where they derived a single 8.7 ns lifetime. We attribute this difference to the fact we probed using a 193 nm pulse while they probed with a 266 nm pulse. They could only probe out of higher energy states and were thus observing a different picture than we observe. This suggests we observe additional details about this initial decay, because it is longer. Further, we observe an excited state that was not observed before, one that is lower in energy and much longer lived.

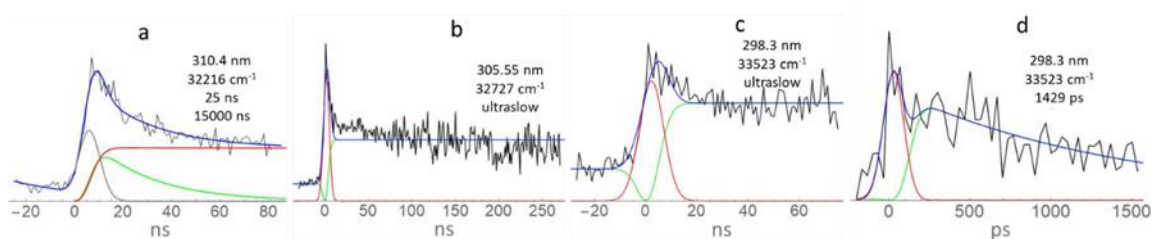


Figure 2. Sample pump probe spectra of 2,6-dAP (7H). (a-c) were pumped with ps pulses and probed with ns 193 nm pulses. (d) was pumped with a ps pulse and probed with ps 213 nm. (a) was fit with a biexponential while (b-d) were fit with a monoexponential. Note the change in x-axis units.

We also measured the next two peaks, +511 and +984 cm^{-1} using the ns 193 nm pump-probe (Fig. 2b). These two decay traces also looked similar. Two decays were again

observed. But the shorter decay could be fit to the IRF, meaning the decay was faster than our laser resolution, and thus we could not measure the actual lifetime in the ns regime. We estimate our IRF with the 193 nm probe to be ~ 10 ns. We could not pump probe these faster decays using ps 213 nm probe due to poor S/N. Therefore, the shorter decay is most likely between 1 ns and 10 ns. Because the shorter decay was assigned to the IRF, we fit the long ns decay using a monoexponential instead, with the fitting program giving a lifetime of 10^{17} . The actual lifetime is not that value, but it does suggest an ultraslow lifetime.

The last peak, $+1307\text{ cm}^{-1}$, was measured using both ns 193 nm (Fig. 2c) and ps 213 nm (Fig. 2d) probe pulses. The ns component was fit to a monoexponential again. This ns decay was again fit to an ultraslow lifetime. A lifetime of 1429 ps was derived using the ps 213 nm pulse (Fig. 2d).

We observed two decay components at all peaks for the 7H tautomer of 2,6-dAP. There is an ultraslow component that is observed at all peaks. For the faster component, it is fitted to 25 ns for the origin and $+214\text{ cm}^{-1}$ peaks. That component then becomes shorter up to between 1 – 10 ns for the $+511$ and $+984\text{ cm}^{-1}$ peaks. It can then be measured in the ps regime with a lifetime of 1429 ps at the last peak, $+1307\text{ cm}^{-1}$. Therefore, the lifetime of the fast component significantly shortens after 400 cm^{-1} and then once more after 1100 cm^{-1} . Again, the ultraslow component is observed at all peaks.

2,6-dAP (9H) dynamics

Figure 3 shows the 2C-R2PI spectrum of the 9H tautomer from 34800 to 35650 cm^{-1} using ps 213 nm as the probe. We assign the band at 34885 cm^{-1} to the origin transition of the 9H tautomer, based on work by Gengliczki et al.³⁴ This is $\sim 2500\text{ cm}^{-1}$ to the blue of the 7H origin. The first vibronic modes are the largest and most well-defined, with the longest

lifetimes. The spectrum quickly becomes diffuse around ~ 500 cm^{-1} excess energy suggesting a corresponding significant drop in excited state lifetime. The lifetime in the ps regime quickly drops by an order of magnitude within an excess 180 cm^{-1} , and then another order of magnitude with an excess 700 cm^{-1} , relative to the origin. All fitted pump probe traces are presented in Fig. S6. The pump probe traces for the origin and the observed highest energy peaks are shown as example traces (Fig. 4).

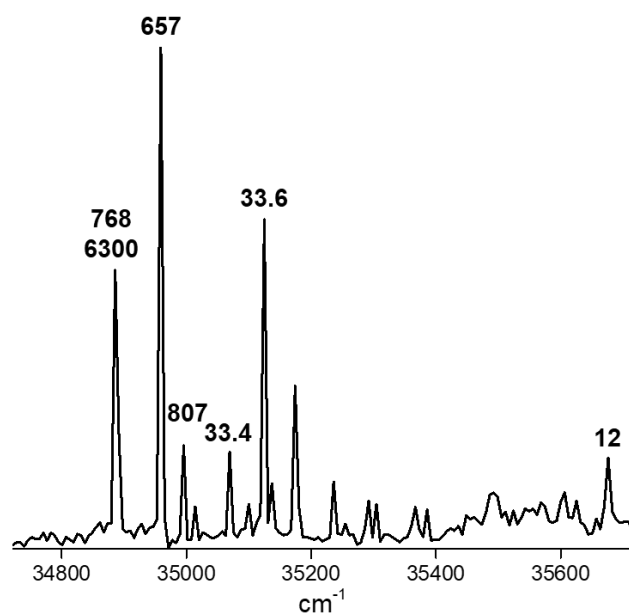


Figure 3. 2C-R2PI spectrum of 2,6-diaminopurine in the gas phase using the ps 213 nm as probe. The origin transition is assigned to 34885 cm^{-1} . Lifetimes for each peak displayed above the corresponding peak, in ps. The lifetime of 6300 ps was taken in the ns regime using 193 nm probe and matches previous published measurements. Lifetimes were measured at the origin, 34885 cm^{-1} , and then $+73$, $+110$, $+183$, $+239$, $+790$ cm^{-1} , relative to the origin.

The spectrum compares well to the spectrum taken by Gengliczki and coworkers³⁴ using ns 266 nm probe pulses, with their spectrum reaching a cut-off point ~ 250 cm^{-1} excess energy. This cut-off value is in line with the faster dynamics we measure in this report. We also obtained a ns pump probe at the origin, deriving a lifetime of 6.3 ns. We expect this nanosecond decay component to exist for the first three peaks, where the spectrum is still

sharp. After that, the broadening of the spectrum leads to the conclusion that the ns relaxation is disappearing, supported by the faster ps decays. This is also supported by the cut-off point at 250 cm^{-1} for the ns spectrum.³⁴

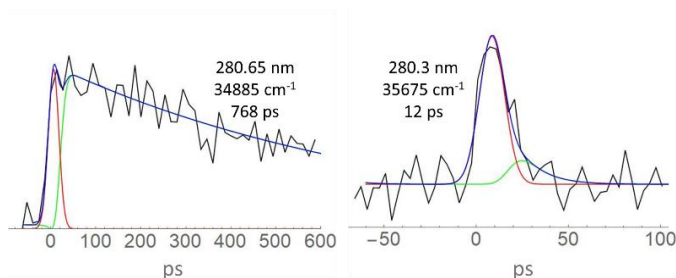


Figure 4. Pump probe traces using ps 213 nm as probe for 2,6-dAP (9H). The left trace was taken at the origin (34885 cm^{-1}) while the right trace was taken at 35675 cm^{-1} .

Table 1 summarizes the spectral and lifetime data of the amino substituted purines in the gas phase. Table 1 also states how much of the spectrum of each molecule has sharp features and broad features. The lifetime of purine has not been reported in the gas phase and we were not able to pump probe it. But purine was observed to have a lifetime of 360 and 645 ps in acetonitrile and aqueous solution, respectively.³⁸ This work also showed theoretically that purine decays to a triplet state near unity. However, these measurements were taken in solution at significant excess energy relative to the origin transition. In the gas-phase Schneider et al. reported a narrow rotational envelope of the origin peak, indicating a long lifetime.³⁹ Thus, we can assume purine has a relatively long lifetime in the gas phase. Purine was also found to exist exclusively in the 9H tautomer in the gas phase.⁴⁰ Following excitation at the origin, adenine and 2AP have excited state lifetimes of single picoseconds and ~ 150 ps, respectively. 2,6-dAP (9H) has a much longer lifetime at the origin of 655 ps as well as a 6.3 ns component. These findings suggest that adding an amino group at either C2

or C6 to the bare purine base significantly decreases the lifetime while adding amino groups at both sites increases the lifetime again relative to an amino group at a single site.

	Tautomer	Origin (cm ⁻¹)	τ_{0-0} (ps)	Range (cm ⁻¹)		References
				sharp	broad	
Purine	9H	31,309	long	2000		39, 41
Adenine	9H	36,101	9; 1 *	500		11, 42-43
	7H	35,824	Unmeasured			44
2AP	9H	32,371	150	700	2000	45-46
	7H	30,723	Unmeasured	600	200	47
Guanine	9H	Unmeasured	Unmeasured			
2,6-dAP	9H	34,881	655 / 6,300	400	800	this work
	7H	32,215	25000/ultralong	1000	800	this work
2,4-dAPy		34459	766	350	300	34, 48

Table 1. Spectral and lifetime data on purine and amino substituted purines. * at 37500 cm⁻¹

As we move progressively to the blue from the origin in the 2,6-dAP (9H) spectrum, the lifetime becomes progressively shorter. Starting at the origin, the first few peaks have lifetimes on the order of 750 ps, in addition to the ns component found earlier. These are significantly slower than adenine and 2AP. We found that the lifetime quickly drops to ~35 ps beyond about 180 cm⁻¹ excess energy for 9H. The last notably large and discrete peak, at +790 cm⁻¹ has a lifetime no longer than 12 ps. The ps decay is thought to be from radiationless decay pathways. The ns decay is most likely from a fluorescence pathway. This ns decay fits well with the usual time for fluorescence and small quantum yield due to another faster rate decay to the same state. From their relative lifetimes, the fluorescence quantum yield should be ~10% of the radiationless decay quantum yield, and thus contribute much less to the pump probe traces. Because the fluorescence quantum yield is much less than the radiationless decay quantum yield, the ps pump probe system is essentially blind to it.

The low fluorescence signal in ps pump probe spectroscopy is drowned out by the higher yield faster process. The ps system can potentially only see the fluorescence signal as a low-amplitude tail after the radiationless pathway has relaxed. Meanwhile, the ns pump probe system is blind to the faster process, because it occurs on a timescale faster than the laser resolution. The ns system can only observe the slower fluorescence process.

2,4-dAPy is the pyrimidine analogue of 2,6-dAP. From rotational contour fitting, it was found to have a lifetime between 10-1000 ps³⁴. We have found 2,4-dAPy to have a 766 ps lifetime near the origin (Fig. S8). This compares well with the rotational contour fitting. Meanwhile, Nachtigallova et al. calculated the relaxation of 2,4-dAPy to occur within single picoseconds at low excitation energy due to low energy barriers to CIs.⁴⁸ Comparison studies between 2,4-dAPy and 4-aminopyrimidine (4APy; the pyrimidine analogue of adenine) showed that they have similar dynamics.^{34, 48} 4-APy can access several CIs at low vibronic energy and thus is short lived in the excited state (similar to adenine). 2,4-dAPy can access a few of these CIs, with other pathways blocked by the additional amino group, such as the C2 deformation. Of notable exception, the C5C6 ethylenic twist is a main CI for 2,4-dAPy, which is blocked in 2,6-dAP allowing 2,4-dAPy to quickly overcome barriers to IC with a minimal amount of excess energy. According to our experimental work and calculations done by Kancheva et al.⁴⁹, the availability of the C5C6 twist in 2,4-dAPy does not play a significant role at energies near the origin though, as it has a long lifetime at low energies. Therefore, just as singly-substituted 4-APy can access CIs at low excess energy and has a short lifetime due to the availability of C2, so does adenine. Meanwhile, the doubly-substituted 2,4-dAPy has some of these CIs blocked due to the second amino group, apparently similar to 2,6-dAP. Both doubly-substituted analogues require a small amount of excess energy to overcome barriers to ultrafast relaxation.

Note, in aqueous solution, 2,6-dAP has a fluorescent quantum yield of 0.02 and a lifetime of ~ 1 ns.⁵⁰⁻⁵¹ As far as we can tell, the tautomer distribution in solution has not been determined. But *in vacuo*, 9H is more stable than 7H³⁴ much like 2AP and adenine. And the 7H tautomers makes up 40% and 20% of the aqueous population for 2AP⁵² and adenine,¹⁵⁻¹⁶ respectively. It is therefore likely that 2,6-dAP (7H) contributes a nonnegligible population to the aqueous solution. It is also likely that both tautomers are then fluorescent in solution.

We propose the following relaxation model for 2,6-dAP (9H). Excitation at the origin (with no excess energy) leads to population of a bright $^1\pi\pi^*$. A barrier on the order of 400 cm^{-1} prevents the system from undergoing nonradiative decay through a $^1\pi\pi^*/S_0$ CI. Therefore, some amount of the wavepacket will relax via fluorescence while the remainder eventually finds its way to a nonradiative decay channel. Increased excitation energy allows the wavepacket to overcome the barrier faster, leading to faster and higher yield nonradiative decay. Quickly, no amount of fluorescence is observed, outcompeted by the more efficient nonradiative decay. This decay mechanism of a barrier leading to $^1\pi\pi^*/S_0$ is similar to both the amino-keto⁵³⁻⁵⁴ and amino-enol^{36, 55} tautomers of guanine. It appears that the height of 9H's barrier is somewhere in between the height of amino-keto and the amino-enol tautomers of guanine. Note 2AP (9H) in the gas phase has a lifetime of 156 ps³¹ at the origin and 88 ps at an excess of 1514 cm^{-1} . For so much excess energy, the lifetime only drops by half. There is also an ultraslow (> 2 μs) decay component due to a triplet state^{31, 47}. 2AP decays via $^1\pi\pi^*/^1n\pi^*$ followed by either $^1n\pi^*/S_0$ or ISC²⁷⁻²⁸. These dynamics are in stark contrast to 2,6-dAP (9H) decay dynamics, further supporting our assignment of $^1\pi\pi^*/S_0$ nonradiative decay through a CI.

In comparison, the 2,6-dAP (7H) tautomer also has two distinct relaxation mechanisms. It has an ultraslow component that appears unchanged for over 1300 cm^{-1} . It also has a faster

component that shortens from 25 ns down to 1429 ps over the same amount of energy. It is not entirely clear if the longer component is actually wavelength-independent as the signal amplitude does decrease with excess energy. But there could be multiple reasons for the decreased signal. First, the system may be favoring faster, more efficient channels with increased energy that we cannot observe. Second, higher energy vibronic modes may have worse Frank-Condon overlap, preventing us from observing them as efficiently. Third, the ionization cross section may change as higher energy vibronic modes are excited leading to fewer ions being created.

But due to the apparent wavelength-independence of the ultraslow decay, both in terms of lifetime and amplitude relative to the faster decay, we assume it must be able to compete with the faster decay. Therefore, it is decaying into this long-lived state just as competitively as the fast decay is occurring. The relative yields do not appear to be qualitatively changing, based on the relative amplitudes of the short peak and the long tail (Fig. 2).

The initially bright $^1\pi\pi^*$ of the 7H tautomer can decay directly to the ground state via a conical intersection or fluorescence, on the order of 25 ns at the origin. Or it can undergo intersystem crossing (ISC) to a $^3\pi\pi^*$. This ISC is not El-Sayed allowed, and it only has a spin-orbit coupling (SOC) of 5-10 cm^{-1} . But the $S_1(\pi\pi^*)$ and $T_2(\pi\pi^*)$ are nearly degenerate, helping to counteract the poor SOC value. The geometry of the ISC point is very similar to the Frank-Condon geometry, while the geometry of the $^1\pi\pi^*/S_0$ conical intersection is significantly distorted. Therefore, much less molecular motion is required to reach the ISC point than the conical intersection. Further, the relatively long time it takes the $^1\pi\pi^*$ to decay back to the ground state (25 ns) gives the system longer time to ISC instead. Thus, even though SOC is small, 2,6-dAP (7H) still has a sizable triplet yield. This overall relaxation pathway is similar to 2-oxopurine.⁵⁶

The increased photostability of the 9H compared to the 7H is also in line with adenine tautomer photostability. Adenine (9H) has a much shorter lifetime than adenine (7H) in solution.¹⁵⁻¹⁶ Unfortunately, the lifetime of adenine (7H) has not been measured in the gas phase for direct comparison. There were no other examples of both the 7H and 9H photostabilities being measured in the gas phase and solution phase that were as clear cut.

It also appears that the 9H tautomer origin transition in the gas phase is always to the blue of the 7H tautomer, for the handful of examples that are available (see table 1). This is the case for 2-aminopurine (30723 vs 32362), adenine (35824 vs 36105), and 2,6-dAP (32216 vs 34885).

Our interest with the origin position is it is a direct measurement of the adiabatic energy of the $\pi\pi^*$ state. And the relative energy levels of the $\pi\pi^*$ versus the nearest $n\pi^*$ states can have serious consequences for the excited state dynamics, as shown with 2AP.³¹ With a few exceptions, it appears most purines and pyrimidines relax from their initially excited $\pi\pi^*$ to an $n\pi^*$ to the ground state. Interestingly, 2,6-dAP appears to follow the other path. It will do the $^1\pi\pi^*/S_0$ CI path exclusively for 9H and $^1\pi\pi^*/S_0$ internal conversion and $^1\pi\pi^*/^3\pi\pi^*$ ISC for 7H. The only difference between the two decay mechanisms is the placement of the hydrogen on N7 vs N9. This minor difference in structure can have significant effects on the excited state dynamics.

This effect is also shown when comparing the dynamics of 2,6-dAP, purine, adenine, 2AP, and guanine. Purine, the base structure, has been shown to have a long excited state lifetime due to significant ISC. Addition of a single amino group to C6 leads to adenine (6-aminopurine) and ultrafast nonradiative decay via $^1\pi\pi^* \rightarrow ^1n\pi^* \rightarrow S_0$ without any measurable ISC. Instead, taking purine and adding an amino group at C2 leads to 2AP and slower relaxation than adenine via the same path. 2AP will also yield a sizable triplet

population in the gas phase and nonpolar solvent.^{27, 31} This juxtaposition is what led the field to think for years the substitution of C2 is what mattered for the excited state dynamics. But if taking 2AP and adding an oxo group to C6, the result is guanine. And guanine undergoes ultrafast nonradiative decay via $^1\pi\pi^*/S_0$.^{54, 57-58} The addition of an oxo group to 2AP led to faster decay and a different decay path. Switching the oxo group on C6 of guanine with an amino group leads to 2,6-dAP. This is also the combination of 2AP and adenine. And 2,6-dAP will follow the same path as guanine, with an additional triplet yield, depending on its tautomerization. Even though 2,6-dAP has elements of both 2AP and adenine, it does not necessarily have the same dynamics. 2,6-dAP is also the least photostable (with the possible exception of purine). The only truly clear effect of structure on dynamics is the case of 2AP (9H) and adenine (9H). Solvation at the C2 amino group of 2AP significantly affects the PES landscape to the point it is fluorescent with a single microhydration.^{28, 31} This is not the case of adenine where solvation does not significantly alter its photostability.

In conclusion, we have attempted to develop a model for the observed differences in photostability of slightly modified purines. We have mapped out two different relaxation mechanisms that appear to fit all purines: direct $\pi\pi^*/S_0$ CI and $\pi\pi^*$ to $n\pi^*$, followed by branching to $n\pi^*/S_0$ internal conversion or ISC. All these decay mechanisms require distortion of the pyrimidine ring of some sort, either puckering, pyramidalization, twisting, or out-of-plane. Xanthine appears to be the one exception with distortion of the 5-membered ring proposed.⁵⁹ 9H tautomerization appears to be more photostable than 7H. Heterosubstituted purines also appear to be more photostable than homosubstituted purines. Photostability also favors single substitution over double substitution. Unfortunately, further refinement of the model is not possible with the data available at this time.

With only a handful of datapoints, more data are needed to see if the trend truly holds up. Our work on the excited state dynamics of xanthine and 9-methylxanthine will be published soon and add another data point. Gas phase results on the singly substituted oxo purines, 2-oxopurine and hypoxanthine, would help fill in some gaps. Solution phase work on 2,6-dAP and 2-oxopurine are also necessary. Hopefully, these results help shed light on the almost unique photostability of the canonical nucleobases and lead to a more mechanistic understanding of the subtle interplay between structure and excited state dynamics.

Supplemental Information

First, an initial R2PI scan was taken of 2,6-dAP to find resonant electronic transitions. Two distinct regions of the spectrum provided signal, offset by $\sim 2500\text{ cm}^{-1}$ (see below). With known electronic resonances, we set about determining which tautomers of 2,6-dAP were in the beam. Figure 1 shows the IR spectra obtained by double resonance spectroscopy mode I (scanning the IR frequency) confirming the tautomer assignment. Probing at 32216 cm^{-1} , we found a single IR peak at 3584 cm^{-1} , corresponding to the 7H tautomer. Probing at 34959 cm^{-1} , we found peaks at 3578 and 3586 cm^{-1} , corresponding to the 9H tautomer. These vibrational modes are in good agreement with Gengeliczki¹, with our results blue-shifted about 10 cm^{-1} , most likely due to calibration. For the 9H tautomer, we chose to probe with 34959 cm^{-1} as opposed to the origin, 34885 cm^{-1} , due to the increased S/N. We confirmed that the signal in the $34800 - 35650\text{ cm}^{-1}$ region was only due to the 9H tautomer using mode II, scanning the ionization wavelength with the IR burn frequency at a constant 3578 cm^{-1} , resonant for the 9H tautomer (Figure 2). Comparison burn spectrum (red trace), with the R2PI spectrum collected without IR in alternating pulses (black trace) show that all the peaks in this UV region dip, and therefore are from the single 9H tautomer.

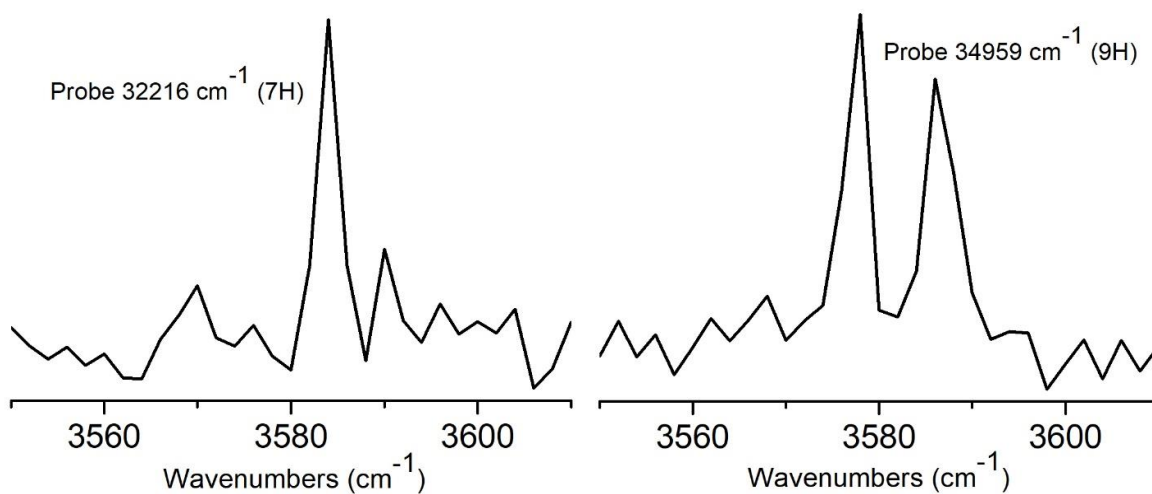


Figure S1. IR-UV mode I spectra with probe set to 32216 cm^{-1} and assigned to the 7H tautomer (left) and to 34959 cm^{-1} assigned to the 9H tautomer (right)

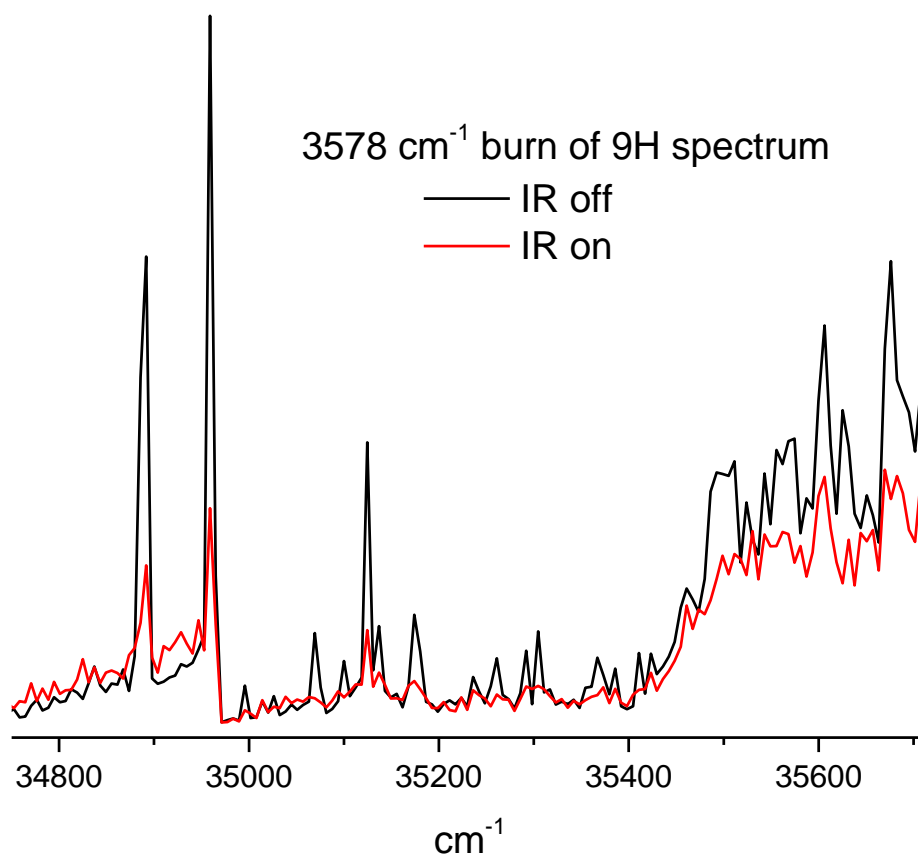


Figure S2. The IR-UV mode II spectrum of the 9H tautomer, generated by burning at 3578 cm^{-1} , resonant for the 9H tautomer. The red trace was generated simultaneously with an

R2PI spectrum (black trace) to show peak alignment and intensity match up. This was done using a digital chopper.

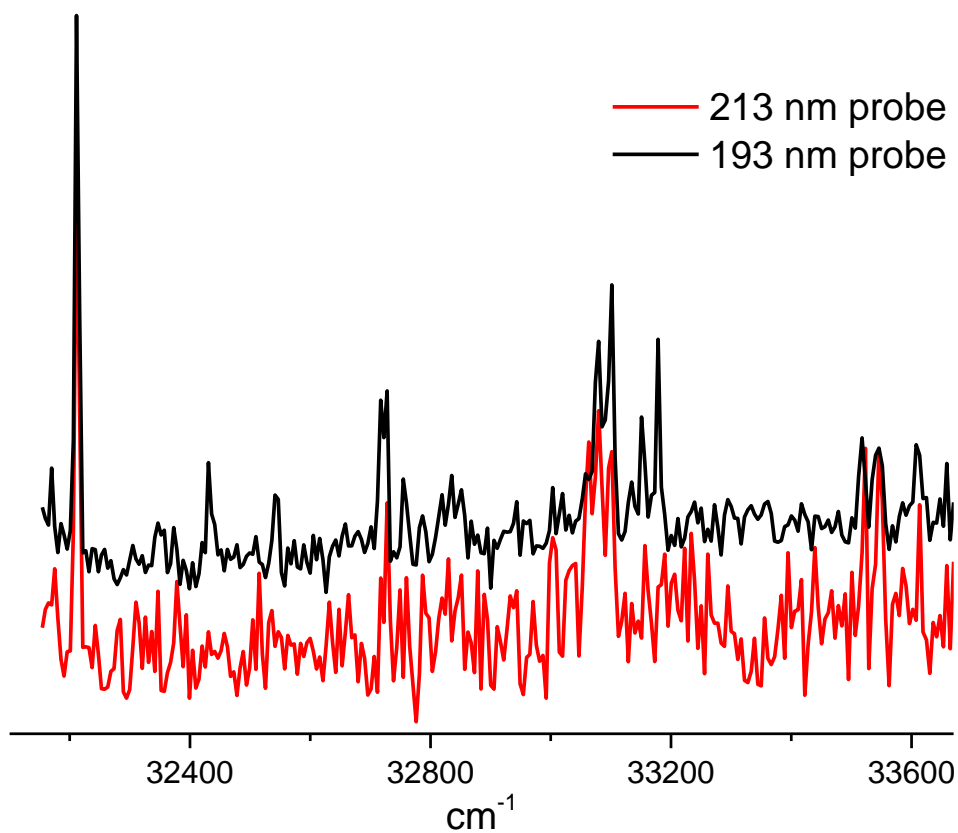


Fig. S3. 2C-R2PI spectrum of 2,6-dAP (7H) using ns 193 nm (black) and ps 213 nm (red) as probes.

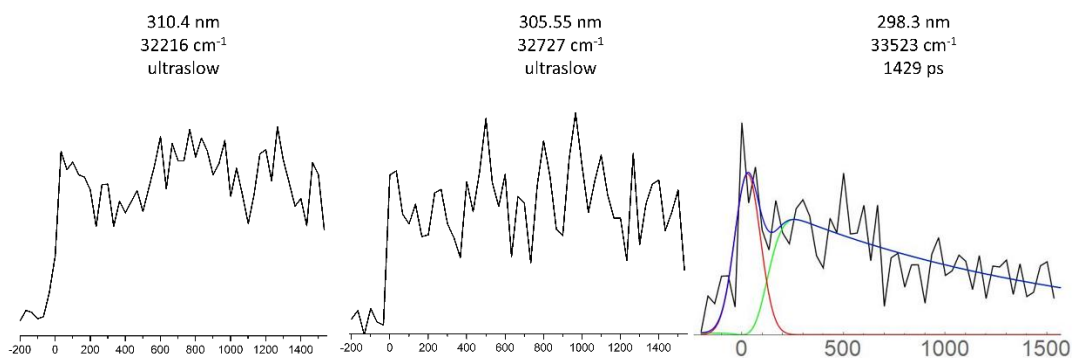


Fig. S4. Pump probe traces using ps 213 nm as the probe. The corresponding wavelength, wavenumber, and fits are displayed above each trace. The x-axis is in ps. The red, green, and blue lines represent the IRF, monoexponential fit, and the sum, respectively. Only the pump probe at 298.3 nm required fitting.

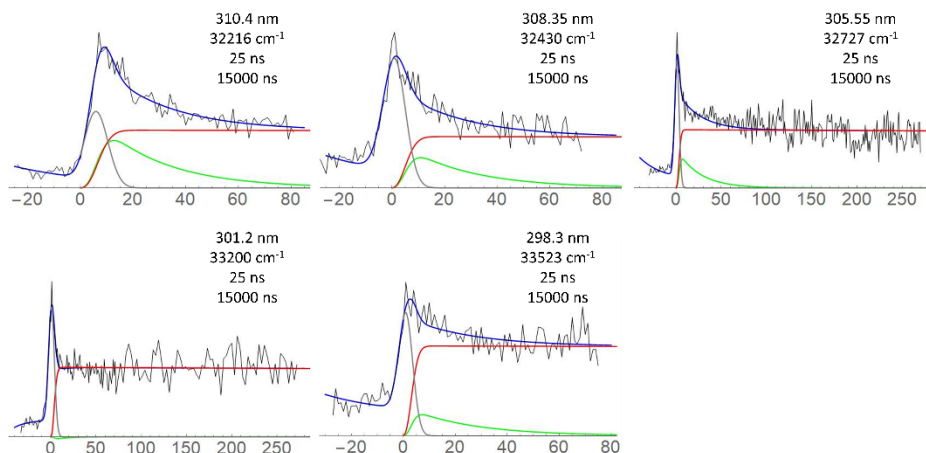


Fig. S5. Pump probe traces of 2,6-dAP (7H) fitted with biexponentials. Only the decays of 32216 and 32430 cm^{-1} really required biexponentials. For the decays of 32727 and 33200 cm^{-1} , the initial spike in signal was fit to IRF and thus biexponential fitting was not completely adequate. 33523 cm^{-1} had a short decay too short for this resolution. The corresponding wavelength, wavenumber, and lifetimes are shown above each decay. The x-axis is in ps. The gray, green, red, and blue lines represent the IRF, short exponential decay, long exponential decay, and the sum, respectively.

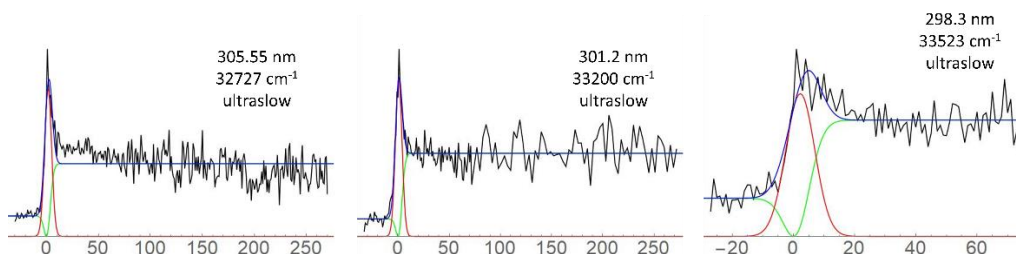


Fig. S6. Pump probe traces of 2,6-dAP (7H) fitted with monoexponentials. The decays of 32216 and 32430 cm^{-1} were excluded because they were fit with biexponentials. For the decays of 32727 and 33200 cm^{-1} , the short decay component (the initial spike in signal) was fit to IRF. The corresponding wavelength, wavenumber, and lifetimes are shown above each decay. The x-axis is in ps. The red, green, and blue lines represent the IRF, monoexponential fit, and the sum, respectively.

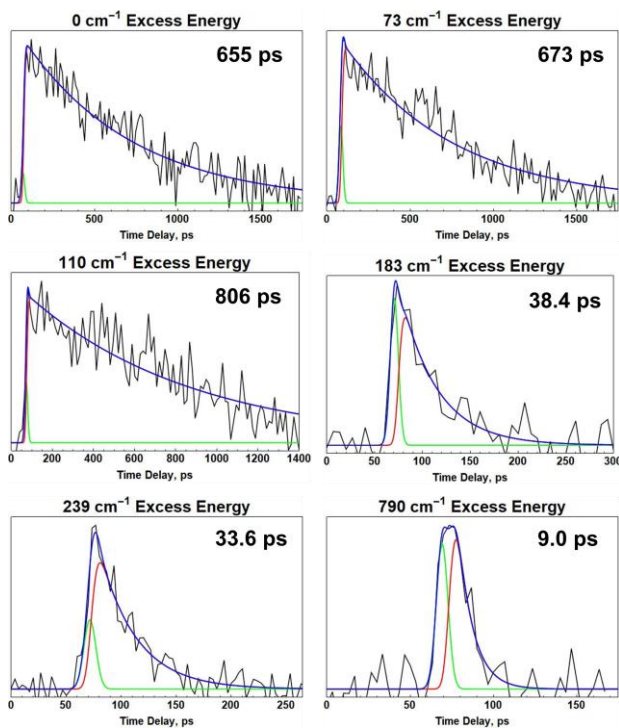


Fig. SX. Pump probes traces using ps 213 nm probe. The red, green, and blue lines represent the IRF, monoexponential fit, and the sum, respectively. Measurements were taken relative to the origin, at 34885 cm^{-1} .

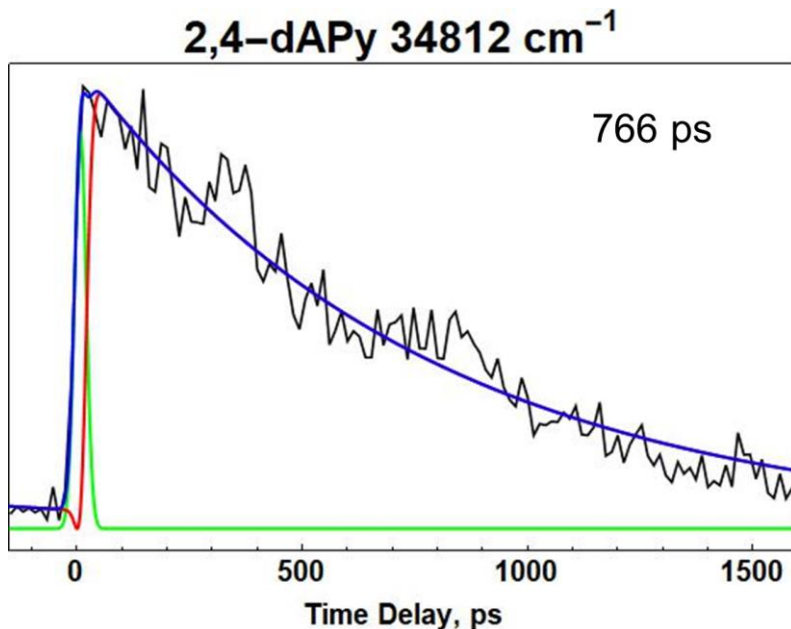


Figure SX. Pump probe spectrum of 2,4-dAPy at 34812 cm^{-1} . The trace was fitted with a monoexponential and found to have a 766 ps lifetime. The red, green, and blue lines represent the IRF, monoexponential fit, and the sum, respectively.

Supplemental Information References

1. Gengeliczki, Z.; Callahan, M. P.; Svadlenak, N.; Pongor, C. I.; Sztaray, B.; Meerts, L.; Nachtigallova, D.; Hobza, P.; Barbatti, M.; Lischka, H.; de Vries, M. S., Effect of substituents on the excited-state dynamics of the modified DNA bases 2,4-diaminopyrimidine and 2,6-diaminopurine. *Phys Chem Chem Phys* **2010**, *12* (20), 5375-88.

References

1. Gustavsson, T.; Improta, R.; Markovitsi, D., DNA/RNA: Building Blocks of Life Under UV Irradiation. *The Journal of Physical Chemistry Letters* **2010**, *1* (13), 2025-2030.
2. Middleton, C. T.; de La Harpe, K.; Su, C.; Law, Y. K.; Crespo-Hernandez, C. E.; Kohler, B., DNA excited-state dynamics: from single bases to the double helix. *Annu Rev Phys Chem* **2009**, *60*, 217-39.
3. De Vries, M. S., Isolated DNA base pairs, interplay between theory and experiment. **2008**, 323.
4. Canuel, C.; Mons, M.; Piuzzi, F.; Tardivel, B.; Dimicoli, I.; Elhanine, M., Excited states dynamics of DNA and RNA bases: characterization of a stepwise deactivation pathway in the gas phase. *J Chem Phys* **2005**, *122* (7), 074316.
5. Kang, H.; Lee, K. T.; Jung, B.; Ko, Y. J.; Kim, S. K., Intrinsic Lifetimes of the Excited State of DNA and RNA Bases. *J Am Chem Soc* **2002**, *124*, 12958 - 12959.
6. Sponer, J., Hydrogen bonding, stacking and cation binding of DNA bases. *Journal of Molecular Structure: THEOCHEM* **2001**, *573* (1-3), 43-53.
7. Beckstead, A. A.; Zhang, Y.; de Vries, M. S.; Kohler, B., Life in the light: nucleic acid photoproperties as a legacy of chemical evolution. *Phys Chem Chem Phys* **2016**, *18* (35), 24228-38.
8. Pecourt, J.-M. L.; Peon, J.; Kohler, B., DNA Excited-State Dynamics: Ultrafast Internal Conversion and Vibrational Cooling in a Series of Nucleosides. *Journal of the American Chemical Society* **2001**, *123* (42), 10370-10378.
9. Rios, A. C.; Tor, Y., On the Origin of the Canonical Nucleobases: An Assessment of Selection Pressures across Chemical and Early Biological Evolution. *Isr J Chem* **2013**, *53* (6-7), 469-483.
10. Gate, G.; Szabla, R.; Haggmark, M. R.; Sponer, J.; Sobolewski, A. L.; de Vries, M. S., Photodynamics of alternative DNA base isoguanine. *Phys Chem Chem Phys* **2019**, *21* (25), 13474-13485.
11. Lührs, D. C.; Viallon, J.; Fischer, I., Excited state spectroscopy and dynamics of isolated adenine and 9-methyladenine. *Physical Chemistry Chemical Physics* **2001**, *3* (10), 1827-1831.
12. Kang, H.; Chang, J.; Lee, S. H.; Ahn, T. K.; Kim, N. J.; Kim, S. K., Excited-state lifetime of adenine near the first electronic band origin. *J Chem Phys* **2010**, *133* (15), 154311.
13. Kang, H.; Jung, B.; Kim, S. K., Mechanism for ultrafast internal conversion of adenine. *The Journal of Chemical Physics* **2003**, *118* (15), 6717-6719.
14. Ullrich, S.; Schultz, T.; Zgierski, M. Z.; Stolow, A., Electronic relaxation dynamics in DNA and RNA bases studied by time-resolved photoelectron spectroscopy. *Physical Chemistry Chemical Physics* **2004**, *6* (10).

15. Cohen, B.; Hare, P. M.; Kohler, B., Ultrafast excited-state dynamics of adenine and monomethylated adenines in solution: implications for the nonradiative decay mechanism. *J Am Chem Soc* **2003**, *125* (44), 13594-601.
16. Buchner, F.; Ritze, H. H.; Lahl, J.; Lubcke, A., Time-resolved photoelectron spectroscopy of adenine and adenosine in aqueous solution. *Phys Chem Chem Phys* **2013**, *15* (27), 11402-8.
17. Ullrich, S.; Schultz, T.; Zgierski, M. Z.; Stolow, A., Direct Observation of Electronic Relaxation Dynamics in Adenine via Time-Resolved Photoelectron Spectroscopy. *J Am Chem Soc* **2004**, *126*, 2262 - 2263.
18. Kim, N. J.; Jeong, G.; Kim, Y. S.; Sung, J.; Keun Kim, S.; Park, Y. D., Resonant two-photon ionization and laser induced fluorescence spectroscopy of jet-cooled adenine. *The Journal of Chemical Physics* **2000**, *113* (22), 10051-10055.
19. Gustavsson, T.; Sharonov, A.; Onidas, D.; Markovitsi, D., Adenine, deoxyadenosine and deoxyadenosine 5'-monophosphate studied by femtosecond fluorescence upconversion spectroscopy. *Chemical Physics Letters* **2002**, *356* (1-2), 49-54.
20. Marian, C. M., A new pathway for the rapid decay of electronically excited adenine. *J Chem Phys* **2005**, *122* (10), 104314.
21. Perun, S.; Sobolewski, A. L.; Domcke, W., Photostability of 9H-adenine: mechanisms of the radiationless deactivation of the lowest excited singlet states. *Chemical Physics* **2005**, *313* (1-3), 107-112.
22. Perun, S.; Sobolewski, A. L.; Domcke, W., Ab initio studies on the radiationless decay mechanisms of the lowest excited singlet states of 9H-adenine. *J Am Chem Soc* **2005**, *127* (17), 6257-65.
23. Barbatti, M.; Lischka, H., Nonadiabatic Deactivation of 9H-Adenine A Comprehensive Picture Based on Mixed Quantum-Classical Dynamics. *J Am Chem Soc* **2008**, *130*, 6831 - 6839.
24. Fabiano, E.; Thiel, W., Nonradiative deexcitation dynamics of 9H-adenine: an OM2 surface hopping study. *J Phys Chem A* **2008**, *112* (30), 6859-63.
25. Plasser, F.; Crespo-Otero, R.; Pedersoli, M.; Pittner, J.; Lischka, H.; Barbatti, M., Surface Hopping Dynamics with Correlated Single-Reference Methods: 9H-Adenine as a Case Study. *J Chem Theory Comput* **2014**, *10* (4), 1395-405.
26. Rachofsky, E. L.; Ross, J. B. A.; Krauss, M.; Osman, R., CASSCF Investigation of Electronic Excited States of 2-Aminopurine. *The Journal of Physical Chemistry A* **2001**, *105* (1), 190-197.
27. Reichardt, C.; Wen, C.; Vogt, R. A.; Crespo-Hernandez, C. E., Role of intersystem crossing in the fluorescence quenching of 2-aminopurine 2'-deoxyriboside in solution. *Photochem Photobiol Sci* **2013**, *12* (8), 1341-50.
28. Barbatti, M.; Lischka, H., Why water makes 2-aminopurine fluorescent? *Phys Chem Chem Phys* **2015**, *17* (23), 15452-9.
29. Perun, S.; Sobolewski, A. L.; Domcke, W., Ab initio studies of the photophysics of 2-aminopurine. *Molecular Physics* **2006**, *104* (5-7), 1113-1121.
30. Evans, N. L.; Ullrich, S., Wavelength dependence of electronic relaxation in isolated adenine using UV femtosecond time-resolved photoelectron spectroscopy. *J Phys Chem A* **2010**, *114* (42), 11225-30.
31. Lobsiger, S.; Blaser, S.; Sinha, R. K.; Frey, H. M.; Leutwyler, S., Switching on the fluorescence of 2-aminopurine by site-selective microhydration. *Nat Chem* **2014**, *6* (11), 989-93.

32. Callahan, M. P.; Smith, K. E.; Cleaves, H. J., 2nd; Ruzicka, J.; Stern, J. C.; Glavin, D. P.; House, C. H.; Dworkin, J. P., Carbonaceous meteorites contain a wide range of extraterrestrial nucleobases. *Proc Natl Acad Sci U S A* **2011**, *108* (34), 13995-8.
33. Miyakawa, S.; Cleaves, H. J.; Miller, S. L., The cold origin of life: B. Implications based on pyrimidines and purines produced from frozen ammonium cyanide solutions. *Orig Life Evol Biosph* **2002**, *32* (3), 209-18.
34. Gengeliczki, Z.; Callahan, M. P.; Svadlenak, N.; Pongor, C. I.; Sztaray, B.; Meerts, L.; Nachtigallova, D.; Hobza, P.; Barbatti, M.; Lischka, H.; de Vries, M. S., Effect of substituents on the excited-state dynamics of the modified DNA bases 2,4-diaminopyrimidine and 2,6-diaminopurine. *Phys Chem Chem Phys* **2010**, *12* (20), 5375-88.
35. Meijer, G.; De Vries, M. S.; Hunziker, H. E.; Wendt, H. R., Laser Desorption Jet-Cooling of Organic Molecules. *Applied Physics B* **1990**, *51*, 395 - 403.
36. Siouri, F. M.; Boldissar, S.; Berenbeim, J. A.; de Vries, M. S., Excited State Dynamics of 6-Thioguanine. *J Phys Chem A* **2017**, *121* (28), 5257-5266.
37. Haggmark, M. R.; Gate, G.; Boldissar, S.; Berenbeim, J.; Sobolewski, A. L.; de Vries, M. S., Evidence for competing proton-transfer and hydrogen-transfer reactions in the S1 state of indigo. *Chemical Physics* **2018**, *515*, 535-542.
38. Crespo-Hernandez, C. E.; Martinez-Fernandez, L.; Rauer, C.; Reichardt, C.; Mai, S.; Pollum, M.; Marquetand, P.; Gonzalez, L.; Corral, I., Electronic and structural elements that regulate the excited-state dynamics in purine nucleobase derivatives. *J Am Chem Soc* **2015**, *137* (13), 4368-81.
39. Schneider, M.; Hain, T.; Fischer, I., Resonance-enhanced multiphoton ionisation of purine. *Chemphyschem* **2009**, *10* (4), 634-6.
40. Caminati, W.; Maccaferri, G.; Favero, P. G.; Favero, L. B., Free jet absorption millimeter wave spectrum of purine. *Chemical Physics Letters* **1996**, *251* (3-4), 189-192.
41. Caminati, W.; Maccaferri, G.; Favero, P. G.; Favero, L. B., Free Jet Absorption Millimeter Wave Spectrum of Purine. *Chem. Phys. Lett.* **1996**, *251*, 189-192.
42. Plützer, C.; Nir, E.; de Vries, M. S.; Kleineremanns, K., IR-UV double-resonance spectroscopy of the nucleobase adenine. *Phys. Chem. Chem. Phys.* **2001**, *3* (24), 5466-5469.
43. Kang, H.; Jung, B.; Kim, S. K., Mechanism for ultrafast internal conversion of adenine. *J. Chem. Phys.* **2003**, *118* (15), 6717-6719.
44. Plützer, C.; Kleineremanns, K., Tautomers and electronic states of jet-cooled adenine investigated by double resonance spectroscopy. *Phys. Chem. Chem. Phys.* **2002**, *4* (20), 4877-4882.
45. Seefeld, K. A.; Plützer, C.; Löwenich, D.; Häber, T.; Linder, R.; Kleineremanns, K.; Tatchen, J.; Marian, C. M., Tautomers and electronic states of jet-cooled 2-aminopurine investigated by double resonance spectroscopy and theory. *Phys. Chem. Chem. Phys.* **2005**, *7* (16), 3021-3026.
46. Lobsiger, S.; Blaser, S.; Sinha, R. K.; Frey, H. M.; Leutwyler, S., Switching on the fluorescence of 2-aminopurine by site-selective microhydration. *Nat Chem* **2014**, *6* (11), 989-993.
47. Lobsiger, S.; Sinha, R. K.; Trachsel, M.; Leutwyler, S., Low-lying excited states and nonradiative processes of the adenine analogues 7H- and 9H-2-aminopurine. *J Chem Phys* **2011**, *134* (11), 114307.
48. Nachtigallová, D.; Barbatti, M.; Szymczak, J. J.; Hobza, P.; Lischka, H., The photodynamics of 2,4-diaminopyrimidine in comparison with 4-aminopyrimidine: The effect of amino-substitution. *Chemical Physics Letters* **2010**, *497* (1-3), 129-134.

49. Kancheva, P.; Tuna, D.; Delchev, V. B., Comparative study of radiationless deactivation mechanisms in cytosine and 2,4-diaminopyrimidine. *Journal of Photochemistry and Photobiology A: Chemistry* **2016**, *321*, 266-274.
50. Virta, P.; Koch, A.; Roslund, M. U.; Mattjus, P.; Kleinpeter, E.; Kronberg, L.; Sjöholm, R.; Klika, K. D., Synthesis, characterisation and theoretical calculations of 2,6-diaminopurine etheno derivatives. *Org Biomol Chem* **2005**, *3* (16), 2924-9.
51. Santhosh, C.; Mishra, P. C., Electronic spectra of 2-aminopurine and 2,6-diaminopurine: phototautomerism and fluorescence reabsorption. *Spectrochimica Acta Part A: Molecular Spectroscopy* **1991**, *47* (12), 1685-1693.
52. Neely, R. K.; Magennis, S. W.; Dryden, D. T. F.; Jones, A. C., Evidence of Tautomerism in 2-Aminopurine from Fluorescence Lifetime Measurements. *The Journal of Physical Chemistry B* **2004**, *108* (45), 17606-17610.
53. Barbatti, M.; Szymczak, J. J.; Aquino, A. J.; Nachtigallova, D.; Lischka, H., The decay mechanism of photoexcited guanine - a nonadiabatic dynamics study. *J Chem Phys* **2011**, *134* (1), 014304.
54. Yamazaki, S.; Domcke, W.; Sobolewski, A. L., Nonradiative decay mechanisms of the biologically relevant tautomer of guanine. *J Phys Chem A* **2008**, *112* (47), 11965-8.
55. Marian, C. M., The guanine tautomer puzzle: quantum chemical investigation of ground and excited states. *J Phys Chem A* **2007**, *111* (8), 1545-53.
56. Martinez-Fernandez, L.; Arslançan, S.; Ivashchenko, D.; Crespo-Hernandez, C. E.; Corral, I., Tracking the origin of photostability in purine nucleobases: the photophysics of 2-oxopurine. *Phys Chem Chem Phys* **2019**, *21* (25), 13467-13473.
57. Miannay, F. A.; Gustavsson, T.; Banyasz, A.; Markovitsi, D., Excited-state dynamics of dGMP measured by steady-state and femtosecond fluorescence spectroscopy. *J Phys Chem A* **2010**, *114* (9), 3256-63.
58. Karunakaran, V.; Kleinermanns, K.; Improta, R.; Kovalenko, S. A., Photoinduced dynamics of guanosine monophosphate in water from broad-band transient absorption spectroscopy and quantum-chemical calculations. *J Am Chem Soc* **2009**, *131* (16), 5839-50.
59. Yamazaki, S.; Sobolewski, A. L.; Domcke, W., Photophysics of xanthine: computational study of the radiationless decay mechanisms. *Phys Chem Chem Phys* **2009**, *11* (43), 10165-74.

IV. Experimental and theoretical photodynamics of xanthine and 9-methylxanthine in the gas phase

Gregory Gate^a, Ann Williams^a, Rafal Szabla^b, Mattanjah de Vries^a

^aDepartment of Chemistry and Biochemistry, University of California Santa Barbara, CA 93106

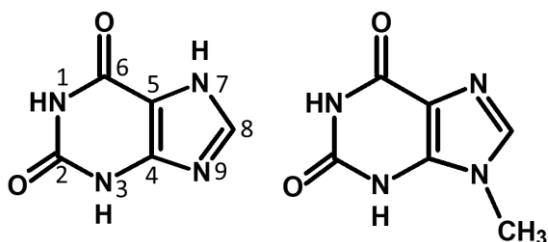
^bDepartment of Chemistry, University of Edinburgh

1. Introduction

The excited state dynamics of the nucleobases, alongside the nucleosides and nucleotides, are well understood at this point¹⁻⁸, thanks to the continuous development of

ultrafast experimental techniques and theoretical calculations. The unique photostability of the canonical nucleobases is thought to have possible consequences for the origins of life and further explains radiative skin damage. With a few exceptions, the canonical nucleobases in their biologically relevant forms are more photostable than their various tautomers, derivatives, and analogues. A handful of these variants will be described later on.

The two canonical purine nucleobases, guanine and adenine, have amino and oxo moieties at their C2 and C6 positions. Their enhanced photostabilities are due to ultrafast nonradiative decays from their excited states. These relaxation channels prevent them from using the absorbed electronic energy to do damaging photochemistry. Structural distortions of the 6-membered rings allow these two systems to reach conical intersections (CI) and enter their respective ground states.⁹⁻¹⁵ Even slight modifications to the structure can change the dynamics significantly. The amino-enol tautomer of guanine was found both experimentally¹⁶ and theoretically¹⁷ to have an excited state lifetime orders of magnitude longer than the biologically relevant amino-keto tautomer. Isoguanine, guanine with its amino and oxo substituents switched, also has significantly worse photostability than guanine.¹⁸ Excited state dynamics is dependent on structure and even slight modifications to the structure can have disproportionate impact on photostability. The dynamics of a few variant purines are highlighted.



Scheme 1. The 7H tautomer of xanthine (left) and 9-methylxanthine (right) with number scheme.

Hypoxanthine (6-oxopurine) is noted for being one of the fastest purine derivatives. It has a single decay channel in solution, with an experimental lifetime of ~ 100 fs.¹⁹⁻²¹ These ultrafast lifetimes are attributed to both the 7H and 9H tautomers, as they are expected to be present in almost equal amount in solution. Theoretical calculations support these experimental findings, with an ultrafast relaxation mechanism via $\pi\pi^*/S_0$ by distortion at C2.²²⁻²³ Unfortunately, experimental gas phase data is lacking.

Guo et al. also theoretically studied 9-methylhypoxanthine in both gas phase and in solution.²⁴ Their motivation was the interest in how substituting the hydrogen on the N9 with a methyl group affects the hydrogen bond network with the solvent. Methylation did not affect the overall photostability, with 9-methylhypoxanthine having similar lifetimes to hypoxanthine, both in gas and solution phase.

2-oxopurine has been studied theoretically in the gas phase and found to have an S_1 minimum that leads to significant ISC.²⁵ Reaching the CI to the ground state required stretching of the C₂-O and N₃-C₄ bonds and overcoming a ~ 0.5 eV barrier. Therefore, 2-oxopurine is expected to have a relatively long lifetime and not be very photostable. Unfortunately, this is the only study on the excited state dynamics of 2-oxopurine that we could find.

Here, we add another data point to the picture, looking at the homosubstituted purines, xanthine and 9-methylxanthine (Scheme 1). Xanthine is the combination of 2-oxopurine and hypoxanthine, with oxo groups on both C2 and C6. We are interested in both the 7H and 9H tautomers of xanthine. But unfortunately we could not observe xanthine (9H) in our molecular beam, so we used 9-methylxanthine instead. Methylation instead of a hydrogen at

N9 has been shown to have small influence on the excited state dynamics of purines.^{24, 26-28} Xanthine is found in the human body, as a degradation product of both guanine and adenine. It is thought to have been present on an early Earth when life was first starting to arise, being found on meteorites.²⁹ It has also been successfully synthesized using chemistry that is believed to have been taking place on an early Earth.³⁰⁻³¹ With its flexible hydrogen bonding and base pairing possibilities, it has also been proposed in an early all-purine system of genetic information.³²

Domcke et al. wrote an extensive theoretical paper on the excited state dynamics of xanthine (7H) and (9H) in the gas phase.³³ They found CIs for both tautomers for both $\pi\pi^*/S_0$ and $n\pi^*/S_0$. The 7H tautomer had an $\pi\pi^*/S_0$ relaxation channel with a small barrier, while the 9H tautomer had a barrier of ~ 1 eV. Thus, they concluded the 7H tautomer to be photostable while the 9H should not be. Interestingly, the CI coordinates were reached via distortion of the 5-membered ring, as opposed to guanine and adenine, which required distortion of the 6-membered ring. The authors excluded crossing of the $n\pi^*/S_0$ CI as it was too high in energy. But the $n\pi^*$ state was isoenergetic or slightly below the $\pi\pi^*$, depending on the method used. Therefore, vibronic coupling between the bright $\pi\pi^*$ and dark $n\pi^*$ states is possible.

Xanthine is very difficult to dissolve, so there have not been any solution phase studies conducted on xanthine itself. Instead, studies have focused on various forms of glycosylated xanthosine, hypoxanthine, and other methylxanthines. Chen and Kohler started in 2012 by looking at hypoxanthine and a few other methylxanthines in aqueous solution using fs transient absorption.¹⁹ They found lifetimes of sub-ps and ~ 1 ps for all systems. Gustavsson et al. then looked at a series of methylxanthines in water and methanol using fluorescence up-conversion and found them to have biexponential decays on the order of 1 ps.³⁴ Rottger

and coworkers did a thorough study on xanthosine monophosphate (XMP) and protonated XMP using fluorescence up-conversion and transient absorption and observed similar ultrafast dynamics.³⁵ All forms of xanthine have been shown to have ultrafast dynamics and high photostability in solution with hypoxanthine noted for being the most photostable.

We have studied the excited state dynamics of xanthine (7H) and 9-methylxanthine in the gas phase using resonant enhanced multiphoton ionization (REMPI) coupled. Our experimental results for both systems show two decay components, one < 30 ps, and another ultraslow relaxation. The dynamics displayed in the gas phase stand in stark contrast to the dynamics displayed for all forms of xanthine in solution phase. 2-aminopurine also shows different photodynamics in solution compared to gas phase and will be compared. And at least for 2-aminopurine, this is due to the rearrangement of the respective $^1\pi\pi^*$ and $^1n\pi^*$ energy levels when solvated. These xanthine results, alongside the results for 2,6-diaminopurine, add to the picture of the behavior of doubly substituted purines, and purines as a whole.

2. Methods

The spectroscopic technique has been described in detail elsewhere and only a brief description follows.³⁶ Samples of xanthine and 9-methylxanthine were purchased from Sigma (99%) and Research Biochemicals International and used without further purification. The sample was placed on a translating graphite bar approximately 1 mm away from the pulsed valve in the vacuum chamber. The fundamental from a Minilite Continuum II pulsed Nd:YAG laser attenuated to ~ 1 mJ and focused to about 1 mm^2 was used for desorption of the sample. Argon gas at 8 atm backing pressure ($30 \mu\text{s}$ pulse width) was produced from an

Amsterdam pulsed valve and used for supersonic jet cooling of the desorbed sample. Ionized sample was detected using a reflectron time-of-flight mass spectrometer.

REMPI was used to ionize the sample. The third harmonic (355 nm) of the Nd:YAG EKSPLA PL2251 was used to pump an optical parametric generator (OPG) (EKSPLA) to create tunable laser light (~0.1 mJ per pulse, 30 ps pulse width). The excess fundamental and second harmonic (532 nm) were combined to generate the 4th (266 nm) or 5th harmonic (213 nm, 0.2 mJ per pulse). These pulses were then recombined in space and used for ionization. We also used the 193 nm output from a GAM excimer for ionization (2 mJ per pulse, 8 ns pulse width).

By scanning the wavelength of the first pulse, always from the OPG, and probing with ps 213 nm, ps 266 nm, or ns 193 nm two-color resonant two photon ionization (2C-R2PI) spectra were generated. To probe faster dynamics, pump probe was conducted where the pump wavelength from the OPG was held constant on a known resonance, and the probe wavelength (ps 213 nm or ps 266 nm) was delayed in time using a mechanical delay stage. This setup allowed for delay up to 1.8 ns. Alternatively, the 8 ns 193 nm output was used as the probe, and was delayed using a digital delay generator. Practically this setup could be delayed up to 2 μ s. These two pump probe setups are complementary, allowing us to observe dynamics on both a faster and slower scale.

3. Results and discussion

The 2C-R2PI spectrum of xanthine (7H) is presented in Fig. 1. It was taken using ns 193 nm as the probe. The R2PI spectrum using ps 213 nm has similar peaks and amplitudes. (Fig. S1) The origin was found at 36751 cm^{-1} , in good agreement with Callahan et al.³⁷ The origin peak is by the far largest amplitude peak. The spectrum is sharp for about 700 cm^{-1} ,

and then broadens out for the next 800 cm^{-1} , at which point it breaks off and no signal is observed. The lifetimes derived from pump probe traces are displayed above each peak. Lifetimes in the ps regime were derived from pump probes using ps 213 nm as the probe and displayed as the top value. We successfully probed every peak using ps 213 nm (Fig. 2(b) and Fig. S3). They all looked similar over this energy range. We attempted to pump probe using ps 266 nm as well, because they ended up showing slightly different dynamics. Unfortunately, due to S/N issues, we could only successfully pump probe the peaks at 36751 and 37334 cm^{-1} using ps 266 nm (Fig. 2(c) and Fig. S2). That reasoning will be described below. Lifetimes using ns 193 nm as the probe are displayed in black (Fig. 2(a) and Fig. S1).

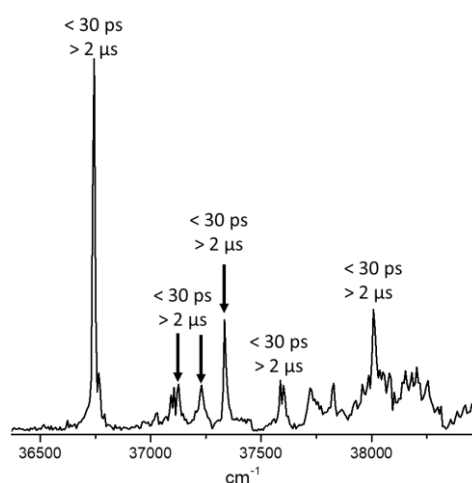


Figure 1. 2C-R2PI spectrum of xanthine (7H). The origin is at 36751 cm^{-1} . Lifetimes derived from pump probe traces using ps 213 nm as probe are on top. Lifetimes derived from pump probe traces using ns 193 nm as probe are on bottom. Pump energies were set to the origin, 37133 , 37230 , 37334 , 37586 cm^{-1} .

The ns decays were measured to be $> 2\text{ }\mu\text{s}$. Looking at figure 2(a) and Fig S1, the traces do not decay exponentially, but linearly. This is attributed to the packet of initially excited molecules flying out of the area of the probe beam within $2\text{ }\mu\text{s}$, not due to excited state relaxation. This means the whole molecular packet will fly $\sim 5\text{ mm}$ in $2\text{ }\mu\text{s}$, which is reasonable. Therefore, the longest in time we can probe is $2\text{ }\mu\text{s}$. Excited molecules flying

outside the beam cross-section would cause a linear decay, as opposed to an exponential decay.

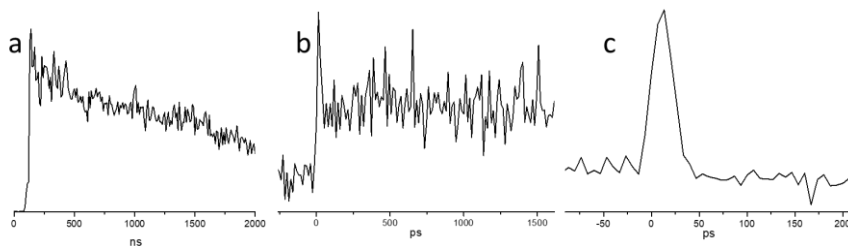


Figure 2. Pump probe of the xanthine (7H). All traces pumped at the origin (36751 cm^{-1}) and probed with ns 193 nm (a), ps 213 nm (b), and ps 266 nm (c). Note the changes in the x-axes. Pump probe traces with ps 213 nm as probe (b) and taken with the pump at the origin, 37133 , 37230 , 37334 , 37586 , and 38008 cm^{-1} all looked similar.

Pump probe was attempted using both ps 213 nm and ps 266 nm as probes, a difference of 1.21 eV. Using the lower energy ps 266 nm, the decay traced the instrument response function (IRF), as seen in figure 2(c), which we estimate to be ~ 30 ps. The trace then returned to baseline. Therefore, the dynamics the ps 266 nm probes is no more than 30 ps, most likely shorter. From our experience, we cannot probe dynamics faster than ~ 1 ps. 1 ps is therefore the lower bound of what the lifetime could be. Alternatively, probing with the higher energy ps 213 nm shows an IRF trace followed by an elevated baseline for the remainder of the measurement. In these ps 213 nm decay traces, we attribute the IRF trace to the same dynamics observed with ps 266 nm and the elevated baseline to the decay channel we observe with ns 193 nm. Because the 213 nm has an IRF trace at each peak, we assume the < 30 ps decay mechanism to be present at every peak.

With this in mind, ps 266 nm is ionizing only the highest excited states. The nature of this state(s) will be discussed later. Quickly, xanthine undergoes intramolecular vibrational redistribution (IVR) and possibly internal conversion (IC), lowering its electronic energy,

disallowing ps 266 nm to probe from these lower-energy states. This relaxation occurs < 30 ps. Ps 213 nm is high enough in energy to probe both these higher- and lower-energy states. The higher-energy, faster states are shown by the IRF trace. The lower-energy, slower relaxation is shown by the elevated baseline. Ns 193 nm cannot observe these faster states due to its much slower time resolution. It can only probe the lower-energy, slower decay. And this slower decay is ultraslow, shown by its lifetime being $> 2 \mu\text{s}$. Note these dynamics do not noticeably change over the 1300 cm^{-1} we observed, though the signal amplitude did change.

The 2C-R2PI spectrum of 9-methylxanthine is presented in Fig. 3. We had to focus the pump and probe beams to get signal on 9-methylxanthine. The spectrum shown was taken using ps 213 nm as probe. Unlike the R2PI spectrum of xanthine (7H), this spectrum has no clear origin or vibronic modes. It is defined by a broad onset of signal. The signal levels off going further to the blue, but no definitive peaks are ever observed. This spectrum is similar to the spectra of both thymine and uracil.³⁸⁻³⁹ Though not entirely clear, this slow rise in signal may be due to poor Frank-Condon factors at the origin with better overlap to the blue. The spectrum is real, as opposed to an artifact, because we were able to pump probe at all energies. The red arrows indicate where pump probes were taken. We chose those energies to pump probe because they provided sufficient signal without imparting too much excess energy.

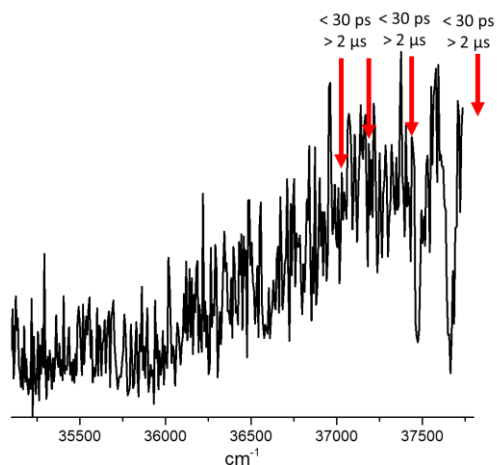


Figure 3. 2C-R2PI spectrum of 9-methylxanthine using ps 213 nm as probe. Red arrows indicate where pump probe traces were taken. Pump energies were set to 37037 cm^{-1} , 37174 cm^{-1} , 37453 cm^{-1} , and 37878 cm^{-1} . The dips around 37500 cm^{-1} are laser power artifacts.

Pump probes for 9-methylxanthine were taken using ps 213 nm with a step size of ~ 30 ps (Fig. 4 and Fig. S4). Decay traces taken at all pump energies looked similar, showing an IRF followed by elevated background. When taken with a step size of 6.6 ps, the traces again match to IRF with an elevated baseline following (Fig. S5). Unfortunately, we could not pump probe using ns 193 nm because we had to focus to get signal. We could not overlap the pump laser with the probe laser well enough to get consistent signal when trying to probe with ns 193 nm.

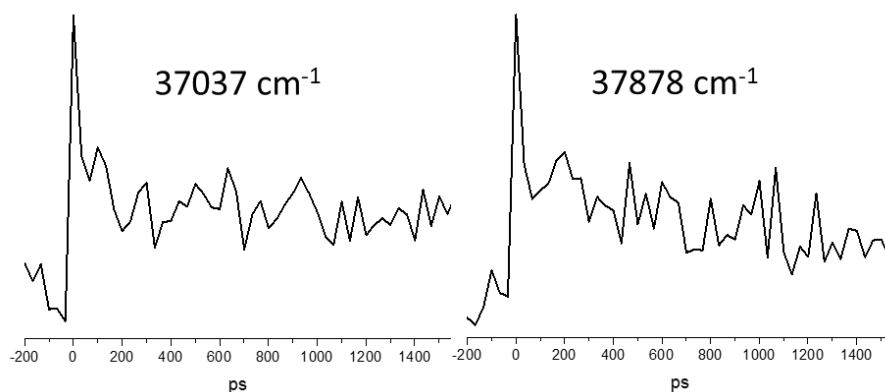


Figure 4. Pump probes of 9-methylxanthine taken in the ps regime using ps 213 nm as probe with step size ~ 30 ps.

The relaxation dynamics of 9-methylxanthine are similar to xanthine (7H). A < 30 ps decay component is observed followed by a long-lived component. Unfortunately, without ns pump probe traces, we cannot say how much longer the long-lived component is. But the ps 213 nm is able to probe the initially fast decay channel and the following slower channel. These dynamics do not noticeably change over the 800 cm^{-1} that we observed.

Domcke et al.³³ confirmed using theoretical calculations that only the 7H tautomer of xanthine should be observed in the gas phase. This was based on the fact that the 7H tautomer is the lowest energy tautomer. Further, the Frank-Condon factors for the origin transition of the 7H tautomer are much greater compared to the 9H tautomer. In fact, they say xanthine (9H) should not be observed in the gas phase due to its poor Frank-Condon factors. And indeed we cannot observe the 9H tautomer. But the poor Frank-Condon factors of xanthine (9H) can potentially explain the R2PI spectrum of 9-methylxanthine. Such spectra with a slow rise in signal have been attributed to poor Frank-Condon factors, such as for thymine and uracil.³⁸⁻³⁹ Potentially, the methylation at the N9 position increases the oscillator strength just enough for it to be observed in the gas phase. Also note that focusing of the pump and probe beams were still required to observe 9-methylxanthine.

The previous studies on xanthine do not support what we observe in the gas-phase. First, gaseous xanthine (7H) and 9-methylxanthine both have two decay components, one < 30 ps and another ultraslow component. They may have faster components, and we just cannot see them. Specifically, the xanthines have been noted for < 1 ps decays in solution, which is supported by theory. This is probably faster than we can observe using R2PI, as stated above. Only Rottger and coworkers noted a small relatively long-lived component of 36 ps when studying XMP in solution.³⁵ They explained this longer decay to either trapping in the

$\pi\pi^*$ or transfer of part of the population to a dark $n\pi^*$. We do not anticipate being able to see (ionize) < 1 ps decays in our beam. The IRF traces we *do* see are most likely attributed to 1-30 ps lifetimes. Therefore, either the ultrafast solution phase dynamics have slowed down in the gas phase or we are observing slower components that could not be seen in solution.

Solvation typically stabilizes $\pi\pi^*$ and destabilizes $n\pi^*$ states. So the nearby $n\pi^*$ state that Domcke describes for isolated xanthine (7H) may not matter in the solution phase because it is too high compared to the $\pi\pi^*$. Therefore, in solution-phase, xanthine may just undergo ultrafast nonradiative decay from $\pi\pi^*$ to S_0 as Domcke described for isolated xanthine (7H). But in the gas-phase, the $\pi\pi^*$ and $n\pi^*$ may be close enough for significant vibronic coupling. After excitation, 7H and 9-methylxanthine may internally convert to $n\pi^*$ and get trapped for a while until it can undergo internal conversion to the ground state. This agrees with Domcke who observed a barrier to $n\pi^*/S_0$ CI. This would explain the faster decay we observe which is still on the order of tens of ps and not ultrafast. But once in the $n\pi^*$, the system can also do ISC to a very long-lived triplet state. This ISC assignment is based on the long-lived state we observe. No other researchers have talked about a triplet state for xanthines.

This overall excited state dynamics behavior for the xanthines contrasts with 2-aminopurine (2-AP), which also has significant differences in its dynamics when going from gas to solution phase. The consensus so far for xanthine is that in solution phase it undergoes ultrafast nonradiative decay and reaches a $^1\pi\pi^*/S_0$ CI via distortion of the five-membered ring.^{19, 33-35} *In vacuo*, xanthine (7H) and 9-methylxanthine experimentally appear to do internal conversion to an $n\pi^*$ state. Once there, they may internally convert to the ground state or undergo ISC to a triplet state. The dynamics of 2-AP are also differentiated by phase.

2-AP is noted for its strong fluorescent signature in solution from a bright $\pi\pi^*$ due to a barrier to internal conversion.⁴⁰ Meanwhile, gaseous 2-AP decays quickly via internal conversion from a bright $^1\pi\pi^*$ to $^1n\pi^*$ due to vibronic coupling, and from there quickly decay to the ground state or undergo ISC to an ultralong-lived triplet state.^{26-27, 41-44} This difference in behavior for 2-AP is attributed to the relative energies of the lowest $\pi\pi^*$ and $n\pi^*$ states. In vacuum, the $^1\pi\pi^*$ and $^1n\pi^*$ are near equal in energy, allowing for significant vibronic coupling and quickly transferring the population into the $^1n\pi^*$.^{26, 40, 44} The wavepacket is trapped in the $^1n\pi^*$ by a slight barrier, allowing for ISC to the near resonant T_2 state while explaining the relatively fast internal conversion of ~ 100 ps.²⁷ Upon solvation of 2-AP, the energy of the bright $^1\pi\pi^*$ lowers and the $^1n\pi^*$ rises. This energy gap creates a barrier, trapping the system in the $^1\pi\pi^*$, causing fluorescence and a longer lifetime. Fluorescence quantum yield increases with solvent polarity. The energy levels are significantly modulated by hydrogen bonding to the amino group on C2, where a single hydrogen bond will cause fluorescence.^{27, 44}

Solvation appears to have similar effects on the energy levels of the lowest $^1\pi\pi^*$ and $^1n\pi^*$ states of xanthine. It is not clear at this time if $^1\pi\pi^*$ stabilization of xanthine is at site-specific as the amino group of 2-AP. But while solvation appears to decrease the photostability of 2-AP, it significantly increases the photostability of xanthine. After excitation, solvated xanthine cannot access the dark $^1n\pi^*$ due to an energy gap between the two states. The energy gap prevents excited xanthine from following the competing decay channel through the $^1n\pi^*$. Instead, it can only follow the $^1\pi\pi^*$ channel down to the $^1\pi\pi^*/S_0$ CI, and undergo ultrafast nonradiative decay. This is a similar relaxation to guanine^{4, 9-10} and hypoxanthine¹⁹⁻²³ in solution. Meanwhile, the amino substitution at the C2 site of 2-AP

prevents it from undergoing ultrafast nonradiative decay. It cannot follow the dynamics of adenine¹¹⁻¹⁵ (6-AP) by $^1\pi\pi^* \rightarrow ^1n\pi^* \rightarrow S_0$ via pyramidalization at C2-N3. Nor can 2-AP follow guanine⁹⁻¹⁰ by $\pi\pi^*/S_0$ CI via out-of-plane distortion at C2. Both of these relaxation channels for 2-AP are prohibited by the C2 amino group.

Many gaseous purines follow the same decay mechanism as xanthine (7H) and 9-methylxanthine in the gas phase. Cytosine⁴⁵⁻⁵¹, 2,6-diaminopurine (7H), 2-AP, and purine⁵²⁻⁵³ all decay from their bright $\pi\pi^*$ states to a dark $n\pi^*$, and then bifurcate to either internal conversion to the ground state or undergo ISC. The relative ratio of internal conversion to ISC greatly affects the photostability of these systems. Clearly substitution at C2 and C6 greatly affects photostability.

For the discussion that follows, all results are for the gas phase systems. 2-AP is relatively photostable with a lifetime of 150 ps at the origin. Interestingly, its lifetime only reduces to 80 ps with 1500 cm^{-1} excess energy. Further, there is a very long-lived triplet state component to 2-AP as well. Addition of an oxo group at C6 to 2-AP creates guanine, which has so far not been seen in the gas phase most likely due to its ultrafast dynamics. But the addition of the oxo group at C6 does not guarantee photostability. Replacing the amino group at C2 of guanine with an oxo group creates xanthine, having oxo substitutions at C2 and C6. And guanine has much higher photostability than xanthine. Though it is clear that modifying C2 and C6 affect photostability, it is not entirely clear how different modifications affect photostability.

We have found the lowest vibronic transitions of xanthine (7H) and 9-methylxanthine. The R2PI spectrum of 9-methylxanthine is noted for its slow, broad onset of signal, most

likely due to poor Frank-Condon overlap. Both systems have two decay channels that appear unchanged over the range of at least 800 cm^{-1} . The faster channel has a lifetime $< 30\text{ ps}$ and is attributed to prompt $\pi\pi^*$ population transfer to $n\pi^*$, and then internal conversion to the ground state. The slower channel was measured to be $> 2\text{ }\mu\text{s}$ for xanthine (7H) and at least tens of ns for 9-methylxanthine, as we were unable to conduct ns pump probe on it. ISC to a long-lived triplet state is assigned to this slower channel.

These dynamics and lack of photostability in the gas phase stand in stark contrast to the behavior of many xanthine derivatives and tautomers in solution. They have been well-studied both experimentally and theoretically, and found to be highly photostable due to ultrafast nonradiative decay. Stabilization of the $\pi\pi^*$ and destabilization of $n\pi^*$ electronic states upon solvation cause the change in photostability going to solution phase.

Supplemental

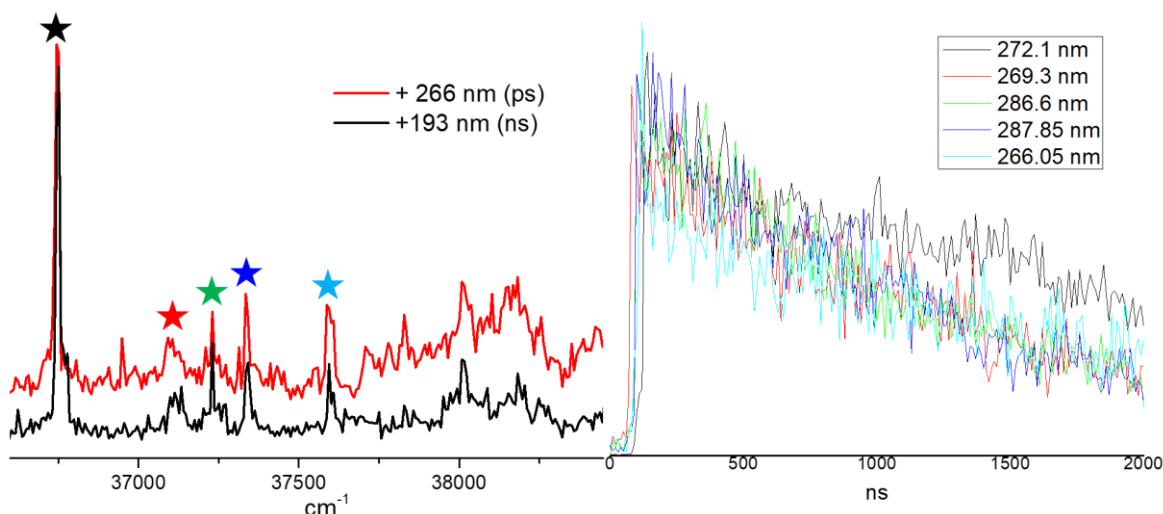


Figure S1. Left: Xanthine (7H) 2C-R2PI spectrum using ps 266 nm (red) and ns 193 nm (black) as probes. Colored stars represent where the pump wavelengths were set for pump with the probe using ns 193 nm. Right: pump probe traces using ns 193 nm, colors refer to the pump wavelength as shown by the colored stars on the left.

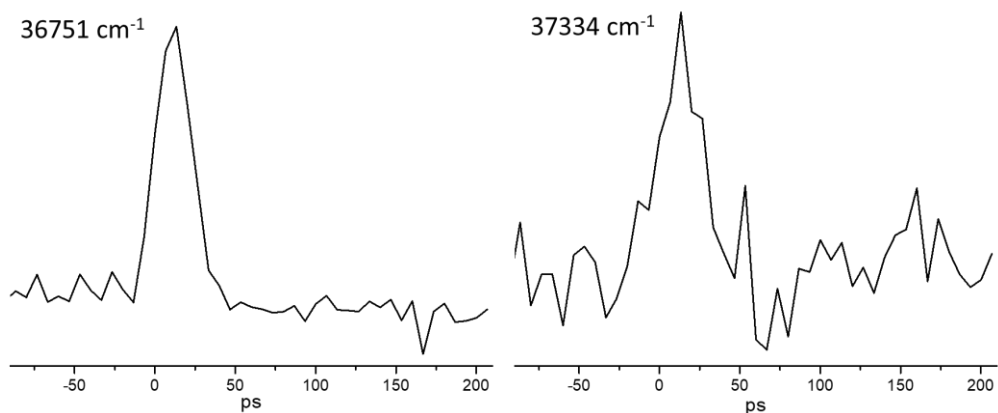


Figure S2. Pump probes of xanthine (7H) using 36751 cm^{-1} (left) and 37334 cm^{-1} (right) as pump and ps 266 nm as probe. Both traces fit to IRF ($\sim 30\text{ ps}$) and can therefore be $< 30\text{ ps}$.

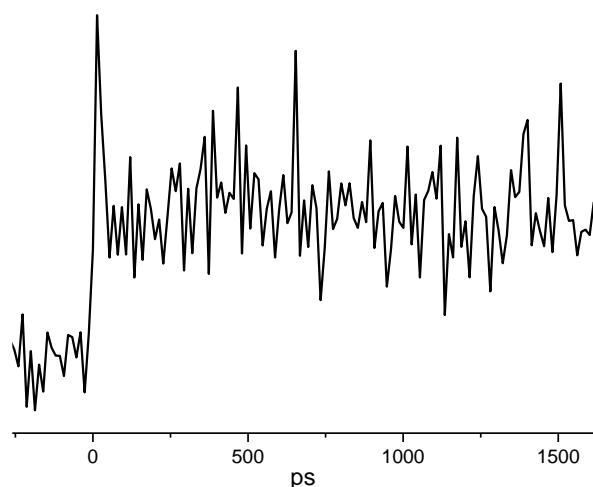


Figure S3. Pump probe trace of xanthine (7H) at the origin (36751 cm^{-1}) with ps 213 nm probe. Traces taken with the pump at 37133 , 37230 , 37334 , 37586 , 38008 cm^{-1} all looked similar.

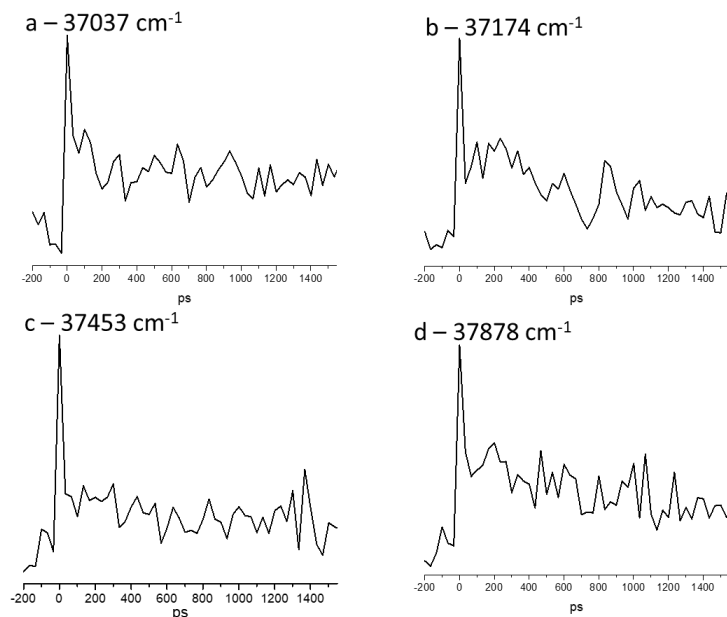


Figure S4. Pump probes of 9-methylxanthine using ps 213 nm as probe with step size ~ 30 ps. Pump energies were at 37037 cm^{-1} (a), 37174 cm^{-1} (b), 37453 cm^{-1} (c), 37878 cm^{-1} (d).

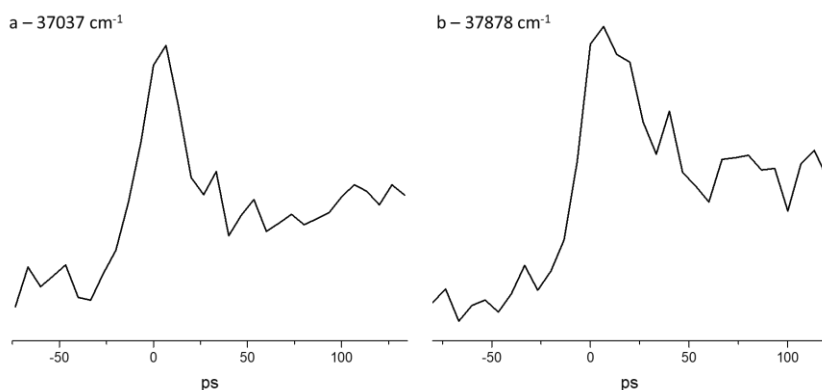


Figure S5. Pump probes of 9-methylxanthine using ps 213 nm as probe with step size of ~ 6.5 ps. Pump energies were at 37037 cm^{-1} (a), 37878 cm^{-1} (b).

References

1. Gustavsson, T.; Improta, R.; Markovitsi, D., DNA/RNA: Building Blocks of Life Under UV Irradiation. *The Journal of Physical Chemistry Letters* **2010**, *1* (13), 2025-2030.
2. Middleton, C. T.; de La Harpe, K.; Su, C.; Law, Y. K.; Crespo-Hernandez, C. E.; Kohler, B., DNA excited-state dynamics: from single bases to the double helix. *Annu Rev Phys Chem* **2009**, *60*, 217-39.
3. De Vries, M. S., Isolated DNA base pairs, interplay between theory and experiment. **2008**, 323.
4. Canuel, C.; Mons, M.; Piuze, F.; Tardivel, B.; Dimicoli, I.; Elhanine, M., Excited states dynamics of DNA and RNA bases: characterization of a stepwise deactivation pathway in the gas phase. *J Chem Phys* **2005**, *122* (7), 074316.

5. Kang, H.; Lee, K. T.; Jung, B.; Ko, Y. J.; Kim, S. K., Intrinsic Lifetimes of the Excited State of DNA and RNA Bases. *J Am Chem Soc* **2002**, *124*, 12958 - 12959.
6. Beckstead, A. A.; Zhang, Y.; de Vries, M. S.; Kohler, B., Life in the light: nucleic acid photoproperties as a legacy of chemical evolution. *Phys Chem Chem Phys* **2016**, *18* (35), 24228-38.
7. Pecourt, J.-M. L.; Peon, J.; Kohler, B., DNA Excited-State Dynamics: Ultrafast Internal Conversion and Vibrational Cooling in a Series of Nucleosides. *Journal of the American Chemical Society* **2001**, *123* (42), 10370-10378.
8. Boldissar, S.; de Vries, M. S., How nature covers its bases. *Phys Chem Chem Phys* **2018**, *20* (15), 9701-9716.
9. Barbatti, M.; Szymczak, J. J.; Aquino, A. J.; Nachtigallova, D.; Lischka, H., The decay mechanism of photoexcited guanine - a nonadiabatic dynamics study. *J Chem Phys* **2011**, *134* (1), 014304.
10. Yamazaki, S.; Domcke, W.; Sobolewski, A. L., Nonradiative decay mechanisms of the biologically relevant tautomer of guanine. *J Phys Chem A* **2008**, *112* (47), 11965-8.
11. Marian, C. M., A new pathway for the rapid decay of electronically excited adenine. *J Chem Phys* **2005**, *122* (10), 104314.
12. Perun, S.; Sobolewski, A. L.; Domcke, W., Photostability of 9H-adenine: mechanisms of the radiationless deactivation of the lowest excited singlet states. *Chemical Physics* **2005**, *313* (1-3), 107-112.
13. Perun, S.; Sobolewski, A. L.; Domcke, W., Ab initio studies on the radiationless decay mechanisms of the lowest excited singlet states of 9H-adenine. *J Am Chem Soc* **2005**, *127* (17), 6257-65.
14. Barbatti, M.; Lischka, H., Nonadiabatic Deactivation of 9H-Adenine A Comprehensive Picture Based on Mixed Quantum-Classical Dynamics. *J Am Chem Soc* **2008**, *130*, 6831 - 6839.
15. Fabiano, E.; Thiel, W., Nonradiative deexcitation dynamics of 9H-adenine: an OM2 surface hopping study. *J Phys Chem A* **2008**, *112* (30), 6859-63.
16. Siouri, F. M.; Boldissar, S.; Berenbeim, J. A.; de Vries, M. S., Excited State Dynamics of 6-Thioguanine. *J Phys Chem A* **2017**, *121* (28), 5257-5266.
17. Marian, C. M., The guanine tautomer puzzle: quantum chemical investigation of ground and excited states. *J Phys Chem A* **2007**, *111* (8), 1545-53.
18. Gate, G.; Szabla, R.; Haggmark, M. R.; Sponer, J.; Sobolewski, A. L.; de Vries, M. S., Photodynamics of alternative DNA base isoguanine. *Phys Chem Chem Phys* **2019**, *21* (25), 13474-13485.
19. Chen, J.; Kohler, B., Ultrafast nonradiative decay by hypoxanthine and several methylxanthines in aqueous and acetonitrile solution. *Phys Chem Chem Phys* **2012**, *14* (30), 10677-82.
20. Villabona-Monsalve, J. P.; Noria, R.; Matsika, S.; Peon, J., On the accessibility to conical intersections in purines: hypoxanthine and its singly protonated and deprotonated forms. *J Am Chem Soc* **2012**, *134* (18), 7820-9.
21. Röttger, K.; Siewertsen, R.; Temps, F., Ultrafast electronic deactivation dynamics of the rare natural nucleobase hypoxanthine. *Chemical Physics Letters* **2012**, *536*, 140-146.
22. Guo, X.; Lan, Z.; Cao, Z., Ab initio insight into ultrafast nonadiabatic decay of hypoxanthine: keto-N7H and keto-N9H tautomers. *Phys Chem Chem Phys* **2013**, *15* (26), 10777-82.

23. Guo, X.; Zhao, Y.; Cao, Z., A QM/MM MD insight into photodynamics of hypoxanthine: distinct nonadiabatic decay behaviors between keto-N7H and keto-N9H tautomers in aqueous solution. *Phys Chem Chem Phys* **2014**, *16* (29), 15381-8.
24. Guo, X.; Yuan, H.; An, B.; Zhu, Q.; Zhang, J., Ultrafast excited-state deactivation of 9-methylhypoxanthine in aqueous solution: A QM/MM MD study. *J Chem Phys* **2016**, *144* (15), 154306.
25. Martinez-Fernandez, L.; Arslançan, S.; Ivashchenko, D.; Crespo-Hernandez, C. E.; Corral, I., Tracking the origin of photostability in purine nucleobases: the photophysics of 2-oxopurine. *Phys Chem Chem Phys* **2019**, *21* (25), 13467-13473.
26. Rachofsky, E. L.; Ross, J. B. A.; Krauss, M.; Osman, R., CASSCF Investigation of Electronic Excited States of 2-Aminopurine. *The Journal of Physical Chemistry A* **2001**, *105* (1), 190-197.
27. Lobsiger, S.; Blaser, S.; Sinha, R. K.; Frey, H. M.; Leutwyler, S., Switching on the fluorescence of 2-aminopurine by site-selective microhydration. *Nat Chem* **2014**, *6* (11), 989-93.
28. Smolarek, S.; Rijs, A. M.; Buma, W. J.; Drabbels, M., Absorption spectroscopy of adenine, 9-methyladenine, and 2-aminopurine in helium nanodroplets. *Phys Chem Chem Phys* **2010**, *12* (48), 15600-6.
29. Callahan, M. P.; Smith, K. E.; Cleaves, H. J., 2nd; Ruzicka, J.; Stern, J. C.; Glavin, D. P.; House, C. H.; Dworkin, J. P., Carbonaceous meteorites contain a wide range of extraterrestrial nucleobases. *Proc Natl Acad Sci U S A* **2011**, *108* (34), 13995-8.
30. Piccirilli, J. A.; Krauch, T.; Moroney, S. E.; Benner, S. A., Enzymatic incorporation of a new base pair into DNA and RNA extends the genetic alphabet. *Nature* **1990**, *343* (6253), 33-7.
31. Saladino, R.; Crestini, C.; Neri, V.; Brucato, J. R.; Colangeli, L.; Ciciriello, F.; Di Mauro, E.; Costanzo, G., Synthesis and degradation of nucleic Acid components by formamide and cosmic dust analogues. *Chembiochem* **2005**, *6* (8), 1368-74.
32. Wachtershauser, G., An all-purine precursor of nucleic acids. *Proc Natl Acad Sci U S A* **1988**, *85* (4), 1134-5.
33. Yamazaki, S.; Sobolewski, A. L.; Domcke, W., Photophysics of xanthine: computational study of the radiationless decay mechanisms. *Phys Chem Chem Phys* **2009**, *11* (43), 10165-74.
34. Changuenet-Barret, P.; Kovacs, L.; Markovitsi, D.; Gustavsson, T., Xanthines Studied via Femtosecond Fluorescence Spectroscopy. *Molecules* **2016**, *21* (12).
35. Rottger, K.; Stellmacher, R.; Stuhldreier, M. C.; Temps, F., Ultrafast Electronic Deactivation Dynamics of Xanthosine Monophosphate. *Molecules* **2017**, *22* (1).
36. Meijer, G.; De Vries, M. S.; Hunziker, H. E.; Wendt, H. R., Laser Desorption Jet-Cooling of Organic Molecules. *Applied Physics B* **1990**, *51*, 395 - 403.
37. Callahan, M. P.; Crews, B.; Abo-Riziq, A.; Grace, L.; de Vries, M. S.; Gengeliczki, Z.; Holmes, T. M.; Hill, G. A., IR-UV double resonance spectroscopy of xanthine. *Phys Chem Chem Phys* **2007**, *9* (32), 4587-91.
38. Ligare, M.; Siouri, F.; Bludsky, O.; Nachtigallova, D.; de Vries, M. S., Characterizing the dark state in thymine and uracil by double resonant spectroscopy and quantum computation. *Phys Chem Chem Phys* **2015**, *17* (37), 24336-41.
39. Brady, B. B.; Peteanu, L. A.; Levy, D. H., The electronic spectra of the pyrimidine bases uracil and thymine in a supersonic molecular beam. *Chemical Physics Letters* **1988**, *147* (6), 538-543.

40. Reichardt, C.; Wen, C.; Vogt, R. A.; Crespo-Hernandez, C. E., Role of intersystem crossing in the fluorescence quenching of 2-aminopurine 2'-deoxyriboside in solution. *Photochem Photobiol Sci* **2013**, *12* (8), 1341-50.
41. Lim, E. C., Proximity effect in molecular photophysics: dynamical consequences of pseudo-Jahn-Teller interaction. *The Journal of Physical Chemistry* **1986**, *90* (26), 6770-6777.
42. Lobsiger, S.; Sinha, R. K.; Trachsel, M.; Leutwyler, S., Low-lying excited states and nonradiative processes of the adenine analogues 7H- and 9H-2-aminopurine. *J Chem Phys* **2011**, *134* (11), 114307.
43. Sinha, R. K.; Lobsiger, S.; Trachsel, M.; Leutwyler, S., Vibronic spectra of jet-cooled 2-aminopurine.H₂O clusters studied by UV resonant two-photon ionization spectroscopy and quantum chemical calculations. *J Phys Chem A* **2011**, *115* (23), 6208-17.
44. Barbatti, M.; Lischka, H., Why water makes 2-aminopurine fluorescent? *Phys Chem Chem Phys* **2015**, *17* (23), 15452-9.
45. Blaser, S.; Trachsel, M. A.; Lobsiger, S.; Wiedmer, T.; Frey, H. M.; Leutwyler, S., Gas-Phase Cytosine and Cytosine-N1-Derivatives Have 0.1-1 ns Lifetimes Near the S₁ State Minimum. *J Phys Chem Lett* **2016**, *7* (5), 752-7.
46. Ismail, N.; Blancafort, L.; Olivucci, M.; Kohler, B.; Robb, M. A., Ultrafast Decay of Electronically Excited Singlet Cytosine via a π, π^* to nO, π^* State Switch. *Journal of the American Chemical Society* **2002**, *124* (24), 6818-6819.
47. Kistler, K. A.; Matsika, S., Radiationless decay mechanism of cytosine: an ab initio study with comparisons to the fluorescent analogue 5-methyl-2-pyrimidinone. *J Phys Chem A* **2007**, *111* (14), 2650-61.
48. Lobsiger, S.; Etinski, M.; Blaser, S.; Frey, H. M.; Marian, C.; Leutwyler, S., Intersystem crossing rates of S₁ state keto-amino cytosine at low excess energy. *J Chem Phys* **2015**, *143* (23), 234301.
49. Mai, S.; Marquetand, P.; Richter, M.; Gonzalez-Vazquez, J.; Gonzalez, L., Singlet and triplet excited-state dynamics study of the keto and enol tautomers of cytosine. *Chemphyschem* **2013**, *14* (13), 2920-31.
50. Richter, M.; Marquetand, P.; Gonzalez-Vazquez, J.; Sola, I.; Gonzalez, L., Femtosecond Intersystem Crossing in the DNA Nucleobase Cytosine. *J Phys Chem Lett* **2012**, *3* (21), 3090-5.
51. Merchan, M.; Serrano-Andres, L.; Robb, M. A.; Blancafort, L., Triplet-state formation along the ultrafast decay of excited singlet cytosine. *J Am Chem Soc* **2005**, *127* (6), 1820-5.
52. Crespo-Hernandez, C. E.; Martinez-Fernandez, L.; Rauer, C.; Reichardt, C.; Mai, S.; Pollum, M.; Marquetand, P.; Gonzalez, L.; Corral, I., Electronic and structural elements that regulate the excited-state dynamics in purine nucleobase derivatives. *J Am Chem Soc* **2015**, *137* (13), 4368-81.
53. Schneider, M.; Hain, T.; Fischer, I., Resonance-enhanced multiphoton ionisation of purine. *Chemphyschem* **2009**, *10* (4), 634-6.

IV. Excited state dynamics of DNA base-stacking free from solvent

Interest in excited state dynamics and the origins of life extend beyond the nucleobases. The oligomeric form of the nucleobases, DNA, is the media form for the storage of genetic material. DNA can exist as a single strand or double strand, which leads to the renowned double-helix structure. Though made of individual nucleobases, DNA actually has notably different dynamics. While the nucleobases are dominated by ultrafast monomer decay, the excited state dynamics of DNA is controlled by its intermolecular interactions: base stacking via π - π interaction between adjacent intrastrand bases, and base pairing via hydrogen bonding across interstrand pairs.

Base stacked complexes will decay by exciton formation and decay. This has been widely studied by in solution (see below for more detail and references). Base paired complexes will decay by proton transfer across the hydrogen-bonded pair. Gas phase studies have focused on this dynamic. The segregation between interaction and phase is because base stacked complexes are heavily stabilized and favored in solution while base pairing is exclusively seen in the gas phase. Thus, base stacking and exciton decay have been studied little *in vacuo* because the π - π interaction requires at least two H₂O molecules to stabilize, a difficult feat in vacuum. And most gas phase instruments cannot study ions, prohibiting the direct study of DNA itself.

A possible work-around to study the DNA base stacking interaction in the gas phase is to use a neutral single-stranded DNA mimic. This mimic can induce the base stacking, allowing for the study of the exciton formation and decay. We have developed peptide nucleic acids (PNA) as a suitable neutral DNA mimic. The experimental and computational work shown below is complete, with the article still being prepared for publication. The published version will probably only slightly differ from the below work.

I. Probing the DNA stacking interaction free from solvent using peptide nucleic acids

Gregory Gate^a, Samuel Boldissar^a, Glake A. Hill^b, Amelia A. Fuller^a, and Mattanjah S. de Vries^a

^a Department of Chemistry and Biochemistry, University of California Santa Barbara, CA 93106-9510

^b Department of Chemistry, Computational Center for Molecular Structures and Interactions, Jackson State University, Jackson, MS 39217

^c Department of Chemistry and Biochemistry, Santa Clara University, 500 El Camino Real, Santa Clara, California 95053, United States

The nucleobases, nucleosides, and nucleic acids and their various analogues and derivatives have been extensively studied for their photostability properties and excited state dynamics. Their ability to safely dissipate potentially harmful electronic energy before damaging photoreactions can occur has implications for the origins of life and the safeguarding of genetic material. There have been many reviews over the past two decades on the development of this theory and the research supporting it.¹⁻⁶

Individual bases in oligonucleotides interact via noncovalent interactions: π - π stacking between adjacent intrastrand bases, and hydrogen-bonding between interstrand base pairs. The excited state dynamics caused by these two interactions are different. In the gas phase nucleobase dimers only interact via hydrogen-bonded interactions. Various intermolecular G-G, G-C, and CC base pairs have been observed, though not in the Watson-Crick (WC) arrangement.^{7-10,11} The dynamics of the G-C Watson Crick base pair have been probed using analogues.¹² Photoelectron spectroscopy has shown adenine dimers with at least three water molecules can form a stacked structure with different dynamics.¹³ It is predicted between 2-8 water molecules are needed to preferentially stabilize stacked structures in the gas phase.¹⁴⁻¹⁶

The structure and dynamics of stacked bases have not been studied in the gas phase much because it is difficult to form microhydrated clusters. Studying single-stranded DNA in the gas phase is also difficult due to its charged phosphate backbone, while in our set-up we can only study neutral molecules. To circumvent this problem, here we study peptide nucleic acids (PNA), a DNA analogue.

PNA is a polymer with a neutral pseudopeptide backbone as opposed to DNA which has an anionic sugar phosphate backbone. Nielsen and co-workers reported the initial development and research on PNA.¹⁷⁻¹⁹ They found PNA-PNA duplexes to have greater stability than any other duplex. PNA can be used for antisense and antigen drugs. PNA-PNA and PNA-DNA duplexes adopt a “P-form” helix noted for its wide and deep major groove and shallow and narrow minor groove.²⁰⁻²³ The hydrophobic backbone is flexible while bases remain rigid. This is due to weaker bonding between the base and backbone and results in single-stranded PNA being the most stable helix. PNA duplexes are more flexible than DNA and thus more likely to remain in a stacked helical geometry.²⁴⁻²⁵ Callahan et al. recently found evidence that PNA could have existed on an early Earth, demonstrating the synthesis of nucleobases with carbonyls attached under prebiotic conditions.²⁶ Nucleobases and amino acids evolved alongside each other prebiotically and PNA fits the genetic requirements for life.

ESI-MS/MS and ion-mobility MS have found DNA duplexes to be metastable in the gas phase, retaining their helicity for a short period of time after electrospray.²⁷⁻²⁸ Longer duplexes were found to retain their helical geometries while shorter duplexes had globular structures.

Herein, we report on a new approach to probe the structure and photodynamics of the stacked base structure in the gas phase free from solvent using PNA. We report on the synthesis and spectroscopic characterization of guanine-guanine (GG) and thymine-thymine (TT) PNA homodimers (Fig. 1). Homodimers are the simplest systems that show excimer character in solution.²⁹

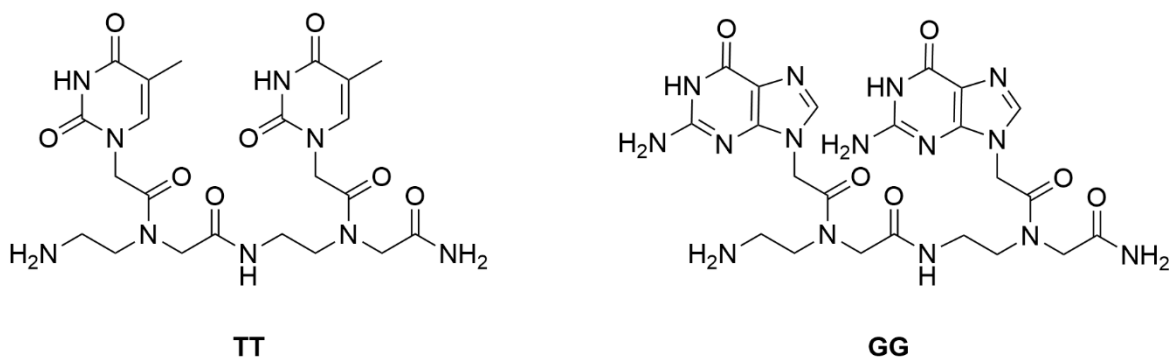


Figure 1. Structure of thymine-thymine (TT) and guanine-guanine (GG) peptide nucleic acid homodimers.

Briefly, TT and GG were synthesized on solid support following reported methods.³⁰ Crude PNA dimers were purified by reverse-phase high-pressure liquid chromatography (RP-HPLC) and identities were confirmed by mass spectrometry. The setup and instrumentation to conduct REMPI has been described in detail elsewhere and only a short description follows.³¹ Solid PNA was laser desorbed from a translating graphite bar. A molecular beam of argon at 8 atm backing pressure quickly cooled the gaseous PNA down to ~10 K. REMPI was then used to excite and ionize PNA, which was then directed into a time-of-flight mass spectrometer for detection. 2 color resonant 2 photo ionization (2C-R2PI) spectra were generated using the tunable output of an optical parametric generator (OPG) (~100 μ J in UV; 30 ps pulse width) as the pump pulse. 213 nm (200 μ J; 30 ps pulse width) or 193 nm (2 mJ; 8 ns pulse width) pulses were used as the probe. Tunable IR light (2 mJ) was generated from an optical parametric oscillator/optical parametric amplifier in the

2800 – 4000 cm^{-1} range. IR-UV double resonance spectroscopy scans the IR wavelength while holding the excitation/ionization pulses on a constant resonance wavelength. The IR pulse was fired 200 ns prior to the probe pulses. This technique was also digitally chopped to simultaneously generate a spectrum without IR contribution. Pump probe spectroscopy was conducted in the ps regime using a ps OPG pulse at a constant wavelength as pump and a ps 213 nm pulse as probe.

A global conformational search was performed using MacroModel (Schrödinger Release 2020-3: MacroModel, Schrödinger, LLC, New York, NY, 2020) found within the Schrodinger Suite. The potential energy surface was searched using Monte Carlo Multiple Minimum (MCOMM) method and the force field, OPLS3e.³² Structures within 20 kcal/mol were then optimized using M06-2X/6-31G(d) in Gaussian16 (Normal Gaussian citation) . Five conformers were within 10 kcal/mol of the lowest conformer. These five conformers and the order of the relative energies were confirmed using a higher basis set, 6-311+G(d). The frequencies of these five conformers were then calculated and compared to experimental values.

We calculated the lowest energy structure of TT and expect the majority of our signal to come from this conformer (Fig. 2). It shows base stacking with some amount of offset to stabilize the π - π interaction. This base offset is similar to what occurs in DNA. All lowest energy structures display base stacking, with some amount of overlap between the thymine bases. The lowest energy conformer that has unstacked bases is characterized by a T-shaped projection of the thymine moieties relative to each other, being perpendicular relative to the plane of the thymines. This conformer is 26.10 kJ/mol higher in energy than the globally lowest energy conformer. Though significantly higher in energy, it is possible for this

conformer to exist in the beam. We have experimentally observed tautomers with similar relative stability energies to exist in other systems.

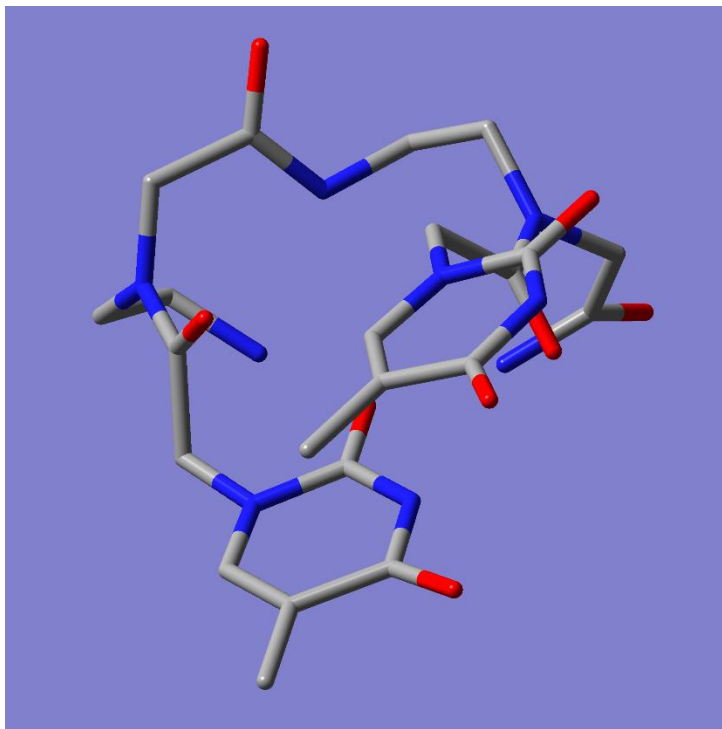


Figure 2. Lowest energy structure of TT calculated at M06-2X/6-31G(d) level

We collected R2PI spectra for the two systems. Figure 3 displays the R2PI spectra for GG and TT. They are remarkably similar with broad onsets and no sharp peaks. These spectra bear resemblance to the R2PI spectra of thymine and uracil, where a broad onset was attributed to poor Frank-Condon factors between the ground state minimum and the lowest energy transitions in the excited state.³³⁻³⁴ By contrast the R2PI spectrum of isolated guanine is marked by discrete peaks. However, the biologically relevant aminoketo N9H tautomer has yet to be observed and a different tautomeric distribution could occur in PNA-GG, since the backbone limits the tautomerization. GG provided about an order of magnitude less signal than TT and therefore at this point we only report further spectroscopic measurements on TT.

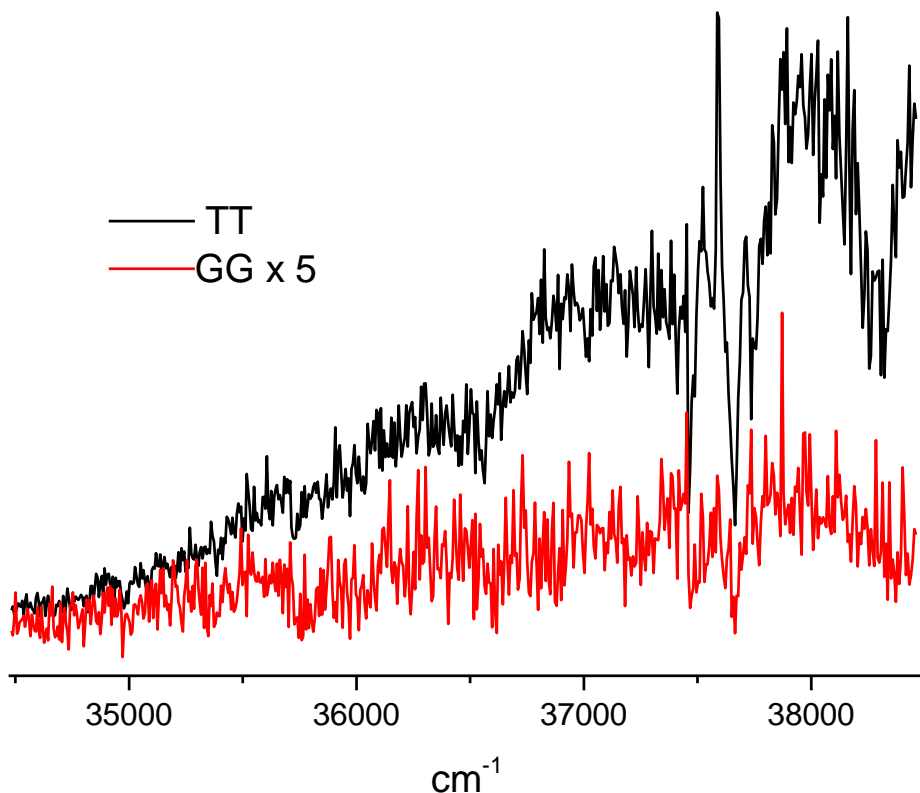


Figure 3. 2C-R2PI of TT (black) and GG (red) using ps OPG and ps 213 as probe. Both beams were focused. The GG signal has been increased by a factor of 5.

Figure 4 shows the experimental and predicted IR spectra of the ground state of TT, obtained by IR-UV double resonance spectroscopy and theoretical calculations. TT broadly absorbs from 2800 – 3500 cm^{-1} , though individual features can still be discerned. The peaks at 3451 and 3506 cm^{-1} in the TT spectrum are consistent with the N3H and N1H stretches of the thymine monomer (Fig. 4 inset).^{33, 35-36} We expect to see the N3H stretch, as it is still free. But N1 is now bound to the PNA backbone so we assign the peak at 3506 cm^{-1} to another N-H stretch from the PNA backbone. The broadening of the IR spectrum is most likely due to the many very similar vibrational modes of TT. These include slightly different electronic environments for similar bonds and intramolecular noncovalent interactions. Further, different conformers may also be present in our molecular beam and contributing to

the signal, causing further broadening. This broadening is in line with other IR spectra of differing thymine complexes in the gas phase.³⁵⁻³⁶ Assignment of a specific geometrical conformer is difficult from these data alone.

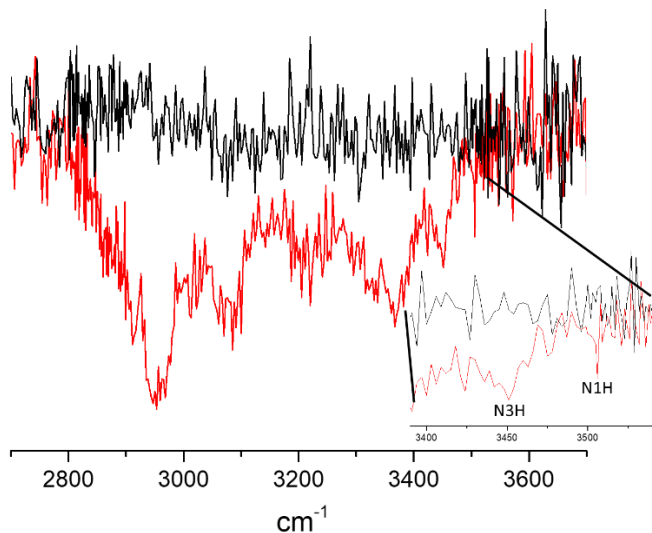


Figure 4. IR-UV spectrum of TT PNA. All pulses were focused. Excitation was at 37037 cm^{-1} . Burn signal is in red and chopped signal is in black for reference. The inset is the zoom-in region of 3390 – 3540 cm^{-1} of TT with the energies of the N3H and N1H stretches of *isolated* thymine labeled.

To assist with geometry assignment, we compare to other thymine studies and our calculated spectra of various conformers. With N1 bound to the PNA backbone and the apparent N3H stretch present, the thymine bases in TT are most likely in the diketo tautomer, similar to thymine monomer in the gas phase. Lack of O-H stretches in the 3700 cm^{-1} region further validates the diketo assignment. C-H stretches are typically found at 3000 – 3300 cm^{-1} but because their intensities are typically weak, they are not expected to significantly contribute to the spectrum here. The broad absorption observed could be due to combination bands of lower energy modes, but they are also not expected to contribute much, especially in comparison to the N3H band intensity. The peak at 3200 cm^{-1} is assigned to a hydrogen-bonded NH stretch or a free CH stretch, according to the calculated spectra for

the TT parallel and T-shaped geometries, respectively. The large peak at 3350 can also be a red-shifted NH stretch due to hydrogen-bonding. We cannot wholly assign the IR spectrum, and the increased signal amplitude in the lower energy region is not understood.

Unfortunately, we cannot decisively identify the TT geometry from these spectra, but there is a good chance that multiple conformers are contributing, likely the global minimum parallel and T-shaped geometries. This also explains the broadening of the experimental spectrum.

Next, we conducted pump-probe on TT using a 37037 cm^{-1} (270 nm) pump and 213 nm probe, both from the ps OPG (Fig. 5a). We can fit the decay with a biexponential using a short lifetime of 30 ps and a much longer decay, shown by the elevated tail at long time points. There is also significant contribution from the instrument response function (IRF), possibly resulting from a process faster than we can resolve. For comparison, a pump probe of isolated thymine was also conducted using 37037 cm^{-1} pump and 213 nm probe from the ps OPG (Fig. 5b). It shows a short decay of almost equal time, but it does not have an elevated baseline at long time points. We also conducted pump-probe using the ps OPG as the pump at 36231 and 37037 cm^{-1} and a ns 193 nm probe (data in Supplemental Information Fig. Sxx). Both show a decay on the order of 100 ns, similar to decays from isolated thymine.³³ The longer decay observed in the ps trace is attributed to be the same decay as the long ns decay observed in ns pump probe. The only difference between the TT and thymine experiments was TT required focusing of the beams to obtain sufficient signal to noise.

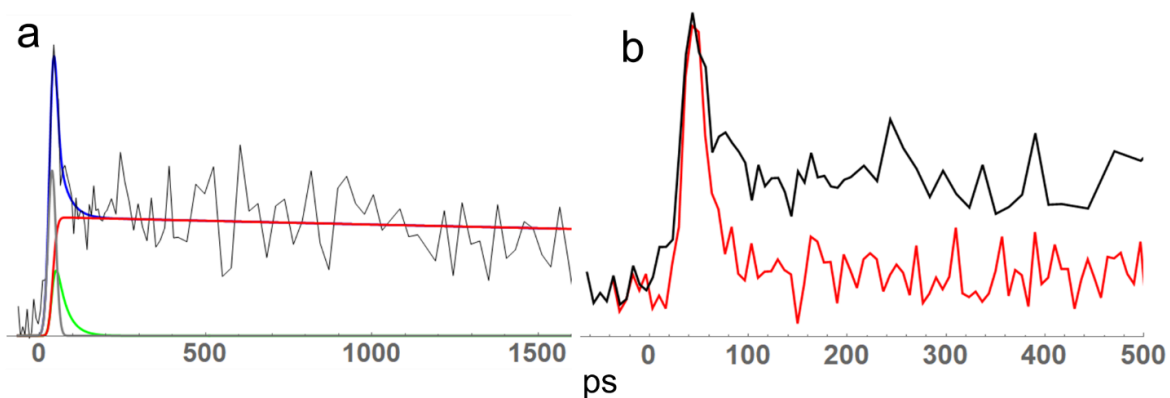


Figure 5. Pump probe trace of TT using 37037 cm^{-1} pump and 213 nm probe from the ps OPG fit with a biexponential decay. Black, blue, green, red, gray lines display raw data, sum, fast monoexponential, slow monoexponential, and the IRF, respectively (a). Decay traces of TT (black) and isolated thymine (red), both taken with 37037 cm^{-1} pump. The two traces were scaled to have similar amplitudes at their point of most signal (b).

After excitation, single stranded DNA undergoes delocalized excimer formation and decay.³⁷⁻³⁸ Su, Middleton, and Kohler later showed that this delocalized state is formed and constrained to an oligonucleotide with two residues.²⁹ Notably, all these studies found excimer decay to have ~ 150 ps lifetime, irrespective of oligomer length, though all were done using adenine homonucleotides.^{29, 37-39} The long relaxation was obvious in every study, though again, only observed for oligonucleotides that contained exclusively adenine residues. This slower, delocalized decay is due to strong electronic coupling between neighboring base stacks and known for its excimer and CT character. These excimer states appear to be largely helix conformation and backbone independent, though base stacking is required.⁴⁰⁻⁴¹ Adenine is widely used most likely because sequences of adenine have greater stacking than other sequences.

Observing the delocalized excimer state of single-stranded DNA and discerning the effect of solvent were the motivations for looking at PNA in the gas phase. With the excited state dynamics of the nucleobase monomers mostly elucidated, we wanted to look at more

complex and biologically relevant forms of genetic material. Again, we cannot look at DNA or RNA oligomers due to their charged phosphate backbones. Base stacking by individual nucleobases is not favored in the gas phase due to energetic reasons. But it is mainly seen in solution phase. We want to study base stacking and its dynamics in the gas phase, and how it compares to solution phase. How much does the solvent affect the excimer states in base-stacked structures? That would give an accurate benchmark for excited state calculations completed on base stacked complexes, which are usually done in gas phase. Studying the solvent effect is further complicated by the difficulty of dissolving DNA in nonaqueous solutions, so there are few studies done using different solvents. Using deep eutectic solvents, de La Harpe et al. have shown for duplexes that excimer formation requires stable base stacking conformation.⁴² The different solvent did not change the dynamics or secondary structure of the DNA duplex, but they did change the stability and lifetime of the charge transfer state.

Single-stranded DNA in aqueous solution has been noted for having three decay components. We will not observe the ultrafast monomer decay, as it is too fast for our setup, though it could be hidden in the IRF peak. And we will not observe the vibrational cooling as there is no solvent. We are interested in the slower excimer decay pathway exhibited in solvated single-stranded DNA. TT exhibits a biexponential decay, with both a relatively fast 30 ps component and a slow component, exhibited by the elevated tail (Fig. 5a). Isolated thymine has a similar 30 ps decay, but lacks the elevated tail for the long time component (Fig. 5b). At short times, thymine and TT have similar dynamics. Thus, TT likely undergoes a relaxation mechanism localized on a single thymine moiety, much like the thymine monomer. Our pump-probe traces do not show any evidence for a decay on the order of 100

ps, nor any evidence for an excimer mechanism. It should be noted that the 30 ps decay observed for both systems is not observed for thymine in solution. This is also the first reporting of the dynamics of thymine in the gas phase on this timescale.

Both TT and thymine have an ultraslow decay mechanism, on the order of 100 ns (Fig. S? and ref. ³³). We assign the slow component of TT, evidenced by the elevated tail at long timepoints in the ps timescale (Fig. 5a), to be the same ultraslow decay observed in the ns pump-probe trace. It is not entirely clear why the elevated signal baseline, or the slow decay, is lacking in the isolated thymine decay, yet is readily apparent for TT. Potentially, focusing increased the ionization rate from the excited state for TT, leading to increased signal at later time points. Alternatively, thymine and TT could decay to different excited states, and it is easier to ionize out of the state TT populates later.

Based on solution phase studies, excimer formation is independent of helix conformation and backbone structure.⁴⁰⁻⁴¹ From our calculations, the five lowest energy conformers of TT have significant overlap of the thymine moieties, allowing for π - π stacking. Further, the first conformer without stacking geometry is 26.1 kJ/mol higher in energy than the global minimum. Therefore, the majority of TT in our molecular beam is likely to have the necessary stacking interaction. We do not exclude the possibility of the higher-energy T-shaped also being present. The sugar phosphate backbone is also not necessary for excimer formation.⁴¹ Yet excimer formation and decay is not easily discernable from the data.

The only other difference to account for these different dynamics is the presence of solvent. Except for reference ⁴², all studies were conducted in aqueous solution. Solvation typically stabilizes $\pi\pi^*$ states and destabilizes $n\pi^*$ states, and can lead to strikingly different

dynamics between a system in the gas phase versus solution phase. A classic example of this is 2-aminopurine, which has a fast decay mechanism *in vacuo*⁴³ but is highly fluorescent in aqueous solution.⁴⁴ This behavior is due to distinct relaxation pathways being favored in different environments. This appears to be the case for TT, where excimer decay is the expected pathway in solution, but with no evidence for it in isolation. Potentially, the solvent is significant in the formation of these long, delocalized excimer states. We should add there is limited evidence that thymine homo-oligonucleotides do not form excimers in solution either.³⁷

More research is necessary to confirm this finding. Our lab continues to study adenine-adenine PNA dimers to compare its dynamics to adenine homo-oligonucleotides in solution, where excimer decay is observed.

We have successfully synthesized two homodimer PNA chains incorporating guanine and thymine as bases. We then spectroscopically characterized them in the gas phase using R2PI, IR-UV double resonance spectroscopy, and pump probe. The R2PI spectra for both molecules are characterized by broad onsets, possibly due to poor Frank-Condon factors. The IR-UV and pump probe spectra are inconclusive at this time. It is likely the TT structure we observe in our beam has base stacking, revealed by the calculated lowest energy conformer. TT exhibits fast monomer decay similar to isolated thymine. The longer relaxation dynamics appear to differ, though the reason for the difference is unclear. This work shows PNA can be studied spectroscopically in the gas phase, though more work is needed to show that it can be used in lieu of DNA to study the stacked base dynamics free from solvent.

Using this structural DNA analogue, we are attempting to study the excited state dynamics of stacked nucleobases free from solvent. This would allow us to study the dynamics of single-stranded DNA after photoexcitation using the electrostatically neutral DNA analogue, PNA in the gas phase. It has been mentioned that PNA could have evolved alongside DNA on an early Earth. The unique excited state dynamics of DNA and its bases have led to the theory that photostability was a prerequisite in the origins of life. Much more work is needed on different PNA systems to validate if PNA is an appropriate DNA analogue in the gas phase.

The lowest energy conformer of TT was calculated to reveal base stacking. Using resonance-enhance multiphoton ionization (REMPI), we collected two-color resonant two photon ionization (2C-R2PI) spectra of GG and TT. We then probed the structure of TT using IR-UV double resonance spectroscopy. The excited state dynamics of TT were observed by pump probe spectroscopy and compared to isolated thymine dynamics. Due to Signal to Noise (S/N) issues, this could not be achieved with GG. The goal using the DNA analogue PNA was to probe the excited state dynamics of the π - π stacking interactions in the cold gas phase. We have shown that we can synthesize and spectroscopically study PNA systems using our technique.

Detailed methods for PNA synthesis and purification

Materials: Tentagel S RAM resin (0.24 meq/g) was purchased from Chem-Impex International (Wood Dale, IL). Fmoc-PNA-G(Bhoc)-OH and Fmoc-PNA-T(Bhoc)-OH were purchased from AIC (Framingham, MA). 2-(1H-benzotriazol-1-yl)-1,1,3,3-tetramethyluronium hexafluorophosphate (HBTU) was purchased from AAptec (Louisville,

KY). Other chemicals were purchased from Sigma Aldrich in the highest purity available: 4-Methylpiperidine, *N*-methylmorpholine (NMM), 1-hydroxybenzotriazole (HOBt), acetic anhydride, pyridine, 2,6-lutidine, methanol, dichloromethane, trifluoroacetic acid (TFA), triisopropylsilane, and *N,N*-dimethylformamide (DMF).

Synthesis of TT and GG PNA dimers: Syntheses were carried out following adaptations of reported procedures.³⁰ Tentagel S RAM resin (0.83 g, 0.2 mmol) was loaded into a glass reaction vessel fitted with a coarse glass fritted filter and a Teflon stopcock. The resin was rinsed three times with DMF, then allowed to swell in DMF for 30 min. Synthesis entailed iterating sequences of deprotection, PNA residue coupling, and capping.

Deprotection. To remove the Fmoc protecting group from the resin-bound amine, 5 mL of a 20% solution of 4-methylpiperidine in DMF was added to the reaction vessel, and the vessel was capped and shaken on a wrist-action shaker for 15 mins at room temperature. The reaction vessel was drained, rinsed five times with DMF, and re-subjected to the deprotection reaction conditions. Following the second deprotection reaction, the resin was rinsed with DMF ten times.

PNA Residue Coupling. Four solutions were mixed in separate a glass vial: Fmoc-PNA-T(Bhoc)-OH (253 mg, 0.5 mmol, 2.5 equiv) or Fmoc-PNA-G(Bhoc)-OH (371 mg, 0.5 mmol, 2.5equiv) in 2.3 mL DMF, 2.5 mL of 0.2 M HOBt (0.5 mmol, 2.5 equiv) in DMF, and 2.5 mL of 0.2 M HBTU (0.5 mmol, 2.5 equiv) in DMF, and 0.2 mL of 0.2 M NMM (0.04 mmol, 0.2 equiv) in pyridine. The mixture was agitated for 1 min, then added to the reaction vessel with the deprotected resin. The reaction vessel was capped and shaken for 30 min at room temperature. The coupling reaction was carried out twice for the more sterically

demanding Fmoc-PNA-G(Bhoc)-OH residue. After draining and rinsing the resin ten times with DMF, a small number of beads were subjected to a Kaiser test. The colorless beads confirmed that the reaction was complete.

Capping. To the reaction vessel was added the capping mixture solution to mask any unreacted amine sites for future reactions: 0.6 mL acetic anhydride and 0.72 mL 2,6-lutidine in 8.9 mL DMF. The mixture was capped and shaken for 20 minutes at room temperature, then the reaction vessel was drained and the resin was washed ten times with DMF.

Iteration. The Fmoc-protecting group removal steps were repeated again, followed by the coupling of the second PNA residue. The capping steps were repeated, and the final protecting group was removed following the procedures described above.

Cleavage from the resin with concomitant nucleobase deprotection. Following the final Fmoc-removal step, the resin was washed with DMF, then methanol, then dichloromethane. The resin was dried under vacuum for 10 mins. To the resin was added 6 mL of a solution of 95% TFA/2.5% water/2.5% triisopropylsilane. The reaction vessel was agitated slightly over the course of the 2.5 h reaction time. The filtrate was collected, and the resin was rinsed with an additional 1 mL of the cleavage mixture. The filtrate was concentrated by rotary evaporation. LC-MS analysis of the crude residue confirmed the presence of the desired product mass. The crude residue was dissolved in a solution of 20% methanol in 0.1% aqueous TFA for purification.

Purification and identification of TT and GG: TT and GG were purified by RP-HPLC on a Hitachi Chromaster 5000 instrument, and chromatographic data were visualized with EZChrom software. A semi-preparative AAPPTEC Spirit C18 column (5 mM, 10.0 mm x 25 cm) was

used, and an elution gradient of methanol (solvent B) in 0.1% aqueous TFA (solvent A) was applied at a flow rate of 3 mL/min. The gradient held the solvent composition at 0% solvent B for the first 10 minutes followed by a linear gradient to 40% B over 40 minutes to elute the compounds. Compounds eluting from the column were detected by absorbance at 220 and 254 nm and collected into individual fractions. Fractions were evaluated by electrospray mass spectrometry (ESI-MS) in positive ion mode using a Thermo LCQ Fleet mass spectrometer to identify which contained the desired product mass. Fractions with the desired product mass were lyophilized to afford white powders.

References

1. Crespo-Hernandez, C. E.; Cohen, B.; Hare, P. M.; Kohler, B., Ultrafast excited-state dynamics in nucleic acids. *Chem Rev* **2004**, *104* (4), 1977-2019.
2. Middleton, C. T.; de La Harpe, K.; Su, C.; Law, Y. K.; Crespo-Hernandez, C. E.; Kohler, B., DNA excited-state dynamics: from single bases to the double helix. *Annu Rev Phys Chem* **2009**, *60*, 217-39.
3. De Vries, M. S., Isolated DNA base pairs, interplay between theory and experiment. **2008**, 323.
4. Kleinermanns, K.; Nachtigallová, D.; de Vries, M. S., Excited state dynamics of DNA bases. *International Reviews in Physical Chemistry* **2013**, *32* (2), 308-342.
5. Beckstead, A. A.; Zhang, Y.; de Vries, M. S.; Kohler, B., Life in the light: nucleic acid photoproperties as a legacy of chemical evolution. *Phys Chem Chem Phys* **2016**, *18* (35), 24228-38.
6. Boldissar, S.; de Vries, M. S., How nature covers its bases. *Phys Chem Chem Phys* **2018**, *20* (15), 9701-9716.
7. Nir, E.; Janzen, C.; Imhof, P.; Kleinermanns, K.; de Vries, M. S., Pairing of the nucleobases guanine and cytosine in the gas phase studied by IR–UV double-resonance spectroscopy and ab initio calculations. *Physical Chemistry Chemical Physics* **2002**, *4* (5), 732-739.
8. Nir, E.; Janzen, C.; Imhof, P.; Kleinermanns, K.; de Vries, M. S., Pairing of the nucleobase guanine studied by IR–UV double-resonance spectroscopy and ab initio calculations. *Physical Chemistry Chemical Physics* **2002**, *4* (5), 740-750.
9. Nir, E.; Kleinermanns, K.; De Vries, M. S., Pairing of isolated nucleic-acid bases in the absence of the DNA backbone. *Nature* **2000**, *408*, 949 - 951.
10. Brauer, B.; Gerber, R. B.; Kabelac, M.; Hobza, P.; Bakker, J. M.; Abo Riziq, A. G.; de Vries, M. S., Vibrational spectroscopy of the G...C base pair: experiment, harmonic and anharmonic calculations, and the nature of the anharmonic couplings. *J Phys Chem A* **2005**, *109* (31), 6974-84.

11. Nir, E.; Hünig, I.; Kleineremanns, K.; de Vries, M. S., The nucleobase cytosine and the cytosine dimer investigated by double resonance laser spectroscopy and ab initio calculations. *Phys. Chem. Chem. Phys.* **2003**, *5* (21), 4780-4785.
12. Abo-Riziq, A.; Grace, L.; Nir, E.; Kabelac, M.; Hobza, P.; De Vries, M. S., Photochemical selectivity in guanine-cytosine base-pair structures. *PNAS* **2005**, *102* (1), 20-23.
13. Smith, V. R.; Samoylova, E.; Ritze, H. H.; Radloff, W.; Schultz, T., Excimer states in microhydrated adenine clusters. *Phys Chem Chem Phys* **2010**, *12* (33), 9632-6.
14. Abo-Riziq, A.; Crews, B.; Grace, L.; de Vries, M. S., Microhydration of Guanine base pairs. *J Am Chem Soc* **2005**, *127* (8), 2374-5.
15. Kabeláč, M.; Ryjáček, F.; Hobza, P., Already two water molecules change planar H-bonded structures of the adenine···thymine base pair to the stacked ones: a molecular dynamics simulations study. *Physical Chemistry Chemical Physics* **2000**, *2* (21), 4906-4909.
16. Kabeláč, M.; Hobza, P., At Nonzero Temperatures, Stacked Structures of Methylated Nucleic Acid Base Pairs and Microhydrated Nonmethylated Nucleic Acid Base Pairs are Favored over Planar Hydrogen-Bonded Structures: A Molecular Dynamics Simulations Study. *Chemistry* **2001**, *7* (10), 2067-2074.
17. Egholm, M.; Buchardt, O.; Christensen, L.; Behrens, C.; Freier, S. M.; Driver, D. A.; Berg, R. H.; Kim, S. K.; Norden, B.; Nielsen, P. E., PNA hybridizes to complementary oligonucleotides obeying the Watson-Crick hydrogen-bonding rules. *Nature* **1993**, *365* (6446), 566-8.
18. Egholm, M.; Buchardt, O.; Nielsen, P. E.; Berg, R. H., Peptide nucleic acids (PNA). Oligonucleotide analogs with an achiral peptide backbone. *Journal of the American Chemical Society* **1992**, *114* (5), 1895-1897.
19. Nielsen, P. E., Peptide Nucleic Acid. A Molecule with Two Identities. *Accounts of Chemical Research* **1999**, *32* (7), 624-630.
20. Eriksson, M.; Nielsen, P. E., Solution structure of a peptide nucleic acid-DNA duplex. *Nat Struct Biol* **1996**, *3* (5), 410-3.
21. Rasmussen, H.; Kastrop, J. S.; Nielsen, J. N.; Nielsen, J. M.; Nielsen, P. E., Crystal structure of a peptide nucleic acid (PNA) duplex at 1.7 Å resolution. *Nat Struct Biol* **1997**, *4* (2), 98-101.
22. Sen, S.; Nilsson, L., Molecular Dynamics of Duplex Systems Involving PNA: Structural and Dynamical Consequences of the Nucleic Acid Backbone. *Journal of the American Chemical Society* **1998**, *120* (4), 619-631.
23. Sen, S.; Nilsson, L., MD simulations of homomorphous PNA, DNA, and RNA single strands: characterization and comparison of conformations and dynamics. *J Am Chem Soc* **2001**, *123* (30), 7414-22.
24. Hatcher, E.; Balaeff, A.; Keinan, S.; Venkatramani, R.; Beratan, D. N., PNA versus DNA: effects of structural fluctuations on electronic structure and hole-transport mechanisms. *J Am Chem Soc* **2008**, *130* (35), 11752-61.
25. Wierzbinski, E.; de Leon, A.; Yin, X.; Balaeff, A.; Davis, K. L.; Reppireddy, S.; Venkatramani, R.; Keinan, S.; Ly, D. H.; Madrid, M.; Beratan, D. N.; Achim, C.; Waldeck, D. H., Effect of Backbone Flexibility on Charge Transfer Rates in Peptide Nucleic Acid Duplexes. *Journal of the American Chemical Society* **2012**, *134* (22), 9335-9342.
26. Rodriguez, L. E.; House, C. H.; Smith, K. E.; Roberts, M. R.; Callahan, M. P., Nitrogen heterocycles form peptide nucleic acid precursors in complex prebiotic mixtures. *Sci Rep* **2019**, *9* (1), 9281.

27. Gabelica, V.; De Pauw, E., Collision-induced dissociation of 16-mer DNA duplexes with various sequences: evidence for conservation of the double helix conformation in the gas phase. *International Journal of Mass Spectrometry* **2002**, *219* (1), 151-159.
28. Gidden, J.; Baker, E. S.; Ferzoco, A.; Bowers, M. T., Structural motifs of DNA complexes in the gas phase. *International Journal of Mass Spectrometry* **2005**, *240* (3), 183-193.
29. Su, C.; Middleton, C. T.; Kohler, B., Base-stacking disorder and excited-state dynamics in single-stranded adenine homo-oligonucleotides. *J Phys Chem B* **2012**, *116* (34), 10266-74.
30. Avitabile, C.; Moggio, L.; D'Andrea, L. D.; Pedone, C.; Romanelli, A., Development of an efficient and low-cost protocol for the manual PNA synthesis by Fmoc chemistry. *Tetrahedron Letters* **2010**, *51* (29), 3716-3718.
31. Meijer, G.; De Vries, M. S.; Hunziker, H. E.; Wendt, H. R., Laser Desorption Jet-Cooling of Organic Molecules. *Applied Physics B* **1990**, *51*, 395 - 403.
32. Roos, K.; Wu, C.; Damm, W.; Reboul, M.; Stevenson, J. M.; Lu, C.; Dahlgren, M. K.; Mondal, S.; Chen, W.; Wang, L.; Abel, R.; Friesner, R. A.; Harder, E. D., OPLS3e: Extending Force Field Coverage for Drug-Like Small Molecules. *J Chem Theory Comput* **2019**, *15* (3), 1863-1874.
33. Ligare, M.; Siouri, F.; Bludsky, O.; Nachtigallova, D.; de Vries, M. S., Characterizing the dark state in thymine and uracil by double resonant spectroscopy and quantum computation. *Phys Chem Chem Phys* **2015**, *17* (37), 24336-41.
34. Brady, B. B.; Peteanu, L. A.; Levy, D. H., The electronic spectra of the pyrimidine bases uracil and thymine in a supersonic molecular beam. *Chemical Physics Letters* **1988**, *147* (6), 538-543.
35. Nosenko, Y.; Kunitski, M.; Brutschy, B., Specific photodynamics in thymine clusters: the role of hydrogen bonding. *J Phys Chem A* **2011**, *115* (34), 9429-39.
36. Casaes, R. N.; Paul, J. B.; McLaughlin, R. P.; Saykally, R. J.; van Mourik, T., Infrared Cavity Ringdown Spectroscopy of Jet-Cooled Nucleotide Base Clusters and Water Complexes. *The Journal of Physical Chemistry A* **2004**, *108* (50), 10989-10996.
37. Crespo-Hernandez, C. E.; Cohen, B.; Kohler, B., Base stacking controls excited-state dynamics in A.T DNA. *Nature* **2005**, *436* (7054), 1141-4.
38. Buchvarov, I.; Wang, Q.; Raytchev, M.; Trifonov, A.; Fiebig, T., Electronic energy delocalization and dissipation in single- and double-stranded DNA. *Proc Natl Acad Sci U S A* **2007**, *104* (12), 4794-7.
39. Kwok, W. M.; Ma, C.; Phillips, D. L., Femtosecond time- and wavelength-resolved fluorescence and absorption spectroscopic study of the excited states of adenosine and an adenine oligomer. *J Am Chem Soc* **2006**, *128* (36), 11894-905.
40. de la Harpe, K.; Crespo-Hernandez, C. E.; Kohler, B., The excited-state lifetimes in a G x C DNA duplex are nearly independent of helix conformation and base-pairing motif. *Chemphyschem* **2009**, *10* (9-10), 1421-5.
41. Chen, J.; Kohler, B., Base stacking in adenosine dimers revealed by femtosecond transient absorption spectroscopy. *J Am Chem Soc* **2014**, *136* (17), 6362-72.
42. de La Harpe, K.; Kohl, F. R.; Zhang, Y.; Kohler, B., Excited-State Dynamics of a DNA Duplex in a Deep Eutectic Solvent Probed by Femtosecond Time-Resolved IR Spectroscopy. *J Phys Chem A* **2018**, *122* (9), 2437-2444.

43. Lobsiger, S.; Blaser, S.; Sinha, R. K.; Frey, H. M.; Leutwyler, S., Switching on the fluorescence of 2-aminopurine by site-selective microhydration. *Nat Chem* **2014**, *6* (11), 989-93.
44. Reichardt, C.; Wen, C.; Vogt, R. A.; Crespo-Hernandez, C. E., Role of intersystem crossing in the fluorescence quenching of 2-aminopurine 2'-deoxyriboside in solution. *Photochem Photobiol Sci* **2013**, *12* (8), 1341-50.

V. Photostability of organic pigments and dyes

Many cultural works of art, mainly paintings and murals, have degraded over the years. Specifically, degradation of their colors. But only some colors appear to fade. The reasoning behind the selective fading of certain pigments was not clear to the artists at the time. They chose the pigments for their color, a property of the systems' steady state absorption. The propensity to photodegrade and fade away has to do with the system's photostability.

Indigo is widely used for its vibrant blue hue, and most commonly found in denim jeans. Cultural artifacts thousands of years old have been found to retain their blue pigmentation, due to the photostability of indigo. This photostability is attributed to a near barrierless proton transfer, while a slower hydrogen atom transfer process is also competitive. These two decay pathways couple to specific vibronic modes, leading to an interesting system that has mode-specific relaxation dynamics.

Substituted hydroxyanthraquinones (HAQ) are used as red colorant pigments. The most common are alizarin and purpurin. Seven different HAQs were studied, and the mechanism for their photostability was determined. HAQs with a single intramolecular hydrogen bonding site were much more stable than those with a two hydrogen bonding sites, due to the availability of a proton transfer.

I. Evidence for competing proton-transfer and hydrogen-transfer reactions in the S₁ state of indigo

Michael R. Haggmark ^a, Gregory Gate ^a, Samuel Boldissar ^a, Jacob Berenbeim ^a, Andrzej L. Sobolewski ^b, Mattanjah S. de Vries ^{a*}

^a Department of Chemistry and Biochemistry, University of California Santa Barbara, CA 93106-9510

^b Institute of Physics, Polish Academy of Sciences, Al. Lotnikow 32/46, PL-02668 Warsaw, Poland

Abstract

Indigo is a blue dye molecule that has been used since antiquity, although it is better known today for its use in blue jeans. Indigo has previously been shown to exhibit remarkable photostability due to fast excited state dynamics mediated by an excited state intramolecular proton transfer. Study of this process is complicated by the fact that the photophysics of indigo is very sensitive to the environment. In order to disentangle the intrinsic photodynamics of indigo from the effects contributed by the environment, we studied indigo in a molecular beam using resonance enhanced multiphoton ionization. We obtained excited state lifetimes of individual vibronic bands with pump-probe spectroscopy ranging from 60 ps to 24 ns. We have mapped a barrier to relaxation at about 700 cm^{-1} , beyond which fast excited state dynamics dominate. Below this barrier two decay processes compete and mode-specific relaxation occurs with certain vibronic bands near the origin relaxing faster than others, or exhibiting different partitioning between the two relaxation channels. Computational studies at the ADC(2)/MP2/cc-pVDZ level indicate that two low-barrier reaction paths exist in the S_1 state of indigo, one corresponding to proton transfer, the other to hydrogen transfer. In both cases the charge distribution changes drastically upon de-excitation. These data provide a sensitive probe of the potential energy landscape, responsible for the response to absorption of light. The results may help in understanding the photostability that preserves the blue color of indigo dyes.

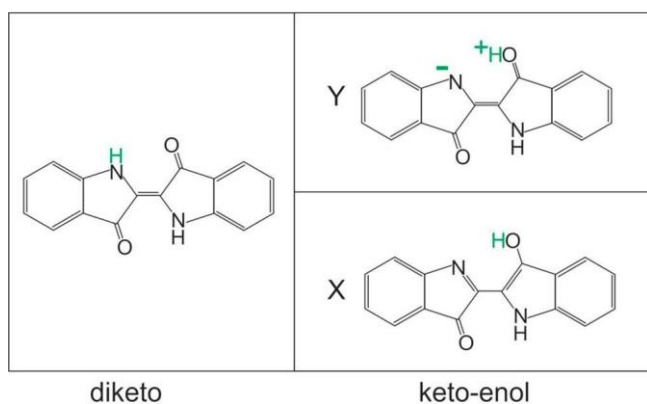
1. Introduction

The blue dye, indigo, is one of the oldest, and still one of the most widely used dyes. It was used by many ancient cultures from the Egyptians, to the Romans, to the Mayans, and remarkably, artifacts from those societies still retain their blue color to this day [1,2]. This lack of fading is due to indigo's high photostability [3].

Generally speaking, photostability is granted by a process that returns a molecule to the ground state at a faster timescale than formation of reactive species [4]. For Indigo, the mechanism providing fast return to the ground state is thought to be due to an excited-state intramolecular proton transfer (ESIPT), first studied computationally in-depth by Yamakazi et al, [5] who found a very short excited state lifetime due to ESIPT from a diketo to a keto-enol tautomer. Moreno et al further examined the relaxation pathway through conical intersections (CI) [6], finding agreement with experimental work. Another possible relaxation process is photoisomerization, which has been shown to only occur when the proton transfer coordinate is blocked [7–9]. A number of studies have attempted to unambiguously observe proton transfer for indigo. Photoelectron spectroscopy of an indigo derivative, indigo carmine, found that the excited-state lifetime in the gas-phase was around 1 ps [10]. Time resolved spectroscopy of an indigo analogue that only allowed a single proton transfer revealed a fluorescence spectrum with a biexponential decay, hinting at fluorescence from two different states, possibly the diketo (KK) and keto-enol (KE) states [11]. Transient absorption spectroscopy of indigo in DMSO revealed a lifetime on the order of 120 ps, but showed no evidence of proton transfer (PT) [12]. Iwakura et al used sub-5 fs resolution coherence experiments to directly observe the new vibrational modes that arise from PT in indigo-carmine [13,14]. Seixas et al. reported a significant blue-shift in the absorption spectrum and an increase in fluorescence quantum yield was seen between indigo and its leuco (reduced) form, due to a slowing down of the relaxation process and increasing

competitiveness of the radiative pathway [15]. The fluorescence spectrum of leuco indigo increased and slightly shifted with prolonged light exposure, thought to be due to photoisomerization [16]. Studies with deuterated indigo and analogues to observe and measure the tunneling mechanism in PT showed an increase in the lifetime with deuteration, consistent with a tunneling assisted proton transfer mechanism [10,14].

PT is the process of transferring a proton from one molecular moiety to another along an intra- molecular hydrogen bridge. A commonly accepted paradigm presumes this situation pertains to the process that occurs in the ground state of a molecular system and often the acronym GSIPT (ground-state intramolecular PT) is assigned to this phenomenon. On the other hand, in the excited electronic state transfer of a proton between molecular moieties is accompanied by transfer of an electron, and often this phenomenon is called ESIHT (excited-state intramolecular hydrogen transfer). The tautomers generated by these processes are illustrated in Scheme 1.



Scheme 1. Tautomeric structures of indigo pertaining to this work.

Yamazaki et al. and Moreno et al. proposed that the single proton transfer from the diketo to the mono-enol tautomer affects the potential energy surfaces (PES), allowing the excited state and ground state energies to intersect and form a CI [5,6]. After ultrafast internal conversion through the CI, the ground state keto-enol will transfer the proton back,

reforming the diketo tautomer and ground state equilibrium geometry. If there is a barrier in the excited state, the proton will have to tunnel through to successfully transfer. The occurrence of a barrier and tunneling implies that the PES has a double-well potential. Tunneling describes the behavior of the proton quantum mechanically, while classically, the proton has to go over the barrier. Therefore, the probability of proton transfer is dependent on the barrier height and width. The barrier height and width are dependent on the distance between the proton donor N and the acceptor O atoms [17]. This is one of the most relevant reaction coordinates [18]. The other significant reaction coordinate is the N–H distance. Dynamical effects, such as vibrational motions, can modulate barrier width and height and significantly affect tunneling probability. Therefore, the tunneling rate is dependent on three factors: (1) total amount of excess energy imparted, (2) specific mode excitation, and (3) internal vibrational redistribution (IVR) of energy to occupy relevant modes [18].

In this study, we confirm the presence of the diketo tautomer of indigo in the gas phase and measure the lifetime of the excited state at various excess energies to generate a picture of the height of the barrier. This work aims to further explore the photostability of indigo and elucidate the main relaxation pathways in the gas phase.

2. Methods

Experimental

The experimental setup has been described in detail elsewhere [19], and only a short description follows. Indigo (Sigma, 95%) is placed on a translating graphite bar and desorbed via a focused Nd:YAG pulse (1064 nm, ~1 mJ/pulse) operating at 10 Hz. Supersonic jet cooling from an argon molecular beam (8 atm backing pressure, 30 μ s pulse width) entrains the gaseous molecules, quickly cooling them. These cold, gaseous molecules are then ionized using resonant two photon ionization (R2PI) and directed into a

reflectron time-of-flight mass spectrometer. Two-color resonant two-photon ionization (2C-R2PI) is performed using an EKSPLA PL2251 Nd:YAG laser system producing ~ 30 ps pulses. The 355 nm output pumps the EKSPLA PG-401 tunable optical parametric generator (OPG) visible output of ~ 0.5 mJ). Residual 1064 nm and 532 nm light from the pump are mixed to harmonically generate 213 nm (0.3 mJ), which is used as the ionization pulse.

IR light is generated using a Laser Vision tunable optical parametric oscillator/optical parametric amplifier (OPO/OPA) (mid-IR output over the range $3000\text{--}3800\text{ cm}^{-1}$ of $\sim 1\text{--}2$ mJ/pulse, 3 cm^{-1} spectral line width). IR light precedes the excitation/ionization pulses by ~ 200 ns. Two variations of IR double resonant spectroscopy are used. In mode I, the IR laser scans across IR wavelengths, while the ionization pulse is held constant at a resonant R2PI transition for a given tautomer. The IR pulse burns out the cold, ground state molecules whenever it hits a vibrational resonance, taking the excitation pulse out of resonance and causing a decrease in signal. This will produce the IR spectrum for the specific tautomer that is being ionized. In mode II, the IR pulse is held constant at a resonant vibrational transition, while the ionization pulse scans the R2PI spectrum. In this way, a tautomer is labeled by a vibrational stretch and signal decreases whenever the transition is shared. All double resonance spectroscopic experiments are chopped to compare the experimental “burn” signal to control signal in situ, with alternating shots collecting burn and control signals.

Pump-probe experiments are performed in both the picosecond and nanosecond regimes. In the picosecond regime, the 30 ps pump pulse from the OPG laser system is tuned to a resonant transition, while the probe is the 5th harmonic (213 nm) from the pump laser for the OPG. The 5th harmonic can be mechanically delayed up to ~ 1.5 ns in time, relative to the OPG pulse, for picosecond pump-probe measurements. In the nanosecond regime, pump pulse is again from the OPG and tuned to a resonant transition, but the probe pulse is from

an excimer laser (193 nm, 1.5–2 mJ/pulse, 6 ns pulsewidth). To account for ionization laser difference, several nanosecond pump probes were also measured by tuning a dye laser (Lumonics HD300 ~0.5mJ) to a resonant transition and probing with the 213 nm light from the ps pump laser. No difference was observed in the ns pump-probe results between 213 nm and 193 nm probe laser wavelengths. Visible-visible hole burning was also performed in an analogous manner to mode II IR by tuning the dye laser to the origin transition ~200 ns prior in time and scanning the OPG across the region of interest to verify only a single tautomer was present.

Pump-probe measurements are taken in two time regimes to help determine what processes are occurring in the excited state. By combining information from both time regimes and observing the changes in lifetime with varying excess energy, conclusions can be drawn about the excited state dynamics. The method for deriving lifetimes is based on previous work, and explained in more detail there [20]. Briefly, lifetimes are derived from kinetic equations and solving the system of ordinary differential equations. This procedure involves convolving the instrument response function (IRF) with a mono- or bi-exponential decay function. The IRF is represented by a Gaussian function centered around t_0 .

Computational

The ground-state tautomers of indigo were optimized and harmonic frequencies calculated using second order Moller-Plesset perturbation theory (MP2) with the cc-pVDZ basis set in Gaussian 09 [21]. A scaling factor of 0.95 and a 2 cm^{-1} Lorentzian width were applied for the simulated IR spectra. Ground state energies of isomers/tautomers have been zero-point energy (ZPE) corrected.

Excitation energies, excited-state reaction paths and energy profiles were calculated with the second-order algebraic-diagrammatic-construction (ADC(2)) method [22,23]. The

reaction path for the ESIPT reaction was constructed as a so-called relaxed scan, that is, for a fixed value of the driving coordinate (the NH distance for PT reaction and CCCC dihedral angle for inter-ring twist) all other internal coordinates of the molecule were relaxed in the S_1 state. The approximate reaction path between the two (X and Y) excited-state conformers of the mono-enol form of indigo was constructed as a linear interpolation in internal nuclear coordinates between equilibrium geometries of both structures. The energy profiles of this reaction path were obtained as single-point energy calculations along the interpolated path.

The MP2 and ADC(2) calculations were carried out with the TURBOMOLE program package, [24] making use of the resolution-of-the-identity (RI) approximation[25] for the evaluation of the electron-repulsion integrals. The cc-pVDZ basis set was used for all calculations.

3. Results

Experimental

Fig. 1 shows the 2C-R2PI spectrum of indigo (black trace). The excitation laser is the same in both panels but the ionization laser is 193 nm/6 ns in the top panel and 213 nm/30 ps in the bottom panel. R2PI was collected with different pulse widths to show the probing ability of the laser systems in different time domains. The top trace truncates at 700 cm^{-1} to a lack of signal beyond that point while peaks continue to appear toward the blue in the bottom trace. The origin transition appears at 18129 cm^{-1} (551.6 nm), and all excitation spectra are presented relative to it. Squares denote lifetimes obtained by pump probe spectroscopy for both the ns (green) and ps (blue) time domains. Fig. 2 shows individual pump probe transients of the first two peaks. Figs. S1–S4 show additional transients.

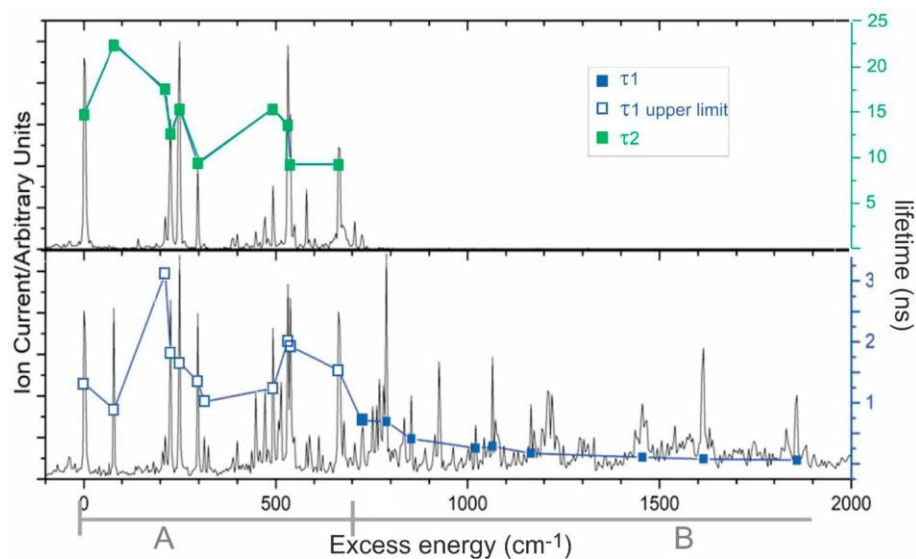


Figure 1. 2C-R2PI spectra (black) collected using ps excitation followed by ionization with 193 nm ns pulses (top panel) and 213 nm ps pulses (bottom panel). Squares denote the lifetimes as recorded from pump-probe measurements in the ns range (green) and ps range (blue). Below 700 cm^{-1} (spectral range A), the lifetimes show the presence of multiple components and only upper limits are reported for the ps pump probe experiments (see discussion). Above 700 cm^{-1} (spectral range B) we observed a single timescale component. For the ns spectra, the lasers are separated in time by a few ns. (For interpretation of the references to color in this figure legend, the reader is referred to the web version of this article.)

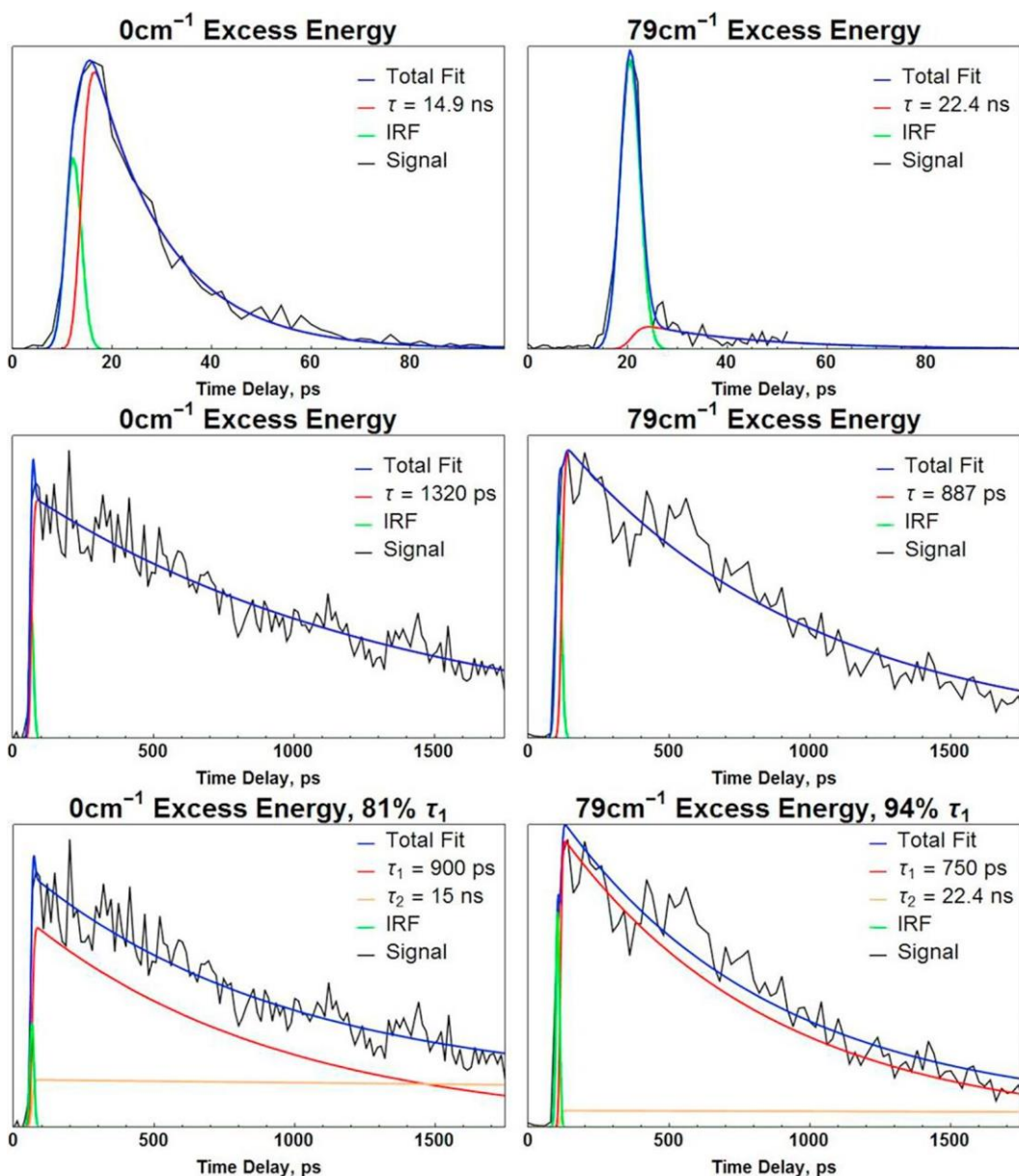


Figure 2. Pump-probe performed in the ns (top two traces) and ps (middle two traces) time domains for the origin transition and the +79 cm⁻¹ peak. The bottom two traces show the biexponential fitting method used as an estimate for the relative quantum yields (see text). The dominant IRF feature seen in the 79 cm⁻¹ ns pump probe spectrum is indicative that a faster process is the major contributor to the signal. The lack of this behavior in other peaks supports the idea of mode specific relaxation (see discussion).

Fig. 3 shows the IR spectrum obtained by IR-Vis double resonance spectroscopy mode I. Peaks at 3084 and 3444 cm⁻¹, correspond to overlapping C–H modes and the N–H stretch, respectively. We did not observe any additional peaks further to the blue, up to 3800 cm⁻¹.

These results agree with the computations, matching the calculated trans-diketo tautomer. To confirm that only the trans-diketo was present in the beam, we carried out visible-visible double resonance spectroscopy (Fig. 4) and mode II IR hole-burning (Fig. S5). From these data, we can confidently conclude that we observe only the trans-diketo tautomer in our beam.

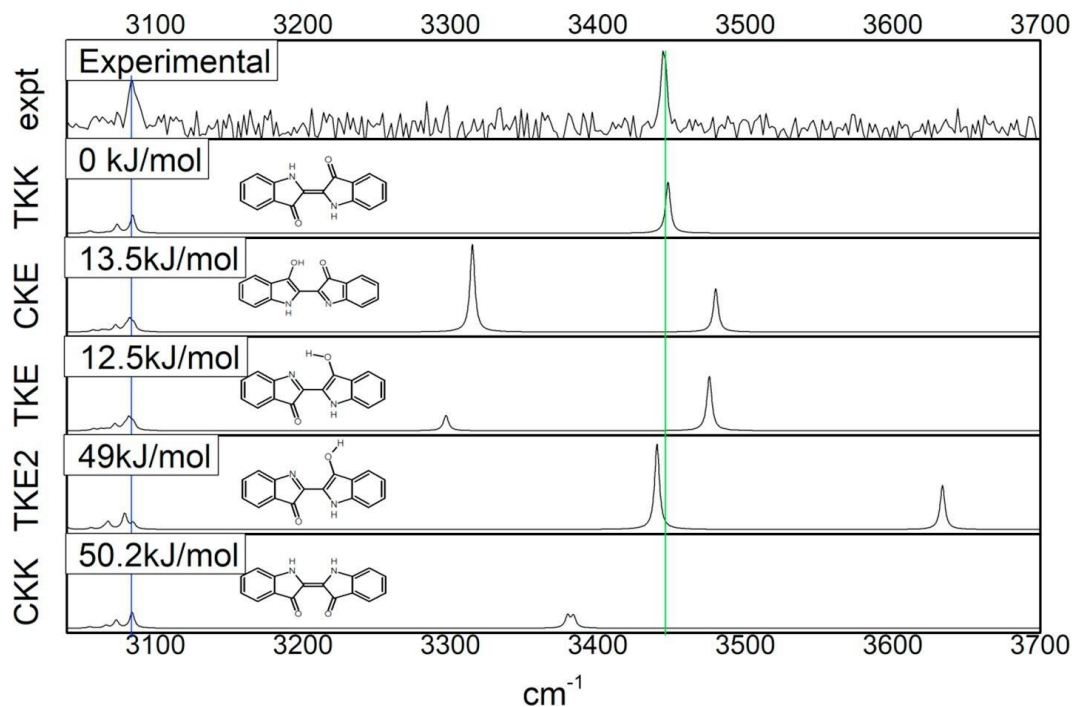


Figure 3. IR-Vis double resonance spectroscopy mode I experimental data (top panel) of indigo from 3040 to 3700 cm^{-1} . Probe was taken at the origin, 18,129 cm^{-1} . For comparison, the vibrational frequencies of the lowest energy tautomers are plotted with a 0.95 scaling factor applied. The abbreviations on the axes correspond to (from top to bottom) the trans diketo, cis keto-enol, trans keto-enol, trans keto-enol 2, and cis diketo tautomers.

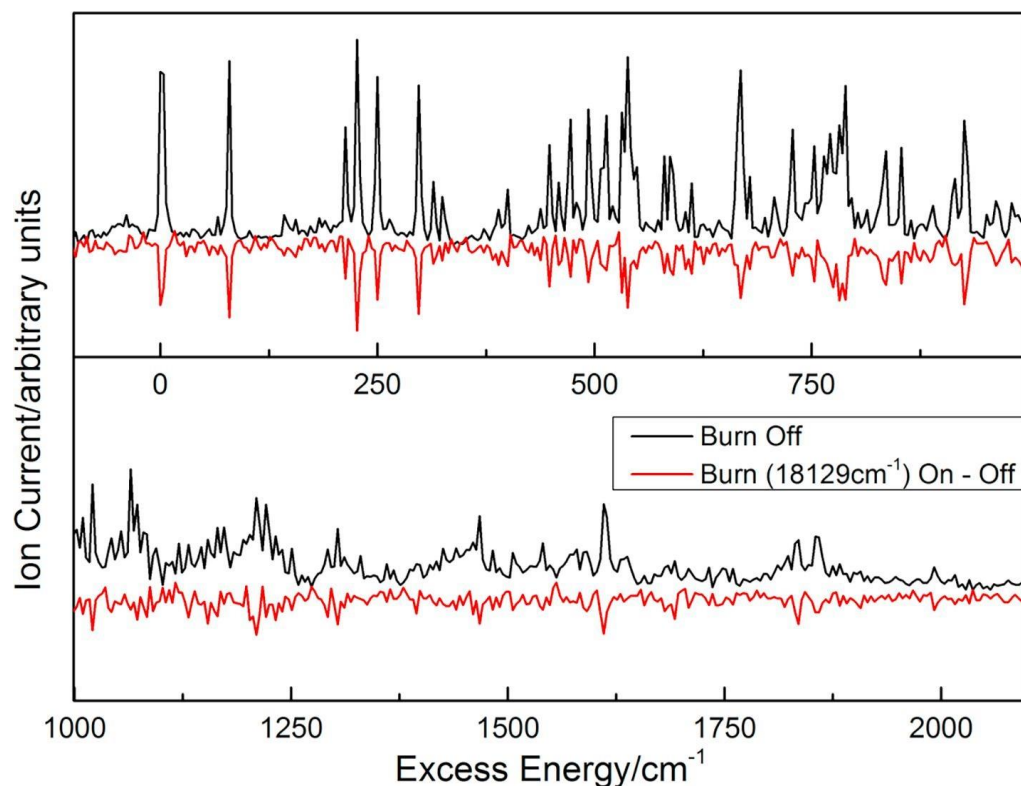


Figure 4. Visible-visible double resonance spectroscopy of indigo. The burn laser was set on the origin while the probe laser (ps OPG + 213 nm) was scanned and fired 200 ns later. Excited molecules were ionized with 213 nm.

Table 1 lists the lifetime values derived by fitting the results of pump probe spectroscopy. For the ns pump probe results, we fit a mono-exponential decay function to the trace. For the ps measurements we can fit with a mono-exponential function and the results appear in Table 1. However, this approach provides an upper limit for the lifetime only. The reason is that we know from the ns measurements that there is also a slower component to the decay so at least one additional exponential needs to be included and the total decay is of the form:

$$I(t) = a_1 e^{(-t/\tau_1)} + a_2 e^{(-t/\tau_2)}$$

Here the coefficients a_1 and a_2 are the relative intensities for each of the two processes and τ_1 and τ_2 are the corresponding lifetimes. Including the second term leads to fits with smaller values of τ_1 . Assuming only two processes occur, the quantum yield for process 1 is

$QY = a_1/(a_1 + a_2)$. In this analysis we assume that the ionization efficiency for the two processes is the same. If that is not the case the values of a_1 and a_2 will differ. Table 2 lists the mono-exponential lifetime fits in spectral region B.

peak	Peak (nm)	excess energy (cm ⁻¹)	Lifetimes (ns)			a ₁ /(a ₁ +a ₂) = QY1 in % for given values of τ ₁ in ps				
			τ ₁	τ ₂ 193 nm	τ ₂ 213 nm	750	900	1050	1200	1500
1	551.6	0	1.320	14.9	15.0	75	81	88	94	
2	549.2	79	0.887	22.4		94	100			
3	545.2	213	3.127	17.0	18.2	39	42	45	48	55
4	544.8	226	1.822	13.9	14.2	60	65	70	76	88
5	544.1	250	1.660		16.1	65	70	76	82	94
6	542.7	297	1.353	9.2	9.1	73	79	85	93	
7	542.2	314	1.019			86	93	100		
8	537	493	1.238	14.8		78	84	91	98	
9	535.9	531	2.017	13.3		57	60	64	70	
10	535.7	538	1.924	9.4		54	59	65	70	83
11	532.1	664	1.540	8.6		70	76	82	90	

Table 1. Observed ps and ns lifetimes fit with mono-exponential functions for both processes in spectral range A. 542.2 nm is a small peak in both ps and ns and we were unable to record a pump probe trace with sufficient signal to noise with the ns system. The QYs for process 1 are shown, calculated for different values of τ₁, as formulated in the text. The highlighted column is discussed in the text.

nm	excess energy/cm ⁻¹	ps lifetime monoexponential fit
530.4	725	710
528.6	789	736
526.8	853	410
522.2	1021	257
521	1065	286
518.3	1165	168
510.6	1456	105
506.5	1614	79
500.3	1859	60

Table 2. Observed lifetime fits with mono-exponential functions in spectral range B.

Fig. 1 and Table 1 show the mono-exponential fits for τ₁, corresponding to a₂=0 and thus representing an upper limit of τ₁ for spectral range A. τ₁ are the lifetimes derived from the ps pump probes and τ₂ are the lifetimes derived from the ns pump probes. We know, in fact,

based on the ns pump-probe results, that $a_2 > 0$ in spectral range A, with particular notice of the 79 cm^{-1} excess energy peak having a_2 very close to zero. We can fit the ps pump-probe data satisfactorily with a range of combinations of τ_1 and τ_2 to give different values of QY for process 1 (the faster decay). Table 1 lists a number of these combinations and Fig. 6 gives a graphic representation of these data. We will discuss the implications of this analysis in the next section. The values of τ_2 as obtained with the 193 nm/ns ionization and 213 nm/ps ionization are identical within 0.3 ns or better, as listed in Table 1, suggesting that both wavelengths probe the same excited state populations.

Computational

We optimized two stable structures of indigo on the ground-state potential-energy (PE) surface: a diketo and a keto-enol tautomeric form. The latter, identified below as the X form, is 0.13 eV higher in energy than the former at this (MP2/cc-pVDZ) theoretical level. The diketo form is non-polar by symmetry with a central CC bondlength of 1.378 \AA (Table S1a) which is typical for a double bond in an aromatic system. The keto-enol tautomer has a dipole moment, μ_0 , of 1.40 Debye and a central CC bondlength of 1.421 \AA (Table S2a). Such a relatively small change of polarity and the reversion of the single/double bond - leading in effect to GSIHT as discussed hereafter.

The calculated electronic absorption spectra of both tautomeric forms (see Tables S1a and S2a of the ESI) are dominated by the transition to the lowest singlet state (S_1) of the $\pi\pi^*$ orbital nature. The adiabatic energy of the S_1 state of the diketo tautomer is estimated as 2.09 eV at this theoretical level and the energy of fluorescence is estimated as 1.98 eV (Table S3a). Notably, electronic excitation of the keto-enol tautomeric form shifts electron density

from the proton accepting molecular moiety back to the proton donating moiety resulting in a highly polar species ($\mu_1 = 6.45$ Debye, Tables S2a and S2b) which can now be classified as a proton transfer (PT) species. This observation implies that this keto-enol form has HT character in the S_0 ground state and PT character in the S_1 excited state. We are not aware of such a phenomenon having been described before in the existing very rich ESIPT related literature.

To our surprise, we found two almost isoenergetic stable forms of the keto-enol tautomer in the S_1 state by excited-state geometry optimization. These forms (denoted as X and Y) are illustrated in Scheme 1, with additional details provided in Tables S4 and S5. Both keto-enol forms exhibit well defined minima on the S_1 PE surface and are more stable than the diketo form by about 0.09 eV. The vertical energy of the ground state computed at these geometries are very different (0.436 eV for X and 1.035 eV for Y, respectively). This suggests a large difference between their equilibrium geometries.

Inspection of the most crucial geometrical parameters (bond lengths and dipole moments) shows that the X form corresponds to the keto-enol form optimized in the ground state with a similar single/double bond pattern within the central molecular unit. The X form has a central bond length of 1.454 Å compared to 1.383 Å of the Y form, or 1.397 Å of the diketo. At its S_1 -optimized equilibrium geometry (Table S4) the X form is highly polar ($\mu_1 = 6.77$ Debye) and its de-excitation to the ground state reduces the dipole moment to $\mu_0 = 1.27$ Debye. As discussed above, this behavior strongly suggests an HT type process in the S_0 state and PT type process in the S_1 state. By contrast, the electronic structure of the Y form is practically the opposite. For the Y form the ground state is more polar ($\mu_0 = 4.14$ Debye) than the S_1 state ($\mu_1 = 3.39$ Debye), cf. Table S5a. The angle between dipole moments in the S_1

state of both forms is about 125 degrees, indicating that they are polarized in different directions. These differences in the electronic structures of the X and Y forms are accompanied by differences in the nuclear geometry. In particular, the forms show different single/double bond-length patterns of the central molecular moiety, with the X form resembling the ground state keto-enol and the Y form resembling the diketo (Scheme 1 and Tables S4a and S5a). The electronic excitation of the X and Y forms only partially shifts the charge from one molecular unit to the other, as can be seen from inspection of the relevant MOs in Tables S4b and S5b, respectively, and this has almost no impact on nuclear geometry.

To estimate the barrier that separates the X and Y forms of the keto-enol tautomer in the S_1 state, we computed the PE profile along the linearly interpolated reaction path that connects their equilibrium geometries, optimized in the S_1 state. The inset of Fig. 5 shows the resulting PE profile and one can notice that estimated barrier separating the X form from the Y form on the S_1 PE surface is rather small (about 0.013 eV). This indicates that in the excited state the two forms of the keto-enol tautomer represent rather two minima of a double-well potential than two separate chemical species. The Y form is unstable in the ground state and converges to the X form upon geometry optimization.

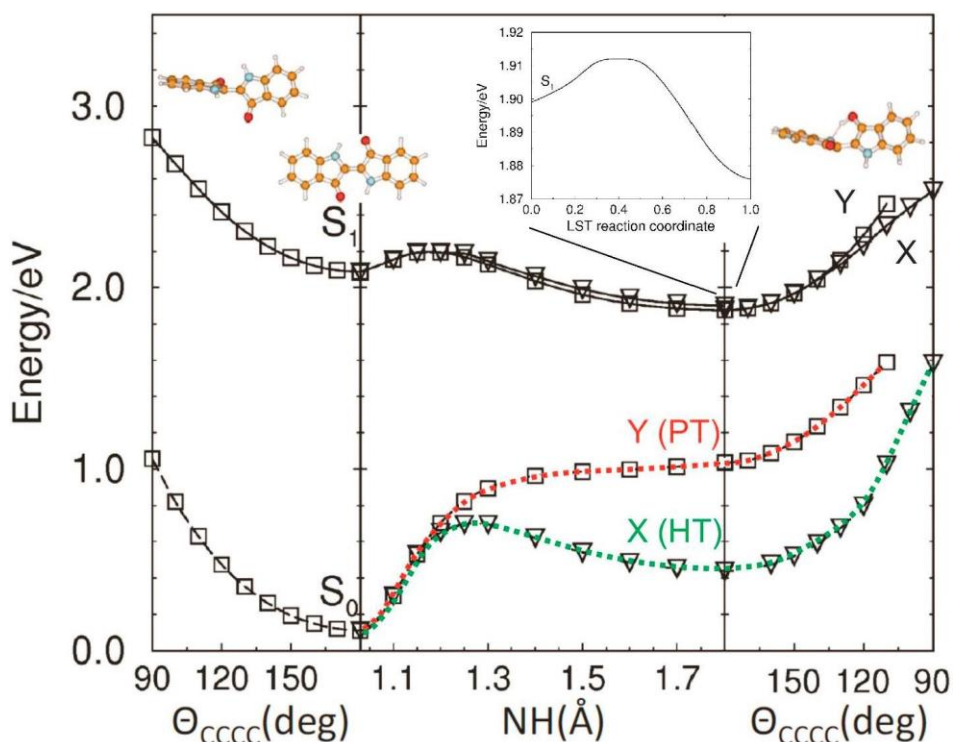


Figure 5. Potential-energy (PE) profiles of the S_0 and S_1 states of indigo computed at the ADC(2)/cc-pVDZ level of theory along the minimum-energy paths optimized in the S_1 state for the PT coordinate (NH distance)-central panel, and the inter-ring twist coordinate (CCCC dihedral angle) of the di-keto (left panel) and the keto-enol (right panel) tautomers. Solid lines denote minimum-energy profiles of the S_1 state. Dashed lines denote vertical-energy profiles of the ground state computed at the geometry of the S_1 state. PE profiles of the X and Y forms are represented by squares and triangles, respectively. The red color indicates proton transfer and the green color indicates H-atom transfer. Inset illustrates the barrier which separates the two tautomeric forms computed along the Linear Synchronous Transit (LST) reaction path connecting the S_1 -state optimized geometries of the X (left) and Y (right) conformers.

Fig. 5 shows potential energy (PE) profiles optimized in the S_1 state along the PT coordinate (NH bond-length) and along the inter-ring twist coordinate (CCCC dihedral angle) together with PE profiles of the ground state computed along these coordinates.

Inspection of the results that are summarized in Fig. 5 leads to the following conclusions:

- (i) The PE profile for proton transfer in the S_1 state shows a barrier of the order of 0.11 eV and the reaction is exothermic by about 0.21 eV.
- (ii) There are two minimum-energy PE

valleys that connect the diketo tautomer with the two forms of the keto-enol tautomer on the PE surface of the S₁ state. (iii) The reaction paths associated with these profiles are different as they result in different ‘vertical’ PE profiles of the ground state computed along these paths. (iv) A significant reduction of the S₁–S₀ vertical energy gap for the Y form of the keto-enol tautomer (0.84 eV) as compared to the X form (1.47 eV) provides the source of more efficient radiationless decay of electronic excitation of the former. The process may involve tunneling through the barrier, which is apparently smaller or thinner for the Y form. Work by Yamazaki et al. [5] points to a possible CI with the ground state but the observed decays on the ps-ns timescale suggest tunneling as the more likely pathway. This conclusion is consistent with the CI at energies higher than the stable equilibria determined at the S₁ PE surface [5,6]. (v) The inter-ring twist of the diketo as well as keto-enol tautomeric forms does not lead to the intersection with the ground state as it is usually found for typical ESIPT systems (cf. [26] for instance).

4. Discussion

The visible-visible double resonance spectrum (Fig. 4) and mode II IR-vis spectrum (Fig. S5), confirm that all peaks observed belong to a single tautomer. Based on the mode I spectrum (Fig. 3), coupled with calculations, we can assign the single tautomer observed in our beam as the trans-diketo.

To describe the excited state dynamics we distinguish two ranges of the R2PI spectrum: spectral range A below 700 cm⁻¹ excess energy and spectral range B with more than 700 cm⁻¹ excess energy. The pump-probe data in range A are characterized by two excited state lifetimes that strongly depend on the vibrational mode of excitation and that differ by an

order of magnitude. The shorter lifetime, τ_1 , is of the order of 1 ns while the longer lifetime, τ_2 , is of the order of 10 ns. For range B we find a single lifetime of less than one ns which gradually decreases with increasing energy. We note that proton transfer is one of the fastest reactions possible. It has been found to occur in less than 1 ps [13,14,18]. Therefore, if proton or hydrogen transfer is involved, these lifetimes likely describe the dynamics of the keto-enol excited state or states once they are formed, rather than the dynamics of the initially excited diketo state.

The two lifetimes in range A likely correspond to two deactivation processes from two different excited states. If both channels originated from a single excited state, the slower decay would correspond to a lower rate and would probably be hard to observe in our experiment. According to the calculations as depicted in Fig. 5, there are two reaction pathways leading from the di-keto tautomer to the keto-enol ones on the PE surface of the S_1 state. They differ in the amount of electric charge that accompanies the proton transfer reaction. Since the S_1 PE profiles of both forms behave in a similar fashion with respect to the inter-ring torsion that does not modulate significantly the S_1 - S_0 energy gap, we can postulate that according to the energy-gap law [27,28] the Y form will undergo a faster decay to the ground state, but we do not have further hard evidence to confidently correlate the faster and slower process with the Y and X form, respectively. Geometrical rigidity of the indole moiety results in a relatively low density of vibrational states at low excess energy above the electronic origin of the S_1 state. Thus the low vibrational levels of indole conserve their quantum identity to a large extent and this makes their coupling to the particular channels along the PT reaction path mode sensitive.

The absence of the slow process beyond 700 cm^{-1} indicates that these excess energies are higher than the relevant barrier separating the Franck-Condon region from a keto-enol minimum. Below that energy, in range A, we observe two processes and beyond that energy, in range B, just one. There could be several causes for the absence of the slow process at higher excitation energies. It is possible that the slow process becomes fast or that beyond 700 cm^{-1} only the form responsible for the fast process is populated. Perhaps more likely is that the X and Y forms are able to interconvert, as IVR provides the energy to overcome the small barrier ($\sim 100\text{ cm}^{-1}$) between the two geometries. The decrease of lifetime with increasing energy in range B could be due to increasing deactivation rates, for example because of increasing internal conversion probability at higher excess energy [28].

In range A we notice mode specificity evidenced by different lifetimes for different vibronic transitions. Fig. 6 shows a graphic representation of the calculated QY data for the faster process from Table 1. If we assume that the fast process is the same for all modes, then a good estimate would be for it to be around 900 ps, as is the case for the $+79\text{ cm}^{-1}$ peak for which there is only a fast component. The values based on these assumptions are listed in the highlighted column of Table 1. The QY for the faster process is between 40% and 100% under all explored parameter values. Even though this is a wide range, there is no single combination of lifetime and QY that fits the data for all modes. Either the initial partitioning amongst X and Y depends strongly on the vibronic mode or so do the lifetimes of the X and Y states once they are formed. The latter would imply that the molecule in the X or Y states remember the original vibrational mode in the diketo state which would suggest slow or inefficient IVR [29,30]. Such slow IVR would also be consistent with

limited intermixing between the X and Y forms below 700 cm^{-1} , thus maintaining separate lifetimes.

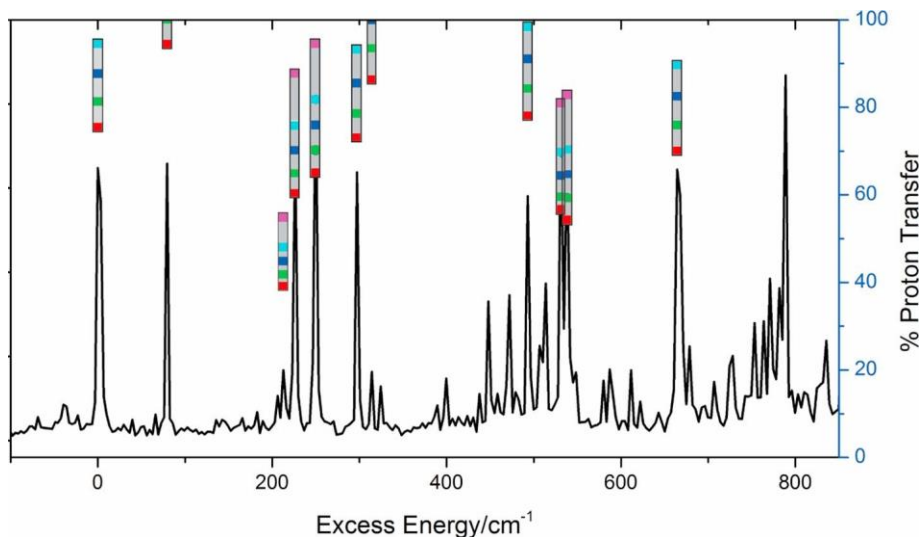


Figure 6. Graphic representation of the data in Table 1, showing QY (percent proton transfer) for specific vibronic peaks and for different values of τ_1 : red-750 ps, green-900 ps, blue-1050 ps, light blue-1200 ps, purple-1500 ps. (For interpretation of the references to color in this figure legend, the reader is referred to the web version of this article.)

Our results lead to the conclusion that indigo represents an exception among molecular systems subject to the ESIPT phenomenon, which generally is accompanied by GSIPT. In the case of indigo GSIPT leads to a structure (Y) which is unstable in S_0 while GSIHT leads to a form (X) that is stable in S_0 . In the S_1 state these processes are accompanied by a shift of electron density (rather than charge transfer) which goes in an opposite direction along the two reaction paths. As illustrated in Fig. 7, optical excitation of the X keto-enol form S_0 to the S_1 state results in a partial back charge transfer from the proton-accepting to the proton-donating moiety and this both raises the dipole moment of the state and changes its direction. A reverse situation occurs for the Y form. The significant polarity of the ground state at its S_1 equilibrium geometry indicates a ‘standard’ proton transfer process in this state and electronic excitation partially neutralizes the polarity of the system. Electronic excitation

qualitatively reverses the dipole moment of a given conformer and the dipole moments in the S_1 state are polarized approximately in the opposite directions to those of the ground states. The estimated angle between dipole moments of the X and Y forms in the S_1 state is about 125 degrees. This observation may have consequences regarding stabilization of these forms by different polar solvents or by specific chemical modifications of the indigo core.

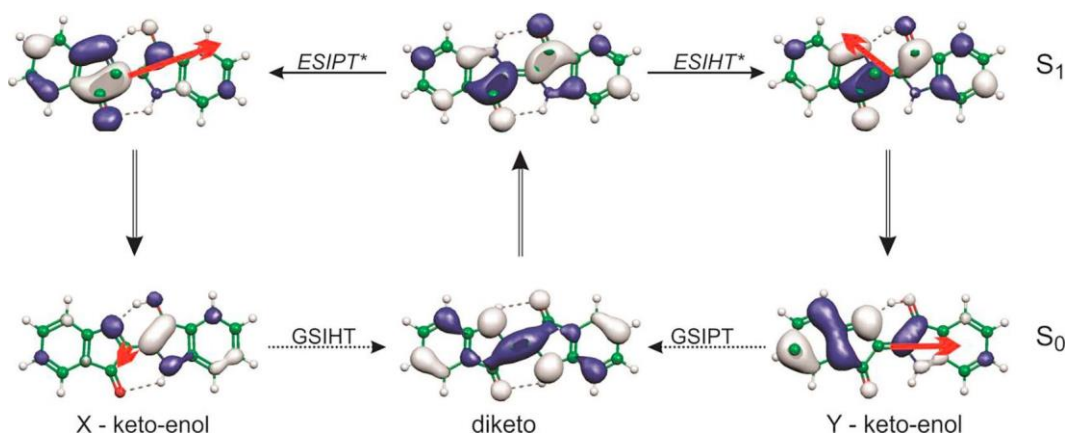


Figure 7. Diagram depicting transitions between the relevant tautomeric forms in ground state and excited state with electron orbitals involved in transitions and dipole moments (red arrows). Double arrows for electronic transitions, dotted arrows for ground state transitions, and solid arrows for transitions between forms in the excited state. (For interpretation of the references to color in this figure legend, the reader is referred to the web version of this article.)

Summarizing, we make the following observations. Unlike in common ESIPT systems, indigo also exhibits hydrogen transfer as part of its photochemistry. Experimentally we observe two deactivation processes. Our calculations predict two pathways as well, involving PT and HT, respectively, in the excited state and the opposite character (HT and PT) in the ground state trajectories. There is a narrow spectral range (up to 700 cm^{-1} above the origin) in which the partitioning among the two pathways depends strongly on vibrational modes. Above 700 cm^{-1} the excited state lifetime shortens considerably, providing a mechanism for indigo's stability against radiative damage. We are undertaking follow-up studies with deuterated indigo to further elucidate the excited state dynamics.

Supplemental Information

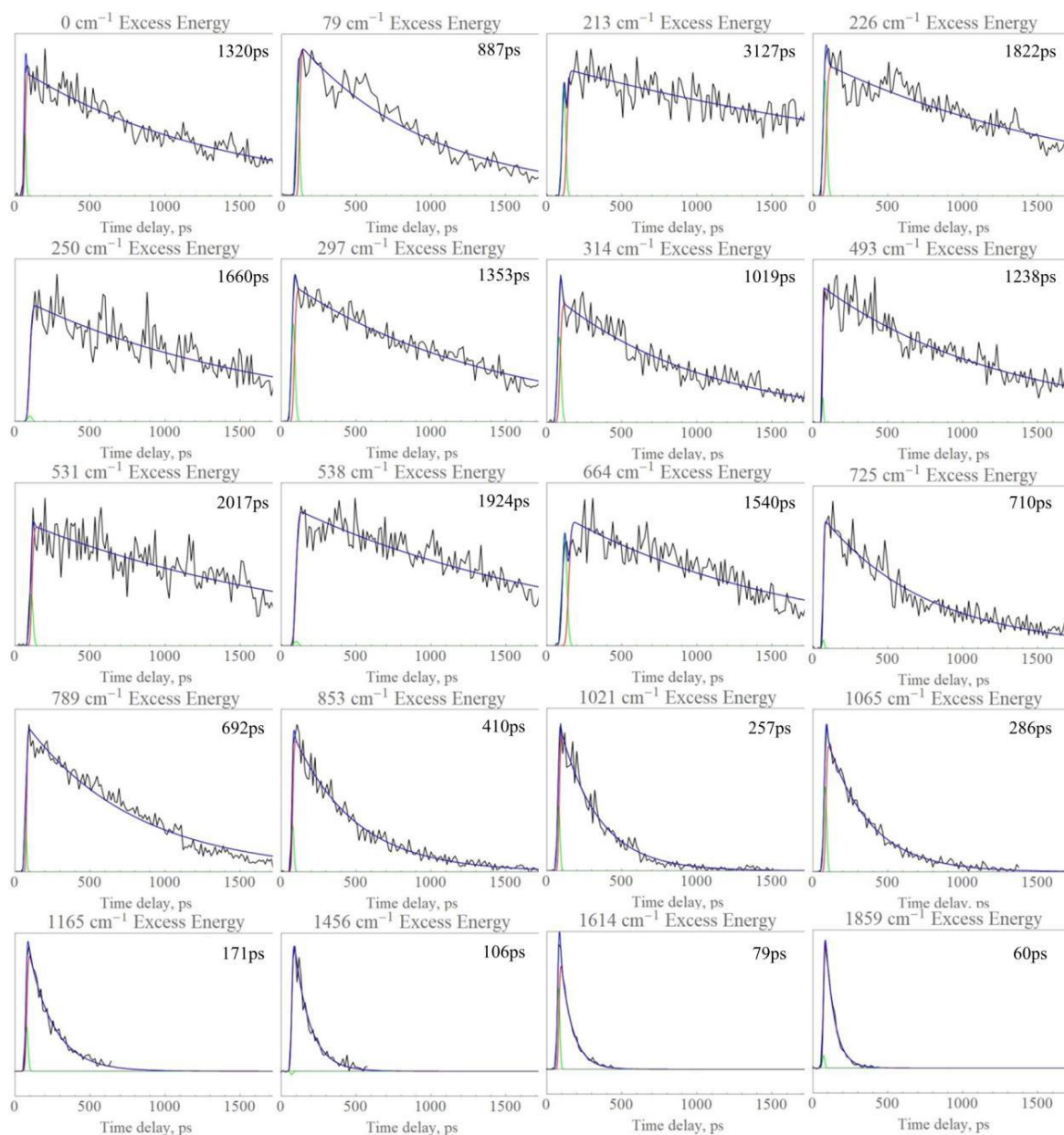


Figure S1. The pump probe transients from the ps pump probe experiments (OPG + 213) with the derived lifetime values. Data is in black, IRF in green, the decaying component in red, and the total fit in blue.

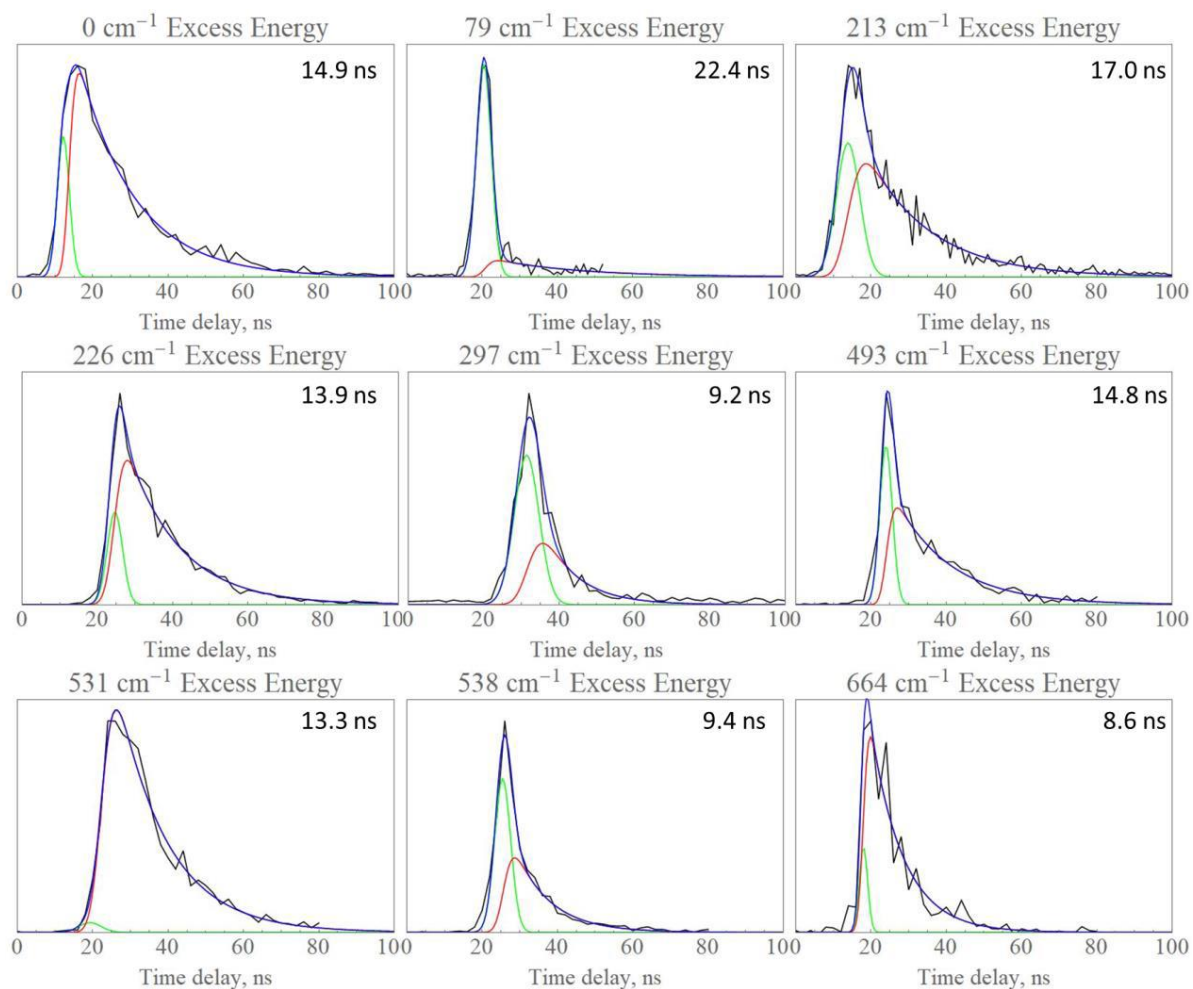


Figure S2. The pump probe transients from the ns pump probe experiments (OPG + 193nm) with the derived lifetime values. Data is in black, IRF in green, the decaying component in red, and the total fit in blue.

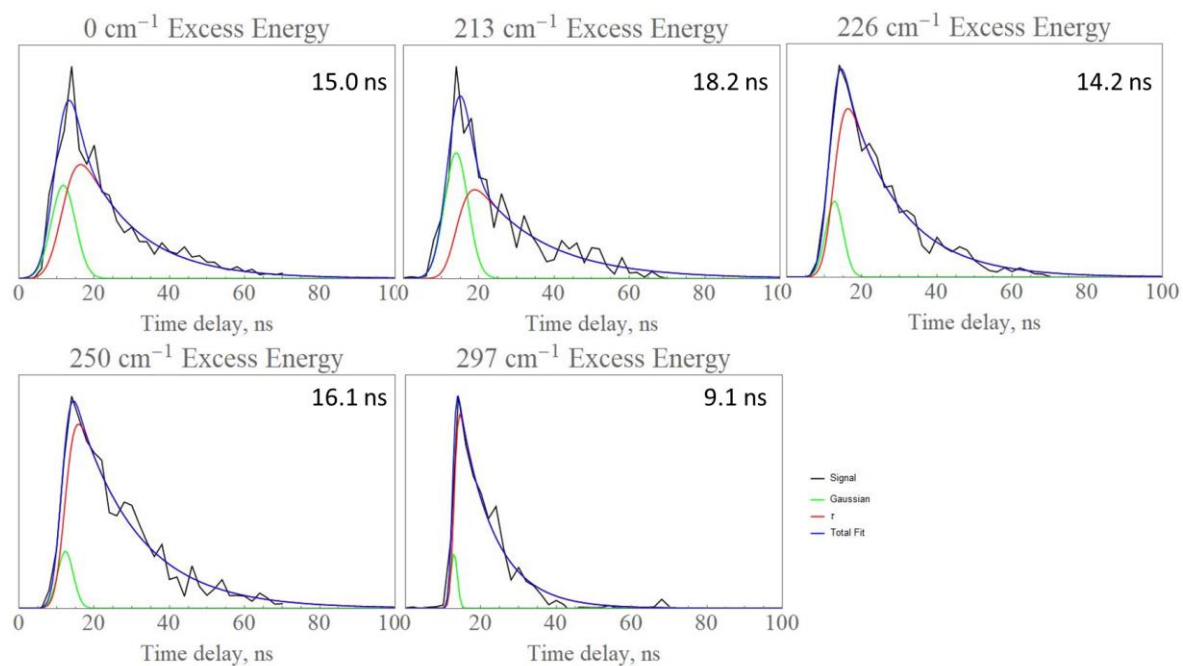


Figure S3. The pump probe transients from the ns pump probe experiments (dye + 213 nm) with the derived lifetime values. Data is in black, IRF in green, the decaying component in red, and the total fit in blue.

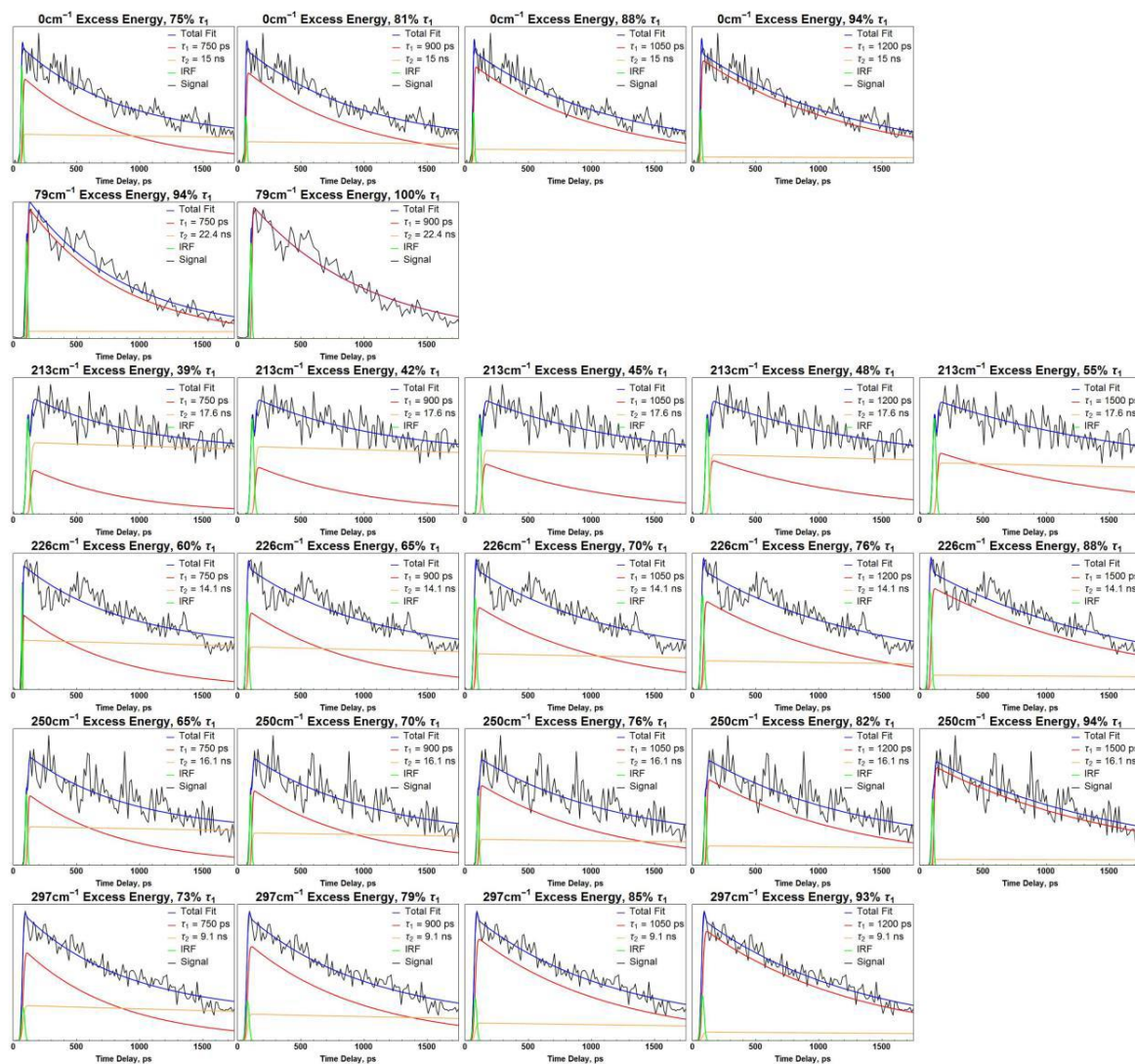


Figure S4a. The first 6 peaks of spectral range A with the different permutations of lifetime values fit in order to derive the range of possible relative quantum yields.

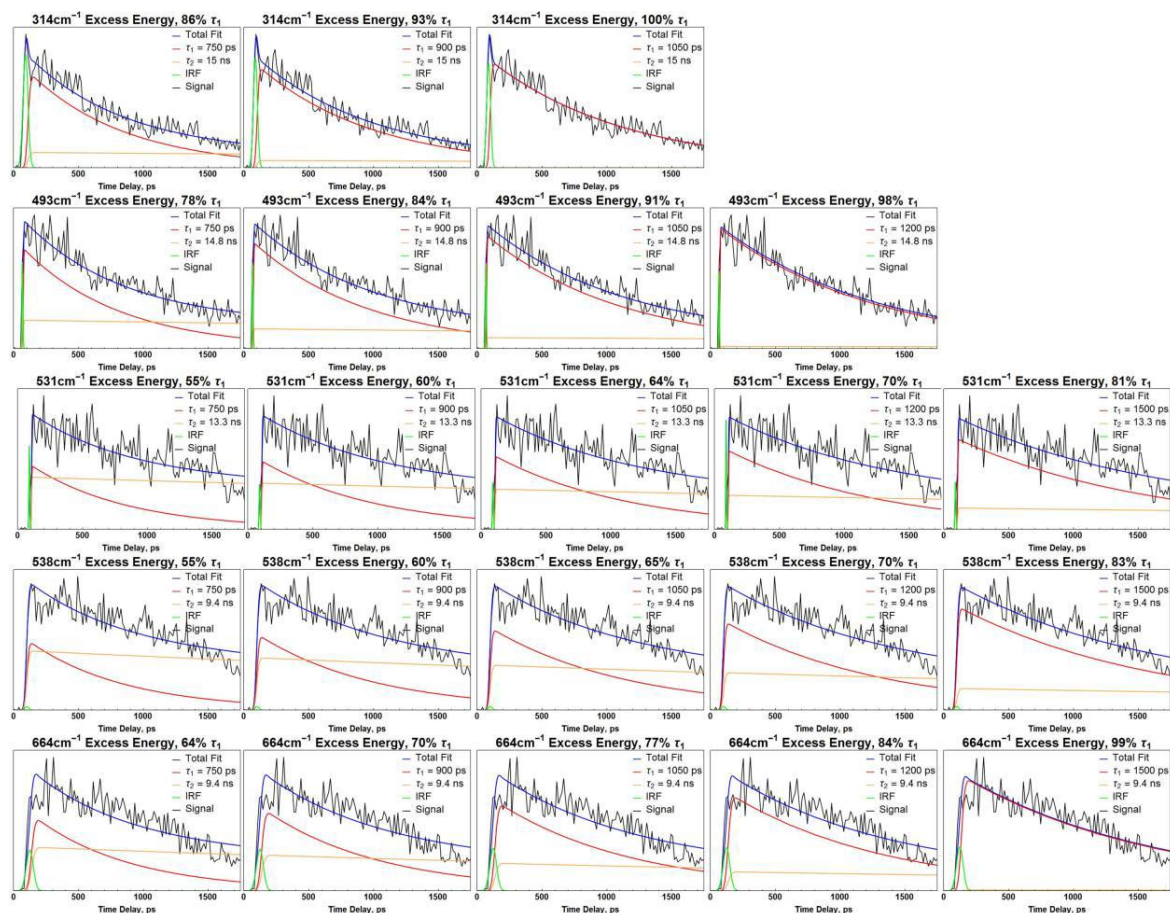


Figure S4b. The latter 5 peaks of spectral range A with the different permutations of lifetime values fit in order to derive the range of possible relative quantum yields.

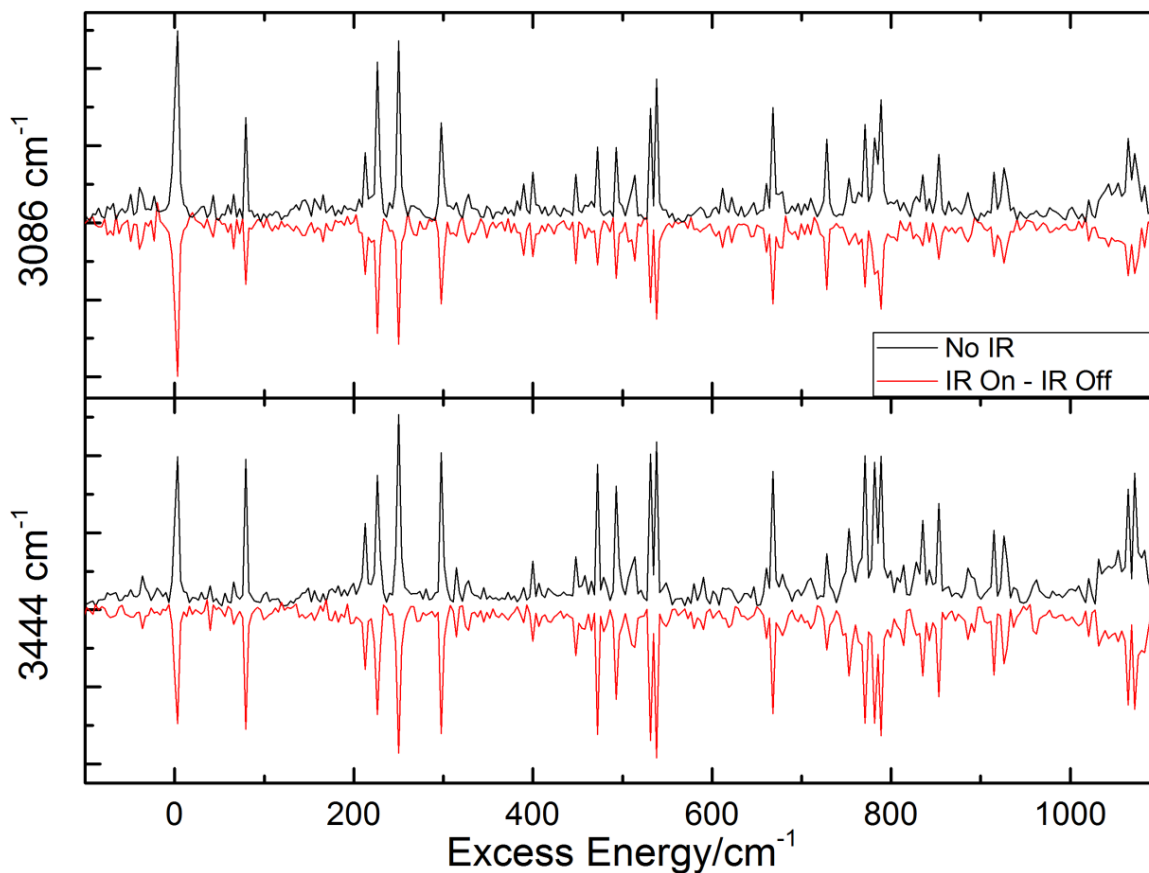


Figure S5. IR-Vis double resonance spectroscopy mode II of indigo with burn pulses set at a) 3084 and b) 3444 cm^{-1} , while probing with 2C from 18018 – 19230 cm^{-1} (555 – 520 nm, ps opp + 213). Burn on and burn off spectra were generated again using a digital chopper.

State	$\Delta E/\text{eV}$	f	μ/Debye	el. config.
S_0	0.0	-	0.0	$(29\text{ag})^2(5\text{bg})^2(6\text{au})^2(28\text{bu})^2$
$S_1(\pi\pi^*)$	2.203	0.351	0.0	0.97(6au-6bg)
$S_2(n\pi^*)$	2.901	0.0	0.0	0.94(29ag-6bg)
$S_3(\pi\pi^*)$	3.185	0.0	0.0	0.90(5bg-6bg)

Table S1a. Vertical transition energy (ΔE), oscillator strength (f), dipole moment (μ), and leading electronic configurations of indigo computed with ADC(2)/cc-pVDZ method at the MP2/cc-pVDZ equilibrium geometry of the $S_0(\text{KK})$ state. Numbers in the figure denote bondlengths in Angstrom.

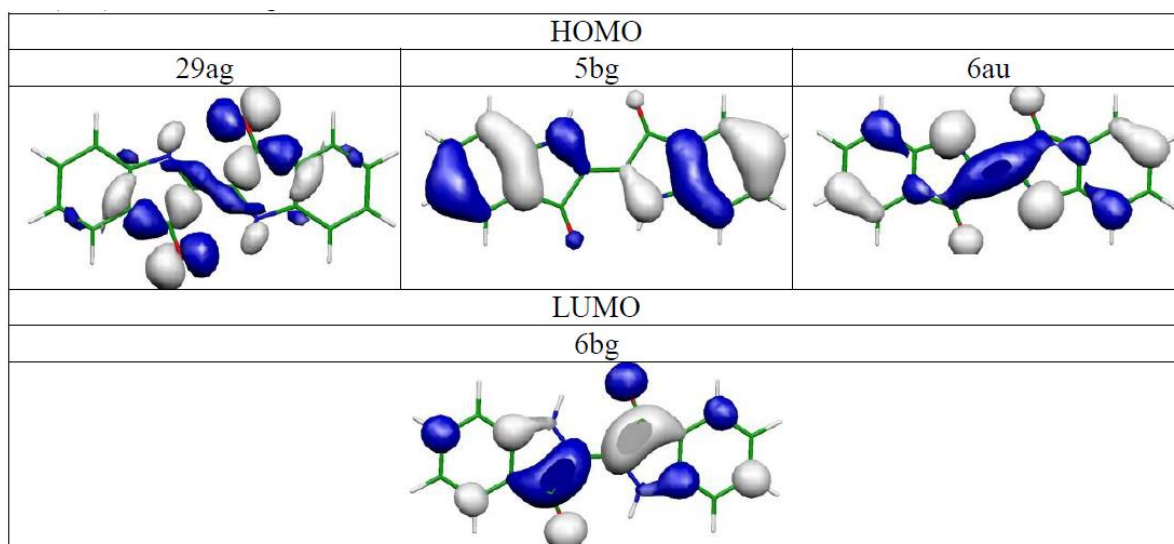


Table S1b. Relevant molecular orbitals involved into the lowest electronic excitations of the $S_0(KK)$ state of indigo.

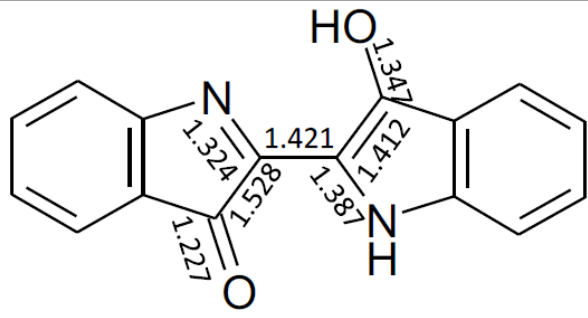
						
State	$\Delta E/eV$	f	$\mu/Debye$	$\mu_x/Debye$	$\mu_y/Debye$	el. config.
S_0	(0.126) ^a	-	1.40	-1.11	-0.86	$(57a')^2(11a'')^2$
$S_1(\pi\pi^*)$	2.101	0.290	6.45	6.09	2.12	$0.95(11a''-12a'')$
$S_2(n\pi^*)$	2.681	0.0	3.03	-0.89	2.89	$0.92(57a'-12a'')$
$S_3(\pi\pi^*)$	3.000	0.046	7.73	7.73	0.13	$0.91(10a''-12a'')$

Table S2a. Vertical transition energy (ΔE), oscillator strength (f), dipole moment (μ), and leading electronic configurations of indigo computed with ADC(2)/cc-pVDZ method at the MP2/cc-pVDZ equilibrium geometry of the $S_0(EK)$ state. Numbers in the figure denote bond lengths in Angstrom.

a) Relative to energy of the KK tautomer.

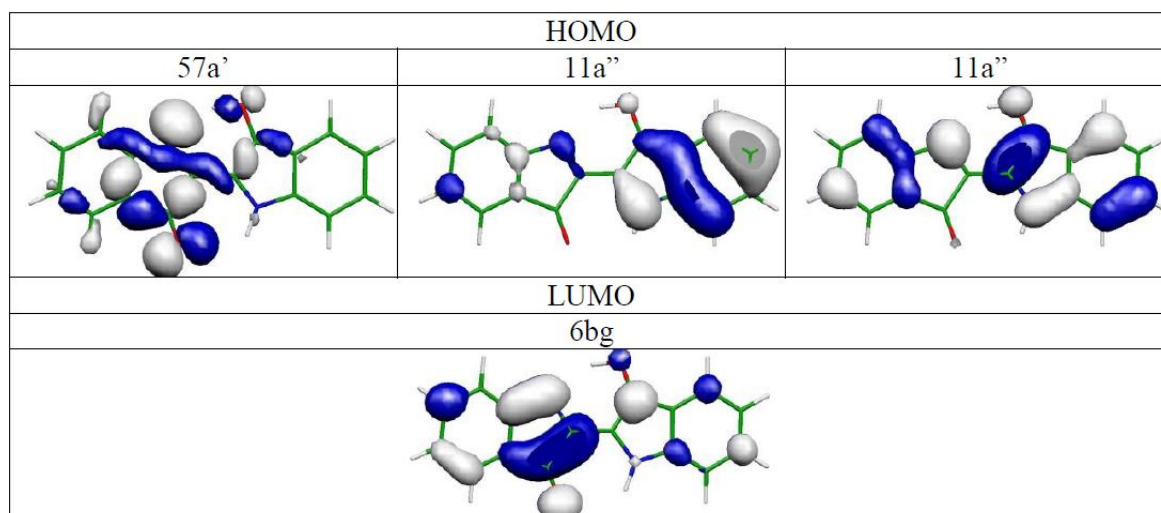


Table S2b. Relevant molecular orbitals involved into the lowest electronic excitations of the $S_0(\text{EK})$ state of indigo.

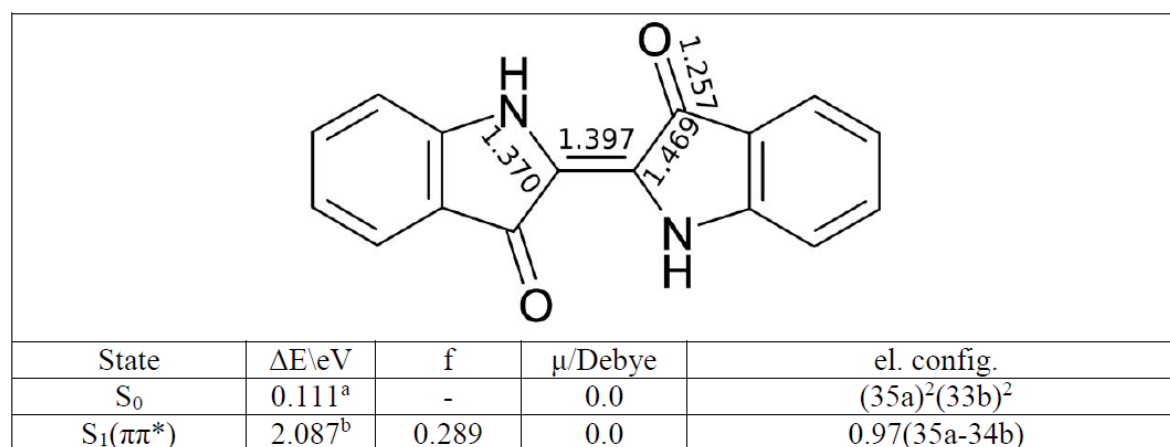


Table S3a. Transition energy (ΔE), oscillator strength (f), dipole moment (μ), and leading electronic configurations of indigo computed with ADC(2)/cc-pVDZ method at the $S_1(\text{KK})$ -state equilibrium geometry. Numbers in the figure denote bondlengths in Angstrom.

- a) Vertical energy computed at the equilibrium geometry of the S_1 state.
 b) Adiabatic energy relative to the energy of the KK tautomer.

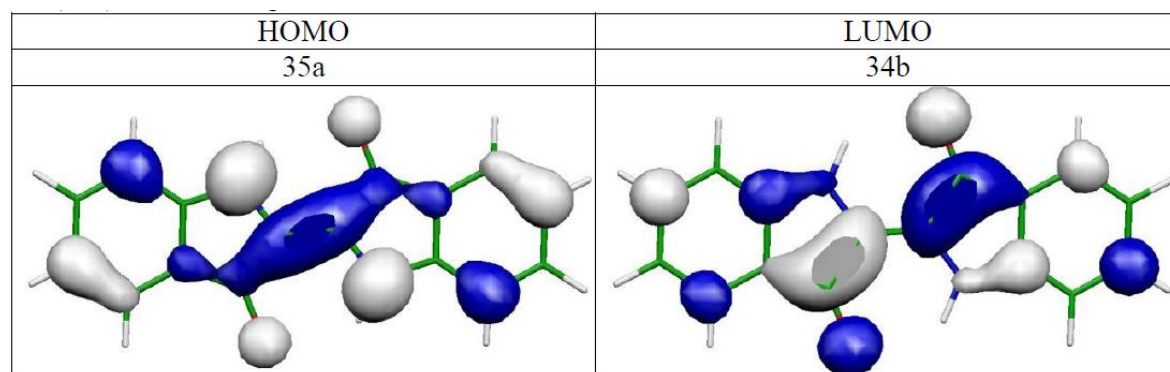
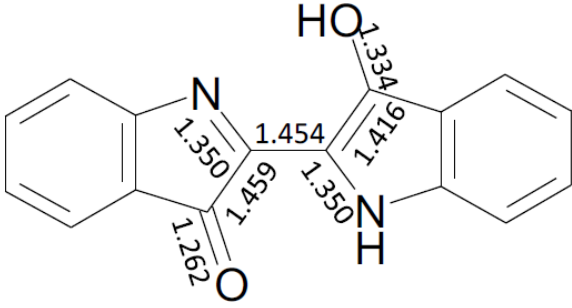


Table S3b. Relevant molecular orbitals involved into the lowest electronic excitation of the $S_1(\text{KK})$ state of indigo.



State	ΔE /eV	f	μ /Debye	μ_x /Debye	μ_y /Debye	el. config.
S_0	0.436 ^a	-	1.27	-1.14	-0.55	$(57a')^2(11a'')^2$
$S_1(\pi\pi^*)$	1.901 ^b	0.198	6.77	6.39	2.22	$0.96(11a''-12a'')$

Table S4a. Transition energy (ΔE), oscillator strength (f), dipole moment (μ), and leading electronic configurations of indigo computed with ADC(2)/cc-pVDZ method at the S_1 (EK)-state equilibrium geometry of the X conformer. Numbers in the figure denote bondlengths in Angstrom.

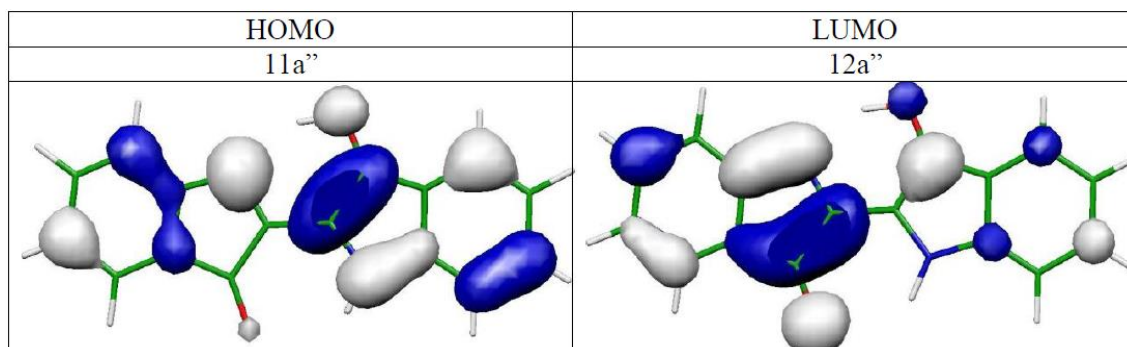


Table S4b. Relevant molecular orbitals involved into the lowest electronic excitation of X conformer.

FINAL HEAT OF FORMATION = -873.0870932672

C 0.6619206 -0.1065775 0.0000000
 C -0.7917185 -0.1084148 0.0000000
 N -1.3985199 1.0978465 0.0000000
 C -2.7676758 0.7926254 0.0000000
 C -3.0043410 -0.6229450 0.0000000
 C -1.6739363 -1.2707338 0.0000000
 C -4.3142052 -1.1177566 0.0000000
 C -5.3770140 -0.1899119 0.0000000
 C -5.1448470 1.2060598 0.0000000
 C -3.8331444 1.7110423 0.0000000
 O -1.3062324 -2.4778345 0.0000000
 N 1.4125181 -1.2288768 0.0000000
 C 2.7734972 -0.8846437 0.0000000
 C 2.8619550 0.5460147 0.0000000
 C 1.5072170 1.0297627 0.0000000
 C 4.1264700 1.1661229 0.0000000

C 5.2664726 0.3450092 0.0000000
 C 5.1626702 -1.0629600 0.0000000
 C 3.9040704 -1.7000052 0.0000000
 O 1.0762926 2.2921322 0.0000000
 H -3.6331386 2.7883907 0.0000000
 H -5.9945195 1.8969170 0.0000000
 H -6.4098504 -0.5563297 0.0000000
 H -4.5014013 -2.1971141 0.0000000
 H 0.0717783 2.2060724 0.0000000
 H 0.9634197 -2.1519527 0.0000000
 H 3.8209729 -2.7918052 0.0000000
 H 6.0707347 -1.6740663 0.0000000
 H 6.2591344 0.8066818 0.0000000
 H 4.2114206 2.2572504 0.0000000

Table S5c. Cartesian coordinates of the X conformer optimized in the S1 state with ADC(2)/cc-pVDZ method.

State	$\Delta E/eV$	f	$\mu/Debye$	$\mu_x/Debye$	$M_y/Debye$	el. config.
S_0	1.035 ^a	-	4.14	4.13	-0.31	$(57a')^2(11a'')^2$
$S_1(\pi\pi^*)$	1.875 ^b	0.097	3.39	-2.71	2.04	$0.96(11a''-12a'')$

Table S5a. Transition energy (ΔE), oscillator strength (f), dipole moment (μ), and leading electronic configurations of indigo computed with ADC(2)/cc-pVDZ method at the S1(EK)-state equilibrium geometry of the Y conformer. Numbers in the figure denote bondlengths in Angstrom.

- Vertical energy computed at the equilibrium geometry of the S1 state.
- Adiabatic energy relative to the energy of the KK tautomer.

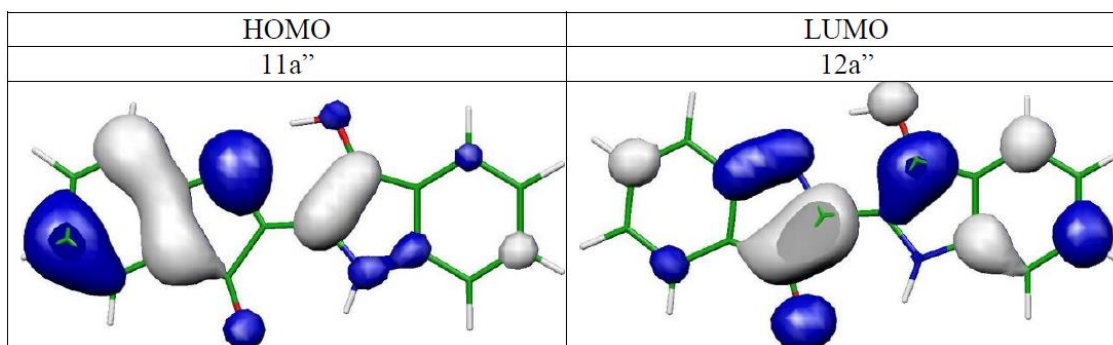


Table S5b. Relevant molecular orbitals involved into the lowest electronic excitations of Y conformer.

FINAL HEAT OF FORMATION = -873.0879616948

C 0.6302364 -0.1642869 0.0000000
 C -0.7531914 -0.1667760 0.0000000
 N -1.4278622 1.1395201 0.0000000
 C -2.7255052 0.8057657 0.0000000
 C -2.9679095 -0.6339839 0.0000000
 C -1.6575612 -1.3006363 0.0000000
 C -4.2757554 -1.1395843 0.0000000
 C -5.3411587 -0.2273084 0.0000000
 C -5.1204606 1.1893114 0.0000000
 C -3.8366860 1.7139106 0.0000000
 O -1.3439359 -2.5217731 0.0000000
 N 1.4343001 -1.2862716 0.0000000
 C 2.7560221 -0.8932104 0.0000000
 C 2.8189884 0.5455082 0.0000000
 C 1.4724280 1.0078886 0.0000000
 C 4.0708499 1.2087497 0.0000000
 C 5.2288439 0.4311086 0.0000000
 C 5.1562485 -0.9887962 0.0000000
 C 3.9300460 -1.6663927 0.0000000
 O 1.0400652 2.2639112 0.0000000
 H -4.4463235 -2.2216296 0.0000000
 H -6.3718698 -0.5984008 0.0000000
 H -5.9849861 1.8617724 0.0000000
 H -3.6511799 2.7931817 0.0000000
 H 0.0376944 2.1858199 0.0000000
 H 1.0332802 -2.2236377 0.0000000
 H 3.8876461 -2.7604011 0.0000000
 H 6.0836323 -1.5718356 0.0000000
 H 6.2101154 0.9159788 0.0000000
 H 4.1139886 2.3024977 0.0000000

Table S6c. Cartesian coordinates of the Y conformer optimized in the S1 state with ADC(2)/cc-pVDZ method.

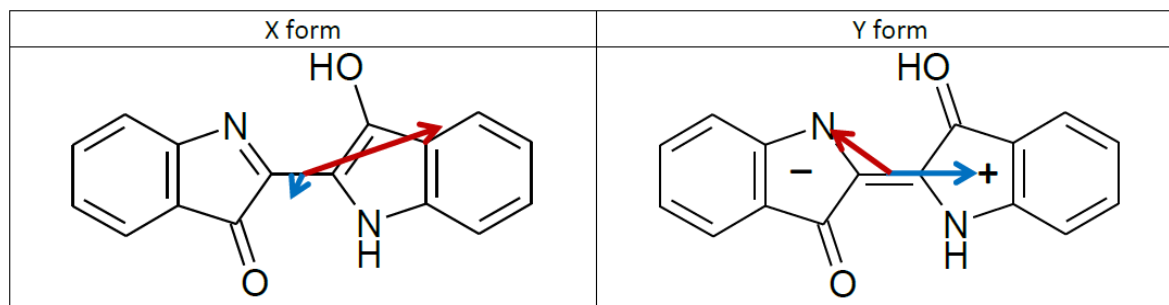


Fig. S6. Geometric structures of the X and Y enol-keto forms of indigo with the electronic structures indicated. Arrows illustrate direction and value of dipole moments computed for the S0 state (blue) and for the S1 state (red) at the S1-optimized geometry.

References

- [1] R.J.H. Clark, C.J. Cooksey, M.A.M. Daniels, R. Withnall, Indigo, Woad, and Tyrian Purple - Important Vat Dyes from Antiquity to the Present, *Endeavour* 17 (1993) 191-199.
- [2] J.C. Splitstoser, T.D. Dillehay, J. Wouters, A. Claro, Early pre-Hispanic use of indigo blue in Peru, *Science advances* 2 (2016) e1501623.
- [3] R.M. Christie, Why is indigo blue?, *Biotech Histochem* 82 (2007) 51-56.
- [4] J.E.A. Otterstedt, Photostability and molecular structure, *The Journal of Chemical Physics* 58 (1973) 5716-5725.
- [5] S. Yamazaki, A.L. Sobolewski, W. Domcke, Molecular mechanisms of the photostability of indigo, *Phys Chem Chem Phys* 13 (2011) 1618-1628.
- [6] M. Moreno, J.M. Ortiz-Sanchez, R. Gelabert, J.M. Lluch, A theoretical study of the photochemistry of indigo in its neutral and dianionic (leucoindigo) forms, *Phys Chem Chem Phys* 15 (2013) 20236-20246.
- [7] G.M. Wyman, B.M. Zarnegar, Excited State Chemistry of Indigoid Dyes. 11. The Interaction of Thio- and Selenoindigo Dyes with Hydroxylic Compounds and Its Implications on the Photostability of Indigo, *The Journal of Physical Chemistry* 77 (1973) 1204-1207.
- [8] A.D. Kirsch, G.M. Wyman, Excited state chemistry of indigoid dyes. 5. The intermediacy of the triplet state in the direct photoisomerization and the effect of substituents, *The Journal of Physical Chemistry* 81 (1977) 413-420.
- [9] G. Miehe, P. Süsse, V. Kupcik, E. Egert, M. Nieger, G. Kunz, R. Gerke, B. Knieriem, M. Niemeyer, W. Lüttke, Light Absorption as well as Crystal and Molecular Structure of N, N'-Dimethylindigo: An Example of the Use of Synchrotron Radiation, *Angewandte Chemie International Edition in English* 30 (1991) 964-967.
- [10] A.S. Chatterley, D.A. Horke, J.R. Verlet, On the intrinsic photophysics of indigo: a time-resolved photoelectron spectroscopy study of the indigo carmine dianion, *Phys Chem Chem Phys* 14 (2012) 16155-16161.
- [11] J. Pina, D. Sarmiento, M. Accoto, P.L. Gentili, L. Vaccaro, A. Galvao, J.S. Seixas de Melo, Excited-State Proton Transfer in Indigo, *J Phys Chem B* 121 (2017) 2308-2318.
- [12] N.D. Bernardino, S. Brown-Xu, T.L. Gustafson, D.L.A. de Faria, Time-Resolved Spectroscopy of Indigo and of a Maya Blue Simulant, *J Phys Chem C* 120 (2016) 21905-21914.

- [13] I. Iwakura, A. Yabushita, T. Kobayashi, Why is Indigo Photostable over Extremely Long Periods?, *Chemistry Letters* 38 (2009) 1020-1021.
- [14] I. Iwakura, A. Yabushita, T. Kobayashi, Kinetic isotope effect on the proton-transfer in indigo carmine, *Chem Phys Lett* 484 (2010) 354-357.
- [15] J.M. Seixas de Melo, A. P.; Melo, M. J., Photophysical and Spectroscopic Studies of Indigo Derivatives in Their Keto and Leuco Forms, *J Phys Chem A* 108 (2004) 6975 - 6981.
- [16] R. Rondao, J. Seixas de Melo, M.J. Melo, A.J. Parola, Excited-state isomerization of leuco indigo, *J Phys Chem A* 116 (2012) 2826-2832.
- [17] J.A. Syage, Ultrafast Measurements of Chemistry in Clusters Excited-State Proton Transfer, *J Phys Chem* 99 (1994) 5772 - 5786.
- [18] A.L. Douhal, Françoise; Zewail, Ahmed H., Proton-transfer reaction dynamics, *Chemical Physics* 207 (1996) 477-498.
- [19] G. Meijer, M.S. De Vries, H.E. Hunziker, H.R. Wendt, Laser Desorption Jet-Cooling of Organic Molecules, *Applied Physics B* 51 (1990) 395 - 403.
- [20] F.M. Siouri, S. Boldissar, J.A. Berenbeim, M.S. de Vries, Excited State Dynamics of 6-Thioguanine, *J Phys Chem A* 121 (2017) 5257-5266.
- [21] M.J. Frisch, G.W. Trucks, H.B. Schlegel, G.E. Scuseria, M.A. Robb, J.R. Cheeseman, G. Scalmani, V. Barone, B. Mennucci, G.A. Petersson, H. Nakatsuji, M. Caricato, X. Li, H.P. Hratchian, A.F. Izmaylov, J. Bloino, G. Zheng, J.L. Sonnenberg, M. Hada, M. Ehara, K. Toyota, R. Fukuda, J. Hasegawa, M. Ishida, T. Nakajima, Y. Honda, O. Kitao, H. Nakai, T. Vreven, J.A.M. Jr., J.E. Peralta, F. Ogliaro, M. Bearpark, J.J. Heyd, E. Brothers, K.N. Kudin, V.N. Staroverov, R. Kobayashi, J. Normand, K. Raghavachari, A. Rendell, J.C. Burant, S.S. Iyengar, J. Tomasi, M. Cossi, N. Rega, J.M. Millam, M. Klene, J.E. Knox, J.B. Cross, V. Bakken, C. Adamo, J. Jaramillo, R. Gomperts, R.E. Stratmann, O. Yazyev, A.J. Austin, R. Cammi, C. Pomelli, J.W. Ochterski, R.L. Martin, K. Morokuma, V.G. Zakrzewski, G.A. Voth, P. Salvador, J.J. Dannenberg, S. Dapprich, A.D. Daniels, Ö. Farkas, J.B. Foresman, J.V. Ortiz, J. Cioslowski, D.J. Fox, Gaussian 09, Revision A.2, Gaussian, Inc., Wallingford CT, 2009.
- [22] J. Schirmer, Beyond the Random-Phase Approximation - a New Approximation Scheme for the Polarization Propagator, *Physical Review A* 26 (1982) 2395-2416.
- [23] A.B. Trofimov, J. Schirmer, An Efficient Polarization Propagator Approach to Valence Electron-Excitation Spectra, *Journal of Physics B-Atomic Molecular and Optical Physics* 28 (1995) 2299-2324.
- [24] TURBOMOLE, 2014.
- [25] C. Hättig, F. Weigend, CC2 excitation energy calculations on large molecules using the resolution of the identity approximation, *Journal of Chemical Physics* 113 (2000) 5154-5161.
- [26] A.L. Sobolewski, W. Domcke, C. Hättig, Photophysics of Organic Photostabilizers. Ab Initio Study of the Excited-State Deactivation Mechanisms of 2-(2'-Hydroxyphenyl) benzotriazole, *The Journal of Physical Chemistry A* 110 (2006) 6301-6306.
- [27] W. Siebrand, Radiationless Transitions in Polyatomic Molecules. II. Triplet-Ground-State Transitions in Aromatic Hydrocarbons, *The Journal of Chemical Physics* 47 (1967) 2411-2422.
- [28] A.L. Sobolewski, On the excess-energy dependence of radiationless decay rate constants, *Chemical physics* 115 (1987) 469-479.
- [29] P.M. Felker, A.H. Zewail, Dynamics of intramolecular vibrational-energy redistribution (IVR). II. Excess energy dependence, *The Journal of chemical physics* 82 (1985) 2975-2993.

[30] P.M. Felker, A.H. Zewail, Observation of restricted IVR in large molecules: Quasi-periodic behavior, phase-shifted and non-phase-shifted quantum beats, Chem Phys Lett 102 (1983) 113-119.

II. Excited State Intramolecular Proton Transfer in Hydroxyanthraquinones: Towards Predicting Fading of Organic Red Colorants in Art

J.A. Berenbeim,¹ S. Boldissar,¹ S. Owens,¹ M.R. Haggmark,¹ G. Gate,¹ F.M. Siouri,¹ T. Cohen,¹ M. F. Rode,² C. Schmidt Patterson,³ and M.S. de Vries^{1*}

¹ Department of Chemistry and Biochemistry, University of California Santa Barbara, California, USA.

² Institute of Physics, Polish Academy of Sciences, Al. Lotnikow 32/46 02-668, Warszawa Poland.

³ Getty Conservation Institute, 1200 Getty Center Drive, Suite 700, Los Angeles, California, USA.

Abstract

Compositionally similar organic red colorants in the anthraquinone family, whose photodegradation can cause irreversible color and stability changes, have long been used in works of art. Different organic reds, and their multiple chromophores, suffer degradation disparately. Understanding the details of these molecules' degradation, therefore, provides a window into their behavior in works of art, and may assist the development of improved conservation methods. According to one proposed model of photodegradation dynamics, intramolecular proton transfer provides a kinetically favored decay pathway in some photo-excited chromophores, preventing degradation-promoting electron transfer (ET). To further test this model, we measured excited state lifetimes of substituted gas phase anthraquinones, utilizing high-level theory to explain the experimental results. The data show a general structural trend: anthraquinones with 1,4-OH substitution are long-lived and prone to damaging ET, while excited state intramolecular proton transfers promote efficient quenching for hydroxyanthraquinones that lack this motif.

1. Introduction

Exposure to light degrades many molecules when absorption of ultraviolet and visible wavelength photons places them in an energetically excited state prone to chemical and physical change. Molecules susceptible to photodegradation are ubiquitous in both natural and synthetic systems and undesired effects of such degradation can include a wide range of phenomena, such as the appearance of abnormal skin cells marking melanoma, and the drop of efficiency in polymer solar cells via photo-bleaching. One notable form of organic photodegradation with relevance to the broad field of cultural heritage research is the fading of certain chromophores in works of art, which leads to visual change in a medium where meaning and value is often predicated on color.

Natural organic red colorants of either plant or scale-insect origin are important traditional sources of red hues.¹ These colorants have high tinting strength and are therefore present on artifacts in low concentration; as little as subnanogram concentrations of these colorants may be required to achieve a desired color saturation.² Many traditional organic red colorants (including madder, alizarin, cochineal, lac dye, brazilwood, and dragonsblood) are compositionally similar: these anthraquinones (AQ) and hydroxyanthraquinones (HAQ) have long been used as lake pigments and contain primarily hydroxyl, carboxylic acid, and carbonyl moieties on a conjugated aromatic backbone. While commercial interest in AQs and HAQs has recently expanded to include pharmaceutical applications,³⁻⁴ the use of natural AQ derivatives (see Fig. 1) as lake dyes (insoluble dye-mordant complexes, typically precipitated with Al or Ca cations) has long attracted the attention of fine artists and craftsmen, and these pigments continue to be used today. The irreversible fading of organic red colorants in art is well-documented, and greatly affects the perception of masterpieces

from antiquity to the present day. Recent publications, for example, have highlighted alteration of organic red colorants in objects as disparate as medieval manuscript illuminations to paintings by Vincent van Gogh.⁵⁻⁷

One of the simplest HAQ molecules to be used as a lake pigment is 1,2-dihydroxyanthraquinone (1,2-HAQ), also known as alizarin. Alizarin is produced naturally by multiple species related to *Rubia tinctorum* (common madder) where it is a primary chromophore along with 1,2,4-trihydroxyanthraquinone (1,2,4-HAQ), also known as purpurin.¹ It is well documented in the cultural heritage and condensed phase scientific communities that alizarin is more photostable than purpurin.⁸⁻¹¹ Condensed phase photodynamics studies of these AQs suggests that the difference in photostability may stem from an excited state pathway, specifically an excited state intramolecular proton transfer (ESIPT), in alizarin which dissipates photonic energy to regain a stable ground state structure on a timescale much faster than the reaction rates of degradation.¹¹⁻¹²

ESIPT constitutes one of the fastest reactions known,¹³⁻¹⁴ and planar organic molecules containing acidic and basic functional groups connected by an intramolecular hydrogen bond often have photophysics driven by such proton transfer. In such molecules, excited state tautomerization occurs through the excitation of the ground state enol-form to an electronically excited intermediate where a rapid (sub-picosecond timescale), often energetically barrierless, enol to keto proton transfer takes place. Radiationless decay follows this transfer, bringing the excited keto form back to the ground state, and the stable ground state enol reforms through a barrierless back proton transfer.¹⁵ Molecules which undergo ESIPT are typically identified by dual band fluorescence with a large degree of Stokes shift from the ESIPT lower well equilibrium geometry.

Formative work examining this mechanism in AQs/HAQs was done in the 1980s¹⁶; laser induced fluorescent spectroscopy studies¹⁷, including by Flom and Barbara,¹⁵ determined that the presence of a dual 1,4- electron donating group (e.g. -OH) precludes dual fluorescence, likely indicating a high barrier towards ESIPT. This qualitative result was later supported by the nodal-plane model by Nagaoka.¹⁸ More recent transient spectroscopic work has measured the rate of ESIPT¹⁹⁻²¹ as a femtosecond process and correlated this with pigment fading^{11, 22}. However these are all condensed phase experiments where the effects of secondary molecules, such as binder or other pigment components, cannot be completely excluded, which is particularly important since intermolecular effects are widely known to affect relaxation.^{20, 23} To measure the unimolecular dynamics of the AQ and HAQ molecules requires gas phase experiments. It should be noted that in the context of art materials, much of the available literature deals only with alizarin and purpurin as exemplars of the HAQ system.²⁴ Therefore, there remains a need to examine a broader range of these important molecules in the gas phase to fully explicate the observed differences in the relative photostabilities of the basic chromophores themselves. By studying a larger set of isolated HAQs it is possible to identify the key structural motifs that determine the photodynamics of this class of compounds and that inform the distinction between alizarin and purpurin characteristics. Such a fundamental study can then inform a fuller understanding of the more complex systems found in works of art, which will include binding media, the support, and other pigments in addition to the organic red colorant in question.

In this paper, we address this need, and report an experimental and computational case study on the effects of proton transfer on the excited state lifetimes of seven related HAQs as isolated chromophores. We measured intrinsic lifetimes of neutral HAQ molecules in a jet-

cooled molecular beam by time resolved, pump-probe, two-color (2C) resonant two-photon ionization (R2PI) spectroscopy to elucidate the relaxation dynamics occurring at the lower limit of the excited state potential energy surface (PES). For each molecule studied, these data provide the first 2C R2PI action spectra. We also obtained the excited state lifetimes from both the lowest energy vibronic transition and at higher internal energy ($\sim 500\text{-}1000\text{ cm}^{-1}$) and, for selected compounds, partial mid-IR characterization of the ground state hydrogen bond vibrations with IR hole burning of the R2PI probe signal. These measurements allow us to study these chromophores in selected unique tautomeric forms. The resulting detailed vibrationally and tautomericly resolved excited state lifetime data reveal the intrinsic properties of the chromophores and serve as the basis for high level quantum computational modeling of the excited state dynamics. We explore the implications of the resulting data for the photodegradation of these compounds. Our results show a trend of shorter excited state lifetimes for the structures for which there is evidence for ESIPT, as derived from dual fluorescence by Flom and Barbara and others. We find that both phenomena correlate with structural motifs with a specific double hydrogen bonding pattern and this observation provides experimental evidence to support predictions for the expected stability of HAQs in works of art.

2. Results

Analytes studied and R2PI spectroscopy

Fig. 1 shows the series of substituted HAQs analyzed. The analytes represent structures with and without the 1,4-OH substitution motif postulated to be determinative of ESIPT properties.^{11, 15}. Several of these molecules are also found in artists' red lake pigments. The

molecular structures shown in Fig.1 are planar in all cases. In each molecule the lowest energy (LE) structure (indicated by the Roman numeral I) is that of the 9,10-anthraquinone, with carbonyl groups rather than hydroxyl moieties on the central ring of the backbone. The interpretation of R2PI and pump-probe spectra requires an understanding of the possible structures present in the molecular beam, which are most likely the lowest energy isomers. Fig. 1 shows all isomers with energies calculated to be within 25 kJ/mol of the lowest energy (LE) structure; isomeric forms with higher energies appear in the supplemental information. The center of Fig. 1 shows the two primary *common madder* chromophores alizarin (1,2-HAQ) and purpurin (1,2,4-HAQ). Both have multiple low energy isomers, as do 1,2,5,8-HAQ and 1,4-HAQ. Three of the molecules examined – 1-HAQ, 1,5-HAQ, and 1,8-HAQ – have only a single lowest energy structure (the rotamers for each of these molecules are 52.3, 53.2, and 47.4 kJ/mol higher in energy than the forms shown, respectively). In the figure and throughout we use the nomenclature of HAQ for all compounds, ignoring the more formal designations of DHAQ and THAQ for the di- and trihydroxy forms, as the numbered prefixes already indicate the number of hydroxyl substituents.

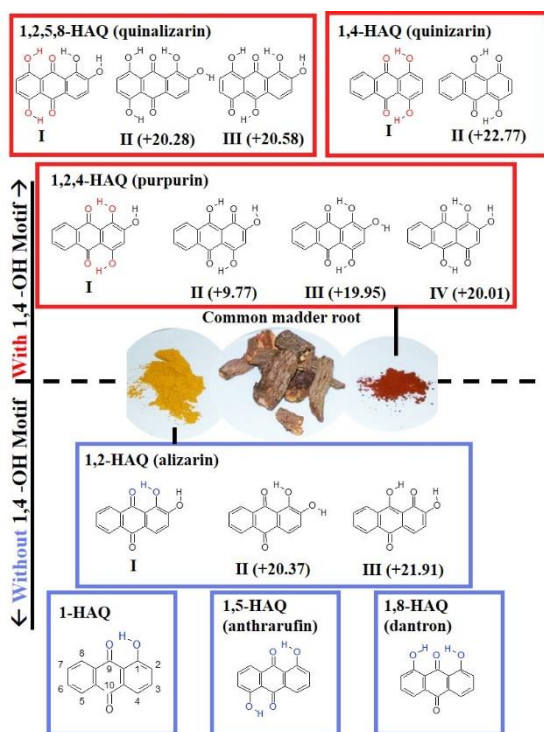


Fig. 1. The molecules of this study. Molecules having a 1,4 -OH motif are above the dotted line and those without 1,4 -OH motif are below it. Isomers within ~ 25 kJ/mol of the lowest energy ZPE corrected structure (labeled I) are also shown with their relative energy values (kJ/mol) with respect to the lowest energy form. Central to this figure is the common madder root and its primary chromophores alizarin and purpurin.

Fig. 2 presents the R2PI spectra of the HAQs from Fig. 1. The origins, corresponding to S_{0-0} transitions, of molecules with a 1,4-motif are about 2000 cm^{-1} lower in energy than those without the 1,4-motif. The origins of 1,2,5,8-HAQ ($19,661\text{ cm}^{-1}$), 1,2,4-HAQ ($19,845\text{ cm}^{-1}$), and 1,4-HAQ ($19,920\text{ cm}^{-1}$) all lie within 300 cm^{-1} of each other, and each is characterized by sharp, laser linewidth limited, bands over a $\sim 1000\text{ cm}^{-1}$ range. In contrast to this, the spectra for HAQs without the 1,4-motif are broader, suggesting shorter excited state lifetimes. Their origins – 1-HAQ ($21,645\text{ cm}^{-1}$), 1,2-HAQ ($21,748\text{ cm}^{-1}$), 1,5-HAQ ($21,321\text{ cm}^{-1}$), and 1,8-HAQ ($22,031\text{ cm}^{-1}$) – are located over a larger energy spread, though still within $\sim 700\text{ cm}^{-1}$ of each other. The difference between these two groups of spectra,

suggests that the excited state properties strongly depend on the presence or absence of the 1,4-OH structural motif.

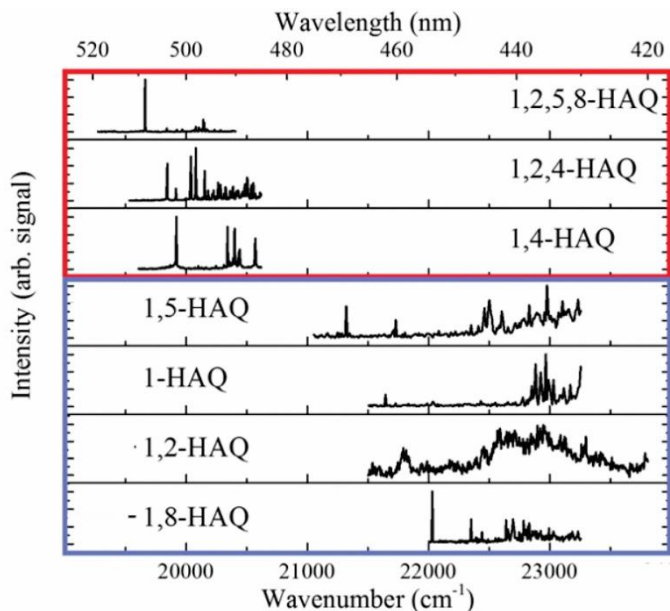


Fig. 2. Picosecond 2C-R2PI spectra of each HAQ in this study (OPG + 213 nm). Intensities have been normalized.

Pump Probe Spectroscopy

We performed picosecond pump-probe measurements for each HAQ from Fig. 1 on both the origin transition and on one additional higher energy transition, determined from the R2PI spectra. The measurement using the higher energy transition probed whether additional relaxation pathways become available at higher energies, which would likely be evidenced by a change in excited state lifetime. Fig. 3 shows the effect of structure on excited state lifetime. The molecules with the 1,4-OH motif, shown at the top in Fig. 3a in a red box, have nanosecond lifetimes at their lowest energy transitions. In contrast, those molecules without the 1,4-OH motif, shown at the bottom of Fig. 3a in a blue box, have sub-nanosecond lifetimes.

Coincidentally, the primary madder chromophores (1,2,4-HAQ and 1,2-HAQ) have the longest and the shortest excited state lifetimes, respectively, of all molecules measured. Fig. 3b shows the pump-probe traces of these two end-members (picosecond pump-probe data for the other molecules are shown in Fig. S1, Supplemental Information). Each of these traces can be adequately fit using a single exponential, providing the excited state lifetime of each molecule. When probed at the origin, 1,2,4-HAQ (purpurin) has an excited state lifetime of 5.4 ns, while 1,2-HAQ (alizarin) has an excited state lifetime of only 120 ps. Others of the HAQ series have lifetimes intermediate between these two: 1-HAQ has a measured lifetime of 290 ps while 1,4-HAQ has a measured lifetime of 1.7 ns, for example. In general, excitation at higher energies shortens the lifetime, as shown in Fig. 3a (black bars). 1,4-HAQ provides an exception to this trend, with a slight increase in excited state lifetime when measured at a transition $+655\text{ cm}^{-1}$ from the origin (from 1.7 ns to 1.9 ns). This slight increase is likely an artifact due to the short observation period relative to the excitation lifetime. For completeness, we also carried out nanosecond pump-probe measurements on the two endmembers (1,2,4-HAQ and 1,2-HAQ, data shown in Fig. S2). These measurements show no component at longer time scale than those found in the ps measurements.

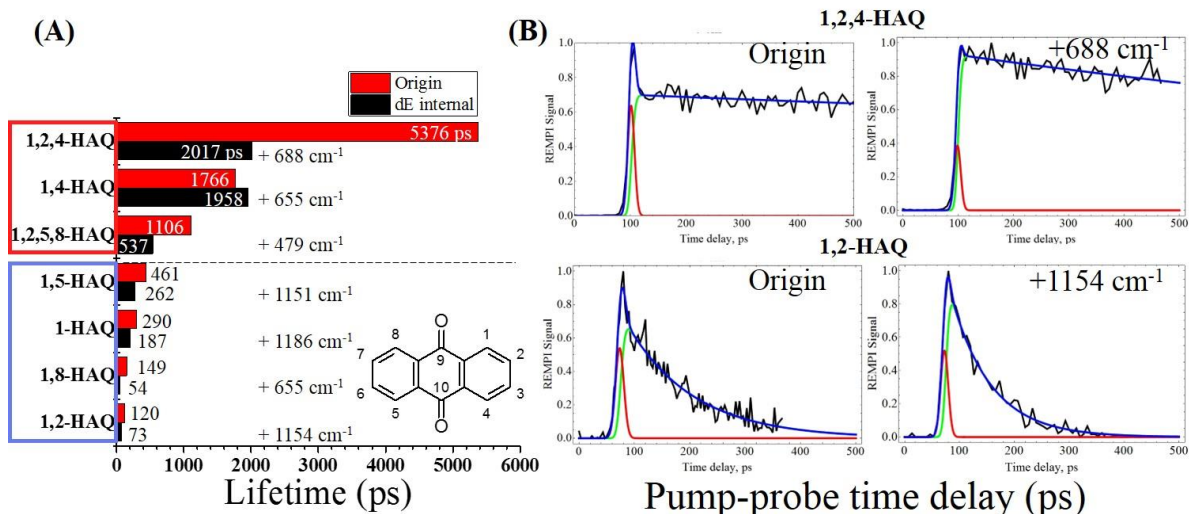


Fig. 3. Results of picosecond pump-probe spectroscopy. (A) Pump-probe lifetime as measured at the origin transition (red bars) and at excess energy (black bars), arranged in order of decreasing measured lifetimes. The excess energy transition used is noted next to the black bars. (B) Pump-probe traces of the molecules with the longest and shortest measured excited state lifetime, 1,2,4-HAQ and 1,2-HAQ respectively, plotted over 500 ps. The pump-probe data are fit to a curve (blue trace) which is the sum of a single exponential decay (green trace) convolved with a Gaussian component (red trace) representative of our instrument response function (IRF).

Intramolecular Hydrogen Bonding Characterization and Structural Confirmation

In order to understand the hydrogen bonding environment of the isomer of species in the molecular beam with and without the 1,4-OH motif, we performed IR hole burning. IR-UV results in mode II indicate that for 1,2,4-HAQ and 1,4-HAQ the R2PI results are from a single conformation (see Supplemental Information Fig. S3).

We also performed hole burning in mode I on 1,2,4-HAQ, 1,4-HAQ, and 1,8-HAQ while probing the origin of each, as shown in Fig. 4. In all three spectra the peak at $\sim 3,100$ cm⁻¹ represents stretching modes associated with the -OH hydrogen bound to a carbonyl group. In the case of 1,8-HAQ this peak is broadened by the competitive sharing of the carbonyl with intramolecular hydrogen bonds 180° about the oxygen atom (9-position). In the case of 1,2,4-HAQ the peak at 3570 cm⁻¹ results from the in-plane hydroxyl (2-position) which is

hydrogen bound to the neighboring hydroxyl (1-position). The 470 cm^{-1} separation is a direct measurement of different hydrogen bond environments: between carbonyl and hydroxy intramolecular bonded -OH stretches.

Fig. S4 in supplemental information also shows calculated LE spectra convoluted with a lorentzian linewidth of 3 cm^{-1} . These calculations reproduce the experimental patterns but not the exact frequencies, reflecting the fact that these are unscaled harmonic calculations. Future work with anharmonic calculations at a higher level may provide further details on structures.

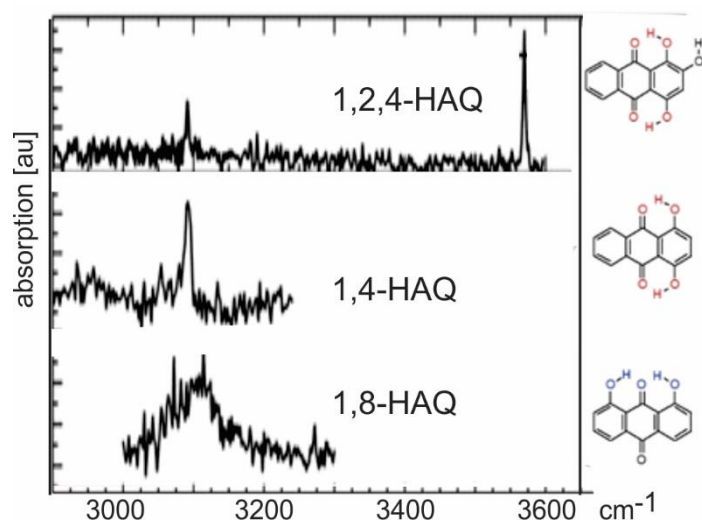


Fig. 4. IR hole burning spectra. Spectra were taken in mode I of 1,2,4-HAQ, 1,4-HAQ, and 1,8-HAQ probed at their origin R2PI transition.

Theoretical calculations: 1-HAQ and 1,4-HAQ

To model computationally the difference in excited state dynamics in the two structural motifs, with and without the 1,4 substitution, we performed detailed calculations on the most basic representatives of the two structural families, namely 1-HAQ and 1,4-HAQ.

1-HAQ: ground and excited state

Fig. 5 shows the calculated energetic landscapes of 1-HAQ. The ground-state global minimum of the keto form (I in Fig 5, hereafter referred to as K(I)) with the proton attached to the O₁ oxygen atom, is planar and stabilized by a single intramolecular hydrogen bond between two oxygen atoms as proton acceptor: O₁-H...O₉. The proton transferred form (enol form, II in Fig. 5, hereafter referred to as E(II)) with the proton attached to the O₉ oxygen atom is not stable in the S₀ state, and its geometry optimization transfers the proton back to the O₁ oxygen atom to reform the global minimum, form K(I). Possible rotation of the O₁H group could generate the second lowest S₀-state minimum, the keto rotamer (III in Fig. 5) structure. However, the O₁H rotation breaks the intramolecular hydrogen bond in the 1-HAQ structure, which destabilizes the rotated form compared to the global minimum K(I) by 0.52 eV (50 kJ/mol). Furthermore, the rotamer (III) minimum is separated from the global minimum by a S₀-state energy barrier of 0.16 eV (15kJ/mol). The fourth form, IV with the proton attached to the O₉ atom, has much higher energy and can be excluded from this study. This energetic profile indicates that the 1-HAQ molecule should exist in the K(I) form in the ground state.

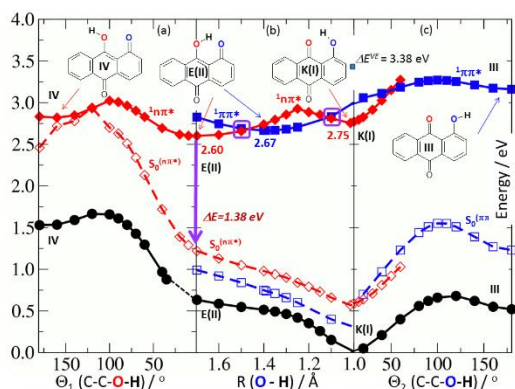


Fig. 5. Potential-energy energy profiles of 1-HAQ. Profiles shown are of the S₀ state (black circles), the S₁($\pi\pi^*$) state (blue squares) and the S₁($n\pi^*$) state (red diamonds) of the 1-HAQ molecule as a function of the torsional reaction path (a, c) and the hydrogen-transfer reaction path (b). Full lines (full symbols): energy profiles of reaction paths determined in the same

electronic state. Dashed lines (empty symbols) represent ground-state energy calculated for the geometry optimized in the given excited state $n\pi^*$ (red) or $\pi\pi^*$ (blue). Purple rectangles highlight the $n\pi^*$ and $\pi\pi^*$ intersections

When 1-HAQ is irradiated, the ground-state K(I) form is photo-excited to the lowest $\pi\pi^*$ excited state, $S_2(\pi\pi^*)$ with vertical energy $\Delta E^{VE} = 3.38$ eV at the S_0 -state minimum geometry. At this optimized ground-state geometry of K(I), S_1 is a dark $n\pi^*$ state below the $S_2(\pi\pi^*)$. The lowest $\pi\pi^*$ excited state does not have a stable minimum in the K(I) form. Therefore, as long as the system remains in the excited $\pi\pi^*$ state, the proton will transfer between the two oxygen atoms (from O_1 toward O_9) along a barrierless path to form the proton-transferred $\pi\pi^*$ excited-state form, E(II), as indicated by the minimum of the blue curve (full squares) in the central panel of Fig. 5.

As depicted in Fig. 5 (highlighted with purple rectangles), the $n\pi^*$ and $\pi\pi^*$ excited states intersect in the vicinity of the $S_1(\pi\pi^*)$ state minimum, E(II). Consequently, the $n\pi^*$ state can be populated directly from the $\pi\pi^*$ excited state. The $n\pi^*$ state has two minima, at the K(I) and E(II) forms, and the adiabatic energies of both minima are lower than that of the $S_1(\pi\pi^*)$ E(II) minimum. Once in the non-fluorescent $n\pi^*$ state the system seeks another decay channel. The S_1 - S_0 energy gap lowers for the $n\pi^*$ state to 1.38 eV for the E(II) excited-state form, as depicted by the vertical purple line in Fig 5. As shown in Fig. 5, if the system is in $n\pi^*$ - E(II) minimum, rotation of the O_9H group may lead to further significant decrease of the S_1 - S_0 energy gap (see red traces) until S_1 and S_0 meet at a C-C- O_2 -H dihedral angle of about 100° . This pathway provides an additional channel for excited-state deactivation. However, the large barrier in the $n\pi^*$ excited state may make this process less efficient.

1,4-HAQ: ground and excited state

The addition of the OH group to position 4 of the 1-HAQ molecule (that is, the introduction of the 1,4-OH motif) results in significant changes, both structurally by forming a second intramolecular hydrogen bond, and photo-physically by changing the ordering of the excited states

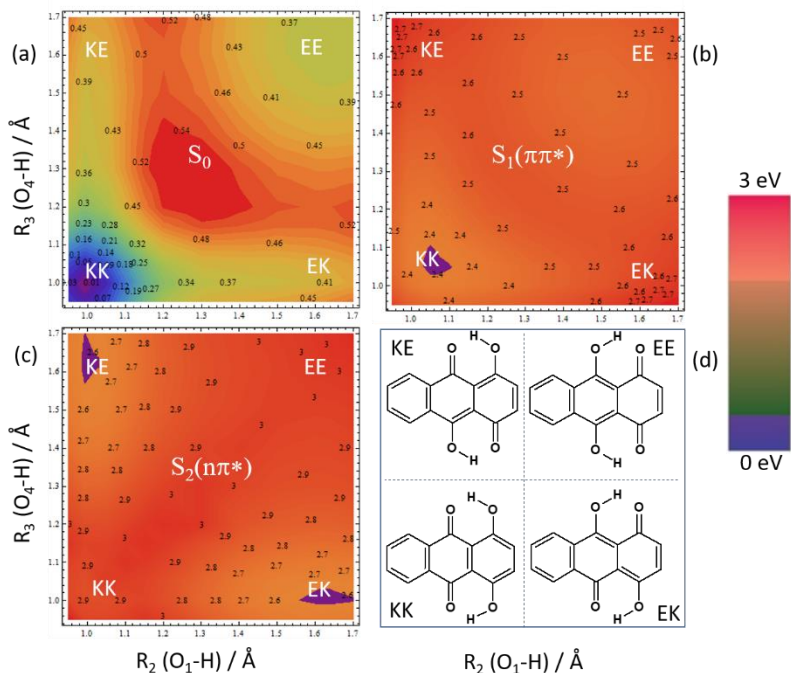


Fig. 6. Potential energy surfaces (PES) of 1,4-HAQ. (a) Minimum PES of the S_0 state, (b) the $S_1(\pi\pi^*)$ singlet excited state, (c) the $S_2(n\pi^*)$ singlet excited state of the **1,4-HAQ** molecule as a function of the hydrogen-transfer reaction path as a function of two coordinates: $R(\text{O}_1\dots\text{H})$ and $R(\text{O}_4\dots\text{H})$. (d) Schematic indication of the structures at the four combinations of minimum and maximum R values. The location of each tautomer on the PES are also labeled.

In contrast to 1-HAQ, 1,4-HAQ possesses two intramolecular hydrogen bonds: $\text{O}_1\text{-H}\dots\text{O}_9$ and $\text{O}_4\text{-H}\dots\text{O}_{10}$ which bridge the molecule on opposite sides and ensure planarity of the system. Fig. 6 displays the 2-dimensional PES of 1,4-HAQ, with panels (a), (b), and (c) showing the S_0 , S_1 and S_2 states, respectively; panel (d) illustrates the possible tautomers of 1,4-HAQ, both single hydrogen transfers (KE and EK), and double hydrogen transfer (EE). The x-axes of Fig. 6(a-c) are the reaction coordinate for the hydrogen displacement from O_1

while the y-axis is the reaction coordinate for the hydrogen displacement from O₄. Moving along the x-axis moves the hydrogen from O₁ to O₉ while the y-axis moves the hydrogen from O₄ to O₁₀. Thus, the top right corner of each energy surface is the EE tautomer, the product of both hydrogen transfers. There exists a tautomer in each corner of each PES, labeled accordingly. In addition to the global minimum form – the KK form with protons attached to O₁ and O₄ – the EE form, with the protons attached to O₉ and O₁₀, provides an additional local minimum, 0.36 eV higher in energy. As shown in Fig. 6a, the EE minimum is separated from the KK form by a relatively small S₀-state energy-barrier of ~ +0.15 eV. The presence of this additional stable tautomer and the energy barrier (in contrast to the 1-HAQ system which lacks an energy barrier) might be explained by the fact that any proton transfer usually requires shortening of the interatomic distance between two proton accepting centers (here, two oxygen atoms). While one interatomic distance, e.g. O₁...O₉, contracts, the other, i.e. O₄...O₁₀, must simultaneously lengthen. This effect is not energetically favorable, creating the barrier in S₀.

In these coordinates for the $\pi\pi^*$ (Fig. 6b), the KK tautomer is the minimum by ~0.15 eV. A single or double proton transfer to generate any other tautomer would be uphill and unfavorable. The vertical excitation energies, ΔE^{VE} , to the lowest excited $\pi\pi^*$ state of the KK and EE forms of the 1,4-HAQ molecule are: 2.80 eV and 2.58 eV, respectively (for a complete tabulation of results, see Tables S1 and S2, Supplemental Information). Both ΔE^{VE} values for 1,4-HAQ are lower than the respective value of 3.38 eV for 1-HAQ which is consistent with the experimental pattern of the origin shifts. This effect is consistent with π -electron donating character of the OH group²⁵ which should result in stabilization of the $\pi\pi^*$ excited state vs the $n\pi^*$ state for a given structure. Indeed, the lowest $n\pi^*$ states (Fig. 6c) in

the absorption ladder of both tautomeric forms of 1,4-HAQ are at least 0.5 eV above the lowest $\pi\pi^*$ states and therefore inaccessible.

The properties of the optimized excited state forms of the molecule are gathered in Table S1. KK and EE, respectively, each have the same ground state and $\pi\pi^*$ excited state geometries. Both excited-state forms are almost isoenergetic. Moreover, a barrier of only 0.15 eV separates the S_1 states of these two forms. At the same time, the $n\pi^*$ state PES lies almost entirely above the fluorescent $\pi\pi^*$ state. Such a situation greatly reduces the probability for nonradiative decay for the 1,4-HAQ in comparison to the 1-HAQ system.

3. Discussion

The experimental and computational results from this series of molecules demonstrate that the presence or absence of a hydroxyl substitution at the 4 position has profound effects on the spectroscopy and dynamics of substituted anthraquinones.

When interpreting spectral and pump-probe results it is important to keep in mind that multiple tautomeric forms are possible (as shown in Fig. 1). Generally, in jet-cooling conditions only the lowest energy forms exist and the mode II IR-UV data for 1,2,4-HAQ and 1,4-HAQ suggest those data to be exclusively from a single tautomer (though it is possible that signal arises from complimentary rotamers in Fig. 1). We assume the other compounds also to be exclusively or at least predominantly in the lowest energy tautomeric form but the possible existence of other tautomers in the beam cannot be definitively excluded.

With this limitation in mind, the experimental and computational evidence can be summarized as follows: (i) The origin transition for HAQs with the 1,4-motif is about 2000 cm^{-1} to the red of those without the 1,4-motif, as shown in Fig. 2.(ii) The excited state lifetime is approximately an order of magnitude shorter for those without the 1,4-motif, going from a few ns to a few hundred ps at the origin transition, as shown in Fig. 3. Relative to the 1-OH motif there is a 15 \times average longer lifetime for the molecular species with the 1,4-OH motif. (iii) In systems without the 1,4 motif (and therefore with short excited state lifetimes), proton transfer between the two oxygen atoms to form the proton-transferred $\pi\pi^*$ excited-state form is likely, while systems with the 1,4 motif more energetically favorable forms are likely to be present, limiting the probability for nonradiative decay pathways.

The photobleaching effects of *common madder* chromophores, 1,2,4-HAQ and 1,2-HAQ, was recently investigated by Tan et al. by counting emissive events in time (photoblinking) of these dyes under inert (N_2) irradiant conditions on glass. They measured that alizarin is able to absorb and emit four times longer (and over many more events) than purpurin, which they argue to be due to a long lived excited state of purpurin which degrades through electron injection to the glass slide.¹¹ This decay pathway is consistent with the literature.^{19, 21, 26} One cannot compare absolute lifetime values between gas phase and condensed phase states but the trend in the condensed phase correlates with the inherent lifetime trends presented here that 1,2-HAQ is ~ 45 times shorter lived at its vibrationless transition than 1,2,4-HAQ. The experimental data presented here seem to suggest that this pathway may be common to other substituted HAQs, with variations in the excited state lifetimes determined by the exact substitution arrangement.

Our theoretical investigation focused on the excited state potentials of 1-HAQ and 1,4-HAQ, since the experimental work showed that these motifs represent two distinct families of molecules. For 1-HAQ, the computations explain the experimentally observed short lifetimes by an energetically downhill process from the initially populated $\pi\pi^*$ state. Along the proton transfer coordinate, the $n\pi^*$ state is crossed twice, leading to the minimum of E(II). Following this pathway, the energy gap to the ground state is 1.38 eV, allowing for nonradiative decay, although there may be additional involvement of an out of plane torsion, leading to a conical intersection. These dynamics are consistent with the relatively short lifetimes observed for the HAQs without a 1,4-motif. After reaching the ground state, it is a downhill path to transfer the proton back and complete the photocycle, recovering the K(I) tautomer.

The addition of the OH group to the 4 position of the HAQ skeleton results in several critical changes to ground and excited state profiles. First, in the 1,4-HAQ molecule there is a second S_0 state minimum, the EE characterized by the two protons being transferred to the oxygens on carbons 9 and 10. Additionally, the shape of the $\pi\pi^*$ -excited state in 1,4-HAQ is much shallower than in 1-HAQ and photoexcitation of the KK form does not result in a barrierless proton transfer to the EE form as in 1-HAQ. The most prominent effect is that the $\pi\pi^*$ excited-state PES lies below the $n\pi^*$ excited-state PES, an effect of electron-donating property of the OH-group, which tends to stabilize the $\pi\pi^*$ excited state versus the $n\pi^*$ state. This explains the red shift of 1,4 motif versus those molecules that lack it^{25, 27}. Due to the stabilization of the $\pi\pi^*$, the $n\pi^*$ is not accessible at the excitation energies utilized. This effect inhibits nonradiative decay from the excited $\pi\pi^*$ to S_0 via crossing to the $n\pi^*$, as is the case for 1-HAQ. A major effect of 4-OH substitution is related to the unique stabilization of

the $\text{KK}(\pi\pi^*)$, lacking the downhill proton transferred minimum of the $\pi\pi^*$ excited state in 1-HAQ. The analogous initial $\pi\pi^*$ state in 1-HAQ undergoes proton transfer in a barrierless manner, leading to ps excited state lifetimes. However, this proton transfer involves shortening of the interatomic distance between the two proton accepting oxygen atoms. With the 1,4 motif, while one interatomic distance, e.g. O1...O9, contracts, the other, i.e. O4...O10, must simultaneously lengthen, which creates a barrier in the excited state potential. As a result, we find a single ns timescale lifetime for the molecules with a 1,4-motif, implying that instead of undergoing ESIPT, they relax from the initially populated $\pi\pi^*$ state. This model also explains why the 1,5-HAQ and 1,8-HAQ – both doubly hydrogen bound – behave photodynamically like the 1-HAQ.

We investigated the possibility of longer-lived states such as triplets with a ns ionization source for 1,2-HAQ and 1,2,4-HAQ, but have not observed such states experimentally. However, Mohamed et al. reported formation of a long lived triplet state with high quantum yield in a study of 1,8-HAQ in a series of nonpolar, polar aprotic, and polar protic solvents.²⁰ Further work in this area is therefore justified to clarify whether long lived triplets may form in some systems.

As seen by Flom and Barbara and explained by Nagaoka et al., the 1-HAQ motif exhibits dual fluorescence due to ESIPT. As the main excited-state pathway, this explains the photostability of molecules lacking the 1,4-HAQ motif observed in works of art (by, e.g. alizarin). In contrast, molecules **with** the 1,4-HAQ motif lack dual fluorescence and the corresponding ESIPT properties. At the same time, molecules with the 1,4-HAQ motif are noted for their photodegradation in works of art (e.g. purpurin). We have corroborated these phenomena both experimentally and theoretically in the gas-phase, indicating that this is a

fundamental characteristic of the anthraquinone molecules used to create lake dyes, and not due to other effects such as the interaction of the binding media or other pigments that may be present in the complex system of a work of art. Molecules with the 1-HAQ motif have ~15x shorter excited state lifetime than molecules with the 1,4-HAQ motif, explaining the former's photostability. The energetically downhill process of ESIPT accounts for the shorter lifetime of the 1-HAQ motif. Meanwhile, the geometries resulting from ESIPT of the 1,4-motif are all higher in energy than the initially excited, non-proton transfer state, making PT highly unfavorable. Without this process available, the 1,4-motif has a much longer excited-state lifetime and worse photostability.

Taken with the body of work done on UV radiation on anthracene by Mallakin on the production of toxic species (i.e. reactive, typically $^1\text{O}_2$) through the stepwise formation and further irradiation of AQs and HAQs²⁸⁻²⁹ and the work by Nagaoka et. Al (18) on the quenching of singlet oxygen ($^1\text{O}_2$) by ESIPT HAQs, the data presented here form a complex picture of the degradation of the madder colorants – and anthraquinone dyes more generally – in cultural heritage materials. These pigments need a way to dissipate photoenergy that they inherently will absorb from the environment. But without a viable energetic channel for decay, such as proton transfer or quenching of singlet oxygen, anthraquinone chromophores with a 1,4- substitutional motif will tend to degrade at a faster pace than their photostable counterparts which lack this motif. Knowledge of the fundamental photochemical response, therefore, allows those who care for culturally significant materials to better predict their photosensitivity: if the specific chemical composition of the organic red dyes in an object can be determined, and a 1,4- substitutional motif is prevalent (either in the only chromophore present, or in high concentration in a mixture of several anthraquinones), a

higher photosensitivity can be presumed than if the structure were lacking, regardless of how many chromophore(s) are present. The data shown here suggests that conservators and curators may therefore use information about the chemical structure to predict general trends in the photosensitivity of the objects in their care if colored with anthraquinone dyes, and protect those objects accordingly.

4. Materials and Methods

Experimental Design

Standards of seven HAQs were purchased from Sigma-Aldrich and used without further purification. Standards were directly applied to individual graphite sample bars as a thin solid layer and examined in isolation to ensure spectral purity for 2C-R2PI and pump-probe measurements.

The instrument has been previously described in detail and only a brief description of the experimental setup follows.³⁰⁻³¹ Samples are laser desorbed in vacuo directly in front of a pulsed molecular beam controlled by a piezo cantilever valve.³² The desorption laser is a tightly focused Nd:YAG laser (1064 nm, ~ 1 mJ/pulse) and the piezo cantilever valve operates at a 45 μ sec pulse duration with 8 bars backing argon gas. The desorbed sample is adiabatically cooled by collisions with the argon jet-expansion to between 10-20 K and the molecular beam is skimmed before being intersected by laser beams and photo-ionized by two-color resonant two photon ionization (2C-R2PI). The subsequent ions are detected by a reflectron time of flight mass spectrometer (2×10^{-6} Torr analyzer pressure, mass resolution $m/\Delta m=500$).

The 2C-R2PI spectroscopic and picosecond (ps) pump-probe delay measurements are performed with an Ekspla PL2251 Nd:YAG laser system producing ~30 ps laser pulses. The

355 nm output pumps an Ekspla PG401 tunable optical parametric generator (OPG) (VIS output of 450-600 uJ/pulse, $\sim 6 \text{ cm}^{-1}$ spectral linewidth). The sample is excited by the OPG and ionized by 213 nm, fifth harmonic of the Ekspla PL2251 laser, which is mechanically delayed up to 600 ps before colineation with the OPG beam. A variable electronic (SRS DG645) delay between OPG UV laser and an excimer laser (193 nm, 1.5-2 mJ/pulse) is used for pump-probe measurements in the nanosecond (ns) time delay range.

For IR-UV double resonant spectroscopy (i.e. IR hole-burning) a Laser Vision optical parametric oscillator/amplifier (OPO/OPA) (mid-IR output over the range 3,000-3,600 cm^{-1} of ~ 3 -5 mJ/pulse, 3 cm^{-1} spectral linewidth) precedes the REMPI by 200 ns. This study utilized double resonant spectroscopy with two different pulse sequences: in mode I, the IR pump is scanned at a fixed UV probe wavelength, while in mode II, the UV is scanned with a fixed IR burn wavelength. In mode I, the UV laser wavelength is selected to correspond to a single vibronic transition, and the resulting 2C-R2PI signal depletes when the IR laser becomes resonant with the ground state population. The resulting ion-dip spectrum therefore represents the ground state IR spectrum of a single tautomer, selected by the UV probe wavelength. This IR spectrum can be compared with calculated IR frequencies to determine the specific tautomer of the selected vibronic transition. In mode II, the IR laser wavelength is selected to correspond to a tautomer-specific vibrational resonance, and spectra are collected both with IR laser on and off. The difference spectrum identifies peaks in the UV spectrum that arise from the same tautomer.

Calculations for IR-UV double resonant spectroscopy

Calculations were performed with the Gaussian 09 program package.³³ Starting structures for hydroxy derivatized anthracene-9,10-dione (HAQ) structures, tautomer and rotamer isomers, were optimized using the B3LYP hybrid functional with CC-pVTZ basis

set. Relative zero-point corrected energy (ZPE) values are used to predict the number of isomers in our molecular beam based on the rule of thumb that for a given species isomers up to 20 kJ/mol of the lowest energy structure are typically kinetically trapped laser desorption jet-expansion. Past work on the nucleobase adenine showed that only the lowest energy isomer was present, where the next lowest energy isomer was calculated to be at ~33 kJ/mol higher energy than the one observed.³⁴ Ground state minima were confirmed by the absence of imaginary frequencies and these geometries were later used to determine electronic transition state strengths for S1-4 by way of TD-DFT with the B3LYP hybrid functional with CC-pVTZ basis set. The simulated IR spectra arise from frequencies with harmonic intensities using a Lorentzian shape and FWHM of 3 cm⁻¹ and are presented without a spectral shift.

Calculations for construction of energy profiles

The ground-state minima forms of the 1-HAQ and 1,4-DHAQ were optimized by means of the MP2 method³⁵ using the cc-pVDZ³⁶ correlation-consistent atomic basis set. The excited-state geometries were optimized with the use of the same basis set while using the CC2³⁷⁻³⁸ method as implemented in TURBOMOLE software package³⁹. In the calculation of the vertical excitation energies, ΔE^{VE} , mimicking the absorption spectra, performed on top of the MP2/cc-pVDZ-optimized S₀-state geometries, the CC2³⁷⁻³⁸ method was used to evaluate the response properties.

To elucidate the photophysical mechanism on the molecular level the important driving coordinates were appropriately chosen for each system so that the ground- and the excited-state minimum potential-energy (MPE) profiles or surfaces could be constructed to estimate the ground- and excited-state energy barriers determining the photophysics of the both

molecules. The 1-HAQ molecule is bound by a single hydrogen bond. In such case one coordinate – the $R_1(\text{O}_1\text{H})$ distance – is needed to be chosen as a driving coordinate to illustrate the photophysical mechanism of the photo-*tautomerization* process. The MPE profile for 1-HAQ is constructed in a way that for fixed given value of the $R_1(\text{O}_1\text{H})$ distance, all the remaining nuclear degrees of freedom are optimized; once in the ground state and twice in the two excited states: $S_1(\pi\pi^*)$ and $S_1(n\pi^*)$.

The 1,4-DHAQ system has an additional intramolecular hydrogen bond binding the molecule and more tautomeric forms are possible to be formed upon photoexcitation. A convenient method for illustrating the *tautomerization* process in such molecule is to construct the MPE surface spanning the two driving reaction coordinates describing the two intramolecular hydrogen bonds by the $R_2(\text{O}_2\text{H})$ and $R_3(\text{O}_4\text{H})$ distances. In that case both the R_2 and R_3 coordinates are being frozen for given values, while the rest of the parameters are being optimized in the constructed MPE surface, separately for the ground (S_0) and the two excited states: $S_1(\pi\pi^*)$ and $S_1(n\pi^*)$ with the C_s symmetry constrain.

Supplemental Materials

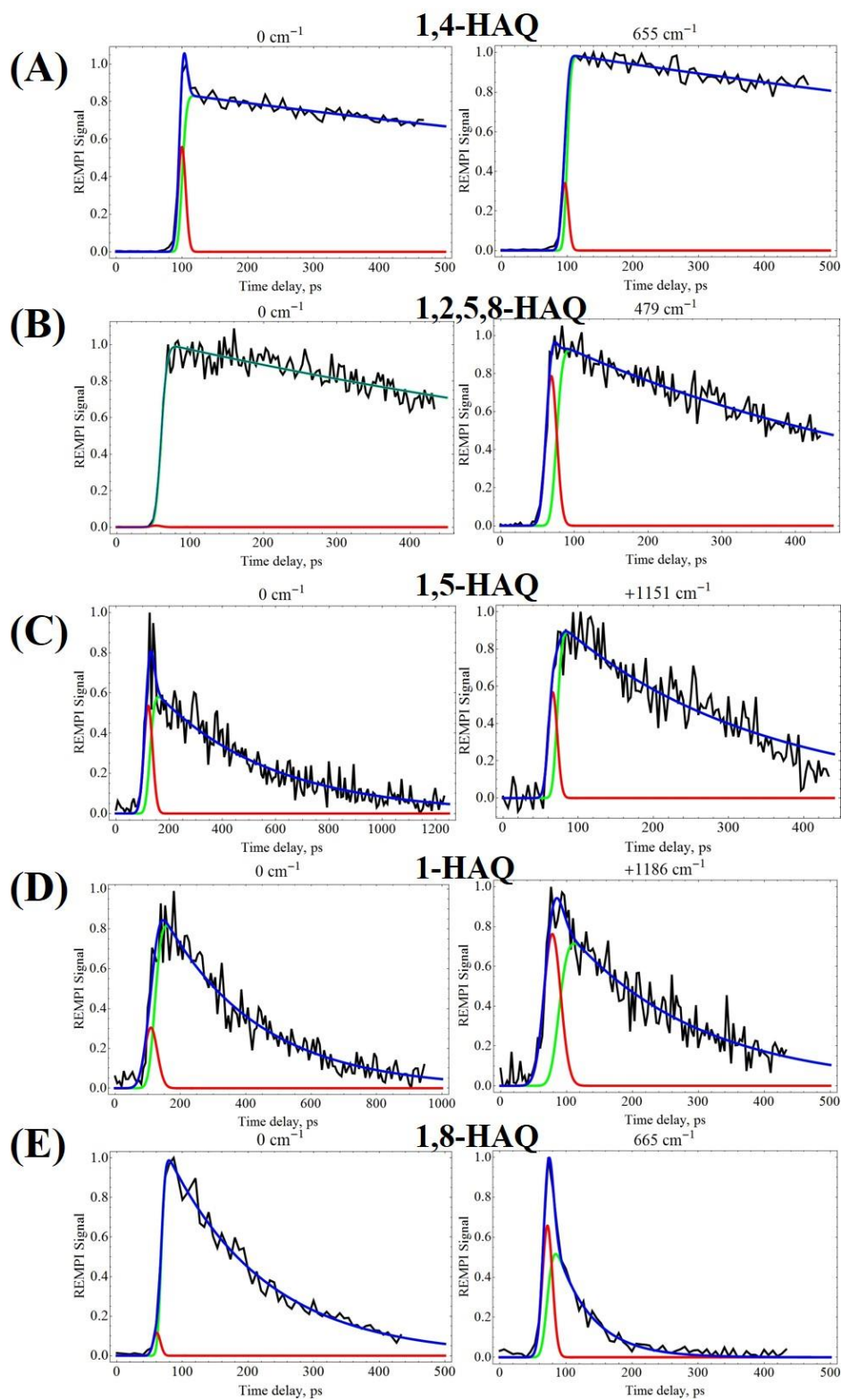


Fig. S1. Picosecond pump-probe spectra. (A) 1,4-HAQ, (B) 1,2,5,8-HAQ, (C) 1,5-HAQ, (D) 1-HAQ, and (E) 1,8-HAQ at vibrationless (left column) and excess probe lengths (right column). The pump-probe data are fit to a curve (blue) which is the sum of a single

exponential decay convolved with a Gaussian component (red) representative of our instrument response function (IRF) the IRF itself (green).

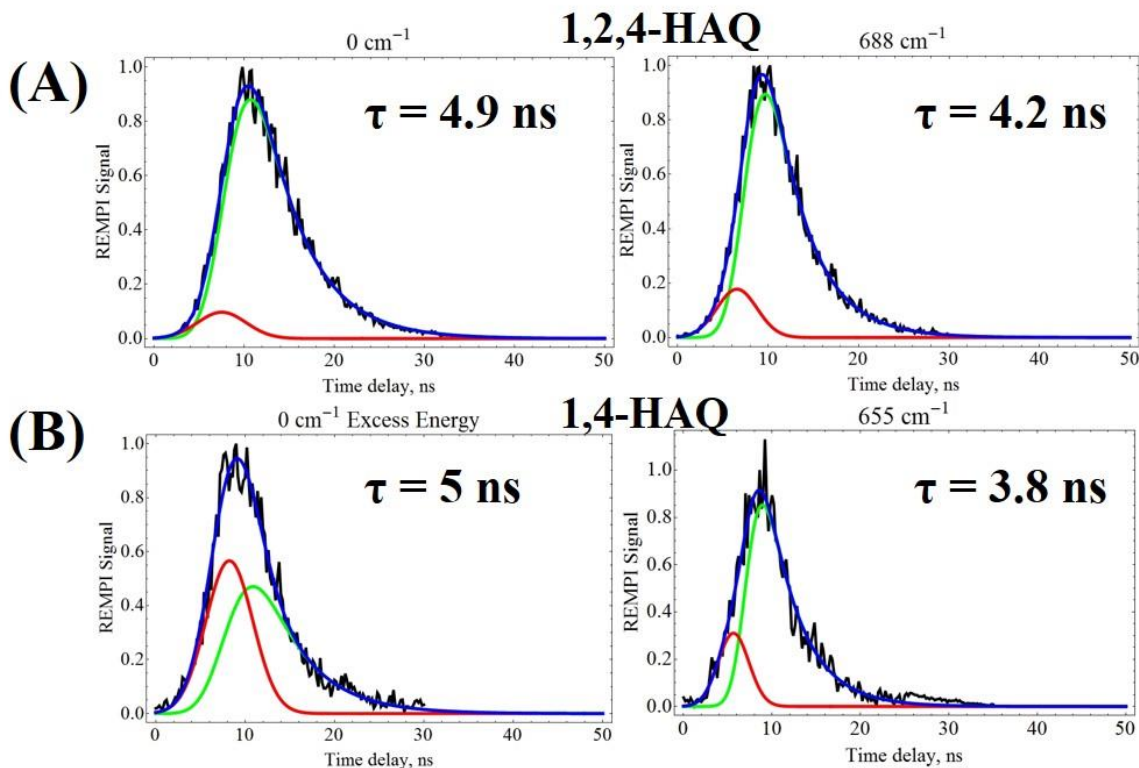


Fig. S2. Nanosecond pump-probe spectra. (A) 1,2,4-HAQ at vibrationless and excess probe lengths and for (B) 1,4-HAQ at vibrationless and excess probe lengths. The lifetime values here agree with those presented in Fig. 3 for pump-probe measurement within the time jitter (± 3 ns) of the 193 nm ns ionization source. The pump-probe data are fit to a curve (blue) which is the sum of a single exponential decay convolved with a Gaussian component (red) representative of our instrument response function (IRF) the IRF itself (green).

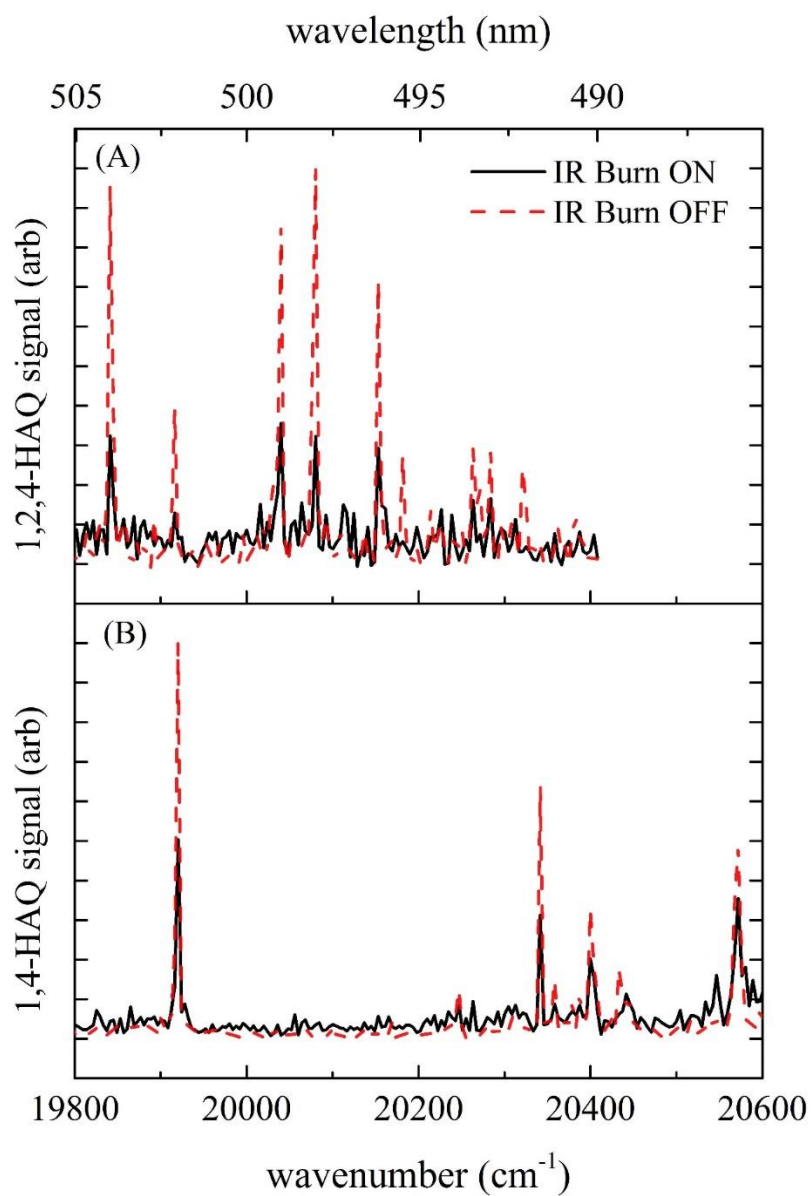


Fig. S3. IR hole burning spectra in mode II with the burn laser set to 3090 cm^{-1} . (A) All 1,2,4-HAQ vibronic transitions share resonance at IR burn wavelength, as do all (B) 1,4-HAQ vibronic transitions, suggesting a single tautomer in each R2PI spectrum.

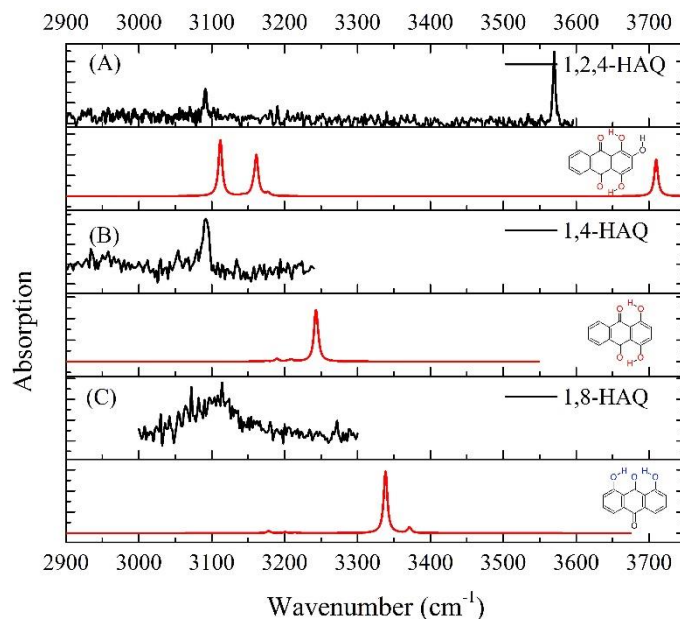


Fig. S4. IR hole burning spectra (in black) taken in mode I of (A) 1,2,4-HAQ, (B) 1,4-HAQ, and (C) 1,8-HAQ probed at their lowest energy R2PI transition. The ground state predicted frequencies for the given LE structure are plotted below each hole burn spectrum (in red). Harmonic analysis is shown unshifted.

1-HAQ			
S_n / Tautomer	ΔE^{VE} / eV	f	μ / D
form K (I)			
S_0	0.0		1.4
$S_1(n\pi^*)$	3.21	0.000	2.8
$S_2(\pi\pi^*)$	3.38	0.145	4.4
$S_3(n\pi^*)$	3.62	0.000	2.6
$S_4(\pi\pi^*)$	4.28	0.029	4.9
$S_5(\pi\pi^*)$	4.31	0.012	1.3
$S_6(n\pi^*)$	4.97	0.000	4.0
form K rot (III)			
S_0	0.52		1.8
$S_1(n\pi^*)$	3.10	0.000	3.6
$S_2(n\pi^*)$	3.43	0.000	2.2
$S_3(\pi\pi^*)$	3.79	0.110	7.2
$S_4(\pi\pi^*)$	4.34	0.035	3.2
$S_5(\pi\pi^*)$	4.55	0.014	0.7
$S_6(n\pi^*)$	4.74	0.000	6.3
1,4-HAQ			
S_n / Tautomer	ΔE^{VE} / eV	f	μ / D
form KK (I)			
S_0	0.0		2.2
$S_1(\pi\pi^*)$	2.80 (a1)	0.209	2.5
$S_2(n\pi^*)$	3.32 (b2)	0.000	1.9
$S_3(n\pi^*)$	3.65 (a2)	0.000	2.1
$S_4(\pi\pi^*)$	4.14 (b1)	0.000	0.4

S ₅ ($\pi\pi^*$)	4.29 (a1)	0.032	7.1
S ₆ ($\pi\pi^*$)	4.43 (b1)	0.006	4.0
form EE (II)			
S ₀	<i>0.36</i>		<i>1.1</i>
S ₁ ($\pi\pi^*$)	2.58 (a1)	0.246	4.8
S ₂ ($n\pi^*$)	3.19 (b2)	0.000	0.6
S ₃ ($n\pi^*$)	3.46 (a2)	0.000	0.4
S ₄ ($\pi\pi^*$)	3.86 (b1)	0.007	0.9
S ₅ ($\pi\pi^*$)	4.16 (b1)	0.051	5.2
S ₆ ($n\pi^*$)	4.34 (a1)	0.002	4.2
form KK rot (I)			
S ₀	<i>0.55</i>		<i>0.9</i>
S ₁ ($n\pi^*$)	3.03	0.188	5.7
S ₂ ($\pi\pi^*$)	3.03	0.000	4.2
S ₃ ($n\pi^*$)	3.60	0.000	2.6
S ₄ ($\pi\pi^*$)	4.29	0.026	4.1
S ₅ ($\pi\pi^*$)	4.38	0.020	0.9
S ₆ ($n\pi^*$)	4.70	0.000	6.8

Table S1: Calculated properties of 1-HAQ and 1,4-HAQ. Vertical excitation energies, ΔE^{VE} (in eV) for the stable minima of the **1-HAQ** and **1,4-HAQ** molecules calculated at the CC2/cc-pVDZ theory level at the geometries optimized with the MP2/cc-pVDZ method. The ground-state properties are marked Italic.

1-HAQ				
state/ tautomer	$E^a(S_n)$ (E _n)	μ_e/D	f	
form K(I)				
S ₀	0.00			
S ₁ $\pi\pi^*$	-	-	-	
S ₁ $n\pi^*$	2.75 (2.18)	$\mu_e = 4.2$ D	0.00	
form E(II)				
S ₀	-			
S ₁ $\pi\pi^*$	2.67 (1.92)	$\mu_e = 1.2$ D	0.200	
S ₁ $n\pi^*$	2.60 (1.38)	$\mu_e = 5.4$ D	0.000	

Table S2: Emission properties of 1-HAQ. Adiabatic energy, (E^a in eV, bold), fluorescence energy, (E_{fl} , given in parenthesis), excited-state dipole moment (μ_e in D) and oscillator strength (f) of the given excited-state form optimized with the CC2/cc-pVDZ method.

1,4-HAQ				
state/ tautomer	S_n (E _n)	μ_e/D	f	
form KK(I)				
S ₀	<i>0.00</i>			
S ₁ ($\pi\pi^*$)	2.39 (2.13)	0.1 D	0.221	
S ₁ ($n\pi^*$)	2.95 (2.42)	3.1 D	0.000	
form EE(II)				
S ₀	<i>0.36</i>			
S ₁ ($\pi\pi^*$)	2.50 (2.01)	2.6 D	0.225	
S ₁ ($n\pi^*$)	3.10 (2.57)	2.0 D	0.000	
form EK ~ KE				
S ₀	-			

S ₁ ($\pi\pi^*$)	-	-	-	
S ₁ ($n\pi^*$)	2.66 (1.70)	3.6 D	0.000	

Table S3: Emission properties of 1,4-HAQ. Adiabatic energy, (E^a in eV, bold), fluorescence energy, (E_{fl} , given in parenthesis), excited-state dipole moment (μ_e in D) and oscillator strength (f) of the given excited-state form optimized with the CC2/cc-pVDZ method.

References

- Hofenk de Graaff, J., *The Colourful Past: Origins, Chemistry, and Identification of Natural Dyestuffs*. Archetype Publications: London, 2004.
- Whitney, A. V.; Van Duyne, R. P.; Casadio, F., An innovative surface-enhanced Raman spectroscopy (SERS) method for the identification of six historical red lakes and dyestuffs. *J. Raman Spectrosc.* **2006**, *37* (10), 993-1002.
- Brown, J. P., A review of the genetic effects of naturally occurring flavonoids, anthraquinones and related compounds. *Mutation Research/Reviews in Genetic Toxicology* **1980**, *75* (3), 243-277.
- Malik, E. M.; Müller, C. E., Anthraquinones As Pharmacological Tools and Drugs. *Medicinal Research Reviews* **2016**, *36* (4), 705-748.
- Melo, M. J.; Claro, A., Bright Light: Microspectrofluorimetry for the Characterization of Lake Pigments and Dyes in Works of Art. *Acc. Chem. Res.* **2010**, *43* (6), 857-866.
- Brosseau, C. L.; Casadio, F.; Van Duyne, R. P., Revealing the invisible: using surface-enhanced Raman spectroscopy to identify minute remnants of color in Winslow Homer's colorless skies. *J. Raman Spectrosc.* **2011**, *42* (6), 1305-1310.
- Fieberg, J. E.; Knutas, P.; Hostettler, K.; Smith, G. D., "Paintings Fade Like Flowers": Pigment Analysis and Digital Reconstruction of a Faded Pink Lake Pigment in Vincent van Gogh's Undergrowth with Two Figures. *Appl Spectrosc* **2017**, *71* (5), 794-808.
- Saunders, D.; Kirby, J., Light-Induced Color Changes in Red and Yellow Lake Pigments. *National Gallery Tech. Bull.* **1994**, *15*, 79-97.
- Clementi, C.; Nowik, W.; Romani, A.; Cibir, F.; Favaro, G., A spectrometric and chromatographic approach to the study of ageing of madder (*Rubia tinctorum* L.) dyestuff on wool. *Anal. Chim. Acta* **2007**, *596* (1), 46-54.
- Grazia, C.; Clementi, C.; Miliani, C.; Romani, A., Photophysical properties of alizarin and purpurin Al(III) complexes in solution and in solid state. *Photochem Photobiol Sci* **2011**, *10* (7), 1249-54.
- Tan, J. A.; Garakyaraghi, S.; Tagami, K. A.; Frano, K. A.; Crockett, H. M.; Ogata, A. F.; Patterson, J. D.; Wustholz, K. L., Contributions from Excited-State Proton and Electron Transfer to the Blinking and Photobleaching Dynamics of Alizarin and Purpurin. *The Journal of Physical Chemistry C* **2017**, *121* (1), 97-106.
- Miliani, C.; Monico, L.; Fantacci, S.; Romani, A.; Melo, M. J.; Angelin, E. M.; Janssens, K., Recent insights into the photochemistry of artists' pigments and dyes: towards better understanding and prevention of colour change in works of art. *Angew. Chem. Int. Ed.* **2018**, *57* (25), 7324-7334.
- Douhal, A.; Lahmani, F.; Zewail, A. H., Proton-transfer reaction dynamics. *Chemical Physics* **1996**, *207* (2), 477-498.

14. Formosinho, S. J.; Arnaut, L. G., Excited-state proton transfer reactions II. Intramolecular reactions. *Journal of Photochemistry and Photobiology A: Chemistry* **1993**, 75 (1), 21-48.
15. Flom, S. R.; Barbara, P. F., Proton transfer and hydrogen bonding in the internal conversion of S1 anthraquinones. *The Journal of Physical Chemistry* **1985**, 89 (21), 4489-4494.
16. El Ezaby, M. S.; Salem, T. M.; Zewail, A. H.; Issa, R., Spectral Studies of Some Hydroxy-derivatives of Anthraquinones. *J. Chem. Soc. B* **1970**, 1293-1296.
17. Navas Diaz, A., Absorption and emission spectroscopy and photochemistry of 1,10-anthraquinone derivatives: a review. *Journal of Photochemistry and Photobiology A: Chemistry* **1990**, 53 (2), 141-167.
18. Nagaoka, S.-i.; Nagashima, U., Effects of node of wave function upon excited-state intramolecular proton transfer of hydroxyanthraquinones and aminoanthraquinones. *Chem. Phys.* **1996**, 206 (3), 353-362.
19. Lee, S.; Lee, J.; Pang, Y., Excited state intramolecular proton transfer of 1,2-dihydroxyanthraquinone by femtosecond transient absorption spectroscopy. *Current Applied Physics* **2015**, 15 (11), 1492-1499.
20. Mohammed, O. F.; Xiao, D.; Batista, V. S.; Nibbering, E. T., Excited-state intramolecular hydrogen transfer (ESIHT) of 1,8-dihydroxy-9,10-anthraquinone (DHAQ) characterized by ultrafast electronic and vibrational spectroscopy and computational modeling. *The journal of physical chemistry. A* **2014**, 118 (17), 3090-9.
21. Jen, M.; Lee, S.; Jeon, K.; Hussain, S.; Pang, Y., Ultrafast Intramolecular Proton Transfer of Alizarin Investigated by Femtosecond Stimulated Raman Spectroscopy. *J Phys Chem B* **2017**, 121 (16), 4129-4136.
22. Smoluch, M.; Joshi, H.; Gerssen, A.; Gooijer, C.; van der Zwan, G., Fast excited-state intramolecular proton transfer and subnanosecond dynamic stokes shift of time-resolved fluorescence spectra of the 5-methoxysalicylic acid/diethyl ether complex. *J Phys Chem A* **2005**, 109 (4), 535-41.
23. Peng, Y.; Ye, Y.; Xiu, X.; Sun, S., Mechanism of Excited-State Intramolecular Proton Transfer for 1,2-Dihydroxyanthraquinone: Effect of Water on the ESIPT. *The journal of physical chemistry. A* **2017**, 121 (30), 5625-5634.
24. Leona, M.; Stenger, J.; Ferloni, E., Application of surface-enhanced Raman scattering techniques to the ultrasensitive identification of natural dyes in works of art. *J. Raman Spectrosc.* **2006**, 37 (10), 981-992.
25. Rode, M. F.; Sobolewski, A. L., Effect of chemical substituents on the energetical landscape of a molecular photoswitch: an ab initio study. *The Journal of Physical Chemistry A* **2010**, 114 (44), 11879-11889.
26. Giacco, T. D.; Latterini, L.; Elisei, F., Photophysical and photochemical properties of 1,2,4-trihydroxy-9,10-anthraquinone adsorbed on inorganic oxides. *Photochemical & Photobiological Sciences* **2003**, 2 (6), 681-687.
27. Rode, M. F.; Sobolewski, A. L., Effect of chemical substitutions on photo-switching properties of 3-hydroxy-picolinic acid studied by ab initio methods. *The Journal of Chemical Physics* **2014**, 140 (8), 084301.
28. Mallakin, A.; George Dixon, D.; Greenberg, B. M., Pathway of anthracene modification under simulated solar radiation. *Chemosphere* **2000**, 40 (12), 1435-1441.
29. Mallakin, A.; McConkey, B. J.; Miao, G.; McKibben, B.; Snieckus, V.; Dixon, D. G.; Greenberg, B. M., Impacts of Structural Photomodification on the Toxicity of

- Environmental Contaminants: Anthracene Photooxidation Products. *Ecotoxicology and Environmental Safety* **1999**, *43* (2), 204-212.
30. Meijer, G.; Devries, M. S.; Hunziker, H. E.; Wendt, H. R., Laser Desorption Jet-Cooling of Organic-Molecules - Cooling Characteristics and Detection Sensitivity. *Appl Phys B-Photo* **1990**, *51* (6), 395-403.
31. Siouri, F. M.; Boldissar, S.; Berenbeim, J. A.; de Vries, M. S., Excited State Dynamics of 6-Thioguanine. *J Phys Chem A* **2017**, *121* (28), 5257-5266.
32. Irimia, D.; Dobrikov, D.; Kortekaas, R.; Voet, H.; van den Ende, D. A.; Groen, W. A.; Janssen, M. H., A short pulse (7 micros FWHM) and high repetition rate (dc-5 kHz) cantilever piezovalve for pulsed atomic and molecular beams. *Rev Sci Instrum* **2009**, *80* (11), 113303.
33. Frisch, M. J.; Trucks, G. W.; Schlegel, H. B.; Scuseria, G. E.; Robb, M. A.; Cheeseman, J. R.; Scalmani, G.; Barone, V.; Mennucci, B.; Petersson, G. A.; Nakatsuji, H.; Caricato, M.; Li, X.; Hratchian, H. P.; Izmaylov, A. F.; Bloino, J.; Zheng, G.; Sonnenberg, J. L.; Hada, M.; Ehara, M.; Toyota, K.; Fukuda, R.; Hasegawa, J.; Ishida, M.; Nakajima, T.; Honda, Y.; Kitao, O.; Nakai, H.; Vreven, T.; Montgomery, J. A.; Peralta, J. E.; Ogliaro, F.; Bearpark, M.; Heyd, J. J.; Brothers, E.; Kudin, K. N.; Staroverov, V. N.; Kobayashi, R.; Normand, J.; Raghavachari, K.; Rendell, A.; Burant, J. C.; Iyengar, S. S.; Tomasi, J.; Cossi, M.; Rega, N.; Millam, J. M.; Klene, M.; Knox, J. E.; Cross, J. B.; Bakken, V.; Adamo, C.; Jaramillo, J.; Gomperts, R.; Stratmann, R. E.; Yazyev, O.; Austin, A. J.; Cammi, R.; Pomelli, C.; Ochterski, J. W.; Martin, R. L.; Morokuma, K.; Zakrzewski, V. G.; Voth, G. A.; Salvador, P.; Dannenberg, J. J.; Dapprich, S.; Daniels, A. D.; Farkas; Foresman, J. B.; Ortiz, J. V.; Cioslowski, J.; Fox, D. J., Gaussian 09, Revision B.01. **2009**.
34. Plutzer, C.; Nir, E.; de Vries, M. S.; Kleineremanns, K., IR-UV double-resonance spectroscopy of the nucleobase adenine. *Physical Chemistry Chemical Physics* **2001**, *3* (24), 5466-5469.
35. Møller, C.; Plesset, M. S., Note on an approximation treatment for many-electron systems. *Physical Review* **1934**, *46* (7), 618.
36. Dunning Jr, T. H., Gaussian basis sets for use in correlated molecular calculations. I. The atoms boron through neon and hydrogen. *The Journal of chemical physics* **1989**, *90* (2), 1007-1023.
37. Christiansen, O.; Koch, H.; Jørgensen, P., The second-order approximate coupled cluster singles and doubles model CC2. *Chem Phys Lett* **1995**, *243* (5-6), 409-418.
38. Hättig, C.; Weigend, F., CC2 excitation energy calculations on large molecules using the resolution of the identity approximation. *The Journal of Chemical Physics* **2000**, *113* (13), 5154-5161.
39. Ahlrichs, R.; Bär, M.; Häser, M.; Horn, H.; Kölmel, C., Electronic-Structure Calculations on Workstation Computers - the Program System Turbomole. *Chem. Phys. Lett.* **1989**, *162* (3), 165-169.